MARTIN MARIETTA ENERGY SYSTEMS LIBRARIES
3 4456 0351036 9

CENTRAL RESEARCH LIBRARY
DOCUMENT COLLECTION

[redacted]

AEC RESEARCH AND DEVELOPMENT REPORT

ORNL-2674
C-84 - Reactors-Special Features of Aircraft Reactors

DECLASSIFIED
CLASSIFICATION CHANGED TO:
BY AUTHORITY OF:
BY:

Cy. 114A

CORROSION OF MATERIALS BY LITHIUM AT ELEVATED TEMPERATURES

Eugene Edward Hoffman

CENTRAL RESEARCH LIBRARY
DOCUMENT COLLECTION
LIBRARY LOAN COPY
DO NOT TRANSFER TO ANOTHER PERSON
If you wish someone else to see this document, send in name with document and the library will arrange a loan.

OAK RIDGE NATIONAL LABORATORY
operated by
UNION CARBIDE CORPORATION
for the
U.S. ATOMIC ENERGY COMMISSION

[redacted]

[redacted]

LEGAL NOTICE

This report was prepared as an account of Government sponsored work. Neither the United States, nor the Commission, nor any person acting on behalf of the Commission:

A. Makes any warranty or representation, express or implied, with respect to the accuracy, completeness, or usefulness of the information contained in this report, or that the use of any information, apparatus, method, or process disclosed in this report may not infringe privately owned rights; or

B. Assumes any liabilities with respect to the use of, or for damages resulting from the use of any information, apparatus, method, or process disclosed in this report.

As used in the above, "person acting on behalf of the Commission" includes any employee or contractor of the Commission to the extent that such employee or contractor prepares, handles or distributes, or provides access to, any information pursuant to his employment or contract with the Commission.

[redacted]

ORNL-2674
C-84 – Reactors-Special Features of Aircraft Reactors

This document consists of 258 pages.
Copy 114 of 350 copies. Series A.

Contract No. W-7405-eng-26

METALLURGY DIVISION

CORROSION OF MATERIALS BY LITHIUM AT ELEVATED TEMPERATURES

Eugene Edward Hoffman

DATE ISSUED
MAR 9 1959

Submitted as a Thesis to the Graduate Council of the University of Tennessee in partial fulfillment of the requirements for the degree of Master of Science

OAK RIDGE NATIONAL LABORATORY
Oak Ridge, Tennessee
operated by
UNION CARBIDE CORPORATION
for the
U. S. ATOMIC ENERGY COMMISSION

[redacted]

[redacted]

[redacted]

MARTIN MARIETTA ENERGY SYSTEMS LIBRARIES
3 4456 0351036 9

ACKNOWLEDGEMENT

The author wishes to acknowledge the contribution of Dr. W. O. Harms of the University of Tennessee, his thesis advisor, in the preparation of this manuscript. He is also indebted to Drs. J. V. Cathcart and J. L. Scott of the Metallurgy Division and Dr. J. W. Prados of the Department of Chemical and Metallurgical Engineering, University of Tennessee, who assisted in the review of the manuscript.

The author was privileged to be able to perform the experimental work at the Oak Ridge National Laboratory which permitted access to and invaluable assistance from a comprehensive organization of scientific personnel, facilities, and equipment. The bulk of the experimental work was made possible by the special talents and equipment available in the Reactor Metallurgy Section of the Metallurgy Division.

Special thanks are extended to W. D. Manly, Associate Director of the Metallurgy Division, for his encouragement and constructive appraisal of the experimental work on this report.

Thanks are also due L. R. Trotter of the General Corrosion Group of the Metallurgy Division for his expeditious performance of both routine and unusual experimental work. A large amount of complementary experimental work was ably performed by W. H. Cook, D. H. Jansen, J. R. DiStefano, J. W. Hendricks, J. E. Pope, and other General Corrosion Group personnel.

The author wishes to express his appreciation to the Fabrication Group of the Metallurgy Division and in particular to H. Inouye of that group for supplying specially prepared test specimens and test containers of the refractory metals.

Thanks are due to the following groups and individuals whose contributions were essential to this work:

The Metallography Section of the Metallurgy Division and particularly E. H. Lee of that section.

The Spectrochemistry, Activation Analyses, and Special Analyses Groups of the Analytical Chemistry Division.

The X-Ray Diffraction Group of the Metallurgy Division.

The Graphic Arts Department and in particular W. C. Colwell of that department.

Louie Mae Pyatt of the Metallurgy Division Reports Office for the typing and preparation of the material for reproduction.

TABLE OF CONTENTS

CHAPTER		PAGE
I.	SUMMARY	1
II.	INTRODUCTION	4
III.	LIQUID METAL CORROSION	12
IV.	REVIEW OF THE LITERATURE	17
V.	OBJECTIVES	22
VI.	EXPERIMENTAL PROCEDURES AND MATERIALS	23
	Development of Procedures and Equipment	23
	Inert Atmosphere Chamber	24
	Static Corrosion Test Systems	27
	Dynamic Corrosion Test Systems	29
	Seesaw Furnace Tests	29
	Thermal Convection Loop Tests	34
	Stripping of Lithium from Test Components	42
	Basic Methods of Examination	43
	Specimens and Container Materials	43
	Test Materials	45
	Materials Tested in Lithium	45
	Preparation of Test Components	45
	Lithium	46
VII.	RESULTS AND DISCUSSION	49
	Static Test Results	49
	Two-Component Static Test Results	49
	Metals	49
	Columbium	55
	1. Initial Observations	56
	2. Effect of Welding Environment	62
	3. The Effects of Oxygen and Nitrogen	76
	Alloys	94
	1. Nickel- and Cobalt-Base Alloys	94
	2. Iron-Base Alloys	96
	Three-Component Static Test Results	110
	Metals	110
	Alloys	115
	1. Nickel- and Cobalt-Base Alloys	115
	2. Iron-Base Alloys	123
	3. Zirconium-Base Alloys	133
	4. Precious Metal-Base Alloys	133

CHAPTER PAGE

VII. (continued)

Cermets 136
Ceramics. 140
Seesaw Furnace Test Results 144
Metals. 144
Alloys. 147
Iron-Base Alloys. 147
1. Austenitic Stainless Steels 147
2. Ferritic Stainless Steel. 150
Nickel-Base Alloys. 158
Thermal Convection Loop Test Results. 159
Columbium 159
Alloys. 163
Nickel-Base Alloy (Inconel) 165
Iron-Base Alloys (Austenitic and Ferritic Stainless Steels). 166
1. Preliminary Tests with Type "A" Loops 166
2. Tests with Modified Types "A" and "B" Loops . 176
3. Chemical Analyses of Mass Transfer Deposits and Hot- and Cold-Leg Surfaces. . . 188
4. Summary of Austenitic and Ferritic Stainless Steel Thermal Convection Loop Results. . . . 193

VIII. CONCLUSIONS AND RECOMMENDATIONS 198
Conclusions 198
Recommendations 204

LIST OF REFERENCES 206

BIBLIOGRAPHY 214

APPENDIX I 218
Impurities in Lithium. 218
A. Sampling Techniques. 218
B. Analytical Methods for Determining Nitrogen and Oxygen in Lithium. 220
C. Purification Experiments 221
D. Solubility of Lithium Nitride and Lithium Oxide in Lithium 231

APPENDIX II. 235
Mechanical Property Studies on Type 316 Stainless Steel after Exposure to Lithium of Varying Purity. 235

APPENDICES REFERENCES. 239

LIST OF TABLES

TABLE		PAGE
I.	Comparison of the Heat Transfer Properties of Several Reactor Coolants at 1000°F (538°C). . . .	8
II.	Purity of Grade LC Lithium as Specified by the Manufacturer	47
III.	Results of Lithium Corrosion Tests on Metals in Two-Component Static Test Systems.	50
IV.	Lithium Concentration as a Function of Distance from Outside of Tube Wall in Columbium-Lithium Thermal-Convection Loop Tests.	61
V.	Effect of Oxygen and Nitrogen Additions on Weight Change of Columbium Specimens Exposed to Static Lithium at 1500°F (816°C) for 100 Hours.	77
VI.	Effect of Heat Treatment and Exposure to Lithium on the Hardness of Contaminated Columbium Weld Specimens.	82
VII.	Relative Thermodynamic Stabilities of Columbium Oxides and Columbium Nitride in Lithium.	90
VIII.	Results of Lithium Corrosion Tests on Eight Lots of Columbium Tubing.	92
IX.	Results of 100-Hour Lithium Corrosion Tests on Nickel-Base and Cobalt-Base Alloys in Two-Component Static Test Systems.	95
X.	Results of 100-Hour Lithium Corrosion Tests on Iron-Base Alloys in Two-Component Static Test Systems at 1500°F (816°C) and 1700°F (927°C)	97
XI.	Results of Lithium Corrosion Tests on Iron-Base Alloys in Two-Component Static Test Systems at 1832°F (1000°C)	98
XII.	Effect of Additions of Lithium Nitride to Lithium on the Corrosion Resistance of Type 316 Stainless Steel.	107

TABLE		PAGE
XIII.	Results of Lithium Corrosion Tests on Metals in Three-Component Static Test Systems	111
XIV.	Results of Lithium Corrosion Tests on Nickel-Base and Cobalt-Base Alloys in Three-Component Static Test Systems	119
XV.	Results of Lithium Corrosion Tests on Iron-Base Alloys in Three-Component Static Test Systems	124
XVI.	Carbon and Lithium Content of Turnings Machined from a 1035 Steel Specimen Following Exposure to Lithium for 100 Hours at 1500°F (816°C) in an Armco Iron Container	127
XVII.	Results of Lithium Corrosion Tests on Zirconium-Base Alloys in 100-Hour Three-Component Static Tests	134
XVIII.	Results of Lithium Corrosion Tests on Cermets in Three-Component Static Tests	137
XIX.	Results of Lithium Corrosion Tests on Various Refractory Metals in Seesaw Furnace Test Systems	145
XX.	Results of Lithium Corrosion Tests on Austenitic Stainless Steels in Seesaw Furnace Test Systems	148
XXI.	Results of Lithium Corrosion Tests on Type 446 Stainless Steel and Inconel in Seesaw Furnace Test Systems	152
XXII.	Results of Lithium Corrosion Tests on Columbium in Thermal Convection Loop Test Systems	160
XXIII.	Results of Lithium Corrosion Tests on Type 316 Stainless Steel in Thermal Convection Loop Test Systems	168
XXIV.	Results of Lithium Corrosion Tests on Types 321 and 347 Stainless Steel in Thermal Convection Loop Test Systems	169

TABLE PAGE

XXV. Results of Lithium Corrosion Tests on Types 430 and 446 Stainless Steel in Thermal Convection Loop Test Systems. 170

XXVI. Results of Lithium Corrosion Tests on Type 316 Stainless Steel in Thermal Convection Loop Test Systems 178

XXVII. Results of Lithium Corrosion Tests on Type 316 Stainless Steel in Thermal Convection Loop Test Systems 182

XXVIII. Comparison of Mass Transfer Crystal Analysis with the Before-Test Analysis of the Thermal Convection Loop Pipe. 191

XXIX. Summary of Analytical Results on Mass Transfer Crystals found in Fourteen Stainless Steel Thermal Convection Loop Tests 192

XXX. Chemical Analysis on 5- and 10-mil Cuts Machined from the Hot- and Cold-Leg Surfaces of Type 316 Stainless Steel Thermal Convection Loops 194

XXXI. Effect of Vacuum Distillation at 1202°F (650°C) on the Nitrogen and Oxygen Content of Lithium . . . 224

XXXII. Standard Free Energy Changes for Reactions between Li_3N and Various Metals 225

XXXIII. Results of Lithium Purification Experiment Utilizing Titanium Sheet as the Gettering Metal 228

XXXIV. Compositions of Yttrium Getter Specimens Before and After Exposure to Lithium Containing Nitrogen and Oxygen 230

LIST OF FIGURES

FIGURE		PAGE
1.	Some Important Physical Properties of Potential Reactor Coolants	6
2.	Temperature-Gradient Mass Transfer	14
3.	Dissimilar-Metal or Concentration-Gradient Mass Transfer	15
4.	Inert Atmosphere Chamber	25
5.	Inert-Gas Arc Welding of a Corrosion Test Container Partially Filled with Lithium	26
6.	Static Corrosion Test Systems	28
7.	Standard Corrosion Test Assembly Procedure	30
8.	Seesaw Furnace Test System	31
9.	Types of Seesaw Furnace Test Capsules	33
10.	Thermal-Convection Loop and Control Equipment	35
11.	Types of Thermal-Convection Loops	36
12.	Method of Testing Thermal-Convection Loops Made of Non-Oxidation Resistant Materials	37
13.	Thermal-Convection Loop Modifications	41
14.	Surfaces of Various Refractory Metals Following Exposure to Lithium	51
15.	Armco Iron Specimens Following Exposure to Lithium at the Indicated Temperatures	53
16.	Temperature-Composition Plot of the Ferrite-Austenite Equilibrium in the Iron-Carbon Diagram	54
17.	Saddle-Weld Area at Top of Hot Leg of Columbium Loop	57
18.	Weld Zone of Columbium Tube Wall from Hot Leg of Thermal-Convection Loop	58

FIGURE PAGE

19. Columbium Tube Wall from Hot Leg of Thermal Convection Loop. 59

20. Results of Dynamic Lithium Corrosion Test on Sintered Columbium Loop Containing Two-Inch Arc-Cast Columbium Insert. 63

21. Weld Zone of Columbium Tube Wall after Exposure to Lithium 64

22. The Effect of Welding Gas Purity on the Microhardness of Fusion-Welded Columbium Specimens Before and After Exposure to Lithium 66

23. Effect of Welding Environment on the Hardness and Lithium Corrosion Resistance of the Fusion-Weld Zone of Columbium Specimens 68

24. Fusion-Weld Zone of Columbium Specimen Welded in Argon + Air Before and After Exposure to Lithium. 69

25. Fusion-Weld Zone of Columbium Specimen Welded in Argon + Air and Exposed to Lithium. 70

26. The Effect of Welding Gas Purity on the Microhardness of Braze-Welded Columbium Specimens Before and After Exposure to Lithium 73

27. Columbium Braze-Welded in Argon + Air 74

28. Effect of Braze-Welding Environment on the Corrosion Resistance of Columbium to Lithium. 75

29. Solubility of Oxygen in Solid Columbium 78

30. Solid Solubility of Nitrogen in Columbium 79

31. Columbium Weld Specimens Following Exposure to Lithium for 100 hr at 1500°F (816°C). 81

32. Weld Zones of Columbium Specimens to which 0.134% N_2 was Added Prior to Welding. 84

33. Weld Zones of Columbium Specimens to which 0.527% O_2 was Added Prior to Welding. 85

FIGURE PAGE

34. Weld Zones of Columbium Specimens Following Exposure to Lithium. 86

35. Fusion-Weld Zones of Columbium Specimens to which Varying Amounts of Oxygen were Added Prior to Welding . . . 87

36. Grain-Boundary Corrosion Products in Weld Zone of Columbium Specimen to which 0.527% Oxygen was Added Prior to Welding. 88

37. Outside and Inside of Tube Wall of Columbium Specimen Following Exposure to Lithium (Both Sides Exposed to Lithium). 93

38. Type 316 Stainless Steel Specimen Following Exposure to Lithium. 99

39. Fe-Ni-Cr Crystals Deposited on a 316 Stainless Steel Specimen During a Static Test in Molten Lithium 101

40. Type 310 Stainless Steel Specimen Following Exposure to Lithium. 102

41. Type 446 Stainless Steel-Lithium "Solubility" Experiment. 104

42. Type 446 Stainless Steel Specimen Following Exposure to Lithium. 105

43. Effect of Additions of Lithium Nitride to Lithium on the Corrosion Resistance of Type 316 Stainless Steel 108

44. Effect of Container Material on the Corrosion Resistance of Beryllium Specimens Exposed to Lithium 112

45. Wall of an Iron Container in which a Beryllium Specimen was Exposed to Lithium 113

46. Cobalt and Nickel Following Exposure to Lithium 114

47. Rhenium Following Exposure to Lithium 116

48. (a) End of Yttrium Specimen which had been "Etched" During Exposure to Lithium in a Columbium Container. (b) Photomicrograph of Exposed Yttrium Surface. 117

FIGURE PAGE

49. Armco Iron Capsule Containing Zirconium Specimen Following Exposure to Lithium. 118

50. Type 316 Stainless Steel Brazed T-Joint Prepared by Placing a Controlled Quantity of Brazing Alloy at One End and Heating to the Flow Point in a Dry-Hydrogen Atmosphere. 121

51. T-Joints Brazed with Nicrobraz (70Ni–14Cr–6Fe–5B–4Si–1C) Following Exposure to Lithium. 122

52. 1035 Steel Specimen Following Exposure to Lithium in an Armco Iron Capsule. 125

53. Alfenol (84Fe–16Al) Specimen Following 100-Hour Exposure to Lithium at 1500°F (816°C). 128

54. Effect of Dissimilar-Metal Container on the Extent of Attack Observed on Type 316 Stainless Steel Exposed to Lithium. 130

55. Preferential Leaching by Lithium of Nickel and Chromium from an Austenitic Stainless Steel. 131

56. Chemical Compositions of Turnings Machined in Ten-Mil Increments from the Surface of a Type 316 Stainless Steel Specimen Following Exposure to Lithium. 132

57. Surfaces of Two Zirconium-Base Alloys Following Exposure to Lithium. 135

58. Cross Sections of Cermet Specimens Following Exposure to Lithium. 138

59. Region A Shown in Figure 58 Illustrating the Leaching Action of Lithium on the Nickel-Rich Binder Phase (White) Surrounding the Angular Carbide Particles (Gray). 139

60. Lithium, Sodium, and Lead Media for 100 Hours at 1500°F (816°C). 141

61. Titanium Carbide (TiC), (97.4% of Theoretical Density), (a) Before and (b) Following Exposure to Lithium in an Iron Container. 142

FIGURE PAGE

62. Cold- and Hot-Zone Specimens from Molybdenum Seesaw Capsule Following Exposure to Lithium. 146

63. Type 316 Stainless Steel Seesaw Test Capsules Following Exposure to Lithium. 149

64. Hot-Zone Sections from Type 316 Stainless Steel Seesaw Capsules Following Exposure to Lithium 151

65. Cold-Zone Sections from Type 446 Stainless Steel Seesaw Capsules Following Exposure to Lithium 153

66. Hot-Zone Wall of Type 446 Stainless Steel Seesaw Test Capsule. 155

67. Hot-Zone Wall of Type 446 Stainless Steel Seesaw Test Capsule. 156

68. Cold-Zone Wall of Type 446 Stainless Steel Seesaw Test Capsule. 157

69. Columbium Saddle Joint Braze Welded with 85Zr-15Cb (Weight Per Cent) Alloy Following Exposure to Lithium. . . 162

70. (a) Low Magnification View of the Longitudinal Weld Zone in the Hot Leg of Columbium Thermal Convection Loop No. 58 which leaked During Test. (b) High Magnification View of Tube Wall Showing Path of Lithium Penetration. . . 164

71. (a) Hot-Leg and (b) Cold-Leg Sections from Inconel Loop Following Exposure to Lithium. 167

72. (a) Hot- and Cold-Leg Sections from Thermal Convection-Loop Test. (b) Enlarged View of Mass-Transfer Crystals. . 172

73. Hot- and Cold-Leg Sections from a Type 347 Stainless Steel Thermal Convection Loop (No. 12) Following Exposure to Lithium for 3000 Hours. 173

74. Cold Leg Surface of Type 316 Stainless Steel Loop (No. 1) Following Exposure to Lithium. 175

75. Effect of Hot-Leg Temperature in Type 316 Stainless Steel-Lithium Thermal Convection Loop System on the Rate of Removal of Metal from a Specimen Suspended in the Hot Leg. 180

FIGURE PAGE

76. The Effect of Temperature on the Corrosion of the Hot Legs of Type 316 Stainless Steel Thermal Convection Loops by Lithium. 183

77. Weight-Loss Specimen from the Hot Leg of Type 316 Stainless Steel Loop No. 21 Following Exposure to Lithium . 184

78. Effect of Nitrogen Addition to Lithium on the Corrosion in the Hot Leg of a Type 316 Stainless Steel Loop 187

79. Radiograph of the Bottom of the Cold Leg of a Type 316 Stainless Steel Thermal Convection Loop (No. 22) which Plugged after 96 hours of Operation 189

80. Corrosion Resistance of Various Metals and Alloys in Molten Lithium. 199

81. Lithium Sampling Procedure. 219

82. Lithium Distillation System 223

83. Standard Free Energy Changes for Lithium Oxide Reduction Reactions 227

84. Surface of Titanium Gettering Specimen Before and Following Exposure to Lithium 229

85. Sampler Used in Li_3N and Li_2O Solubility Studies. 232

86. Solubility of Lithium Oxide in Lithium. 234

87. The Effect of Adding Li_2O and Li_3N to Lithium on the Corrosion Resistance of Type 316 Stainless Steel. 236

88. Type 316 Stainless Steel Specimens Tested in Tension at Room Temperature Following Treatments Indicated. 238

CHAPTER I

SUMMARY

The purpose of this investigation was to determine the corrosion resistance of various materials to lithium in the temperature range 1000 to 1832°F (538 to 1000°C) in both static and dynamic systems. Evaluation of test results was based primarily on metallographic examination, weight-change data, dimensional changes, and chemical analyses.

The static tests were conducted in constant temperature systems in the range 1500 to 1900°F (816 to 1038°C) for time periods of 100 to 400 hours. Pure metals, alloys, cermets, and ceramics were included in the studies. The following materials exhibited good corrosion resistance in static systems: beryllium, chromium, cobalt, columbium, iron, molybdenum, rhenium, tantalum, titanium, tungsten, vanadium, zirconium; cobalt-, iron-, and zirconium-base alloys; cobalt-bonded tungsten carbide cermets and the ceramic carbides of chromium, titanium, and zirconium.

Materials which showed promise in static tests and which were available in the form of tubing or pipe were tested in dynamic systems containing temperature gradients. Lithium flow velocities of one-to-eight feet per minute and temperature differences of 100 to 600 Fahrenheit degrees (56 to 333 Centigrade degrees) between hot and cold sections were used. Hot-zone temperatures ranged from 1000 to 1900°F (538 to 1038°C), and test periods varied between

100 and 3000 hours. Inconel, stainless steels, columbium, molybdenum, vanadium, and zirconium were the materials studied. All but Inconel and the stainless steels were found to be satisfactory at hot-zone temperatures of at least 1500°F (816°C).

Columbium and the stainless steels were investigated extensively in this corrosion study. Columbium was observed to undergo a type of intergranular corrosion attack in preliminary static and dynamic tests. This type of attack was found to be particularly severe in and near weld zones. A systematic investigation revealed that the attack was due primarily to contamination of the metal by oxygen. Subsequent tests showed that columbium containing less than 100 ppm oxygen was completely resistant to attack in static systems at temperatures as high as 1800°F (982°C) and in dynamic systems at temperatures as high as 1600°F (871°C) and for time periods up to 300 hours.

The austenitic and ferritic stainless steels containing less than 0.12 weight per cent carbon normally exhibited good corrosion resistance in static systems. Occasionally, intergranular penetration was observed in both static and dynamic tests with austenitic stainless steels. This type of attack was found to be particularly severe under the combined circumstances of high-nitrogen content lithium and precipitated grain-boundary carbides. The high carbon ferritic stainless steels, such as type 446, always exhibited excessive grain-boundary attack. Both the ferritic and austenitic stainless steels exhibited temperature-gradient mass transfer in flowing, non-isothermal systems at hot-leg temperatures of 1300°F (704°C) and above. In thermal

convection loops, lithium flow velocity was found to have a major influence on the rate of mass transfer in the range of velocities studied in this investigation. An analysis of the data indicated that this effect was primarily attributable to the velocity dependence of liquid diffusion in the hot leg.

In order to determine the effects of nitrogen and oxygen contamination of lithium on its corrosiveness, sampling techniques and methods of purifying lithium were developed. The solubilities of lithium oxide and lithium nitride in molten lithium were also determined.

CHAPTER II

INTRODUCTION

For several years nuclear power reactor engineers have shown an interest in liquid metals as heat transfer media. This interest is due primarily to the need for effective accommodation of the extremely high heat fluxes available in certain types of nuclear reactors. The removal of very large quantities of heat from a reactor of relatively small volume can be accomplished only through the combined physical and heat transfer properties of certain liquid metals.

The properties desired in a nuclear reactor coolant are: (1) low neutron absorption cross section (for thermal* reactors), (2) low melting point, (3) high boiling point, (4) low vapor pressure at high temperatures, (5) low density, (6) high heat capacity, (7) high thermal conductivity, and (8) low viscosity.

Of all the liquid metals, two of the alkali metals, lithium and sodium, come closest to meeting the property requirements listed above. Of these elements, lithium-7 (the most abundant isotope of lithium) is definitely superior from an over-all point of view.

---

*Nuclear reactors are usually classified as thermal, intermediate, or fast, according to the velocity of the neutrons used to sustain the fission reaction.

It is of interest to note that the results of a study, conducted as early as 1949,[1] indicated that lithium-7 was the most attractive liquid metal coolant for nuclear reactors for use in ships, airplanes, submarines, and in other applications where the space allotted for the reactor and its auxiliary cooling equipment is limited. The need for the development of lithium-7 for use in mobile reactor systems is even more apparent today.

Several pertinent physical properties of lithium and other potential reactor coolants are represented graphically in Figure 1. Certain ranges on each plot in Figure 1 are designated as "undesirable areas." For example, a range of temperatures corresponding to high melting points or low boiling points is indicated as undesirable in the first plot. The temperature range over which a proposed coolant exists as a liquid at normal pressures is important for two reasons: (1) a coolant which has a melting point substantially higher than room temperature would necessitate cumbersome preheating of the system during reactor start-up, and (2) low boiling point coolants would have to be contained in a pressurized system if the reactor were to operate at temperatures high enough to produce steam suitable for efficient utilization of modern power plant equipment.

The superiority of lithium as a reactor coolant is evident from the following considerations (Figure 1):

1. Lithium has a liquid temperature range greater than any of the other alkali metals and could be used at temperatures as high as 1300°C at near atmospheric pressure.

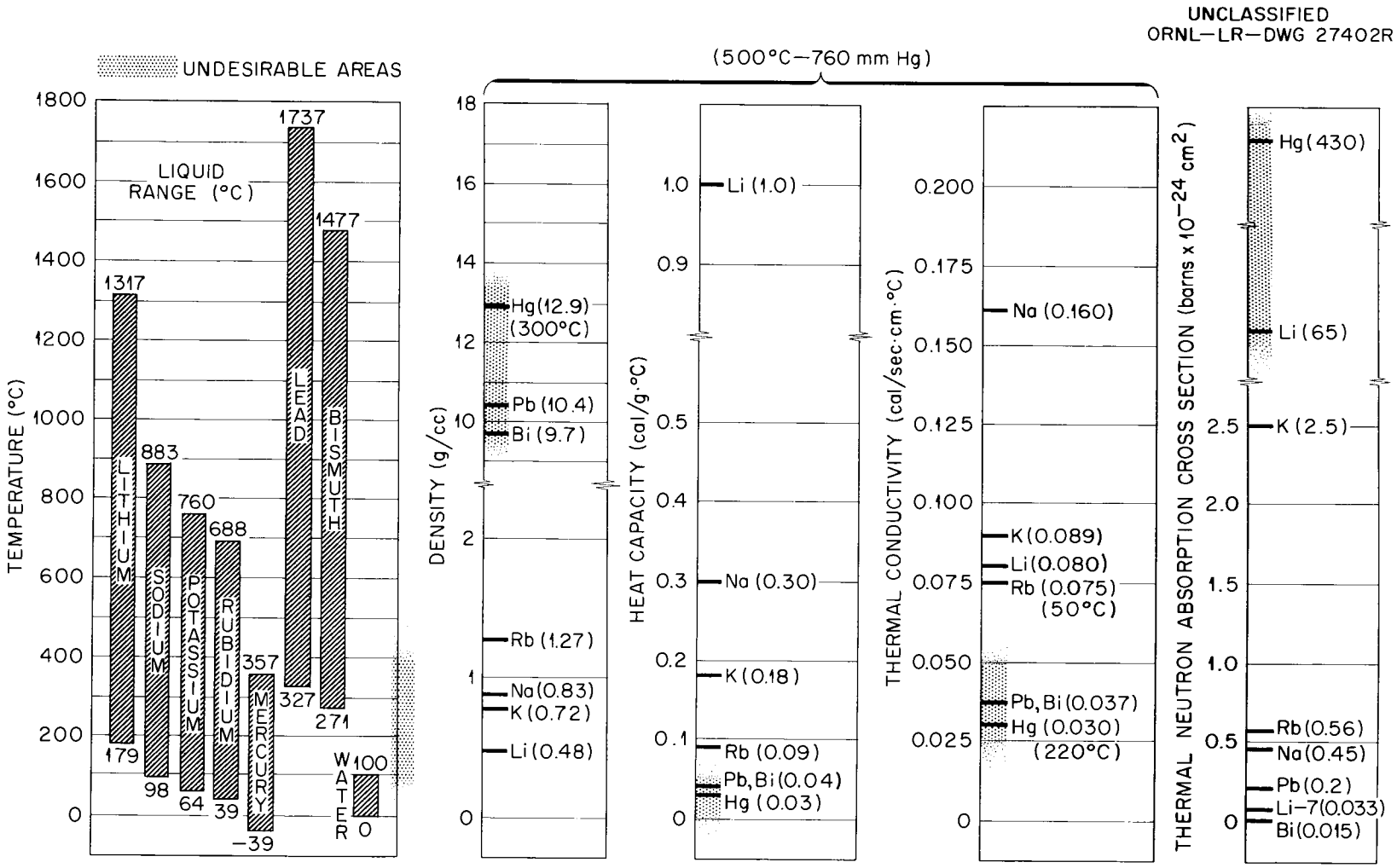

Figure 1. Some Important Physical Properties of Potential Reactor Coolants.

2. Lithium has the lowest density of the materials considered.

3. The heat capacity of lithium is the largest of the potential coolants, being greater than that of sodium, the second best in this category, by a factor of more than three.

4. The thermal conductivity of lithium is below that of sodium and potassium, but it is higher than most of the potential liquid-metal coolants.

5. The high thermal neutron absorption cross section of 65 barns[Ref. 2] prohibits the use of naturally occurring lithium as a primary coolant in a thermal reactor. This difficulty may be overcome, however, by isotopic separation of the lithium-7 isotope from naturally occurring lithium, which contains 7.5 per cent lithium-6. The thermal neutron absorption cross sections of these isotopes are 0.033 and 945 barns,[Ref. 2] respectively.

A comparison of the heat transfer properties of several potential reactor coolants (Table I[3]) shows that while both lithium and sodium are superior in regard to heat transfer coefficient, lithium is by far more favorable from the standpoint of pumping power requirements under the conditions specified.

Using the properties cited in Figure 1 and Table I as a basis, it is clear that lithium-7 and sodium are the most attractive potential reactor coolants. Since the relative merits of lithium-7 and sodium are frequently discussed in connection with mobile reactors where minimum weight is a primary consideration, it is of interest to

TABLE I

COMPARISON OF THE HEAT TRANSFER PROPERTIES OF SEVERAL REACTOR COOLANTS AT 1000°F (538°C)

Coolant	Pressure (Psia)	Heat Transfer Coefficient[a] (Btu/Hr-Ft^2-°F)	Pumping Power For Equivalent Heat Removal[b] For °F Temperature Rise
Lithium	14.7	13,900	3.41
Sodium	14.7	13,200	34.0
56 Sodium-44 Potassium	14.7	7,400	63.4
55.5 Bismuth-44.5 Lead (Eutectic Alloy)	14.7	8,120	133.0
Water (500°F)	1500	6,030	0.67

[a]Determined for a velocity of 20 feet per second in a 1/2-inch inside diameter tube.

[b]Normalized to a value for water at 100°F and 14.7 psia with a velocity of 20 feet per second in a 1/2-inch inside diameter, 10-feet long tube.

compare these metals from the standpoint of nuclear characteristics which affect reactor shielding requirements.

According to the analysis of Goldstein,[4] a mobile reactor system using lithium-7 as the coolant would, in principle, require a smaller primary shield and, therefore, would be preferred to one using sodium. Lithium-7, upon neutron capture, forms lithium-8 which is a weak beta emitter with a half-life of 0.841 second.(Ref. 2) Only neutrons and gamma rays pose any difficulty in shielding. Thus, it appears that the heat exchanger in a lithium system could be positioned outside of the primary reactor shield. Gamma-ray production due to attenuation of beta rays by structural materials containing elements of high atomic number is not regarded as a serious problem. On the other hand, sodium-23 (natural abundance, 100 per cent) when activated by neutron capture converts to sodium-24, which is a strong gamma emitter with a half-life of 15.0 hour.(Ref 2) The heat exchanger in a sodium-cooled system, therefore, would have to be contained within the primary shield which would have to be larger and heavier than the shield for a lithium-cooled system. Sodium presents the additional disadvantage of requiring several days waiting time for decay of gamma activity to a level which would permit access to the heat exchanger area by reactor personnel.

There have appeared within the last several years numerous proposed applications which indicate to some extent the interest in

lithium as a nuclear reactor coolant. Several of these proposals are listed below:

1. A lithium-7 cooled nuclear power reactor using columbium as the container metal and employing a maximum temperature of 1650°F (899°C).[5]

2. A fast-neutron aircraft reactor, proposed in the USSR, involving the circulation of lithium in a nickel-base alloy system at temperatures as high as 1742°F (950°C).[6]

3. A hypothetical space vehicle in which lithium is used as the primary coolant. The lithium is passed through a heat exchanger where liquid sodium is vaporized and used to drive a turbine which in turn provides the electricity for operation of either an ion accelerator or a plasma accelerator.[7]

4. A controlled thermonuclear device using lithium both as a heat transfer fluid and a tritium-producing blanket. The lithium would be circulated at temperatures in the range of 1000 to 1830°F (538 to 1000°C).[8]

Despite the wide-scale interest in lithium as a heat transfer fluid at temperatures in excess of 1000°F (538°C) not a single engineering system employing lithium at these temperatures is known to be in operation at the present time. The use of lithium at elevated temperatures in such systems must await the solution of two major problems. The first relates only to the application of lithium in thermal neutron reactors, while the second is common to all high-temperature systems involving lithium.

The first of these problems is concerned with the economical separation of the undesirable lithium-6 isotope from the lithium-7 isotope. Recent information[9,10] indicates that a solution to the lithium-7 isotopic separation problem is imminent. A production run of 99.99 per cent lithium-7 is scheduled to begin on February 1, 1959, and a cost estimate of forty-five dollars per pound is given.

The second major problem deals with the severe corrosion encountered in high-temperature systems containing liquid lithium. The research reported here is concerned with this problem.

CHAPTER III

LIQUID METAL CORROSION

There are many corrosion mechanisms possible in liquid-metal–solid-metal systems. In addition, the results observed in any one corrosion experiment may be influenced by a large number of possible test variables, some of which are not consistently controllable. It is the purpose of this section to present a brief discussion of the types of liquid-metal corrosion and the factors which affect corrosion by liquid metals.

The principal types of liquid-metal corrosion are:[11,12] (1) simple solution, (2) alloying between liquid metal and solid metal, (3) intergranular penetration, (4) impurity reactions, (5) temperature-gradient mass transfer, and (6) dissimilar-metal or concentration-gradient mass transfer.

Solution of a solid container material in a liquid metal and alloying between the liquid and solid metal are the simplest forms of liquid-metal corrosion. The amount of corrosion due to these phenomena could readily be predicted if adequate phase-diagram information were always available. Static, isothermal tests are usually adequate for determining the extent of solution and alloying.

Intergranular penetration of a container material occurs as a result of preferential attack on a constituent of the metal which segregates in the grain boundaries.

Impurities in either the liquid metal or the container material can affect the nature and the extent of the corrosion observed.

The two most troublesome forms of liquid-metal corrosion are temperature-gradient mass transfer and dissimilar-metal mass transfer. These corrosion phenomena are very often difficult to observe in a simple static test. In some cases, they may be detected only after a flow system containing temperature gradients has been operated for an extended time period.

The mechanism of temperature-gradient mass transfer is illustrated in Figure 2.[13] This type of corrosion may be studied in a thermal-convection loop, as shown schematically in Figure 2. Since the solubility of most container materials in a particular liquid metal is temperature dependent, solution in the hot section and subsequent deposition in a cooler section may occur and the system eventually will become plugged.

Dissimilar-metal or concentration-gradient mass transfer (Figure 3) can occur in solid-metal—liquid-metal systems in the absence of temperature gradients. Where two or more solid metals are in contact with the same liquid metal, the liquid metal may act as a carrier in transferring atoms of one of the solid metals to the surface of the other solid metal. Such alloying would, in most cases, have an adverse effect on the mechanical properties of the dissimilar metals and, in some cases, might even cause plugging of small tubes.

The principal factors affecting liquid-metal corrosion are: (1) temperature, (2) temperature gradient, (3) cyclic temperature

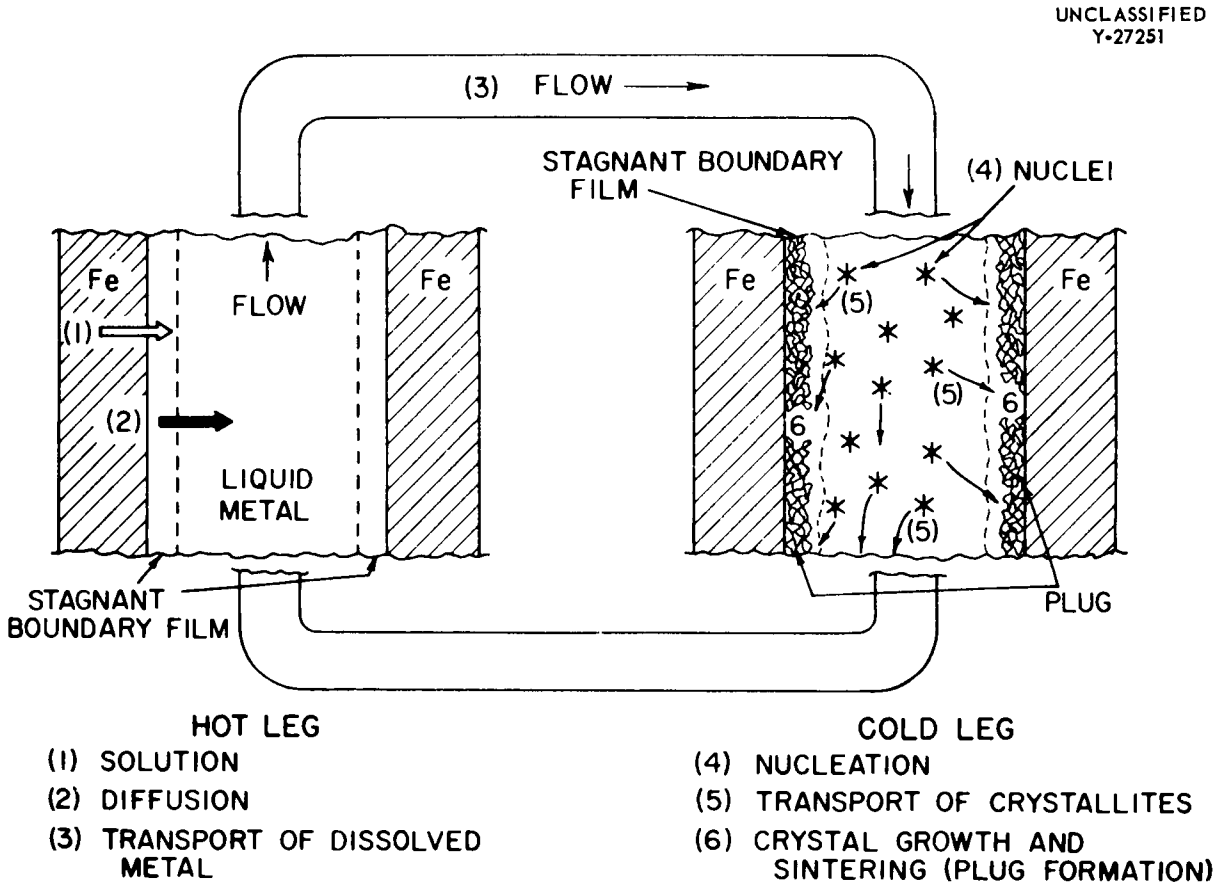

Figure 2. Temperature-Gradient Mass Transfer.

UNCLASSIFIED
ORNL-LR-DWG 5612

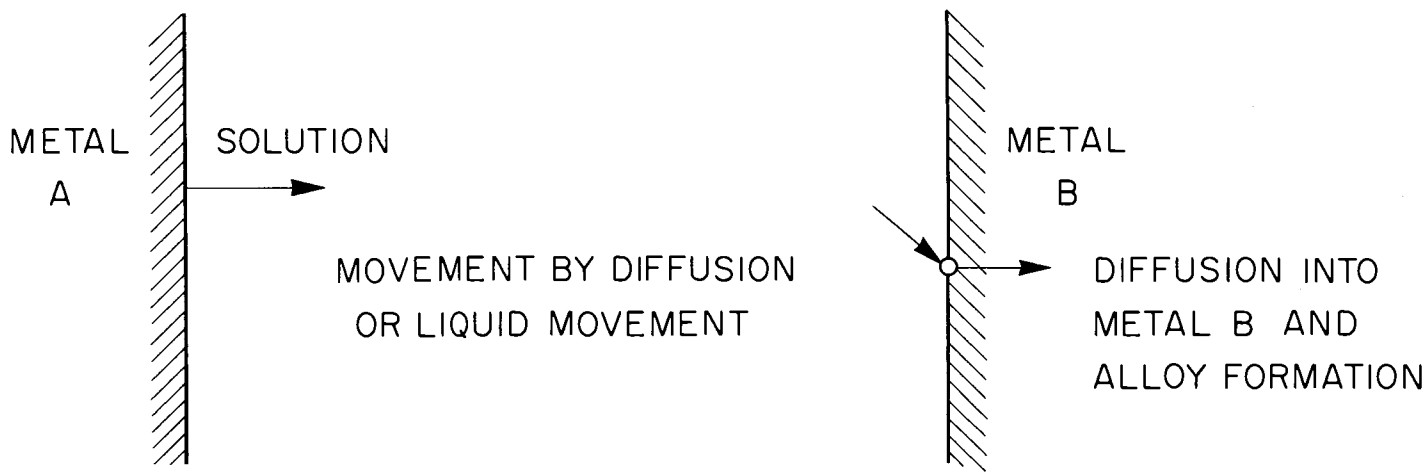

Figure 3. Dissimilar-Metal or Concentration-Gradient Mass Transfer.

fluctuation, (4) ratio of container material area-to-coolant volume, (5) purity of liquid metal, (6) flow velocity, (7) surface condition of container material, (8) two or more materials in contact with liquid metal, and (9) physical metallurgical condition of container material. Generally speaking, these variables are listed in order of decreasing importance. The relative importance of these factors might change, depending on the liquid metal and the container system under consideration.

CHAPTER IV

REVIEW OF THE LITERATURE

Very little information regarding the compatibility of lithium with materials at elevated temperatures existed prior to 1949 when Burton, et al.,[14] in a comprehensive review paper on lithium, presented a qualitative evaluation of container materials based on observations during physical property studies. This evaluation, which was limited for the most part to temperatures less than 1112°F (600°C), showed pure iron to be preferable to stainless steels.

The results of a corrosion screening program were reported by the U. S. Naval Ordnance Test Station, Inyokern, California, in 1950.[15] Various metals and alloys were exposed to static lithium at 600°F (316°C) and 900°F (482°C) for 72 hours. The effect of the exposure to lithium on the tensile properties of the test materials was also reported. The austenitic stainless steels were found to have good corrosion resistance and showed no change in tensile properties.

A total of twenty-six different materials, including six Stellite alloys, four Hastelloy alloys, and several cobalt- and nickel-bonded titanium carbide cermets, were tested in static lithium at 842°F (450°C) for 100 hours by Edler.[16] It was concluded that the metals which best withstood corrosion were Kennametal K151A, Stellite No. 6, and Stellite Star J Metal.

Five metals and seven alloys were tested in static lithium for 144 hours at 572°F (300°C) and 1112°F (600°C) by Wilkinson and

Yaggee.[17,18] Iron, beryllium, thorium, uranium, and the stainless steels were reported to have good corrosion resistance.

A comprehensive program to determine the corrosion behavior of lithium at elevated temperatures was conducted by the NEPA Project and the Babcock and Wilcox Company during the years 1950 – 1952. The findings may be summarized as follows:

1. Solubility of Metallic Elements in Lithium.[19] Twelve metals having melting points above 2300°F (1260°C) were investigated in the temperature range of 900° to 1850°F (482° to 1010°C) for periods of 4, 24, and 100 hours in lithium. Molybdenum, vanadium, and zirconium were reported to have solubilities of less than 250 ppm in lithium at 1800°F (982°C).

2. Materials Tested in Lithium.[20] Tests were conducted in agitated and unagitated capsules at temperatures from 900° to 2200°F (482° to 1204°C) for times of 5 to 200 hours. Materials studied were molybdenum, tantalum, columbium, titanium, zirconium, nickel, iron, stainless steel types 304, 309, 310, 316, 321, 347, and 446, Inconel, L-605 (Haynes Alloy No. 25), cemented carbides, and ceramics, including oxides, nitrides, carbides, and graphite. Molybdenum appeared to be least affected of all the materials investigated.

3. Constant Temperature – Forced-Circulation Lithium Loops.[21] Seven essentially constant temperature, forced-circulation lithium loops made of type 310 stainless steel were operated at temperatures ranging from 960°F (516°C) to 1600°F (871°C) and at velocities up to 55 feet per second. Heavy metallic mass transfer deposits were

detected in loops operated at temperatures in excess of 1400°F (760°C) for time periods of 500 to 1000 hours. The maximum temperature difference in these systems was 40°F.

4. Non-isothermal Forced-Circulation Lithium Loops.[22] Four type 310 stainless steel loops were operated at hot- and cold-leg temperatures of 1350°F (732°C) and 850°F (454°C), respectively, and lithium velocities of 8 to 10 feet per second. The loops were plugged with nickel-rich mass transfer crystals in time periods ranging from 23 to 53 hours. Stainless steel specimens in the hot leg were corroded at a rate of 38 $mg/cm^2/100$ hours.

The static corrosion resistance of metallic materials to high-temperature lithium in iron containers was investigated by Cunningham.[23,24] Tests were conducted on pure metals and numerous high-temperature alloys at 1112°F (600°C), 1472°F (800°C), and 1832°F (1000°C) for times of 4, 40, and 400 hours. Based on weight changes and metallographic examinations, Armco iron, columbium, tantalum, zirconium, uranium, and titanium were reported to have good corrosion resistance.

Much of lithium corrosion data reported prior to 1952 were summarized in the Liquid-Metals Handbook issued in June, 1952.[25]

A study by Parkinson[26] of the effect of alpha-particle irradiation on the corrosion resistance of iron to lithium at 1670°F (910°C) indicated that corrosion was no greater than that previously reported without irradiation.

The results of a study of the corrosion resistance of type 316 stainless steel to distilled lithium circulated in thermal-convection loops at hot- and cold-leg temperatures of 1600°F (871°C) and 1100°F (593°C), respectively, were reported by McKee.[27] The effect of nitrogen in the lithium was investigated and it was concluded that "The corrosiveness of lithium cannot be blamed on its nitrogen content."

Recent experiments have been conducted by Minushkin[28] to determine the solution rate of metals in distilled lithium by gravimetric techniques. Austenitic stainless steel specimens were found to dissolve in lithium at 1600°F (871°C) at an initially high rate of 3.0 mg/in.^{2}-hour due to preferential leaching of nickel. The solution rate of molybdenum in lithium at 1600°F (871°C) was found to be less than 0.1 mg/in.^{2}-hour.

An extensive study of the corrosiveness of lithium at elevated temperatures under a variety of test conditions has been underway at Pratt and Whitney Aircraft[29 – 41] since April, 1955. Iron- and nickel-base alloys, refractory metals, and ceramics have been studied in static and dynamic tests. Most of the tests have been on the austenitic stainless steels, columbium, and columbium-base alloys in dynamic systems. The stainless steels have been found to suffer extensive temperature-gradient mass transfer, while columbium and columbium-base alloys have generally exhibited good corrosion resistance at temperatures up to 1600°F (871°C) for time periods up to 250 hours in flowing, non-isothermal test systems.

A list of 222 references pertaining to corrosion by molten lithium and related subjects was compiled for use in connection with a Lithium Symposium held in August, 1957.[42]

CHAPTER V

OBJECTIVES

The general objective of this investigation was the determination of the corrosion resistance of various materials to lithium in the temperature range 1000°F (538°C) to 1830°F (1000°C).

The specific objectives may be summarized briefly as follows:

1. To determine the corrosion resistance of various materials to lithium under static, constant temperature conditions.

2. To determine the corrosion resistance of those materials having relatively good resistance to static, isothermal lithium in flow systems containing temperature gradients.

3. To determine the temperature limitations of systems using the most promising commercially available structural materials, such as the stainless steels, in flow systems containing temperature gradients.

4. To investigate the effect of alloying elements in conventional structural materials on the corrosion resistance of these materials to lithium at elevated temperatures.

5. To determine the effect of non-metallic impurities, such as oxygen, nitrogen, and carbon, in lithium on the corrosive properties of lithium in systems involving conventional structural materials.

CHAPTER VI

EXPERIMENTAL PROCEDURES AND MATERIALS

Development of Procedures and Equipment

The procedures and equipment used to test the corrosion resistance of pure metals, alloys, cermets, and ceramics in molten lithium were based on corrosion testing techniques developed in studies with lithium and other liquid metals and fused salts over a period of ten years.[43,44,45,46]

Two basic types of tests were used: static and dynamic. In static tests, the test assembly was maintained in a stationary position at a controlled constant temperature. In dynamic tests, on the other hand, controlled temperature differences were maintained within the system, and flow of molten lithium relative to the test material was effected either by rocking the test assembly in a seesaw fashion or by thermal convection currents in a closed loop.[47,48]

Static systems were used primarily to determine whether potential structural materials held any promise of resisting attack in the more severe dynamic tests, where the conditions more nearly simulated those which would exist in a lithium-cooled nuclear reactor system. Static tests were used also for systematic studies of those aspects of corrosion mechanisms not related to flow or to temperature gradients. The static systems were not only cheaper and easier to

fabricate than dynamic systems but also provided for closer control of important test variables.

It should be noted that the dynamic tests used in this investigation were capable of producing lithium flow rates in the range of one to ten feet per minute, whereas actual heat transfer systems using liquid metal coolants are designed to operate at flow rates of ten to forty feet per second. From the standpoint of expense and operational difficulties, however, high-velocity flow systems requiring mechanical or electromagnetic pumps are not suitable for use in a liquid metal corrosion testing program designed to evaluate a variety of potentially useful materials.

Inert Atmosphere Chamber

Lithium metal used in this investigation was handled either under vacuum or in an inert gas atmosphere at all times. The stainless steel, inert atmosphere chamber shown in Figure 4 was used for (1) opening gas-tight containers or lithium, (2) melting and casting of lithium, (3) loading of corrosion test assemblies, and (4) welding of test assemblies made of metals such as molybdenum and beryllium which are sensitive to contamination during welding by even trace amounts of oxygen and nitrogen. A typical welding operation is illustrated in Figure 5.

Prior to conducting any of the operations above, the stainless steel chamber with a plexiglas dome was first evacuated to a pressure of one micron of mercury or less. The leak rate of the chamber was

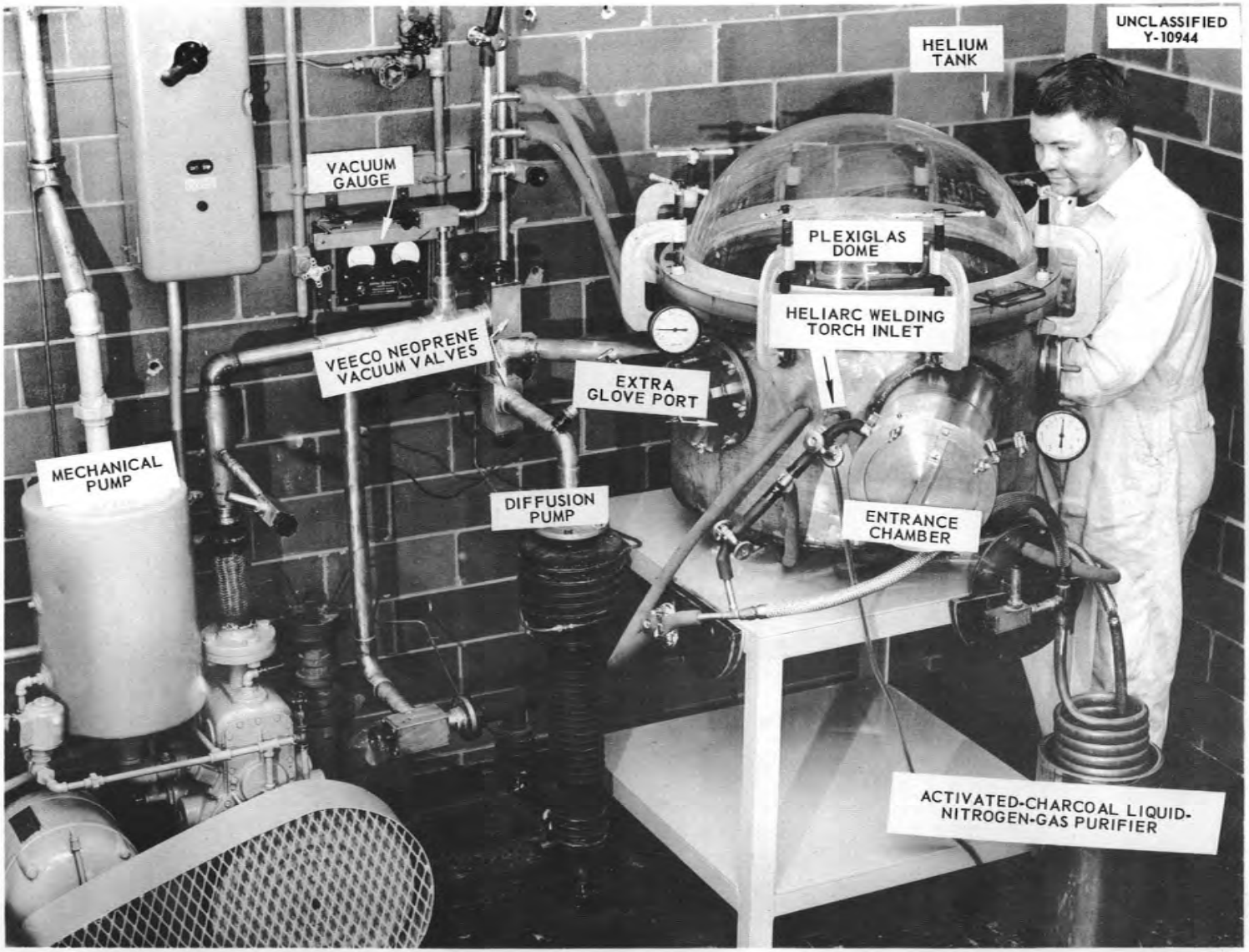

Figure 4. Inert Atmosphere Chamber.

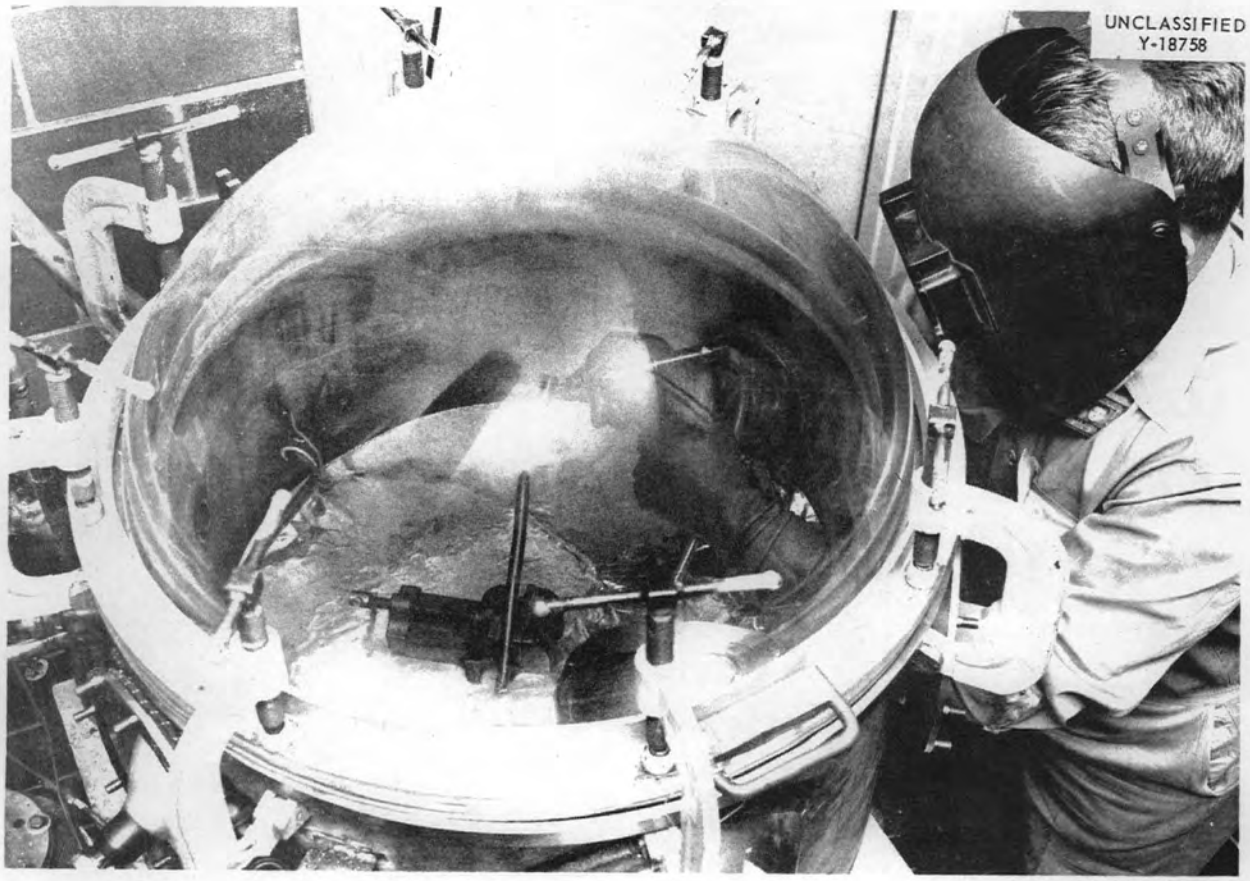

Figure 5. Inert-Gas Arc Welding of a Corrosion Test Container Partially Filled with Lithium.

checked periodically and was never greater than four microns of mercury per hour. Following evacuation, the system was brought to atmospheric pressure by filling with argon. Each tank of argon was analyzed prior to use and only the tanks which contained less than 10 ppm oxygen and less than 50 ppm nitrogen were used. With gas of this purity level the following observations were made: (1) it was possible to maintain a mirror-like surface on such reactive metals as sodium and potassium during melting and casting operations, (2) bare tungsten filaments of 100-watt light bulbs operating across 110 volts lasted as long as three hours, and (3) contamination of melted and cast lithium was not detectable by chemical analyses.

Static Corrosion Test Systems

The two types of static corrosion test systems used are illustrated in Figure 6. Two-component systems of the type shown in Figure 6a were used in most of the static tests. The specimens for this test were prepared from a flattened section of the tube wall when this was possible.

Three-component static test systems such as the one illustrated in Figure 6b were employed for either of the following two reasons: (1) it was desired to evaluate the corrosive effects of lithium on two different materials* in contact with a common lithium test bath, or (2) no container made of the material to be evaluated was available.

*For reactor design considerations it is often desirable to place more than one material in contact with the reactor coolant.

UNCLASSIFIED
ORNL-LR-DWG 33531R

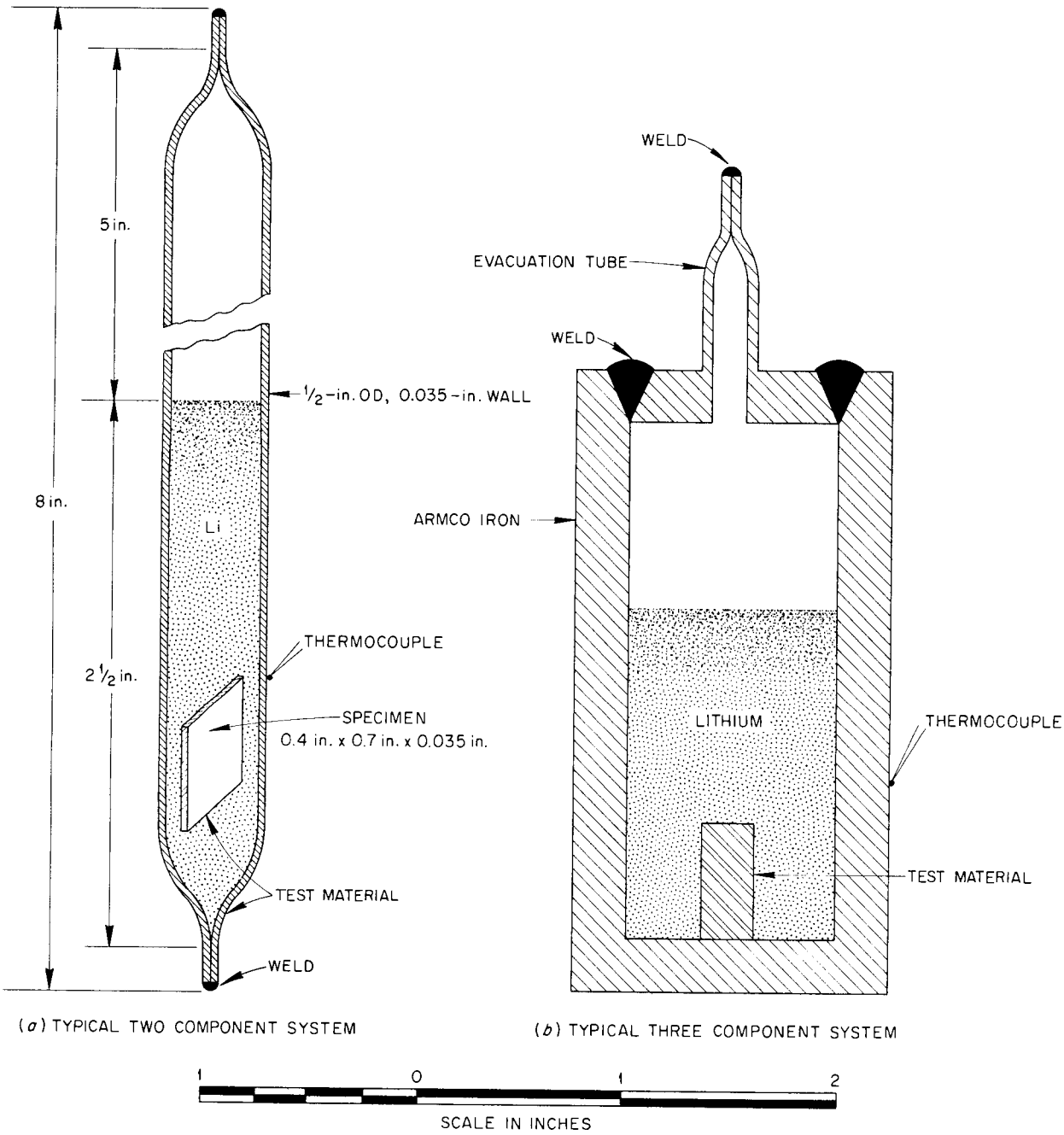

Figure 6. Static Corrosion Test Systems.

In the latter case, the most inert container available (generally pure iron or columbium) was used.

The standard corrosion test assembly procedure used for both static and seesaw test systems is outlined in stepwise fashion in Figure 7. It should be noted that the entire loading and sealing operation could be carried out inside the inert atmosphere chamber. Test capsules of metals or alloys which did not possess adequate oxidation resistance at the desired test temperature were placed in stainless steel containers prior to testing.

Chromel-alumel thermocouples were attached to the test capsule by spot welding, when possible, as shown in Figure 6. The temperature was controlled by Brown Pyr-o-vane type controllers and was recorded on multipoint recorders. The maximum temperature variation was ± 18°F (10°C).

Several types of commercially available electric furnaces were used in the static testing program.

Dynamic Corrosion Test Systems

Seesaw Furnace Tests.* The essential components of the seesaw furnace test system are shown in Figure 8. Figure 8a is a photograph of the six-furnace test rack including the control panel. The configuration of a test system in a single seesaw furnace, the relative movement of the components, and the location of hot and cold zones of

*Often referred to as "tilting" furnace tests.

UNCLASSIFIED
ORNL-LR-DWG 18341

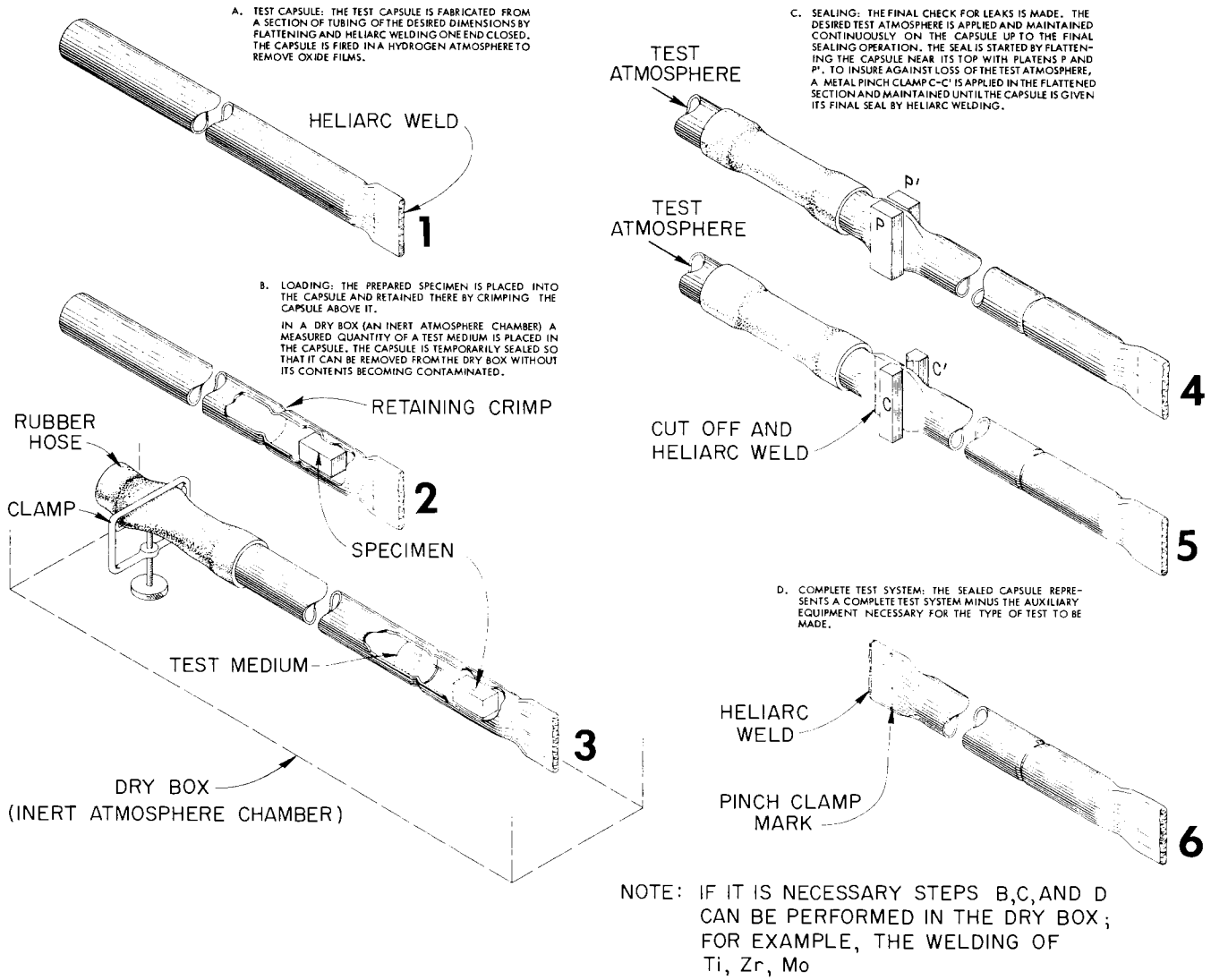

NOTE: IF IT IS NECESSARY STEPS B, C, AND D CAN BE PERFORMED IN THE DRY BOX; FOR EXAMPLE, THE WELDING OF Ti, Zr, Mo

Figure 7. Standard Corrosion Test Assembly Procedure.

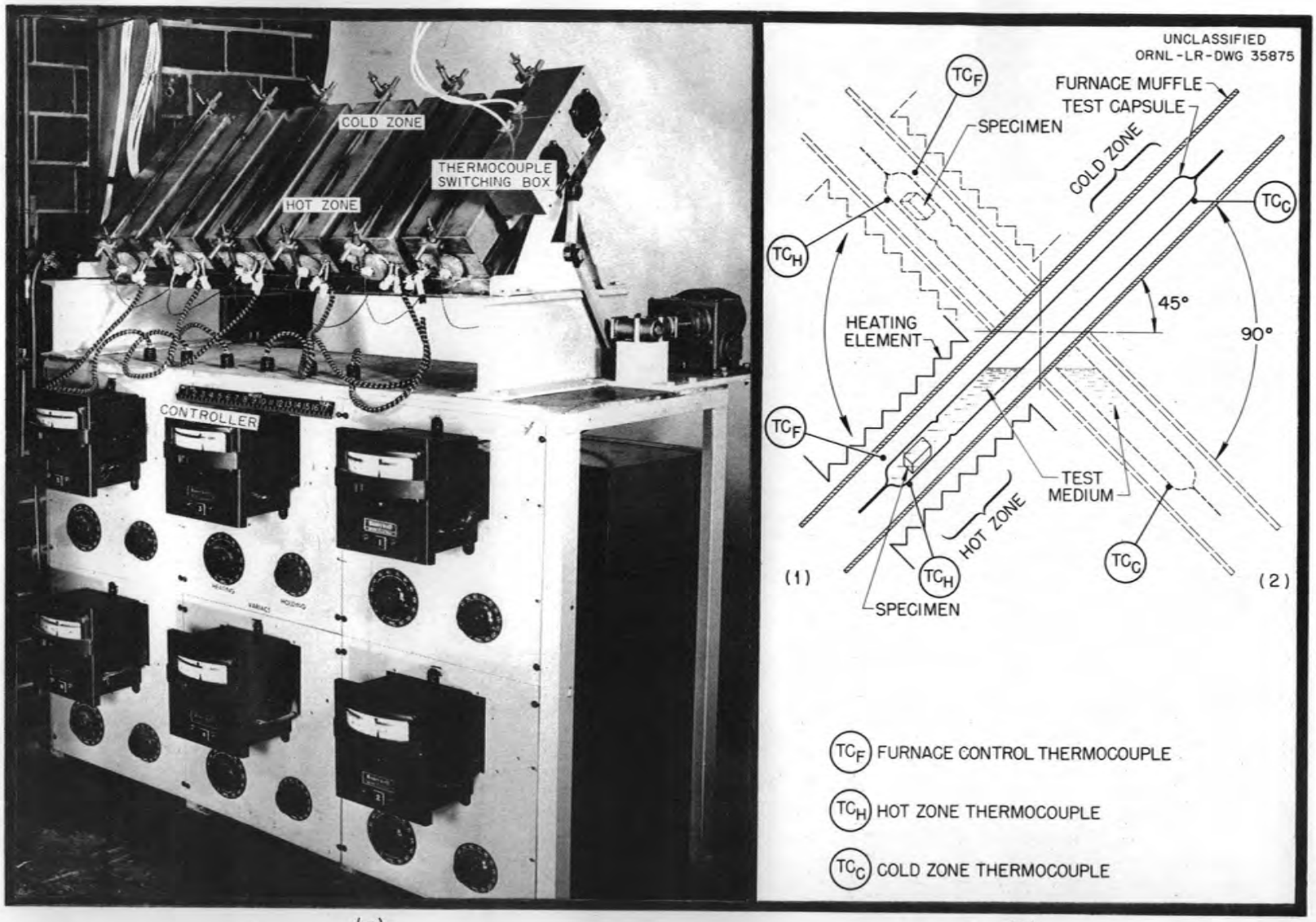

(a) (b)

Figure 8. Seesaw Furnace Test System.

the test capsule are shown schematically in Figure 8b. The maximum angle of tilt of the seesaw furnaces with the horizontal was 45 degrees. Cycling rates of one-half and one per minute were used in this investigation.

The thermocouple leads from the test capsules were connected to a switching box, and the hot- and cold-zone temperatures of each test capsule were monitored by means of the switching box and a continuous recorder. Each of the six furnaces was physically separated from the other furnaces and had its own power supply and temperature controller.

The three types of seesaw test capsules used are shown in Figure 9. The test system illustrated in Figure 9a was the type most commonly used in this investigation. The test temperatures reported for the systems shown in Figure 9a and 9b were the maximum temperatures reached in each zone during one cycle of the furnace. (The temperature at the interface of the lithium and the capsule wall was determined in an independent experiment and found to be approximately 30 Fahrenheit degrees below the recorded test temperature.)

One experimental difficulty encountered in the seesaw testing of lithium, which to some extent limited the use of this testing device, was the reluctance of lithium to flow in test capsules having inside diameters of less than 0.6 inch. Many of the metals and alloys were not available in sizes larger than this and consequently were not evaluated in this system.

Special techniques were required to test materials having limited oxidation resistance at elevated temperatures. The method

UNCLASSIFIED
ORNL-LR-DWG 33532R

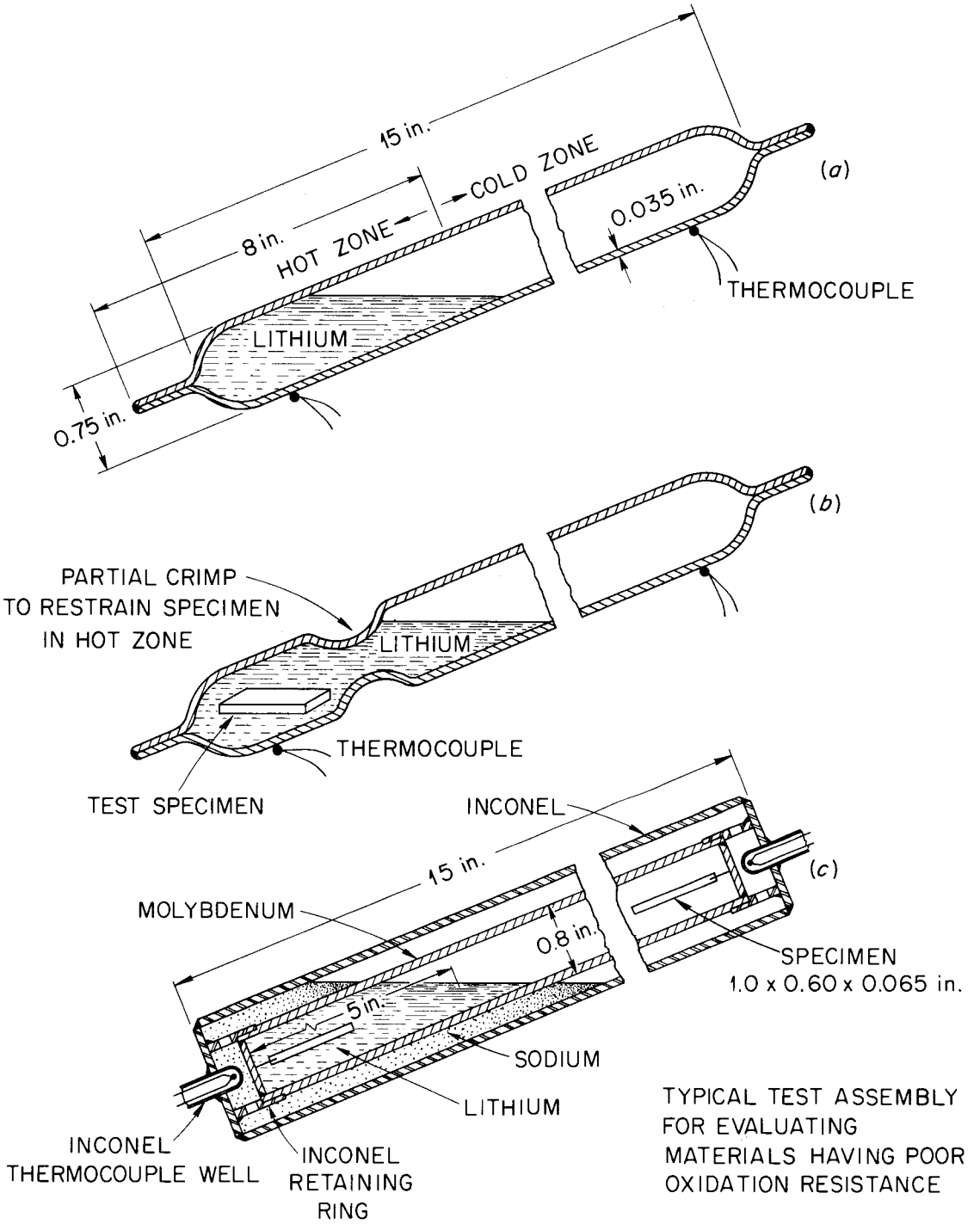

Figure 9. Types of Seesaw Furnace Test Capsules.

used is illustrated in Figure 9c. The annular space between the test metal (molybdenum) in the example shown, and the outer Inconel protective capsule was partially filled with sodium. The sodium acted as a thermal bond between the two materials and permitted the establishment of the desired temperature differences in the hot and cold zones of the test capsule.

Seesaw test capsules were loaded with lithium using techniques similar to those described in Figure 7.

Thermal-Convection Loop Tests. A thermal-convection loop test stand and a bank of controllers and recorders used to operate four loop stands are shown in Figure 10. The stainless steel loop shown was circulating lithium at maximum hot-leg and minimum cold-leg temperatures of 1600°F (871°C) and 1200°F (649°C), respectively.

The three basic thermal-convection loop designs used in this study are shown in Figures 11 and 12. Descriptions of these designs are as follows:

1. Type A. Early thermal-convection loops made of oxidation-resistant materials such as the stainless steels were designed in such a manner that the entire loading and sealing operation could be performed in the inert atmosphere chamber illustrated in Figure 4. A schematic diagram of this type of loop is shown in Figure 11. The loading procedure was as follows: (1) a predetermined volume of lithium was cast into the fill-pot and allowed to solidify, (2) the fill-pot was joined to the loop by heliarc welding in the chamber,

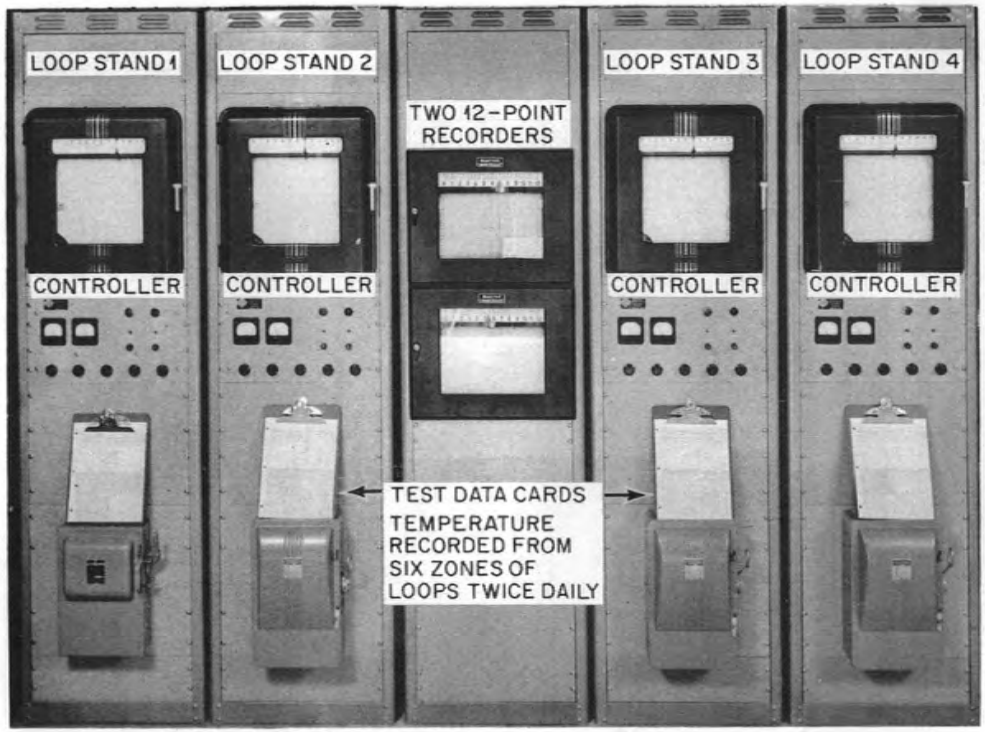

Saturable Reactor Controllers and Multipoint Recorders for Thermal Convection Loop Tests.

UNCLASSIFIED
ORNL-LR-DWG 33536

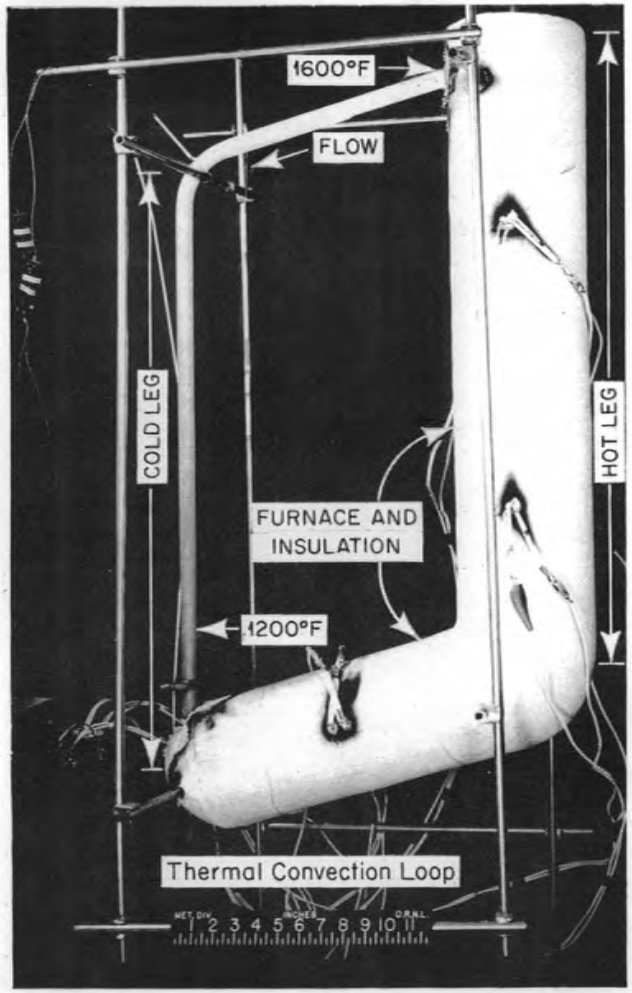

Figure 10. Thermal Convection Loop and Control Equipment.

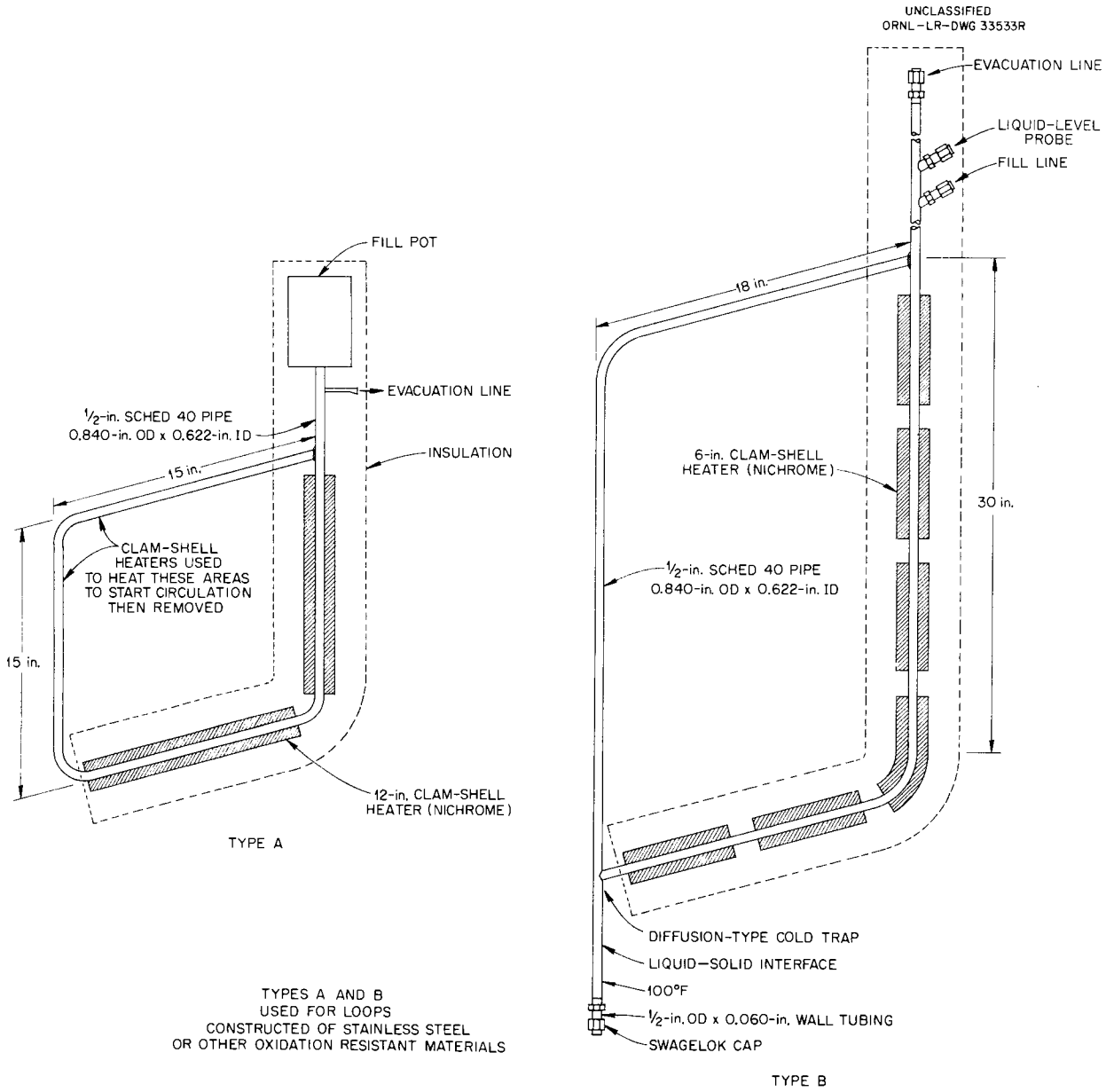

Figure 11. Types of Thermal Convection Loops.

UNCLASSIFIED
ORNL-LR-DWG 33534R

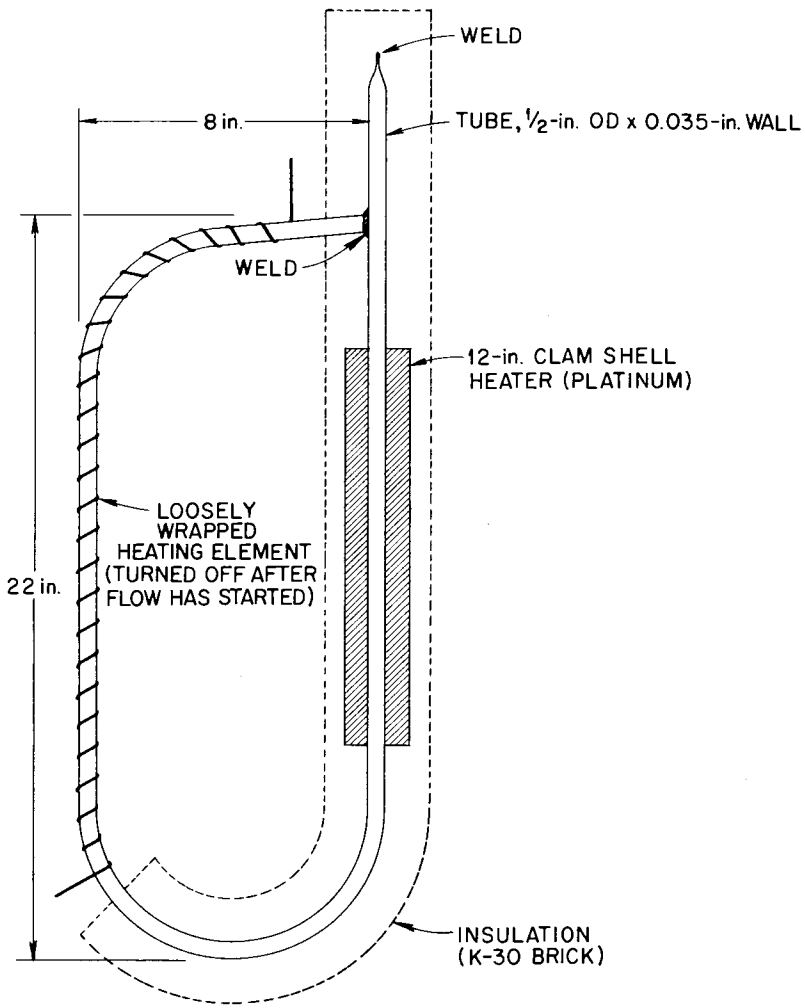

TYPE C

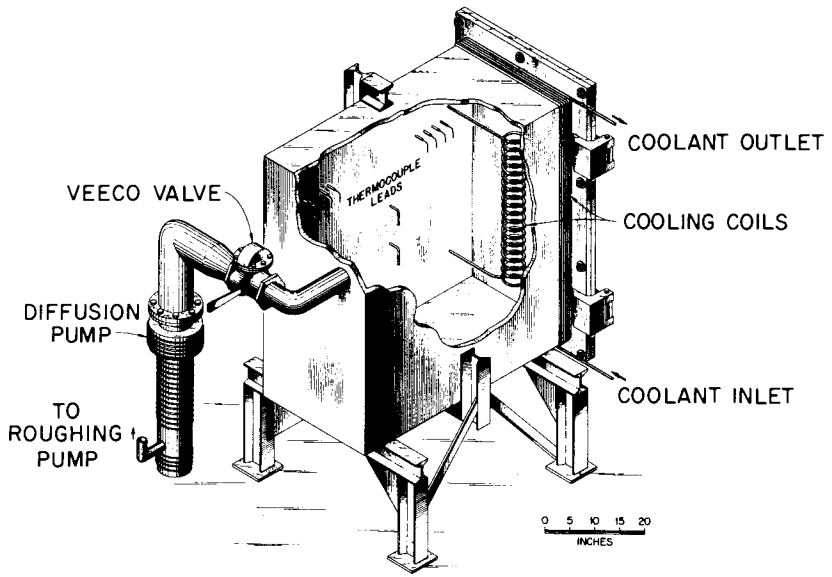

STAINLESS STEEL VACUUM BOX

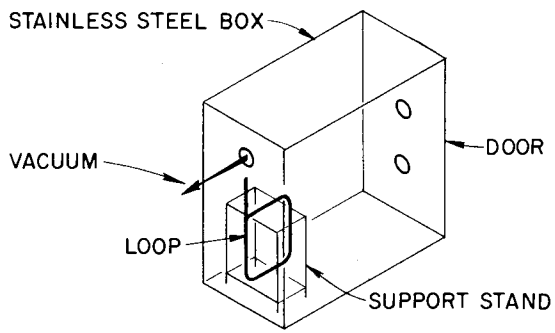

LOCATION OF LOOP IN VACUUM BOX

Figure 12. Method of Testing Thermal Convection Loops Made of Non-Oxidation Resistant Materials.

and (3) the loop was then evacuated to a pressure of less than five microns of mercury and the evacuation line was sealed.

Following the loading operation the loop was removed from the inert atmosphere chamber and resistance heaters and insulation were applied. Circulation of lithium in the loop began when the lithium became molten and flowed from the fill-pot, at which time the heaters and insulation on the cold-leg sections were removed. Following completion of the test, the loop was inverted in order that the lithium would drain from the loop back into the fill-pot.

2. Type B. Improved lithium-handling techniques and a cooperative lithium corrosion testing program between Nuclear Development Corporation of America and the Oak Ridge National Laboratory led to the alteration of the thermal-convection loop design. The modified loop, designated as Type B, is illustrated in Figure 11 and was used for the latter portion of stainless steel loop studies. Loops of this design were loaded with lithium in the following manner: (1) the empty loop was heated to 1000°F (538°C) while a reduced pressure of less than five microns of mercury was maintained in the system, and (2) the evacuation line was then sealed off and liquid lithium at approximately 700°F (371°C) was forced into the evacuated loop by argon pressurization of a charging container.

When circulation of lithium in the loop was established, the heaters and insulation were removed from the cold-leg sections of the

loop. The cold-leg temperature could be controlled by placing varying amounts of insulation on the cold leg.

The diffusion-type cold trap shown at the bottom of the Type B loop in Figure 11 was used on some loops in an attempt to purify the lithium by precipitation of contaminants of limited solubility.* These loops were drained of lithium following test by heating the cold trap and applying argon pressure at the top of the loop.

Lithium flow rates in loops of Type B were approximately seven feet per minute as compared to values of approximately four feet per minute in loops of the Type A design. These values are for hot- and cold-leg operating temperatures of 1500°F (816°C) and 1100°F (593°C), respectively. The flow rates were not determined for each loop test but were checked several times for each type of loop by two methods. The first method used was based on heat balance measurements as described by McKee.[49] The second method was as follows: (1) a twenty-gauge chromel-alumel thermocouple encased in a 1/4 x 0.020-inch wall stainless steel protection tube was welded into the bottom of the cold leg of a loop, (2) an intense heat source (two acetylene-oxygen torches) was applied to a small area of the upper portion of the cold leg for several seconds, and (3) the time required for the "hot slug" to reach the thermocouple in the cold leg was measured.

---

*See Appendix I - C.

The flow rates determined by the heat balance and "hot slug" methods differed by not more than 15 per cent.

3. Type C. In order to evaluate metals which had limited oxidation resistance at elevated temperatures, it was necessary to design special thermal convection loop testing facilities. Cladding of the test metals with oxidation-resistant alloys, such as the stainless steels, was not satisfactory because thermal stresses resulting from the differences in the temperature coefficients of expansion between the test metal and the cladding metal led to cracking in certain critical areas of the systems.

It was necessary, therefore, to design and build a stainless steel vacuum box for the corrosion testing of metals having poor oxidation resistance. The vacuum box and a typical test loop are shown in Figure 12. Tests were run either under vacuum or in argon, the former being preferred from the standpoint of heat transfer to the vacuum box walls. This system was employed to test six Type C columbium loops.

The two minor loop design modifications shown in Figure 13 were employed so that test specimens could be included in the hottest portion of the hot zone for studying mass transfer effects. Modification No. 1 shown in Figure 13 was used on several stainless steel loop systems to determine the weight loss per unit area for flat specimens suspended in the flowing lithium, as compared to the weight loss on sleeve specimens incorporated into the tube wall. Modification No. 2 shown in Figure 13 was used in determining the

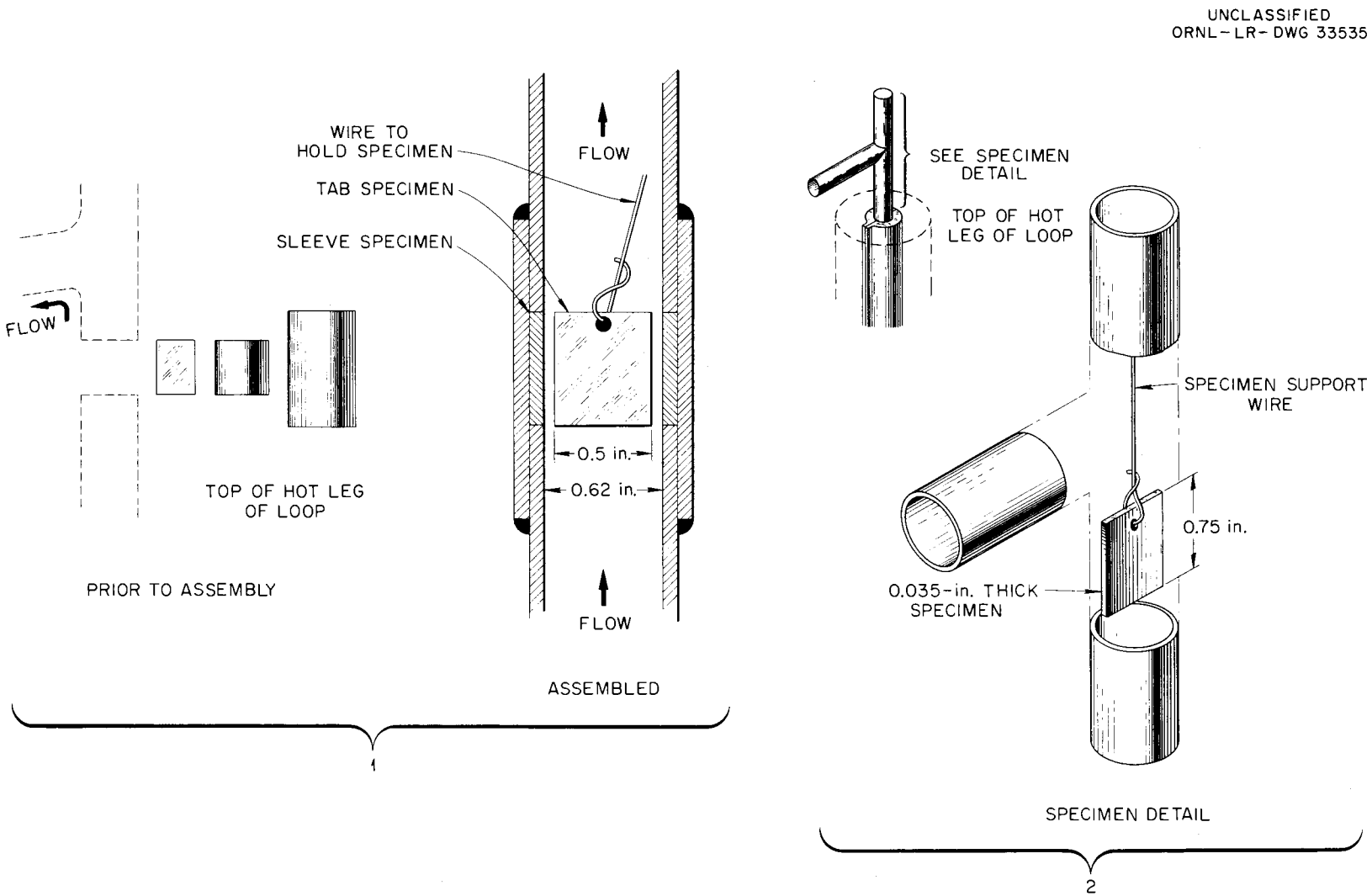

Figure 13. Thermal Convection Loop Modifications.

weight loss for columbium specimens suspended in the hot legs of columbium thermal-convection loops.

Stripping of Lithium from Test Components

The removal of lithium from the static and seesaw test specimens and containers was normally accomplished by submerging the test components in water and allowing the reaction of lithium with the water to proceed until no lithium metal remained.*

Lithium was drained from the thermal-convection loops at the end of the test period when possible. The loops were then cut into five-inch lengths and the residual lithium removed from the walls of the loop sections by reaction with water. In the tests which were terminated by plugging due to metal crystal deposition, the lithium could not be drained from the loops. These loops were sectioned into five-inch lengths and the lithium in each section was removed by reaction with water.

It was necessary to exercise considerable care during the stripping operation to avoid the loss of mass transfer crystals. In several cases the loops were radiographed to determine the location

*It is important to note that the stripping operation was carried out in a well-ventilated area to avoid the accumulation of hydrogen gas which was evolved during the reaction. It was also found necessary to keep the lithium metal completely submerged to prevent the lithium from igniting any hydrogen which might be present.

of the mass transfer crystals in the cold leg of the loops prior to the sectioning and stripping operations.

Basic Methods of Examination

The methods used to determine the extent and nature of the corrosion encountered in the various tests included most of the metallurgical and chemical analytical techniques currently available. The methods of examination described below apply in general to both static and dynamic test systems.

Specimens and Container Materials.

1. Weight Change. Weight determinations were made on specimens before and after test. The results were reported as weight changes and not as rates based on the length of test, since the latter are often incorrectly construed as inferring linear corrosion rates. Weight-change data were considered to be of limited usefulness as acceptability criteria since the attack by lithium on materials was rarely uniform.

2. Dimensional Changes. Specimen-dimension changes as determined metallographically and by micrometer measurements were useful only when the attack was heavy and uniform.

3. Metallographic Methods. Metallographic methods, including both reflected light and electron microscopy, were by far the most useful for evaluating the resistance of materials to attack by lithium.

Three specimens from each static and seesaw furnace test and six from each thermal-convection loop test were examined metallo-

graphically in both the as-polished and etched conditions. Electroplated nickel deposits ranging in the thickness from 0.010 to 0.050 inch were used for edge preservation of metallographic specimens during polishing since many of the surface corrosion products were less than 0.001 inch in thickness.

Allowing as-polished test specimens to stand in air for several days was found to be an excellent method of locating grain boundaries which had been penetrated by lithium.

Microhardness measurements across exposed specimens and on corrosion product phases were found to be extremely useful in evaluating the effects of corrosion on many materials.

A magnetic-etch technique[50,51] was effective in detection of regions of austenitic stainless steel specimens which had become ferromagnetic due to the leaching action of lithium on particular alloying elements.

4. X-Ray Analysis. Specimens or sections of test systems exposed to lithium were routinely examined by x-ray diffraction methods to determine changes in the crystal structure of the surfaces or to identify surface deposits.

5. Chemical Analysis.* Chemical analysis was used to determine the changes in chemical composition of specimens as a result of

---

*All chemical analyses were performed by the Analytical Chemistry Division, Oak Ridge National Laboratory.

exposure to lithium and to identify mass transfer crystals. In many cases successive layers of material were milled from the surfaces of specimens following exposure in order to determine the changes in composition as a function of distance from the specimen surface. The resulting data were useful, for example, in determining the extent of preferential leaching by lithium of such elements as carbon, chromium, and nickel from stainless steels. Spectrographic analyses, including the micro-spark technique, was used extensively in this connection.

Samples of lithium from test containers were analyzed routinely in the early static test portion of this study but the results were of only limited usefulness.

Vacuum-fusion analysis was used to determine the oxygen and nitrogen contents of various test materials before and after testing.

Test Materials

Materials Tested in Lithium

The test materials and their chemical compositions are listed in the tables which summarize the corrosion test results in Chapter VII.

Preparation of Test Components

Procedures used in preparation of specimen surfaces prior to testing included polishing by mechanical and chemical methods, degreasing treatments in appropriate solvents, and annealing in a hydrogen environment to reduce surface oxide films. Porous ceramic

materials were subjected to degassing treatments by heating at elevated temperatures under vacuum to remove adsorbed gases from the surfaces prior to testing in lithium.

Special care was taken to assure that all cutting burrs were removed from specimen edges prior to testing since these could easily lead to weighing errors and false metallographic observations. Metallographic specimens of all test materials were examined before testing to determine the condition of the surface prior to exposure to lithium.

Lithium

All lithium metal used in this study was LC Grade obtained from the Maywood Chemical Works, Maywood, New Jersey. Maximum impurity contents for this grade of lithium are given in Table II. Throughout the work a continuous effort was exerted to minimize contamination of the lithium metal by employing careful handling techniques and to develop practical and effective methods of purifying the best available commercial product. Sampling and purification techniques which were developed are discussed in Appendix I - A and I - C, respectively. A comparison of the various analytical methods used for oxygen and nitrogen determinations is given in Appendix I - B.

The bulk of the corrosion testing was carried out using lithium which was received in the form of two-inch cubes packed under helium gas inside small gas-tight, tin-plated cans. These cans were

TABLE II

PURITY OF GRADE LC LITHIUM AS SPECIFIED BY THE MANUFACTURER

LC Grade	Per Cent
Silicon	0.015 maximum
Iron and aluminum	0.03 maximum (calculated as iron)
Calcium	0.03 maximum
Sodium	0.02 maximum
Heavy metals	0.07 maximum (calculated as nickel)
Nitrogen	0.03 maximum
Chlorine	0.003 maximum
Lithium	99.80 minimum

opened in the inert atmosphere chamber previously described. The cubes were melted in stainless steel crucibles, heated to approximately 450°F (232°C), drossed until free of visible lithium nitride or lithium oxide, and finally cast into ingots or "sticks" of the desired size. The lithium metal was cast only when the atmosphere in the chamber was pure enough so that a mirror-like surface could be maintained on the molten lithium for several minutes. No additional purification techniques were normally employed on the lithium prior to test. The lithium ingots used in the majority of the tests contained from 200 to 600 ppm nitrogen and from 100 to 400 ppm oxygen.

In the latter portion of this study, lithium was obtained in fifty-pound batches which had been loaded by the supplier into stainless steel shipping containers in a helium-filled dry box. This metal was purified in the manner described in Appendix I - C.

The desired weight of lithium for each test was obtained by cutting and weighing the lithium "sticks" in the inert atmosphere chamber.

CHAPTER VII

RESULTS AND DISCUSSION

Static Test Results

Two-Component Static Test Results

Most of the static corrosion data were obtained using two-component test systems of the type illustrated in Figure 6a, Chapter VI. The results of tests of this type on several metals and alloys are reported in this section. Because the behavior of columbium in static lithium was investigated more extensively than that of other metals, the results of the columbium studies are considered separately.

Metals. The results of two-component static tests on relatively pure metals are listed in Table III.

The poor corrosion resistance of copper and nickel is apparently attributable to the high solubility of these metals in lithium at elevated temperatures.

Beryllium and the refractory metals, molybdenum, tantalum, titanium, vanadium, and zirconium, were found to be quite resistant to attack. The outstanding corrosion resistance of the refractory metals is shown in the photomicrographs of Figure 14. It is in order to note that in an earlier study[52] in which iron capsules were used, beryllium, molybdenum, and vanadium were rated as having poor corrosion resistance to lithium. This result is now known to have been due to dissimilar metal mass transfer of these metals to the iron

TABLE III

RESULTS OF LITHIUM CORROSION TESTS ON METALS IN TWO-COMPONENT STATIC TEST SYSTEMS

Metal	Temperature °F	Temperature °C	Time Hour	Surface Area / Volume of Lithium in.^{2}/in.^{3}	Weight Change mg/in.^{2}	Metallographic Observations
Beryllium	1500	816	100	10	+ 1.7	2 mils of intergranular attack.
Beryllium	1832	1000	100	10	+ 1.6	3 mils of intergranular attack.
Copper[a]	1500	816	100	13	--	Portions of 35-mil tube wall completely dissolved.
Iron[a]	1500	816	100	13	0	No attack.
Iron	1500	816	400	7	- 2.0	Up to 20 mils of very faint intergranular penetration.
Iron	1832	1000	400	7	- 1.9	No attack.
Molybdenum	1500	816	100	13	0	No attack.
Nickel[a]	1500	816	100	13	--	Portions of 35-mil tube wall completely dissolved.
Tantalum	1500	816	100	13	+ 7.6	No attack.
Titanium[a]	1500	816	100	13	+ 2.5	No attack.
Vanadium	1500	816	100	13	+ 8.4	No attack.
Zirconium	1500	816	100	13	0	No attack.

[a]Duplicate tests.

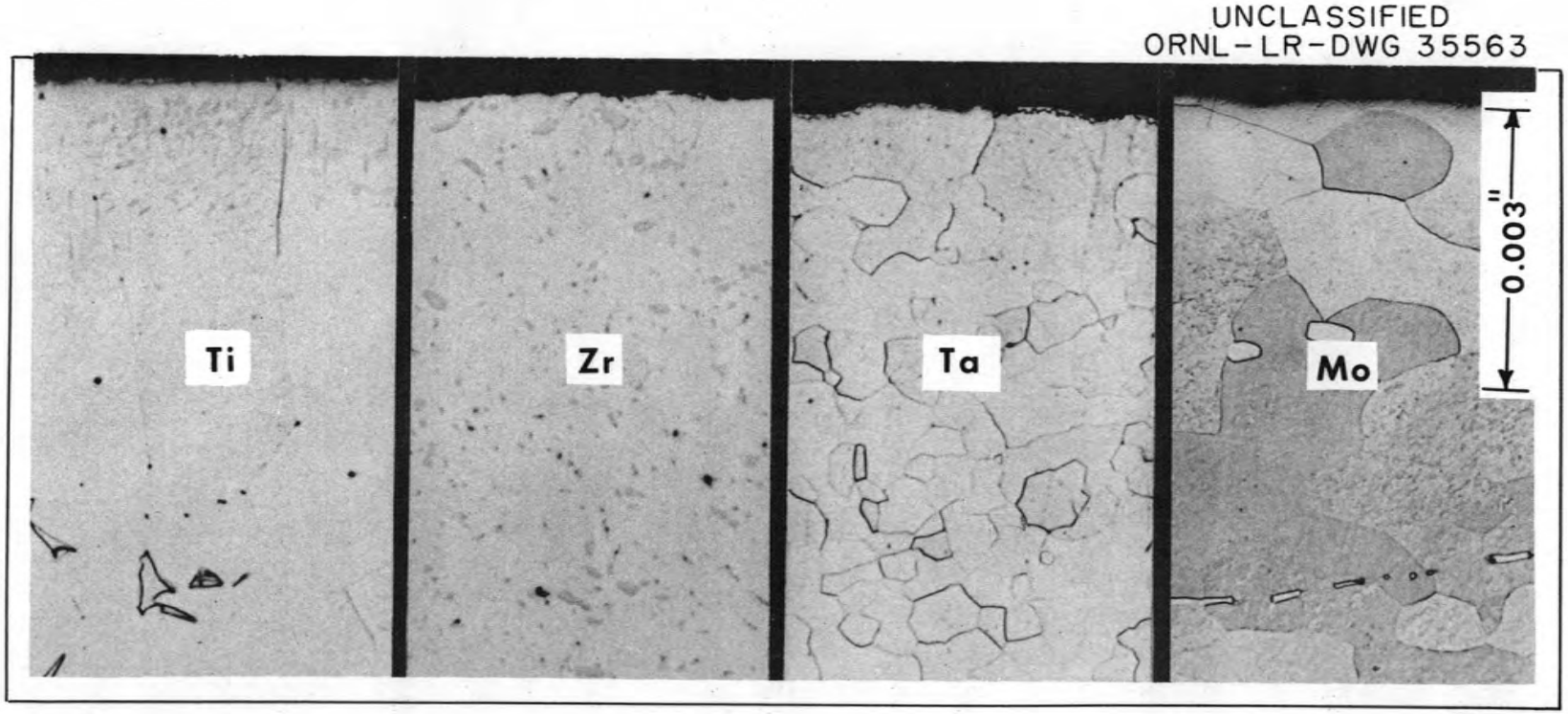

Figure 14. Surfaces of Various Refractory Metals Following Exposure to Lithium. Test Conditions: Static, 1500°F (816°C), 100 hr. Specimens Shown in the Etched Condition.

container walls. The results of the present study, then, serve to emphasize that the two-component test technique provides a more accurate evaluation of the corrosion resistance of a material to a liquid metal than does the three-component technique.

Although pure iron generally has been found to be quite resistant to attack by lithium, iron containing small amounts of carbon often is penetrated intergranularly by lithium in certain temperature ranges. This is illustrated in Figure 15 which shows that Armco iron, containing 0.014 weight per cent carbon, is attacked intergranularly when tested for 400 hours at 1500°F (816°C) but is not attacked when tested at 1832°F (1000°C) for a similar time period. Figure 15b shows the penetration observed in the grain boundaries at very high magnification. This attack is attributed to a reaction of lithium with carbon in the grain boundaries, a phenomenon which is discussed later in connection with the behavior of iron-base alloys in two-component systems and of mild steels in three-component tests. Several cases have been noted in which small particles of a hygroscopic material containing lithium were found on the exterior surfaces of Armco iron capsules tested at 1500°F (816°C) for periods of 100 hours. A distinct acetylene (C_2H_2) odor was associated with these capsule wall penetrations.

The iron-carbon phase diagram, a portion of which is shown in Figure 16, indicates that at 1832°F (1000°C) the single homogeneous phase, austenite, is stable. However, at 1500°F (816°C) the equilibrium phases are ferrite, containing approximately 0.010 per cent

UNCLASSIFIED
ORNL-LR-DWG 35565

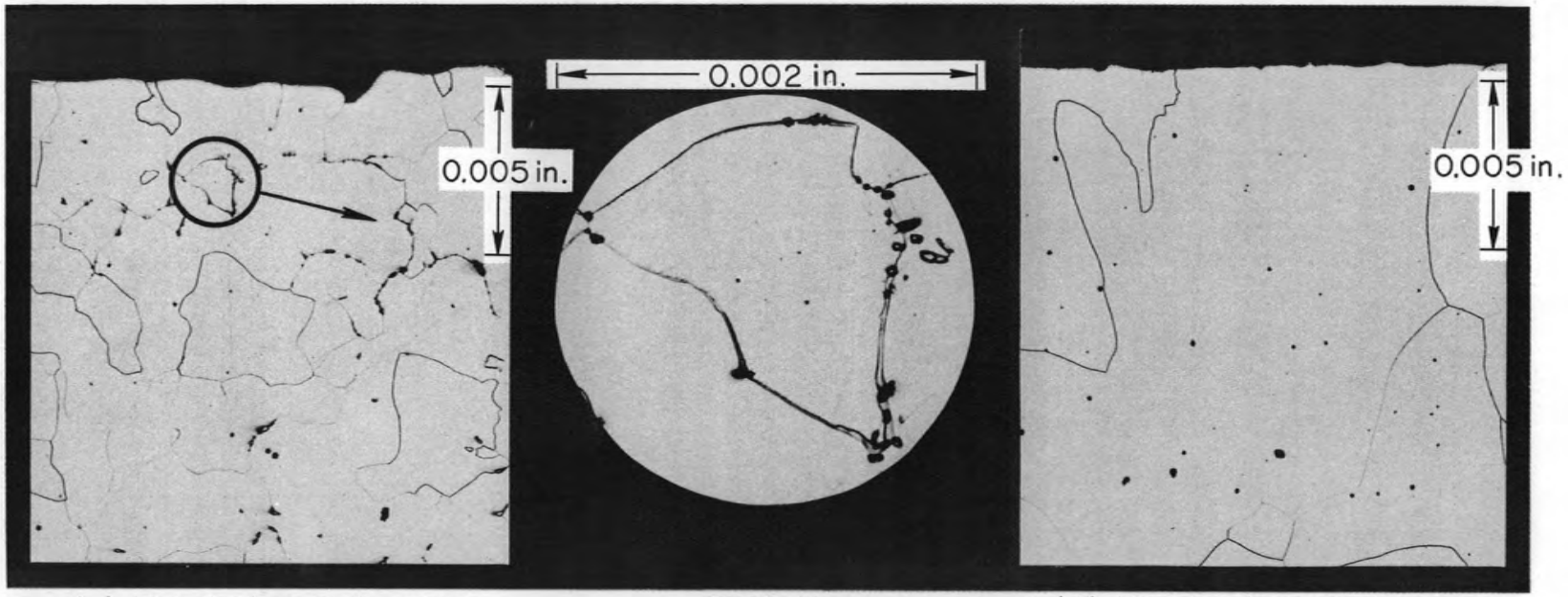

(*a*) 1500°F (816°C) 250X 1500 X (*b*) 1832°F (1000°C) 250X

Figure 15. Armco Iron Specimens Following Exposure to Lithium at the Indicated Temperatures. Test Conditions: Static, 400 hr. Note the Faint Intergranular Attack in (*a*) and the Lack of any Attack in (*b*). Etch: Nital. Reduced 28%.

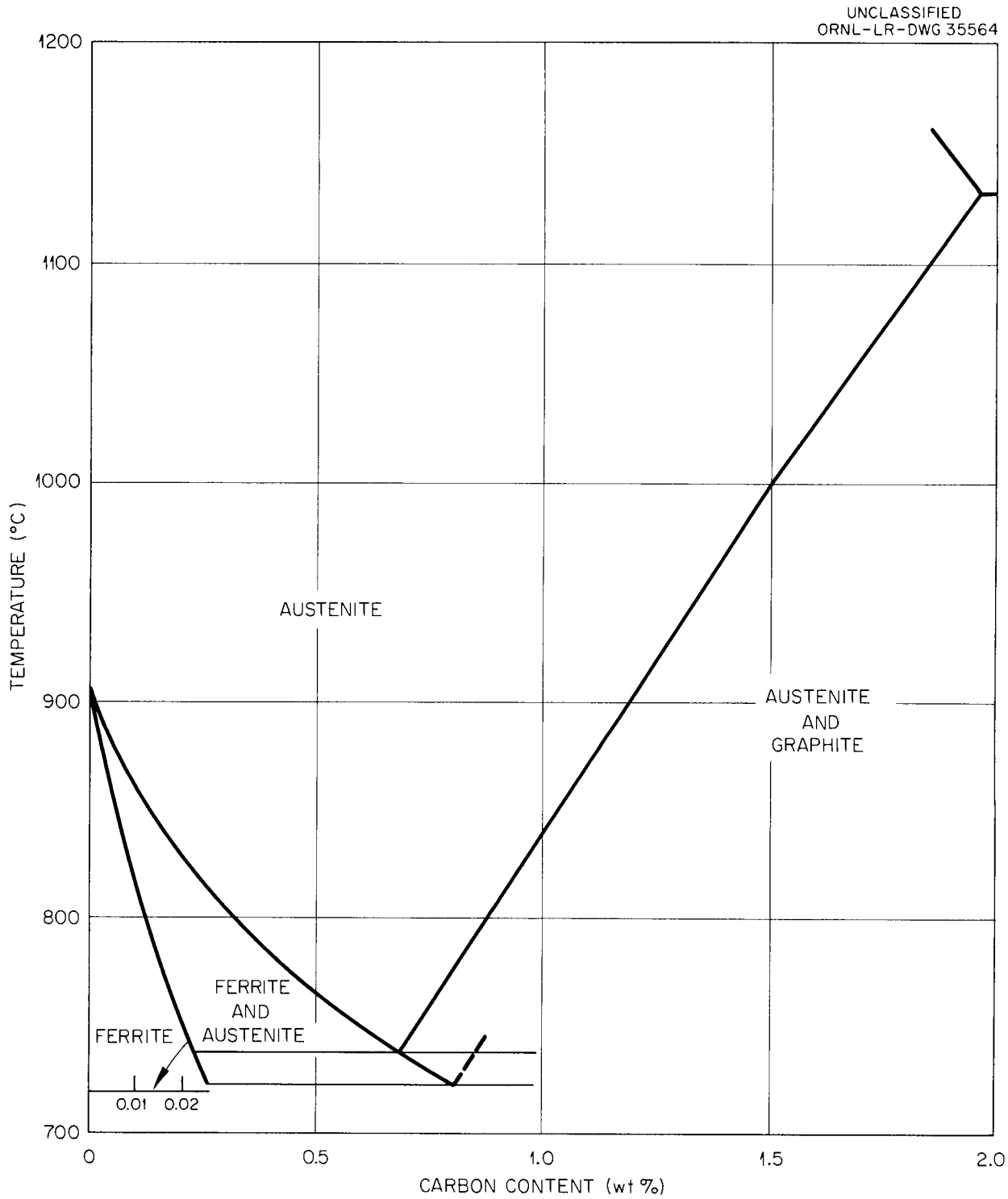

Figure 16. Temperature-Composition Plot of the Ferrite-Austenite Equilibrium in the Iron-Carbon Diagram. (From R. P. Smith, *J. Am. Chem. Soc.*, 68, 1163) (1946).

carbon, and a very small amount of austenite, containing approximately 0.3 per cent carbon. The most probable location of this carbon-rich austenite is in the ferrite grain boundaries.

Several cases have been reported in the literature[53,54] of Armco iron being attacked intergranularly at 900°F (482°C) and 1200°F (650°C) where ferrite and iron carbide (Fe_3C) are the equilibrium phases. If the carbide phase were present in the grain boundaries, where nucleation is easiest, it would afford a path whereby the lithium could penetrate the metal and would account for these observations.

Columbium. Early screening-type static corrosion tests indicated columbium to be a promising container material for molten lithium. Subsequent tests of this material under flowing, non-isothermal conditions in thermal convection loops, however, revealed a type of intergranular corrosion attack, particularly in and near weld zones, which had not been detected in the more cursory preliminary evaluations in static systems. Because columbium rates high as a potential high-temperature nuclear reactor structural material, an intensive study was undertaken to determine the cause of the observed intergranular attack.

Additional static tests as well as a more thorough examination of the weld zones of the early static test systems established that columbium is attacked intergranularly by lithium in the absence of flow and of temperature gradients. The research which followed, therefore, was carried out using static test systems since, relative

to thermal convection loops, static systems not only are easier to fabricate but also lend themselves to more stringent control of important test variables.

The lithium corrosion studies on columbium are presented chronologically, beginning with the initial observations in thermal convection loops and terminating with systematic studies in static systems. On the basis of the latter, an hypothesis is developed to explain the intergranular attack of columbium by lithium.

1. Initial Observations. In the first columbium-lithium thermal convection loop test, severe cracking was observed in the saddle-weld area at the top of the hot leg as shown in Figure 17. In this test, the loop was operated for 500 hours at a hot-leg temperature of 1500°F (816°C). The columbium was protected from oxidation by cladding it with type 310 stainless steel. The saddle-weld area was protected by a type 310 stainless steel shroud which was welded to the cladding as shown in Figure 17.

Subsequent loop tests were performed in a stainless steel vacuum chamber at pressures from 1 to 5 microns of mercury to eliminate the effect of stresses due to the difference in thermal expansion of stainless steel and columbium in the clad-and-shroud test design. In all cases the vacuum-chamber tests on non-clad loops were terminated as the result of actual penetration of the columbium tube walls by lithium, especially at weld zones. Typical grain-boundary penetrations in a weld zone and in base material not affected by welding are shown in Figures 18 and 19, respectively. The

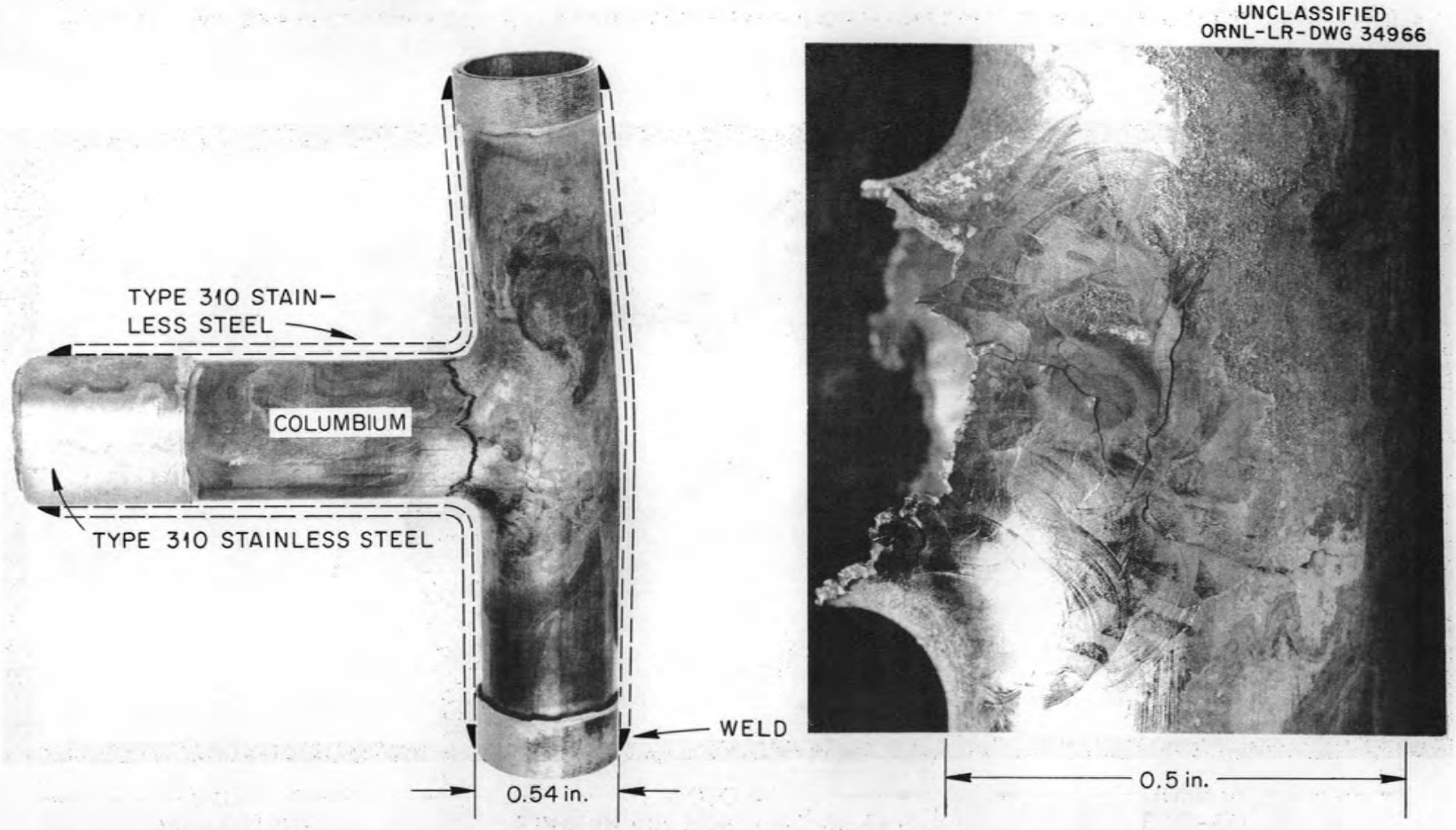

Figure 17. Saddle-Weld Area at Top of Hot Leg of Columbium Loop. Dotted Line Shows the Location of Protective Stainless Steel Shroud which was Removed Following Test to Reveal Cracks in the Columbium. Photograph on Right Shows the Weld Area of the Columbium at Higher Magnification. Reduced 3%.

[redacted]

ORNL-LR-DWG 34967

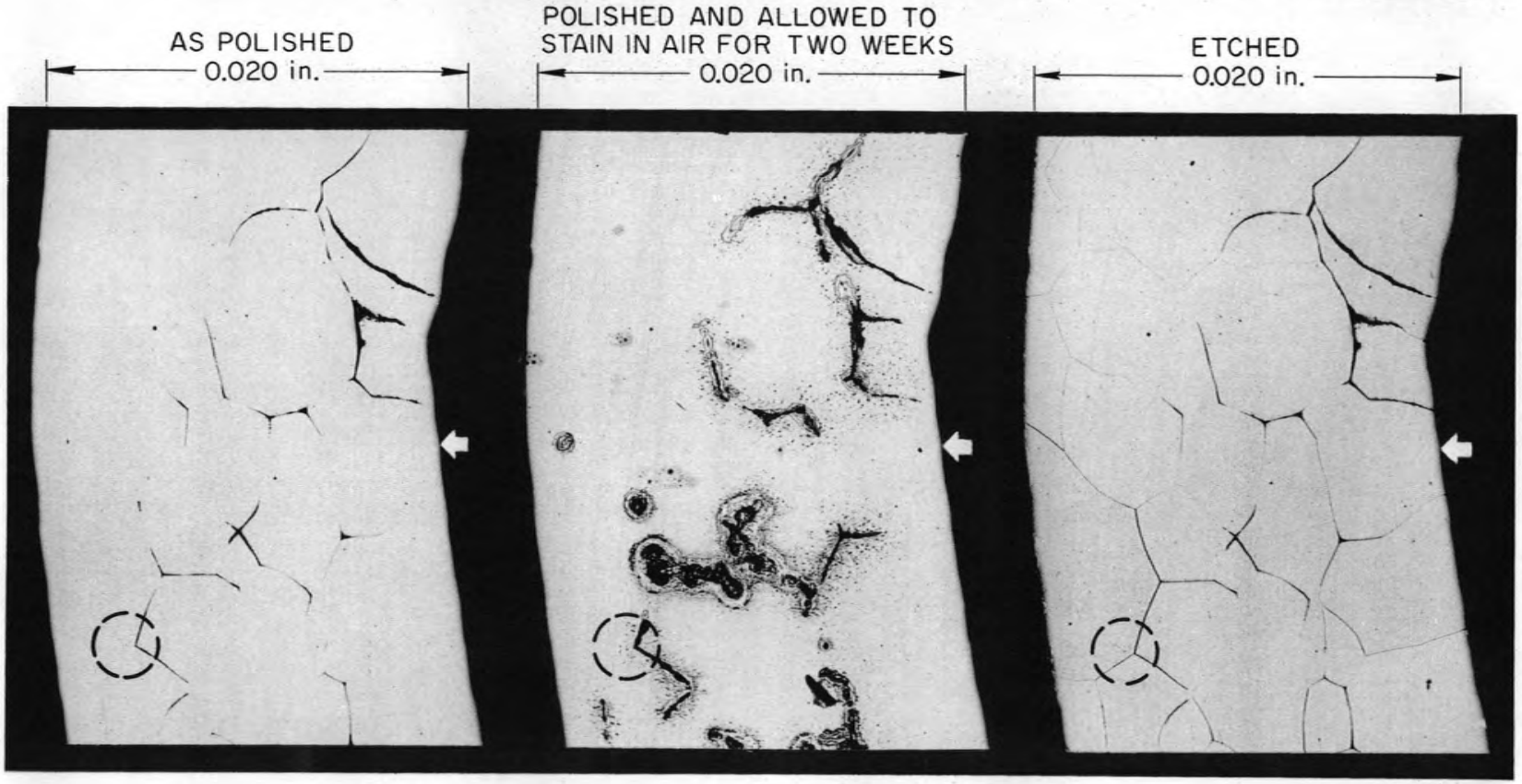

150X

Figure 18. Weld Zone of Columbium Tube Wall from Hot Leg of Thermal Convection Loop. Loop No. 54 Test Conditions: 1600°F (871°C) for 23 hr. Arrow Indicates Surface Exposed to Lithium. Reduced 21%.

[redacted]
ORNL-LR-DWG 34968

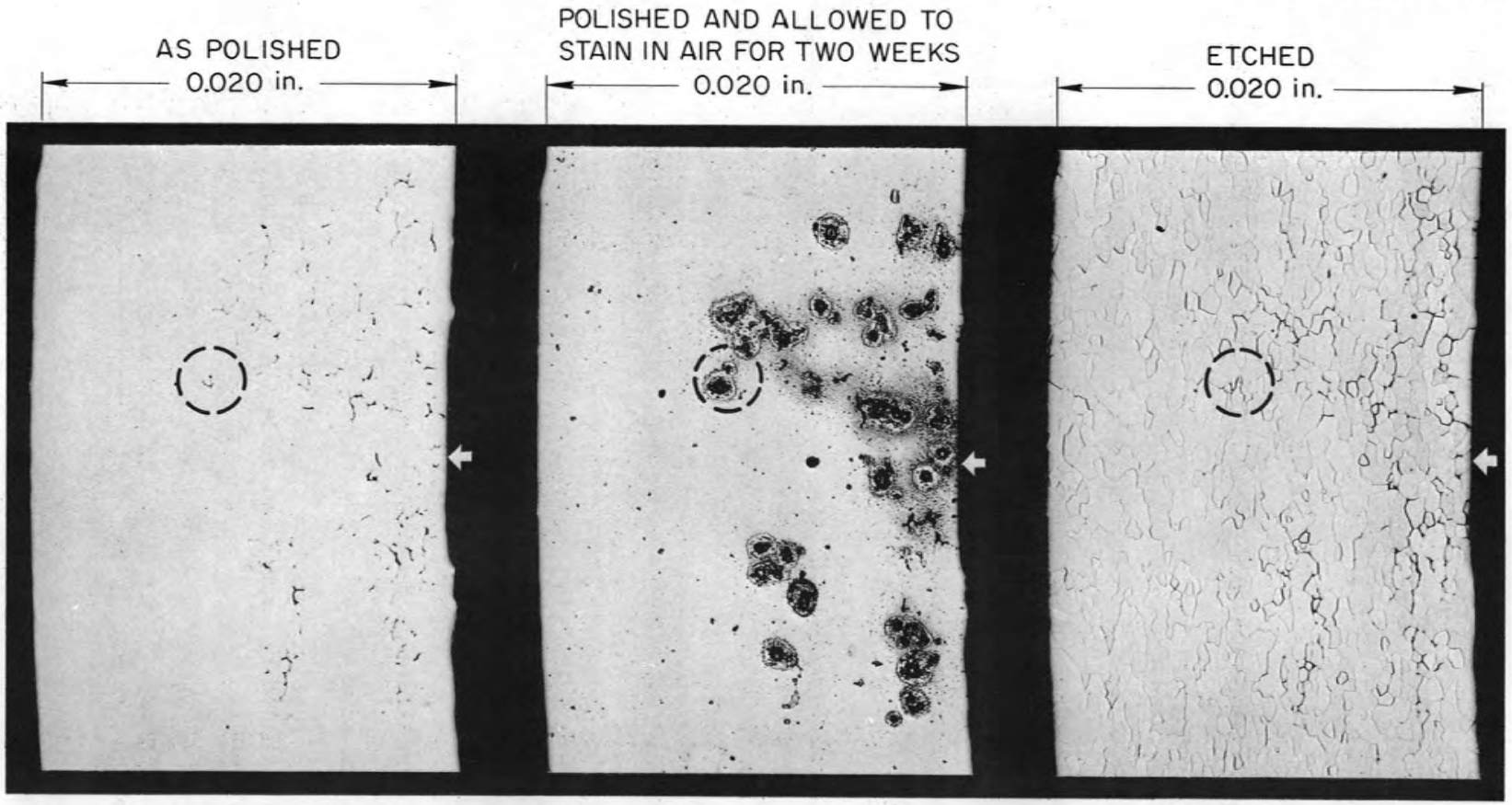

150X

Figure 19. Columbium Tube Wall from Hot Leg of Thermal Convection Loop. Loop No. 54 Test Conditions: 1600°F (871°C) for 23 hr. Arrow Indicates Surface Exposed to Lithium. Reduced 19%.

photomicrographs in each of these figures show a given penetrated region in three different stages of metallographic preparation: (a) as polished, (b) polished and allowed to "stain" in air for two weeks, and (c) polished and etched.* The extent of penetration is detected most readily in the "stained" specimens, as shown by the areas enclosed by dashed circles. The staining effect was attributed to the formation of lithium hydroxide by the reaction of lithium, or lithium compounds, with water vapor in the atmosphere.

The presence of lithium in penetrated grain boundaries was confirmed by chemical analysis of successive five-mil turnings machined from both hot and cold legs of several loops. The excellent correlation between lithium content, as a function of distance from the outside surface of the tube wall, and the extent of intergranular attack observed metallographically is shown in Table IV.

The corrosion test results described thus far were on sintered** columbium tubing formed by powder metallurgy techniques. For comparison of these results with those for denser and perhaps purer arc-cast material, a two-inch section of arc-cast tubing was inserted by braze welding as part of the hot leg of a sintered columbium loop. A vacuum-chamber corrosion test using this loop was

---

*The columbium specimens shown in the etched condition in this report were etched by immersion in H_2O-HF-H_2SO_4-HNO_3, 55-25-10-10 volume per cent.

**The terms "sintered" and "arc-cast" as applied to columbium tubing in this report refer to the method of preparing the starting material which is used in the subsequent fabrication of tubing.

TABLE IV

LITHIUM CONCENTRATION AS A FUNCTION OF DISTANCE FROM OUTSIDE OF TUBE WALL IN COLUMBIUM-LITHIUM THERMAL CONVECTION LOOP TESTS[a]

LOOP NO.	CUTS[b] MACHINED FROM O.D. OF TUBE WALL (MILS)	LITHIUM CONCENTRATION (ppm)		METALLOGRAPHIC RESULTS	
		HOT LEG	COLD LEG	HOT LEG	COLD LEG
52 Test Conditions: Hot Leg: 1600°F Cold Leg: 1300°F Time: 155 hr	0–5 5–10 10–15 15–20	<1 <1 <1 25	<1 <1 2 4	Up to 10 mils attack in longitudinal weld and heat affected zone. No attack on base material.	No attack
54 Test Conditions: Hot Leg: 1600°F Cold Leg: 1300°F Time: 23 hr	0–4 4–8 8–12 12–16 16–20	135 230 450 450 470	<1 <1 <1 <2 11	Complete penetration (20 mils) of longitudinal weld. Up to 10 mils attack on base material.	No attack
55 Test Conditions: Hot Leg: 1600°F Cold Leg: 1400°F Time: 55 hr	0–5 5–10 10–15 15–20	1 7 42 70	1 1 25 65	Complete penetration (20 mils) of longitudinal weld, heat affected zone and base material.	3 mils penetration in heat-affected region of weld. No attack in base material.

[a]LOOP TESTS PERFORMED IN VACUUM BOX.

[b]0 MILS = OUTSIDE SURFACE.
20 MILS = INSIDE SURFACE.

terminated after 36 hours by heater failure due to lithium contamination, the penetration having occurred in a longitudinal seam weld in the sintered tubing. Metallographic examination of this loop after the test showed that severe attack had occurred in both types of tubing and that a non-metallic gray phase was present in the attacked regions. These results are shown in Figure 20. The absence of a micro-hardness gradient across the tube walls indicated that evacuation to pressures of 1 to 5 microns of mercury in the vacuum-chamber test apparatus was adequate to prevent contamination of the columbium by interstitial oxygen and nitrogen.

Additional static tests, conducted on sintered columbium tubes, showed that the type of corrosion attack observed in the thermal-convection loop tests was not related to flow of lithium or to temperature gradients in the system. An examination of weld zones of components used in the earlier screening-type static tests confirmed this conclusion. Figure 21 shows a typical static test result. Grain-boundary phases, both metallic and non-metallic in appearance, were observed, as indicated by arrows in Figure 21. The attack was found to be heaviest in weld zones and heat-affected zones adjacent to welds.

2. Effect of Welding Environment. The predominance of intergranular penetrations at and near weld zones in both static and dynamic test components suggested the possibility that the corrosion of columbium by lithium was associated with contamination of the metal by either oxygen or nitrogen, or both, during conventional

ORNL-LR-DWG 31069

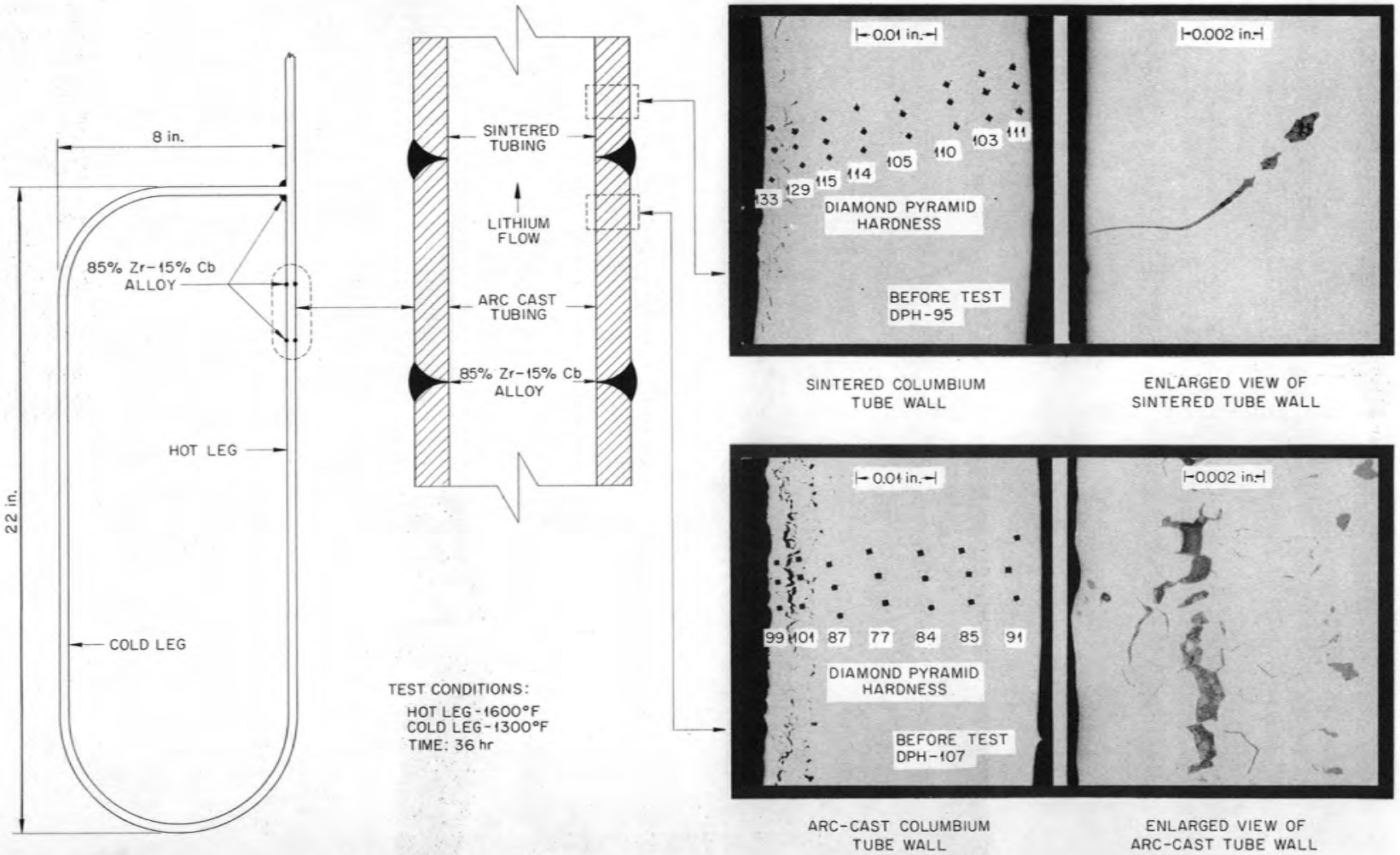

Figure 20. Results of Dynamic Lithium Corrosion Test on Sintered Columbium Loop Containing a Two-Inch Arc-Cast Columbium Insert.

[redacted]

ORNL-LR-DWG 34970

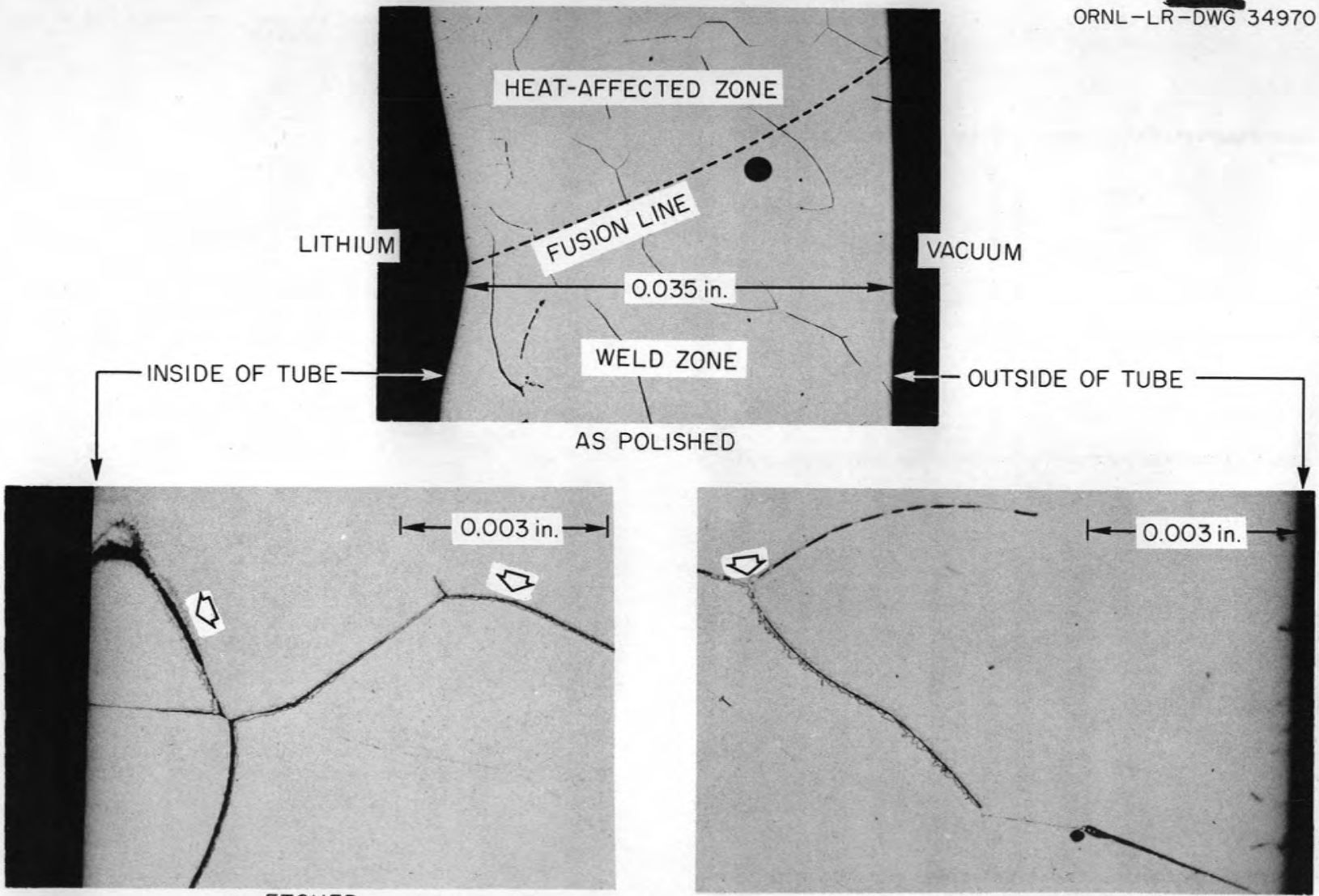

[redacted]

Figure 21. Weld Zone of Columbium Tube Wall after Exposure to Lithium. Arrows Indicate Corrosion Product Phases in Attacked Grain Boundaries. Test Conditions: Static, 1500°F (816°C), 100 hours.

shielded-arc or inert-gas-chamber welding. This consideration led to the second phase of the study in which the corrosion resistance of specimens welded in inert-gas environments containing varying amounts of oxygen and nitrogen was investigated.

In this study, both the fusion-welding and braze-welding techniques were used in preparing the specimens. The joining processes were carried out in three different environments: (1) argon plus air, (2) argon containing 1600 ppm nitrogen and 400 ppm oxygen, and (3) argon containing 67 ppm nitrogen and 3 ppm oxygen. The "argon plus air" designation is used to describe that environment associated with welding in air using conventional inert-gas coverage. The controlled environment welding was carried out in an inert-atmosphere chamber. Gas compositions were determined by the mass spectrograph technique and the values reported represent the average of results on duplicate samples taken prior to welding. Evaluation of the effects under consideration was based primarily on metallographic examination and on hardness determinations, the latter being a sensitive measure of the extent of contamination of columbium by the interstitial solutes, oxygen and nitrogen.[55,56]

The results of hardness determinations on fusion-welded specimens both before and after exposure to lithium are tabulated in Figure 22. Significant effects shown in this tabulation are: (1) the marked sensitivity of fusion-zone hardness to welding environment purity, and (2) the decrease in hardness following exposure to lithium of all specimen regions, including the non-heat-affected base

[redacted]

ORNL-LR-DWG 34971R

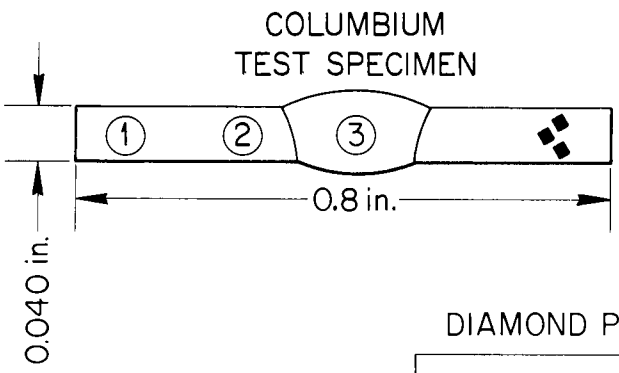

① BASE MATERIAL
② HEAT-AFFECTED ZONE
③ WELD ZONE

DIAMOND PYRAMID HARDNESS * (500 g LOAD)

FUSION-WELDING ENVIRONMENT	AS WELDED			FOLLOWING TEST IN LITHIUM		
	①	②	③	①	②	③
ARGON + AIR	127	127	356	97	90	128
ARGON + 1600 ppm N_2 + 400 ppm O_2	128	116	155	107	93	105
ARGON + 67 ppm N_2 + 3 ppm O_2	127	118	131	93	92	95

[a]As-received Arc Cast Cb: O_2–0.038%, N_2–0.002%, C–0.014% (supplier's analysis) D.P.H. – 137.
[b]Each hardness value is average of three determinations taken as shown schematically in sketch.
[c,d,e]O_2 and N_2 content (weight per cent) of Cb specimens in base material ① and weld ③ following welding operation.

[c] ① O_2–0.062%, N_2–0.014%; ③ O_2–0.34%, N_2–0.21%
[d] ① O_2–0.061%, N_2–0.015%; ③ O_2–0.086%, N_2–0.026%
[e] ① O_2–0.061%, N_2–0.015%; ③ O_2–0.060%, N_2–0.014%

Figure 22. The Effect of Welding Gas Purity on the Microhardness of Fusion-Welded Columbium Specimens Before and After Exposure to Lithium. Test Conditions: Static, 1500°F (816°C), 100 hours.

metal of the specimen welded in the purest atmosphere. The extent of oxygen and nitrogen pickup which occurred in the base material and weld zones during the welding operation in the various environments is also given in Figure 22. The base material was essentially unaffected by the type of gaseous environment employed while the weld zone was quite sensitive to the purity of the welding environment.

The results of metallographic studies on specimens containing fusion welds are shown in Figures 23, 24, and 25. The photomicrographs in Figure 23 demonstrate that welds representative of all three environments were corroded intergranularly by lithium, but that the severity of attack decreased with increasing purity of welding environment. The intergranular penetrations in the weld made in the purest environment may be related to grain-boundary segregation of existing base-metal impurities during solidification of the weld.

Catastrophic intergranular failure of the "argon plus air" weld is apparent in all three figures. The surface of this weld contained numerous macroscopic cracks which were easily visible upon removal of the specimen from the lithium bath. The apparent soundness of this weld prior to corrosion testing is demonstrated in Figure 24.

The thin but continuous white surface layer present on the specimens after corrosion testing was identified by x-ray diffraction analysis as columbium nitride. This nitride layer is formed by reaction of columbium with nitrogen in the lithium. The white-etching feathery constituent adjacent to attacked grain boundaries and the rod-like white phase in unattacked grain boundaries shown in

[redacted]

ORNL-LR-DWG 34972

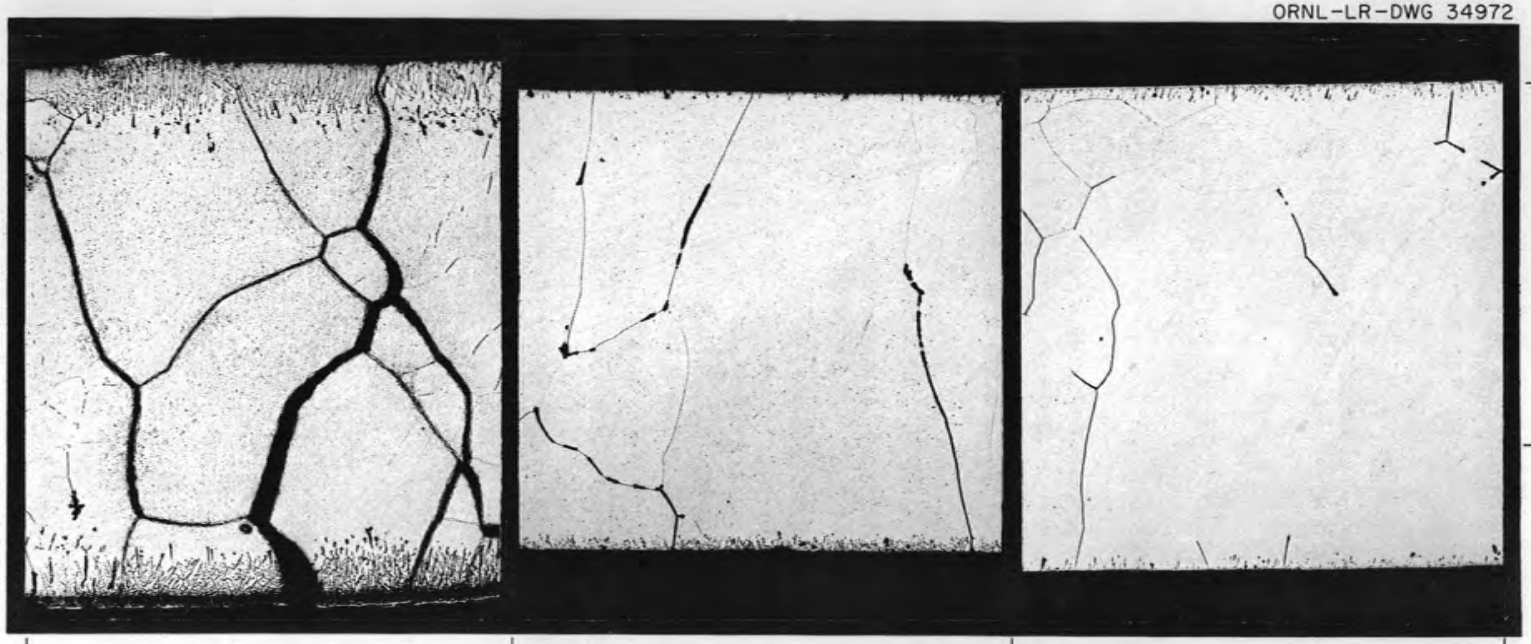

WELDED IN: ARGON + AIR	ARGON + 1600 ppm N_2 + 400 ppm O_2	ARGON + 67 ppm N_2 + 3 ppm O_2
DIAMOND PYRAMID HARDNESS:		
UNWELDED SHEET – 137	137	137
WELDED – 356	155	131
WELDED AND TESTED – 128	105	93

ALL SPECIMENS IN ETCHED CONDITION

Figure 23. Effect of Welding Environment on the Hardness and Lithium Corrosion Resistance of the Fusion-Weld Zone of Columbium Specimens. Test Conditions: Static, 1500°F (816°C), 100 hours.

[redacted]

ORNL-LR-DWG 34973

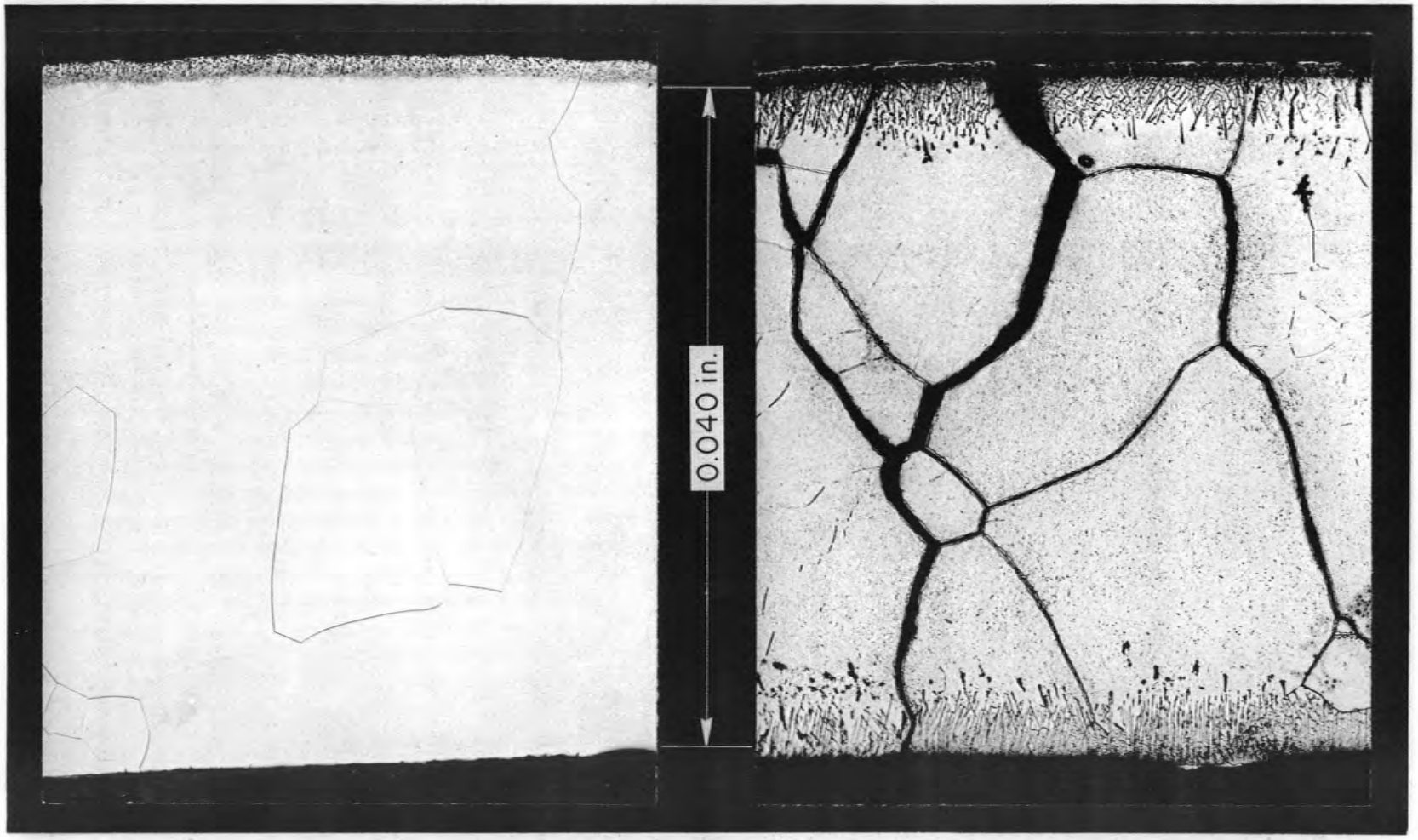

BEFORE (ETCHED,100X) AFTER (ETCHED,100X)

Figure 24. Fusion-Weld Zone of Columbium Specimen Welded in Argon + Air Before and After Exposure to Lithium. Test Conditions: Static, 1500°F (816°C), 100 hours. Reduced 5%.

[redacted]

ORNL-LR-DWG 34974

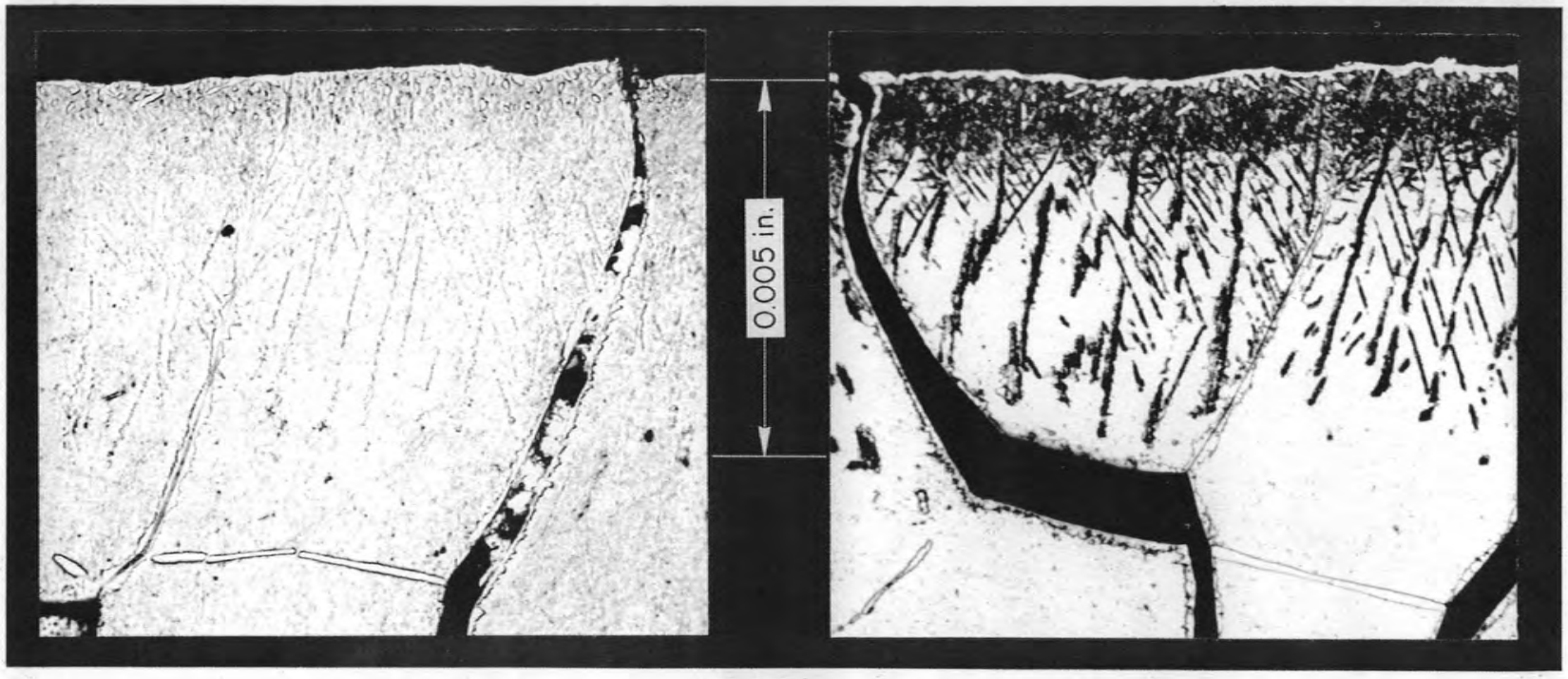

UNETCHED 500X ETCHED 500X

Figure 25. Fusion-Weld Zone of Columbium Specimen Welded in Argon + Air and Exposed to Lithium. Test Conditions: Static, 1500°F (816°C), 100 hours. Reduced 15%.

[redacted]

Figure 25 were presumed to be columbium nitride also, since when viewed at a magnification of 1500X these phases were found to be continuous with the white surface layer.

Surface contamination during "argon plus air" welding resulted in the precipitation of either oxides or nitrides to a depth of approximately 0.001 inch as shown in the as-welded microstructure in Figure 24. It is to be noted that this region was so severely attacked by the etchant following the corrosion test that it appears almost totally black at a magnification of 100X. Some white-etching constituents, similar in appearance to the white nitride layer, are visible in this region at the higher magnification shown in Figure 25.

A dense but more or less shallow Widmanstätten-type precipitate was present in the microstructures of all specimens after corrosion testing. This type of precipitation was also observed in similar specimens which were heat treated in argon for 100 hours at 1500°F (816°C) and not exposed to lithium. This microstructural feature was discernible in the unetched specimens as shown, for example, in Figure 25 but was not pronounced after metallographic etching. The microconstituents responsible for this effect are believed to be oxides or nitrides of columbium formed as the result of the heat treatment. The presence of the continuous, unattacked surface layer of columbium nitride and the general behavior of this region during metallographic preparation suggest that exposure to lithium, per se, was not a factor in the development of the Widmanstätten-type microstructure.

An 85 Zr–15 Cb weight per cent filler-wire alloy[57] was used in the braze-welding studies. This alloy, which melts at a temperature about 1400 Fahrenheit degrees less than the melting point of columbium, was used in an effort to reduce both contamination and grain growth during welding. The effect of braze-welding environment on the hardness of various zones of the specimens before and after exposure to lithium is given in Figure 26. Of particular significance is the marked reduction in hardness of the heat-affected zones after corrosion testing. The hardness in all zones was uniform to within ± 10 diamond pyramid hardness units across the wall thickness except for the heat-affected zone of the "argon plus air" specimen shown in Figure 27. It is important to note that the hardness gradient in the heat-affected zone of this specimen was reversed as a result of exposure to lithium. This effect was attributed to gettering by lithium of oxygen which with nitrogen was responsible for the high as-braze-welded hardness in this zone. The gettering characteristics of lithium were demonstrated in an independent experiment in which the oxygen content of one-eighth-inch cube-shaped columbium specimens were reduced from 4000 to 1500 ppm by exposure to lithium for 100 hours at 1500°F (816°C) while the nitrogen content remained essentially unchanged.

The effect of braze-welding environment on the extent of corrosion attack on columbium is illustrated in Figure 28. The specimen joined in the purest environment showed no attack while the specimen joined in the most contaminated environment was heavily

[redacted]

ORNL-LR-DWG 34975

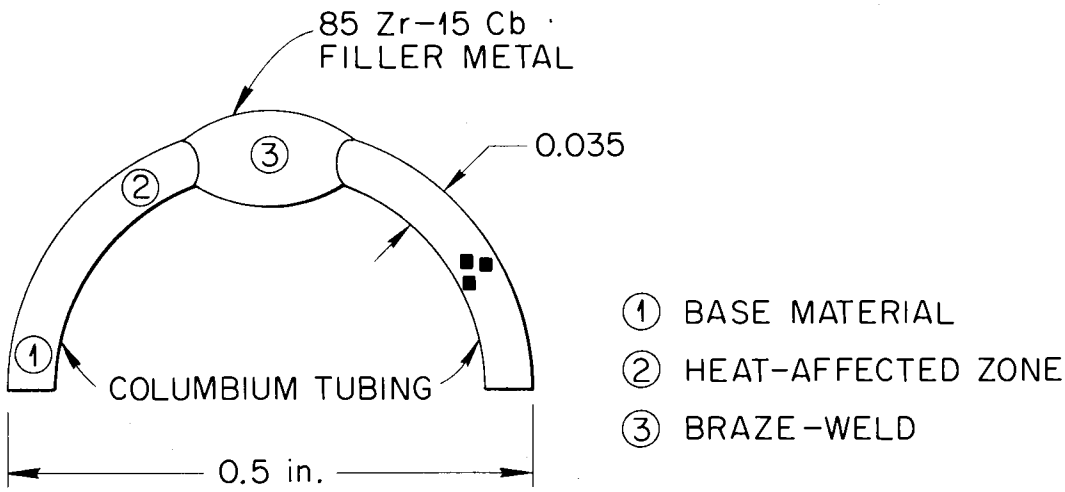

BRAZE-WELDING ENVIRONMENT	DIAMOND PYRAMID HARDNESS* (500g LOAD)					
	AS BRAZE-WELDED			FOLLOWING TEST IN LITHIUM		
	①	②	③	①	②	③
ARGON + AIR	129	360	361	112	94	343
ARGON + 1600 ppm N_2 + 400 ppm O_2	120	114	285	104	98	246
ARGON + 67 ppm N_2 + 3 ppm O_2	113	122	289	105	98	242

*AS-RECEIVED ARC CAST Cb: O_2-0.038%, N_2-0.002%, C-0.014%; D.P.H. -137. EACH HARDNESS VALUE IS AVERAGE OF THREE DETERMINATIONS TAKEN AS SHOWN SCHEMATICALLY IN SKETCH.

Figure 26. The Effect of Welding Gas Purity on the Microhardness of Braze-Welded Columbium Specimens Before and After Exposure to Lithium. Test Conditions: Static, 1500°F (816°C), 100 hours.

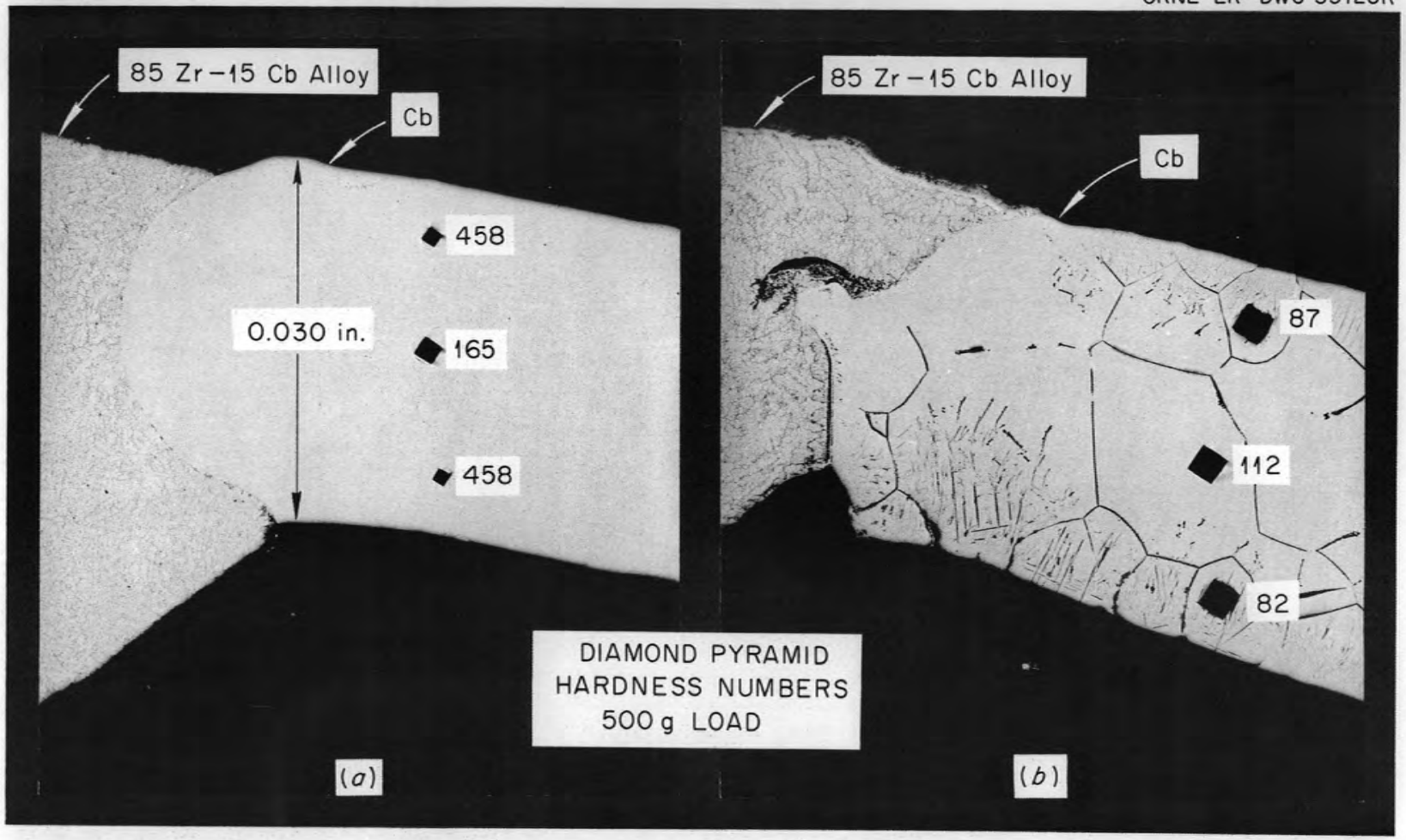

SPECIMENS IN THE AS POLISHED CONDITION
(*a*) AFTER BRAZE-WELDING
(*b*) AFTER BRAZE-WELDING AND EXPOSURE TO LITHIUM

Figure 27. Columbium Braze-Welded in Argon + Air. Test Conditions: Static, 1500°F (816°C), 100 hours.

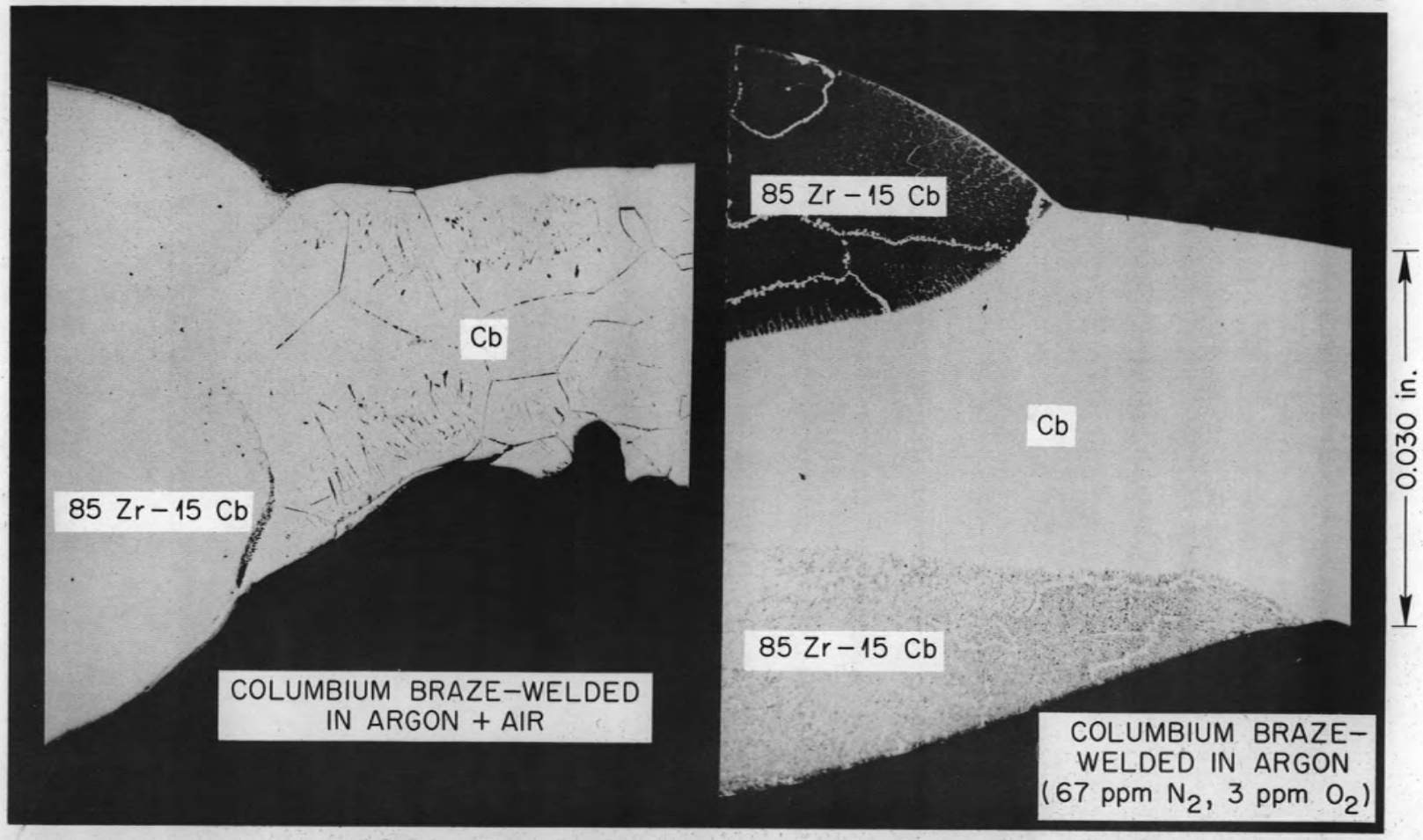

AS POLISHED – 75X

AS POLISHED – 75X

Figure 28. Effect of Braze-Welding Environment on the Corrosion Resistance of Columbium to Lithium. Test Conditions: Static, 1500°F (816°C), 100 hours. Reduced 10%.

attacked. A Widmanstätten-type precipitate similar to that observed in the fusion-welded specimens is visible in the as-polished microstructures of the "argon plus air" specimen after corrosion testing, shown in Figures 27 and 28. In brief summary, the welding environment studies showed clearly that contamination by oxygen and nitrogen renders columbium susceptible to corrosion attack by lithium and indicated that an investigation of the effect of each of these contaminants considered individually was in order.

3. The Effects of Oxygen and of Nitrogen. The separate effects of oxygen and nitrogen were investigated using specimens to which controlled amounts of these gases had been added in a modified Sieverts' gas-absorption apparatus. The concentration levels studied are given in Table V. According to the portions of phase diagrams[58,59] shown in Figures 29 and 30, concentrations in excess of the limit of solid solubility at the corrosion test temperature of 1500°F (816°C) were represented in both the oxygen series and the nitrogen series.

The specimens were tested in static lithium for 100 hours in three heat-treated conditions: (1) homogenized at 1832°F (1000°C) for 2.5 hours, (2) homogenized and aged at 1000°F (538°C) for 336 hours, and (3) homogenized and "welded" by subjection to a single fusion pass in relatively pure argon containing 20 ppm oxygen and 75 ppm nitrogen. All specimens were tested in a single columbium capsule to eliminate lithium purity as a test variable. The lithium used contained 245 ppm oxygen and 69 ppm nitrogen.

TABLE V

EFFECT OF OXYGEN AND NITROGEN ADDITIONS ON WEIGHT CHANGE OF COLUMBIUM SPECIMENS EXPOSED TO STATIC LITHIUM AT 1500°F (816°C) FOR 100 HOURS

ADDITIONS[a]		WEIGHT CHANGE (mg/in.^{2}) AFTER TEST		
OXYGEN, Wt %	NITROGEN, Wt %	HOMOGENIZED[b]	HOMOGENIZED AND AGED[c]	HOMOGENIZED AND "WELDED"[d]
0	0	+0.3	+0.5	+0.8
0.056	0	0	0	+0.3
0.111	0	0	0	+0.5
0.237	0	−1.2	−0.9	−1.2
0.371	0	−3.3	−4.2	−3.9
0.527	0	−7.2	−7.7	−5.5
0	0.061	−0.5	+0.3	0
0	0.134	−0.3	0	−1.7[e]

[a]AS-RECEIVED ANALYSIS IN WEIGHT PER CENT: O_2 – 0.0061; N_2 – 0.0046; C – 0.0007; H_2 – 0.0005; Zr – 0.074.

[b]HOMOGENIZED AT 1832°F (1000°C) FOR 2.5 HOURS.

[c]AGED AT 1000°F (538°C) FOR 336 HOURS.

[d]FUSION PASS MADE IN CENTER OF 0.5-INCH × 0.5-INCH × 0.040-INCH SPECIMEN IN ARGON ATMOSPHERE CONTAINING 20 ppm O_2 AND 75 ppm N_2.

[e]PART OF WEIGHT LOSS DUE TO CHIPPING OF SPECIMEN EDGE FOLLOWING TEST.

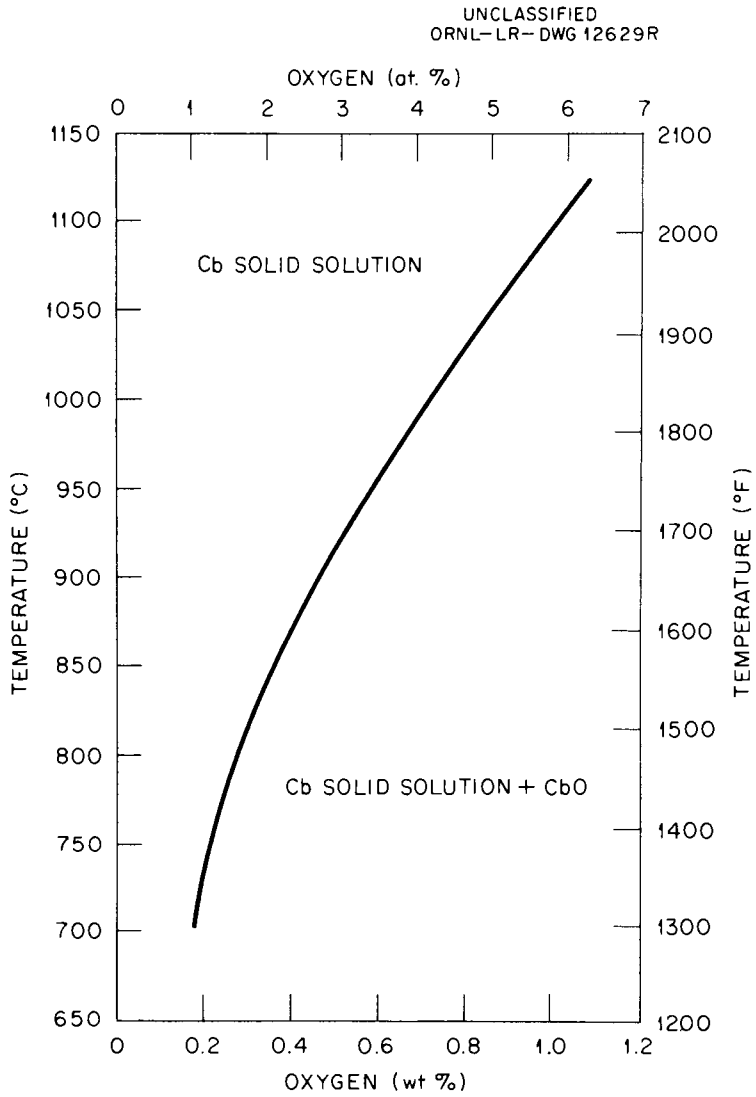

Figure 29. Solubility of Oxygen in Solid Columbium.

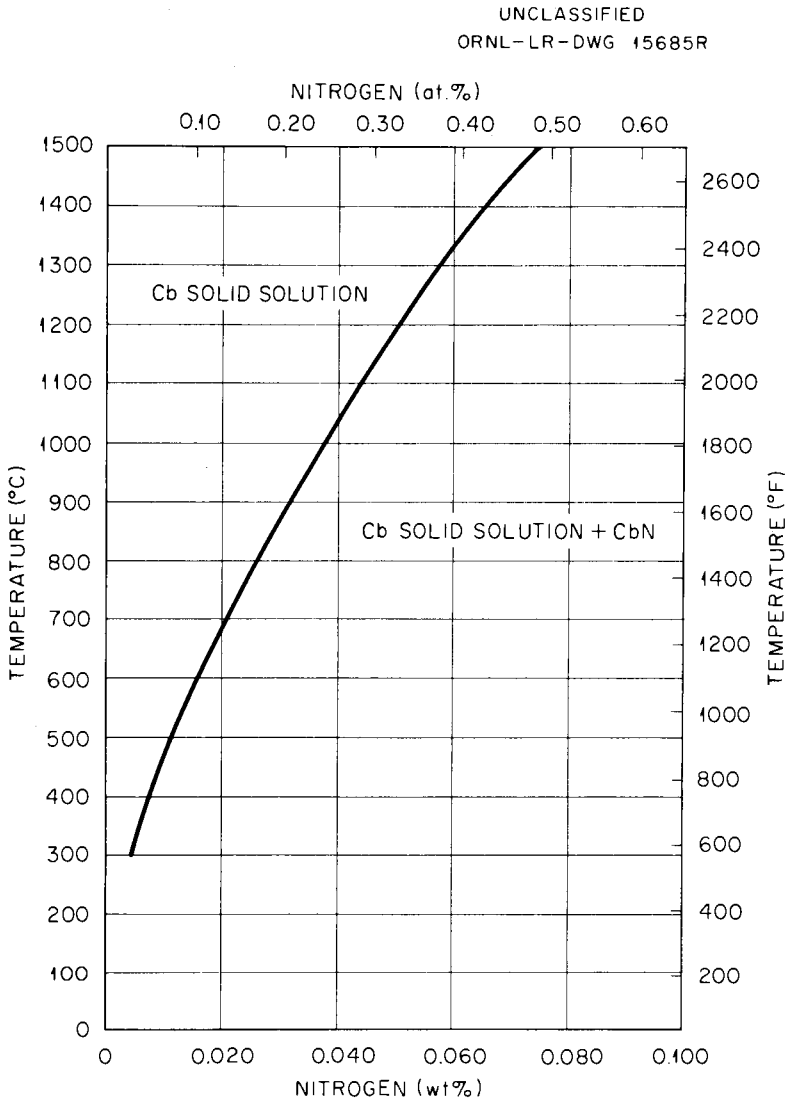

Figure 30. Solid Solubility of Nitrogen in Columbium.

Evaluation of the test results was based on metallography and on weight and hardness changes. Since the heat treatments performed were found to have no effect on the corrosion resistance, the results of metallographic and hardness studies on specimens representing only one condition of heat treatment were selected for presentation in this report. In view of the data presented in the previous sections, the "welded" specimens were chosen for this purpose.

Weight changes after exposure to lithium are given in Table V. It is to be noted that regardless of heat treatment the high-oxygen specimens showed substantial weight losses while the specimens charged with nitrogen were affected only slightly. The surfaces of the most heavily contaminated specimens after corrosion testing are compared in the photomacrographs of Figure 31. The mottled appearance of the high-oxygen specimen is indicative of surface grain removal. Severe cracking can be seen in the weld and heat-affected zones of this specimen.

The results of hardness studies are given in Table VI. The drastic reduction in hardness of the high-oxygen specimen after corrosion testing is attributed to the removal of interstitial oxygen by the gettering action of lithium, as discussed in the previous section. The relatively moderate softening which occurred in the high-nitrogen specimens after exposure to lithium appears to have been due to the effects of heat treatment alone. The specimens to which no contaminants had been added showed essentially no change in

[redacted]

ORNL-LR-DWG 34978

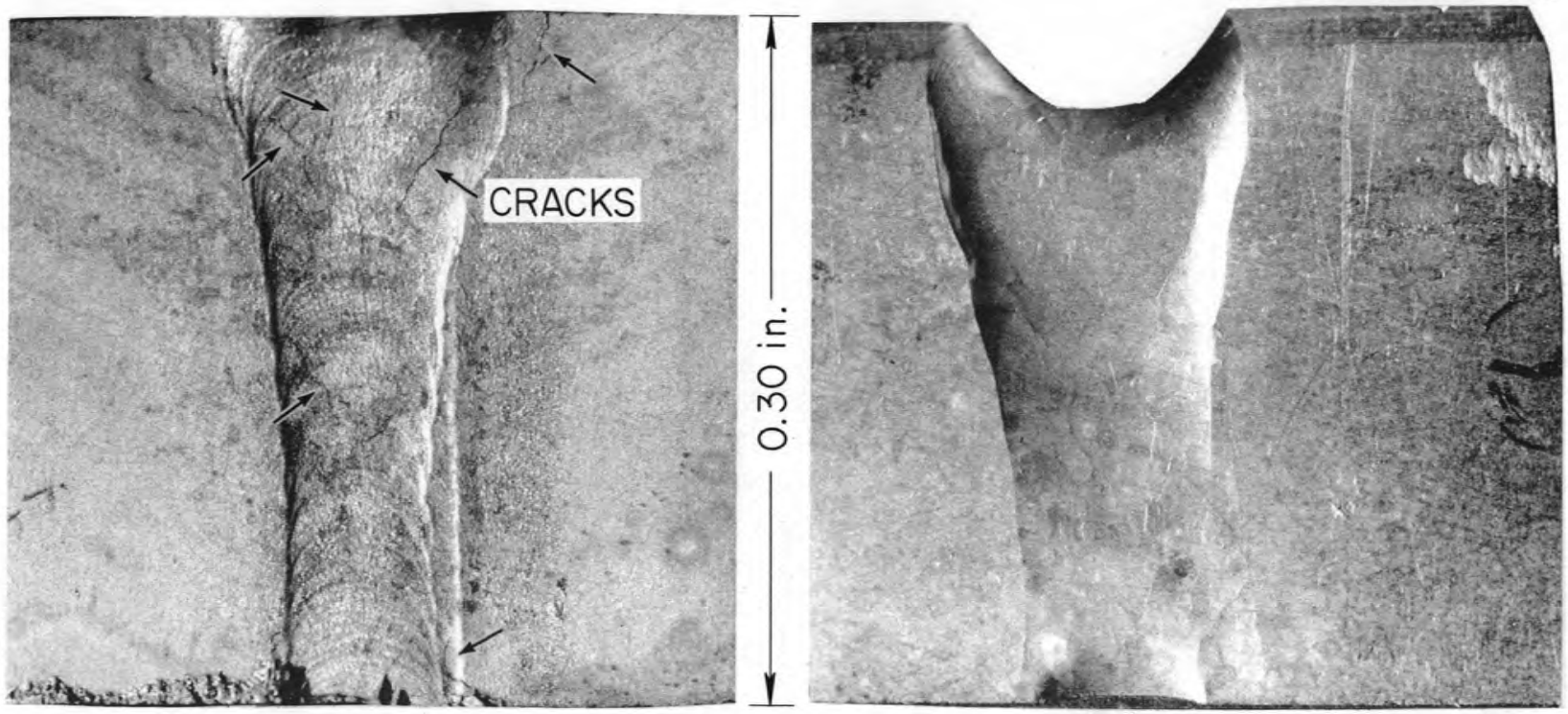

WEIGHT CHANGE IN Li = −5.5 mg/in.^{2}

(*a*) 0.527% O_2 ADDED TO Cb PRIOR TO WELDING

WEIGHT CHANGE IN Li = −1.7 mg/in.^{2}

(*b*) 0.134% N_2 ADDED TO Cb PRIOR TO WELDING

Figure 31. Columbium Weld Specimens Following Exposure to Lithium for 100 hr at 1500°F (816°C). Specimens Welded in Argon Containing 20 ppm O_2 and 75 ppm N_2.

TABLE VI

EFFECT OF HEAT TREATMENT AND EXPOSURE TO LITHIUM ON THE HARDNESS OF CONTAMINATED COLUMBIUM WELD SPECIMENS

Specimen Treatment	Diamond Pyramid Hardness (500 gram load)	
	Base Material	Weld Zone
1. As-Received Columbium Sheet[b]		
(a) following welding[c]	80	96
(b) a) plus 100 hr-1500°F in Argon	91	101
(c) a) plus 100 hr-1500°F in Lithium	87	84
2. Oxygen Added (0.527 weight per cent)		
(a) following welding	330	366
(b) a) plus 100 hr-1500°F in Argon	242	241
(c) a) plus 100 hr-1500°F in Lithium	71	85
3. Nitrogen Added (0.134 weight per cent)		
(a) following welding	220	231
(b) a) plus 100 hr-1500°F in Argon	151	155
(c) a) plus 100 hr-1500°F in Lithium	122	137

[a]Each hardness value is an average of three determinations.

[b]As-received analysis in weight per cent: O_2 - 0.0061; N_2 - 0.0046; C - 0.0007.

[c]All specimens homogenized at 1832°F (1000°C) for 2-1/2 hours prior to welding.

hardness. Metallographic examination revealed that these specimens had undergone no attack and no change in microstructure after corrosion testing.

As-polished microstructures of the most heavily contaminated specimens in both series are shown in Figures 32 through 36. Figures 32 and 34 show that the high-nitrogen specimen was not attacked and that the grain-boundary phase, which at the higher magnification in Figure 34 is seen to extend to the surface of this specimen, was not affected by lithium during the test. This phase has been identified metallographically as columbium nitride.

The marked effect of oxygen is illustrated in Figures 33 through 36. In Figure 33, it is evident that in the high-oxygen specimen every grain boundary suffered attack. In spite of the extreme care exercised in metallographic preparation, several grains in the interior of this specimen became dislodged during polishing. The nickel plate shown on the specimen in Figure 34 was deposited for purposes of edge preservation during polishing.

The increase in attack by lithium as a function of the oxygen content of the columbium is illustrated in Figure 35. It is to be observed in this series of photomicrographs that the extent of grain-boundary attack was appreciable even at oxygen levels considerably less than the reported oxygen solubility limit of about 0.3 per cent at 1500°F (816°C).

Examination of the weld zone of the high-oxygen specimen in Figure 36 at a magnification of 750X reveals two corrosion products

[redacted]

ORNL-LR-DWG 34979

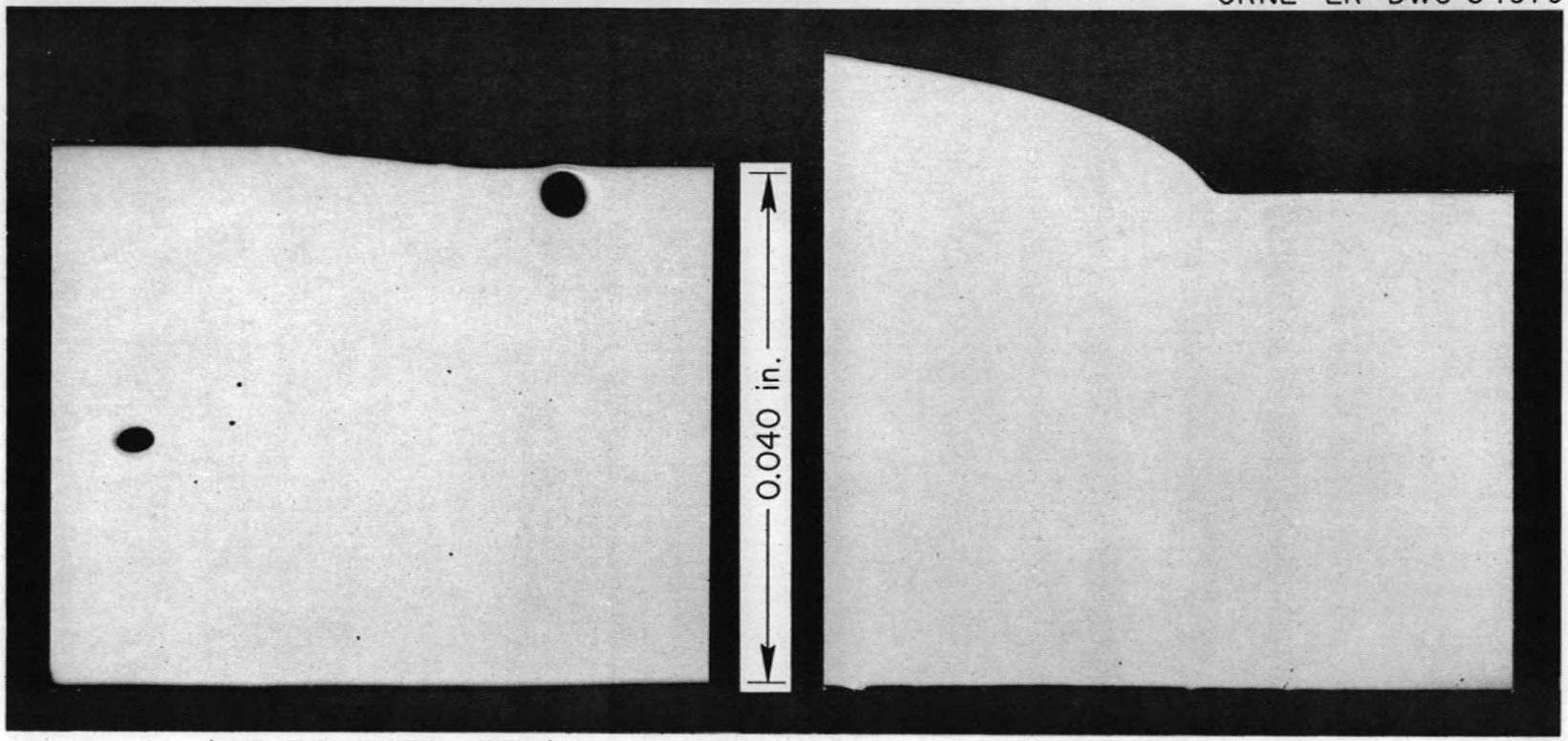

(AS POLISHED—75X) (AS POLISHED—75X)

(*a*) BEFORE EXPOSURE TO LITHIUM (*b*) AFTER EXPOSURE TO LITHIUM

Figure 32. Weld Zones of Columbium Specimens to Which 0.134% N_2 was Added Prior to Welding. Test Conditions: Static, 1500°F (816°C), 100 hours. Reduced 4%.

[redacted]

ORNL-LR-DWG 34980

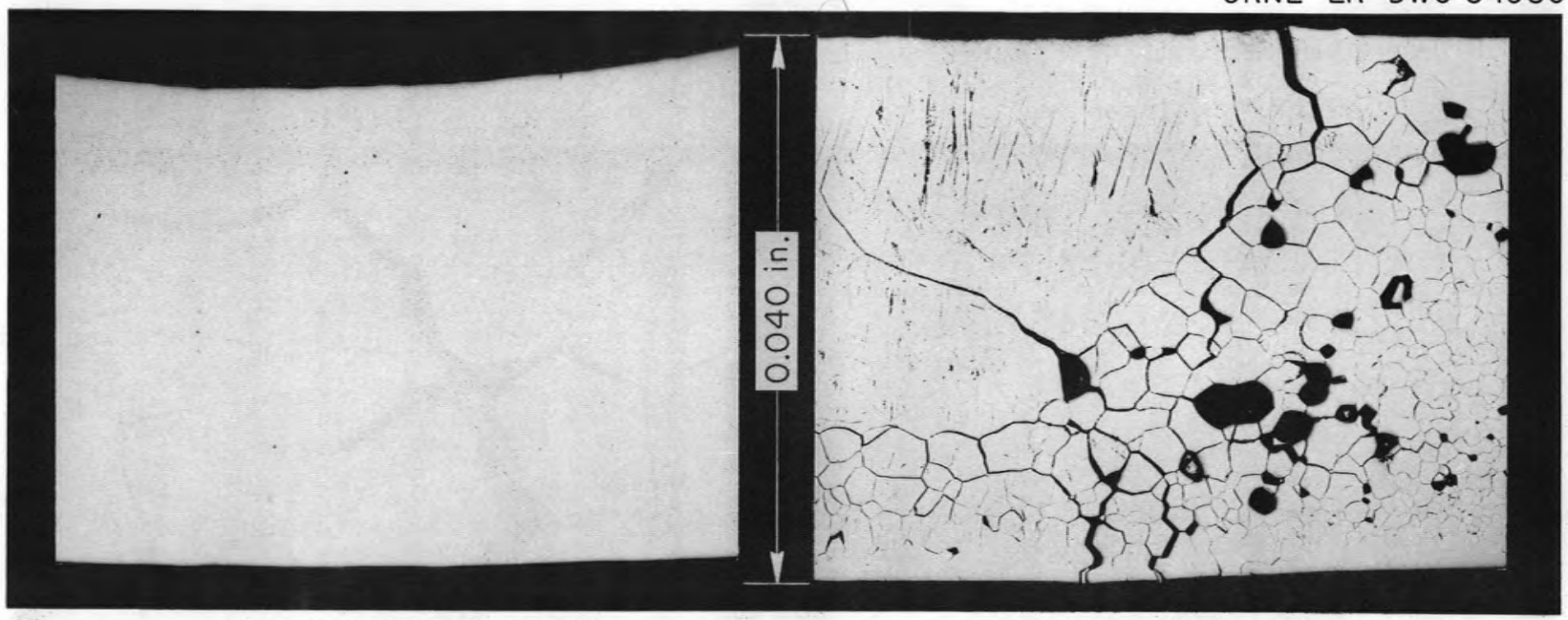

(AS POLISHED-75X)

(*a*) BEFORE EXPOSURE TO LITHIUM

(AS POLISHED-75X)

(*b*) AFTER EXPOSURE TO LITHIUM

Figure 33. Weld Zones of Columbium Specimens to which 0.527% O_2 was Added Prior to Welding. Test Conditions: Static, 1500°F (816°C), 100 hours. Reduced 5%.

[redacted]

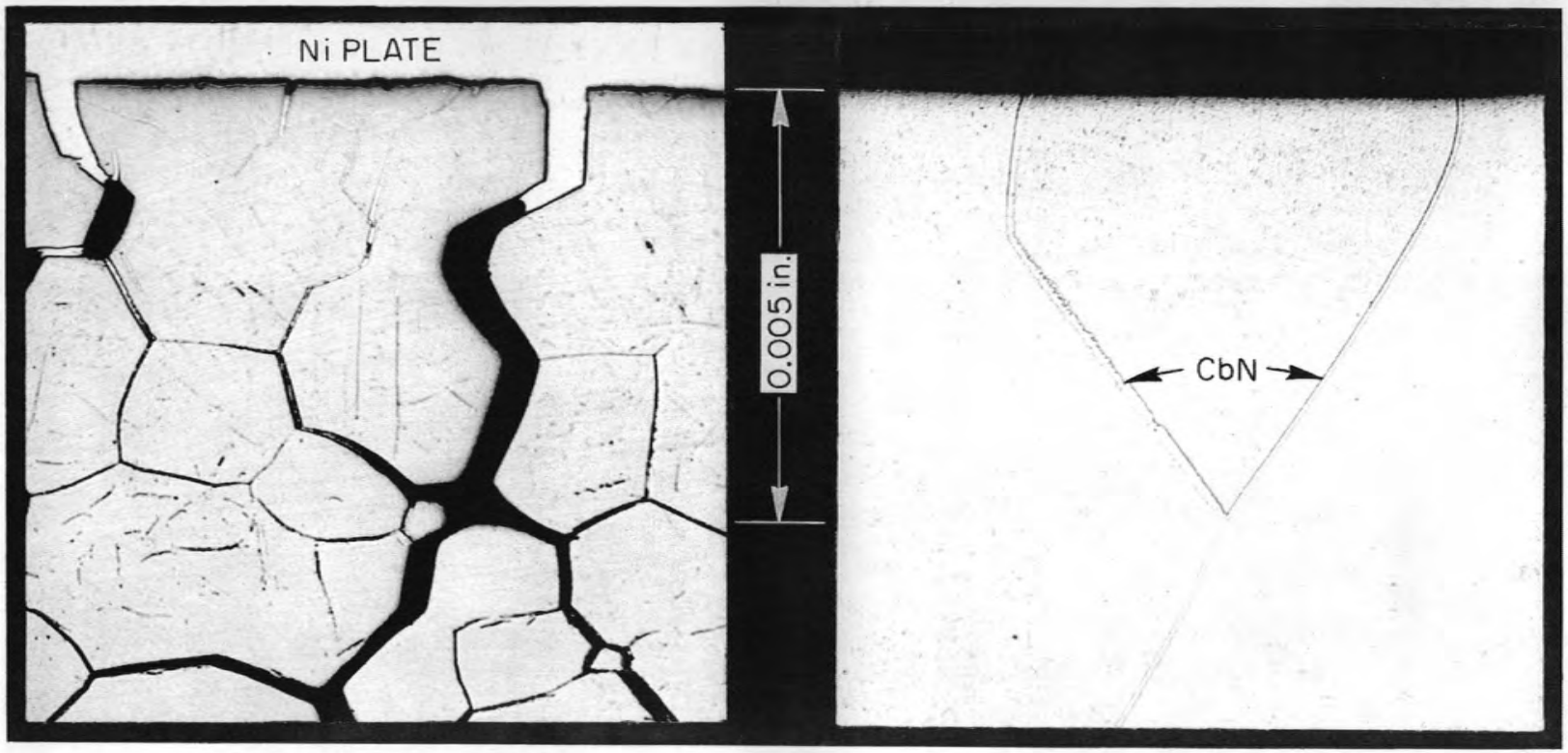

(AS POLISHED-500X)

(*a*) 0.527 % O_2 ADDED PRIOR TO WELDING

(AS POLISHED-500X)

(*b*) 0.134 % N_2 ADDED PRIOR TO WELDING

Figure 34. Weld Zones of Columbium Specimens Following Exposure to Lithium. Test Conditions: Static, 1500°F (816°C), 100 hours. Reduced 7%.

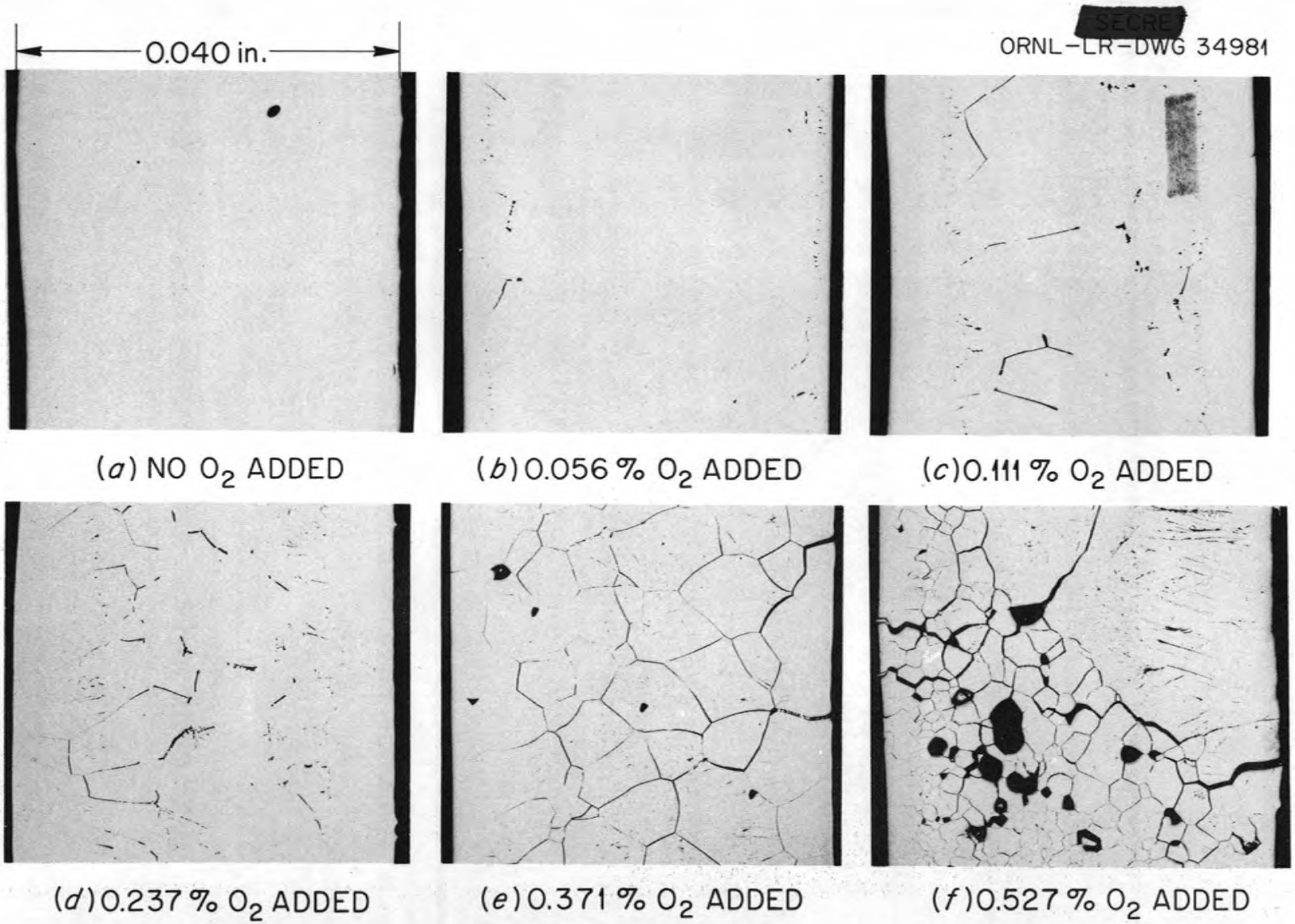

Figure 35. Fusion-Weld Zones of Columbium Specimens to which Varying Amounts of Oxygen were Added Prior to Welding. Specimens Shown in As-Polished Condition after Exposure to Lithium. Test Conditions: Static, 1500°F (816°C), 100 hours.

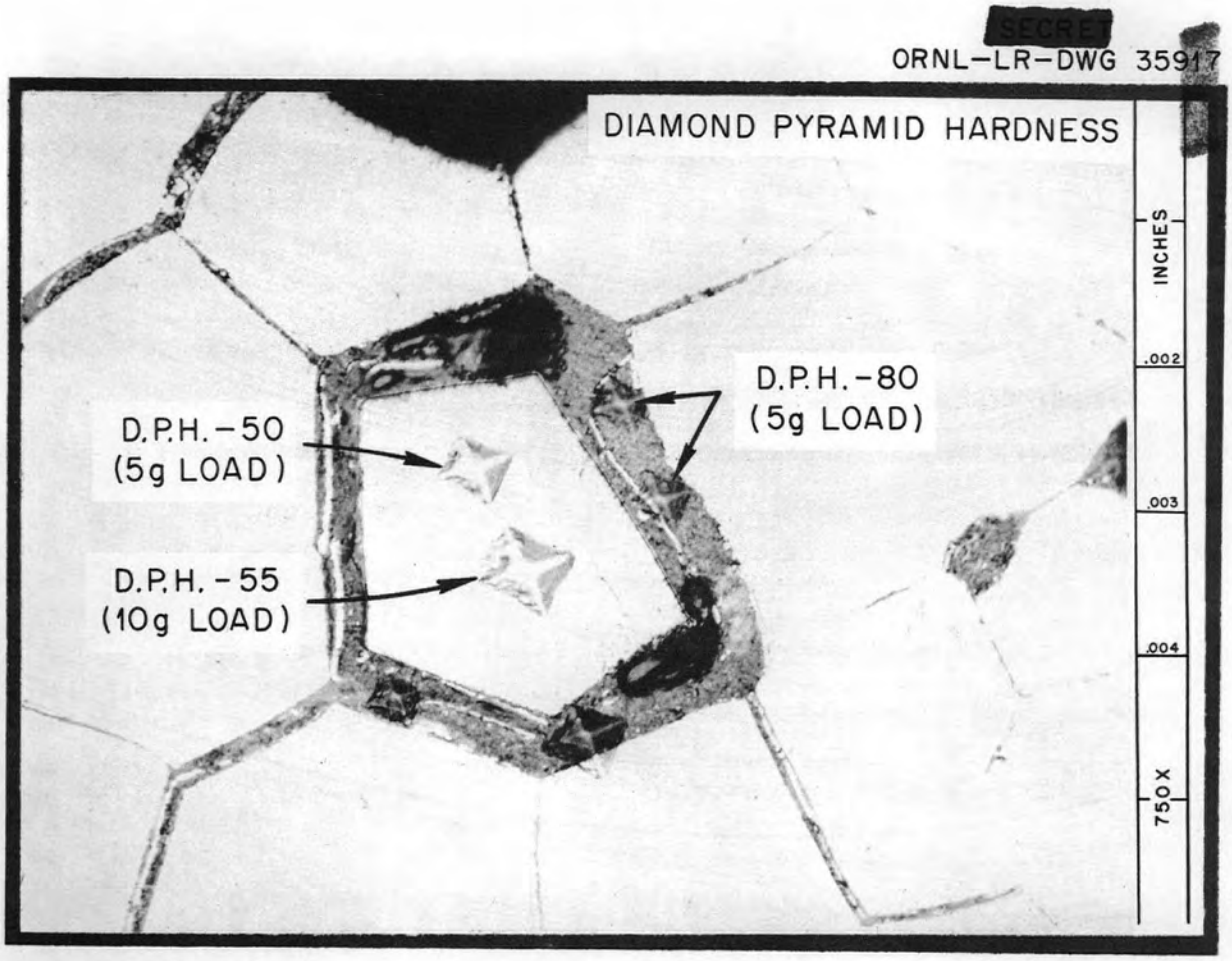

Figure 36. Grain-Boundary Corrosion Products in Weld Zone of Columbium Specimen to which 0.527% Oxygen was Added Prior to Welding. Specimen was Exposed to Lithium for 100 hours at 1500°F (816°C). As Polished, 750X.

in the grain boundaries. One of these phases is metallic in appearance and is present in the form of long stringers and small particles. The darker and more continuous grain-boundary phase has a ceramic-like appearance and was extremely difficult to retain during metallographic polishing.

The hardness of the grain-boundary corrosion products was DPH 80. The extreme softness of the columbium grains is interpreted as indicating that exposure to lithium resulted in drastic lowering of the oxygen content in these areas.

The evidence cited thus far clearly indicates that oxygen is by far more effective than nitrogen in promoting the susceptibility of columbium to grain-boundary attack by lithium. Moreover, it is evident that oxygen is particularly detrimental when present in amounts grater than its reported solubility limit in columbium and that nitrogen has no effect at comparable concentration levels. That these observations are consistent with the relative thermodynamic stabilities of columbium nitride and columbium oxides in molten lithium is shown by the calculated standard free energy of reaction values[60,61] listed in Table VII. In view of this correlation, it is proposed that the metallic phase in the duplex grain-boundary corrosion product shown in Figure 36 is columbium metal and the ceramic-

TABLE VII

RELATIVE THERMODYNAMIC STABILITIES OF COLUMBIUM OXIDES AND COLUMBIUM NITRIDE IN LITHIUM

Reaction	$\Delta F^\circ_{816°C}$ (K cal)
$2\ Li + CbO = Li_2O + Cb$	- 31.7
$2\ Li + 1/2\ CbO_2 = Li_2O + 1/2\ Cb$	- 34.2
$2\ Li + 1/5\ Cb_2O_5 = Li_2O + 2/5\ Cb$	- 37.7
$3\ Li + CbN = Li_3N + Cb$	+ 24.9

like phase is lithium oxide.* The staining phenomenon mentioned earlier is accordingly attributed to the formation of lithium hydroxide by the reaction of lithium oxide in the grain boundaries with moisture in the atmosphere. The cracks observed on the surface of the high-oxygen specimens are attributed to the volume expansion which would occur as a result of the grain-boundary corrosion reaction. Based on room-temperature densities,[62,63] the formation of the proposed reaction products would be accompanied by a 47 per cent increase in volume.

Additional corrosion tests were performed on eight different lots of columbium tubing at 1500°F (816°C) and at 1800°F (982°C). At each temperature the specimens were contained in a single columbium capsule to eliminate lithium purity as a test variable. The results of these tests are presented in Table VIII in the form of metallographic observations. It is to be noted that the attack on most of the tube specimens was quite erratic. The inside surfaces of some specimens were attacked while the outside surfaces were not; in other cases the reverse was true. An example of this type of inconsistent behavior is shown in Figure 37. These metallographic results suggest that the tubing was contaminated with oxygen during manufacture and

*In this connection a comment is in order concerning experiments in which the effects of additions of oxygen and nitrogen to lithium were studied. Approximately 5000 ppm of each of these contaminants were added in separate experiments in the form of lithium oxide and lithium nitride, respectively. After 100-hour exposures at 1500°F (816°C), no attack was observed in any of the specimens in this study in spite of the impurity additions to the lithium. The only effect noted was the formation of a thin columbium-nitride surface layer on the specimens exposed to lithium to which nitrogen was added.

TABLE VIII

RESULTS OF LITHIUM CORROSION TESTS ON EIGHT LOTS OF COLUMBIUM TUBING[a]

TEST CONDITIONS: STATIC, 100 HOURS

TUBING CODE	COMPOSITION (Wt %)				RESULTS			
					1500°F (816°C)		1800°F (982°C)	
	O_2	N_2	H_2	C	INSIDE	OUTSIDE	INSIDE	OUTSIDE
WC-1	0.033	0.042	0.0053	0.030	No attack	No attack	No attack	No attack
WC-2	0.050	0.018	0.0026	0.0077	Subsurface phase to *1.5 mils*	No attack	No attack	No attack
ST-2	0.061	0.022	0.0009	0.017	No attack	Subsurface phase to *1 mil*	No attack	Subsurface phase to *1 mil*
F-8	0.013	0.0088	0.0008	0.0041	No attack	No attack	No attack	No attack
WC-3[b]	0.051	0.050	0.0004	0.0031	No attack	Subsurface phase to *2 mils*	No attack	Subsurface phase to *1 mil*
WC-4[b]	0.045	0.037	0.0001	0.0018	No attack	Subsurface phase *2–4 mils*	No attack	Subsurface phase to *2.5 mils*
WC-5[b]	0.026	0.0066	0.0002	0.0045	No attack	Subsurface phase to *1.5 mils*	No attack	No attack
ST-1[b]	0.080	0.032	0.0005	0.016	Subsurface phase to *1.5 mils*	Subsurface phase to *2 mils*	Subsurface phase to *1.5 mils*	Subsurface phase to *2.5 mils*

[a]0.5 IN. O.D. × 0.030 IN. WALL.

[b]TYPE 446 STAINLESS STEEL CLADDING MECHANICALLY STRIPPED FROM COLUMBIUM TUBING PRIOR TO CORROSION TESTS.

ORNL-LR-DWG 34984

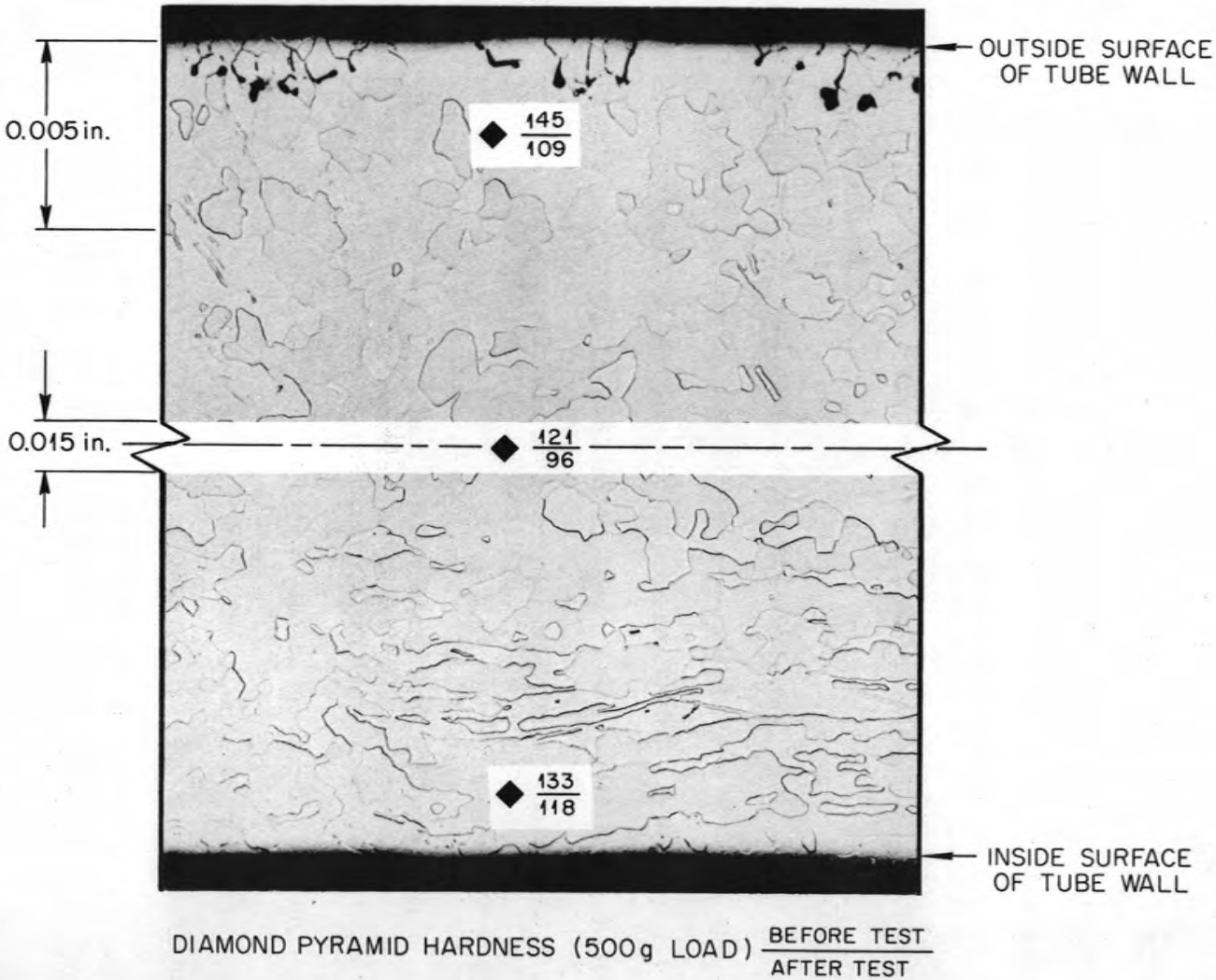

Figure 37. Outside and Inside of Tube Wall of Columbium Specimen Following Exposure to Lithium (Both Sides Exposed to Lithium). Test Conditions: Static, 1500°F (816°C), 100 hours. Etched.

that careful control of processing techniques will be required to produce columbium tubing which is totally corrosion resistant to lithium. It is of interest to note that according to the data in Table VIII the specimen with the highest oxygen content sustained the heaviest and most consistent attack and that no attack was observed on the specimen of lowest oxygen content. These specimens are designated in the table as St-1 and F-8, respectively.

Alloys. Nickel-, cobalt-, and iron-base alloys have been tested in two-component static test systems. The results of these tests are discussed below:

1. Nickel- and Cobalt-Base Alloys. The results of tests on various nickel- and cobalt-base alloys are listed in Table IX. The alloying elements, chromium, iron, and molybdenum, improve the corrosion resistance of nickel. Additions of copper to nickel (Monel) and aluminum to nickel (Duranickel), on the other hand, lead to rapid attack by lithium.

Many of the nickel-base alloy test specimens were covered with small, well-bonded metal crystals which probably precipitated from the liquid solution during cooling from the test temperature.

The one test on a cobalt-base alloy indicated that its corrosion resistance was not as good as that of the better nickel-base alloys, such as the Hastelloys and Inconel. This is believed to be due to the relatively high carbon content of the particular cobalt-base alloy studied.

TABLE IX

RESULTS OF 100-HOUR LITHIUM CORROSION TESTS ON NICKEL-BASE AND COBALT-BASE ALLOYS IN TWO-COMPONENT STATIC TEST SYSTEMS
Surface Area/Volume of Lithium = 13 in.^{2}/in.^{3}

Alloy	Nominal Composition Weight Per Cent	Weight Change mg/in.^{2}	Metallographic Observations
1500°F (816°C)			
D-Nickel[a]	95Ni-4.5Mn	--	Solution-type attack to depth of 2 mils. Mass transfer crystals on tube and specimen.
Duranickel[a]	94Ni-4.5Al	--	Complete intergranular penetration of 35-mil tube wall.
Nichrome V[a]	80Ni-20Cr	+ 12.5	1 mil of intergranular attack. 0.2 mils of crystals attached to specimen surface.
Inconel[a]	80Ni-14Cr-6Fe	+ 6.1	1 mil of intergranular attack and solution. Extremely hard crystals (0.5 mil thick) attached to surface.
Inconel X[a]	73Ni-15Cr-7Fe-2Ti	+ 17.5	1 mil of intergranular attack. Small crystals attached to surface.
Monel[a]	67Ni-30Cu	--	Portions of 35-mil-thick tube wall completely dissolved. Copper-colored crystals (composition 95Cu-5Ni) in lithium.
Hastelloy R	65Ni-14Cr-10Fe-6Mo	- 4.7	Attacked to a depth of 0.25 mils.
Hastelloy B	64Ni-28Mo-6Fe	0	1 mil of attack in a few scattered areas.
Haynes Alloy 25[a]	50Co-20Cr-15Mo-10Ni	- 1.5	Intergranular attack to a maximum depth of 8 mils.
1832°F (1000°C)			
Inconel	80Ni-14Cr-6Fe	+ 12	Up to 4 mils scattered attack in the form of small subsurface voids. Specimen covered with 0.25-mil layer of nickel crystals.

[a]Duplicate tests.

2. Iron-Base Alloys. The results of two-component tests on thirteen different commercial iron-base alloys are listed in Table X and Table XI. Except for the 1035 plain-carbon steel and Multimet, the alloys studied belong to that classification of materials known as the stainless steels, with chromium and nickel or chromium alone as major alloying elements. For the most part, tests were carried out at 1400°F (816°C) for 100 hours (Table X) and at 1832°F (1000°C) for 400 hours (Table XI). Four main features of the experimental results are treated separately in the following discussion.

(a) The 35-mil tube wall of the plain-carbon 1035 steel underwent complete intergranular penetration after 100 hours at 1500°F (816°C). This result is consistent with that reported in the previous section for Armco ingot iron in which austenite containing approximately 0.3 weight per cent carbon was present as a second phase at 1500°F (816°C).

(b) Examination of the surfaces of the stainless steels tested for 100 hours at 1500°F (816°C) revealed the presence of carbide crystals in all but two cases. An example of this is shown in Figure 38 for type 316 stainless steel. Crystals of this type have been detected in larger amounts on type 446 stainless steel in seesaw and thermal-convection loop systems and have been identified by x-ray analysis as the chromium carbide ($Cr_{23}C_6$). Because their etching behavior, microhardness, and shape were similar to those of the crystals formed on the type 446 alloy in seesaw and loop tests, crystals of the type shown in Figure 38 and reported in Table IX are

TABLE X

RESULTS OF 100-HOUR LITHIUM CORROSION TESTS ON IRON-BASE ALLOYS IN TWO-COMPONENT STATIC TEST SYSTEMS[a] AT 1500°F (816°C) AND 1700°F (927°C)

Alloy[b]	Nominal Composition Weight Per Cent	Weight Change mg/in.^{2}	Metallographic Observations
1500°F (816°C)			
1035 Steel[c]	98Fe-0.35C	- 1	Complete intergranular penetration of 35-mil tube wall.
304 SS[c]	69Fe-19Cr-10Ni-0.08C max.	0	No attack. Carbide crystals on surface.
309 SS[c]	62Fe-23Cr-13Ni-0.02C max.	- 1	Scattered intergranular penetration to maximum depth of 4 mils. Carbide crystals on surface.
310 SS[c]	53Fe-25Cr-20Ni-0.25C max.	- 1	Intergranular penetration to depth of 7 mils. Carbide crystals on surface.
316 SS[c]	67Fe-17Cr-12Ni-2Mo-0.10C max.	0	Intergranular penetration to depth of 0.5 mils. Carbide crystals on surface.
317 SS[c]	64Fe-19Cr-12Ni-3Mo-0.10C max.	+ 1	No attack. Carbide crystals on surface.
330 SS	48Fe-15Cr-35Ni-0.25C max.	- 5	Subsurface voids to depth of 2 mils. Carbide crystals on surface.
347 SS[c]	69Fe-18Cr-10Ni-1Cb-0.08C max.	0	No attack.
446 SS	73Fe-25Cr-0.35C max.	+ 3	Intergranular penetration to depth of 10 mils.
Incoloy[c]	42Fe-34Ni-21Cr-0.10C max.	0	Intergranular penetration to depth of 1 mil. Carbide crystals on surface.
Multimet[c]	32Fe-21Cr-20Ni-20Co-0.12C max.	0	No attack.
1700°F (927°C)			
446 SS[c]	82Fe-16Cr-0.35C max.	-12	Intergranular penetration to depth of 35 mils.

[a]Surface area/volume of lithium = 13 in.^{2}/in.^{3}

[b]SS stands for Stainless Steel.

[c]Duplicate tests.

TABLE XI

RESULTS OF LITHIUM CORROSION TESTS ON IRON-BASE ALLOYS IN TWO-COMPONENT STATIC TEST SYSTEMS[a] AT 1832°F (1000°C)

Alloy[b]	Nominal Composition Weight Per Cent	Time Hour	Weight[c] Change mg/in.^{2}	Metallographic Observations
304 SS	69Fe-19Cr-10Ni-0.08C max.	400	- 12	Intergranular penetration to depth of 2 mils. Ferrite formation.
304L SS	69Fe-19Cr-10Ni-0.03C max.	400	--	Intergranular penetration to depth of 2 mils. Ferrite formation. Crystal platelets on specimen surface.
309 SS	62Fe-23Cr-13Ni-0.20C max.	400	- 2	No attack. A few carbide crystals on surface.
316 SS	67Fe-17Cr-12Ni-2Mo-0.10C max.	100	- 3	Intergranular penetration to depth of 2 mils.
316 SS	67Fe-17Cr-12Ni-2Mo-0.10C max.	400	- 4	Intergranular penetration to depth of 3 mils.
316 SS	67Fe-17Cr-12Ni-2Mo-0.10C max.	400	--	Intergranular penetration to depth of 2 mils. Ferrite formation. Crystal platelets on specimen surface.
347 SS	69Fe-18Cr-10Ni-1Cb-0.08C max.	400	--	Intergranular penetration to depth of 10 mils on one end of specimen. Many crystal platelets on specimen surface.
430 SS	82Fe-16Cr-0.12C max.	400	--	Intergranular penetration to depth of 7 mils. Crystal platelets on specimen surface.

[a]Surface area/volume of lithium = 13 in.^{2}/in.^{3}

[b]SS stands for Stainless Steel.

[c]Specimens covered with mass transfer crystals were not weighed after test.

UNCLASSIFIED
Y-10026, Mn-7303

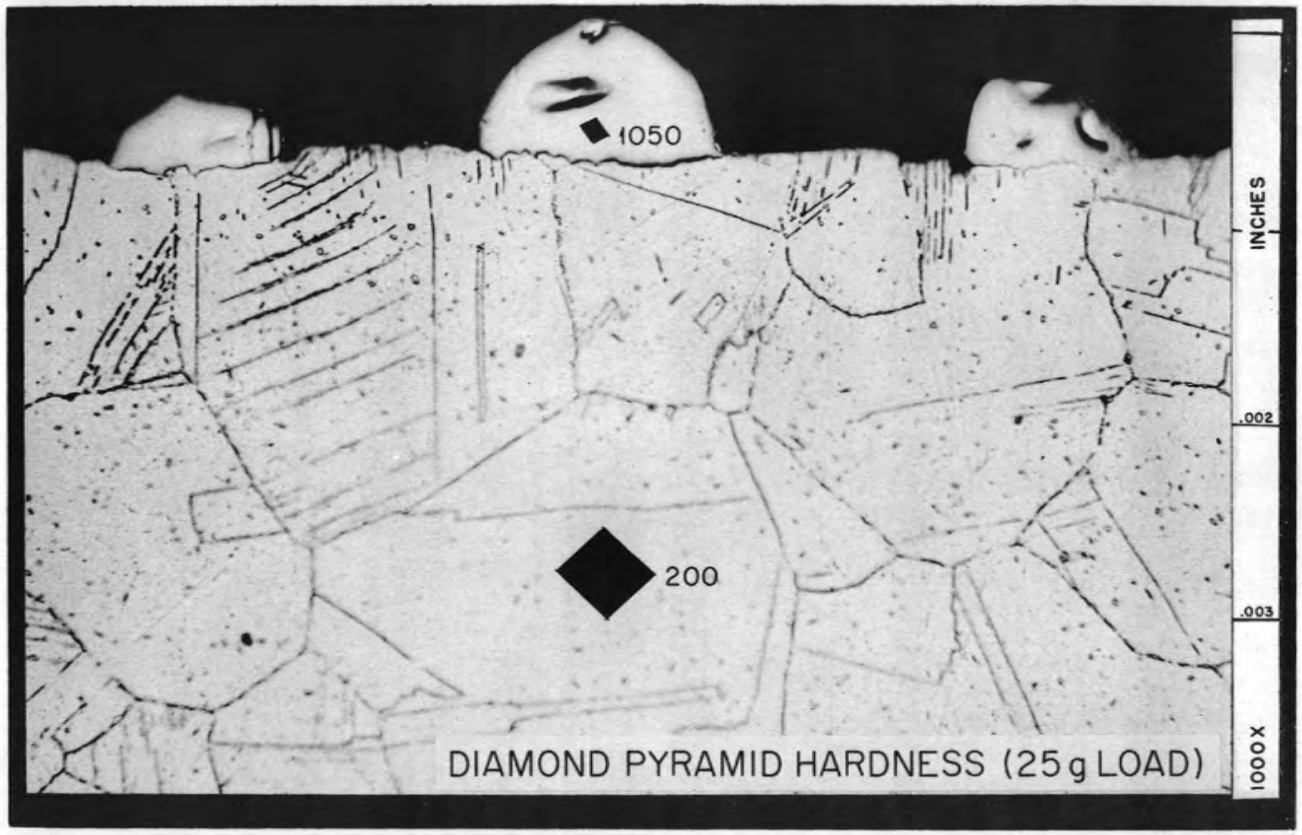

Figure 38. Type 316 Stainless Steel Specimen Following Exposure to Lithium. Test Conditions: Static, 1500°F (816°C), 100 Hours. Note Carbide Crystals on Surface. Etched with Glyceria Regia. 1000X.

considered to be $Cr_{23}C_6$ also. The carbide crystals are believed to deposit during cooling from 1500°F (816°C) to room temperature.

(c) Massive deposits of thin metallic crystal platelets of the type shown in Figure 39 were observed on four of the stainless steels tested at 1832°F (1000°C). These diamond-shaped crystals were approximately two-mils thick and up to one-sixteenth inch in length. The chemical composition of the platelets was found to be essentially the same as the base alloy upon which deposition occurred. The three-fold cubic symmetry displayed in the photomicrograph of an unpolished, unetched crystal platelet in Figure 39 suggests that growth of the platelets was primarily in directions parallel to (111) planes.

(d) Many of the stainless steel specimens listed in Tables IX and X exhibited intergranular penetration by lithium. This type of attack is illustrated in Figure 40. The penetration of the grain boundaries by lithium was often difficult to establish in specimens in the etched condition. However, when specimens in the as-polished condition were allowed to stand in air for several days, staining was observed along the boundaries in which lithium was present (see Figure 40a). The thick grain boundaries in Figure 40b are representative of grain boundaries which contained lithium and which were heavily attacked by the etchant. This erratic intergranular penetration by lithium was attributed to interaction between impurities in the lithium and grain-boundary carbides in the steel.

Additional static tests were conducted on two types of stainless steel in order to elucidate two of the observations cited above,

UNCLASSIFIED
ORNL-LR-DWG 35874

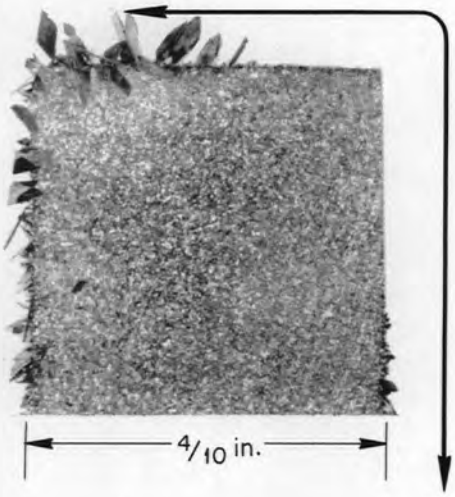

Figure 39. Fe-Ni-Cr Crystals Deposited on a 316 Stainless Steel Specimen During a Static Test in Molten Lithium (316 Stainless Steel Container) Held at 1832°F (1000°C) for 400 hr. Reduced 15%.

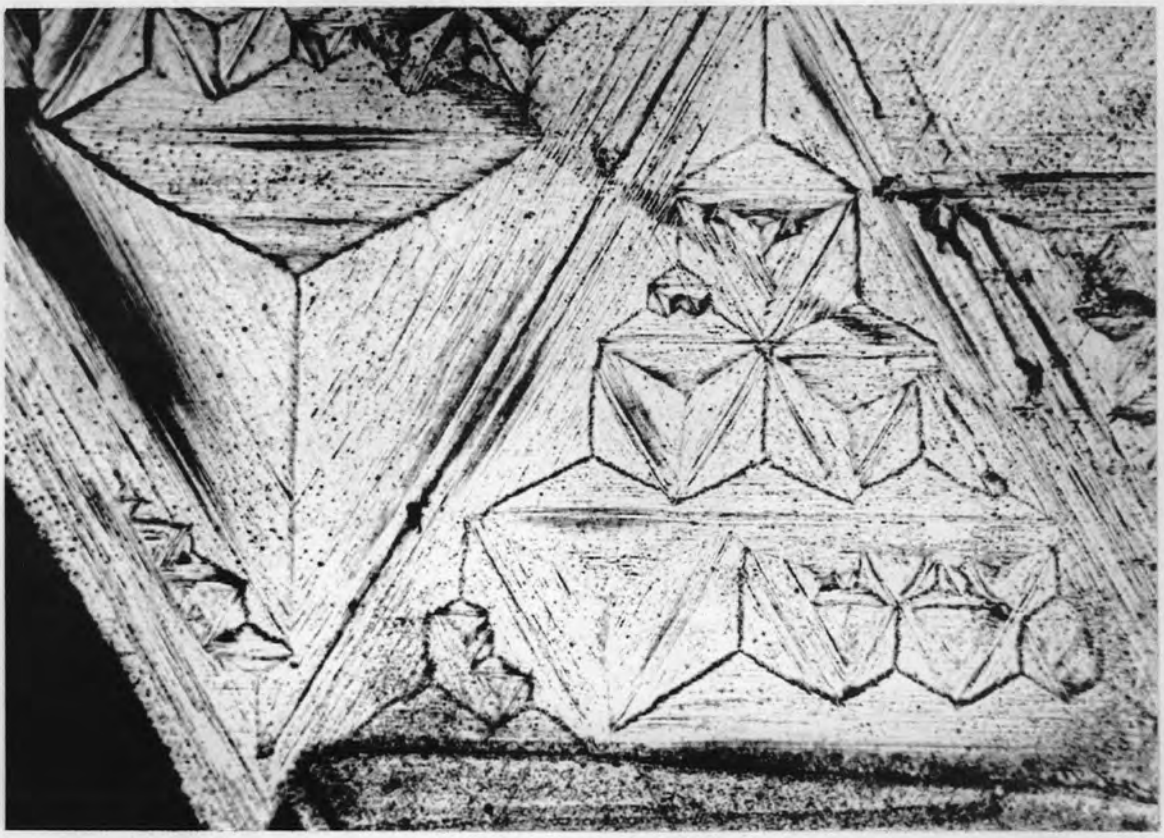

SURFACE OF DEPOSITED Fe-Ni-Cr CRYSTAL INDICATED ABOVE

BRIGHT FIELD ILLUMINATED

UNETCHED
UNPOLISHED

MAGNIFICATION 375X

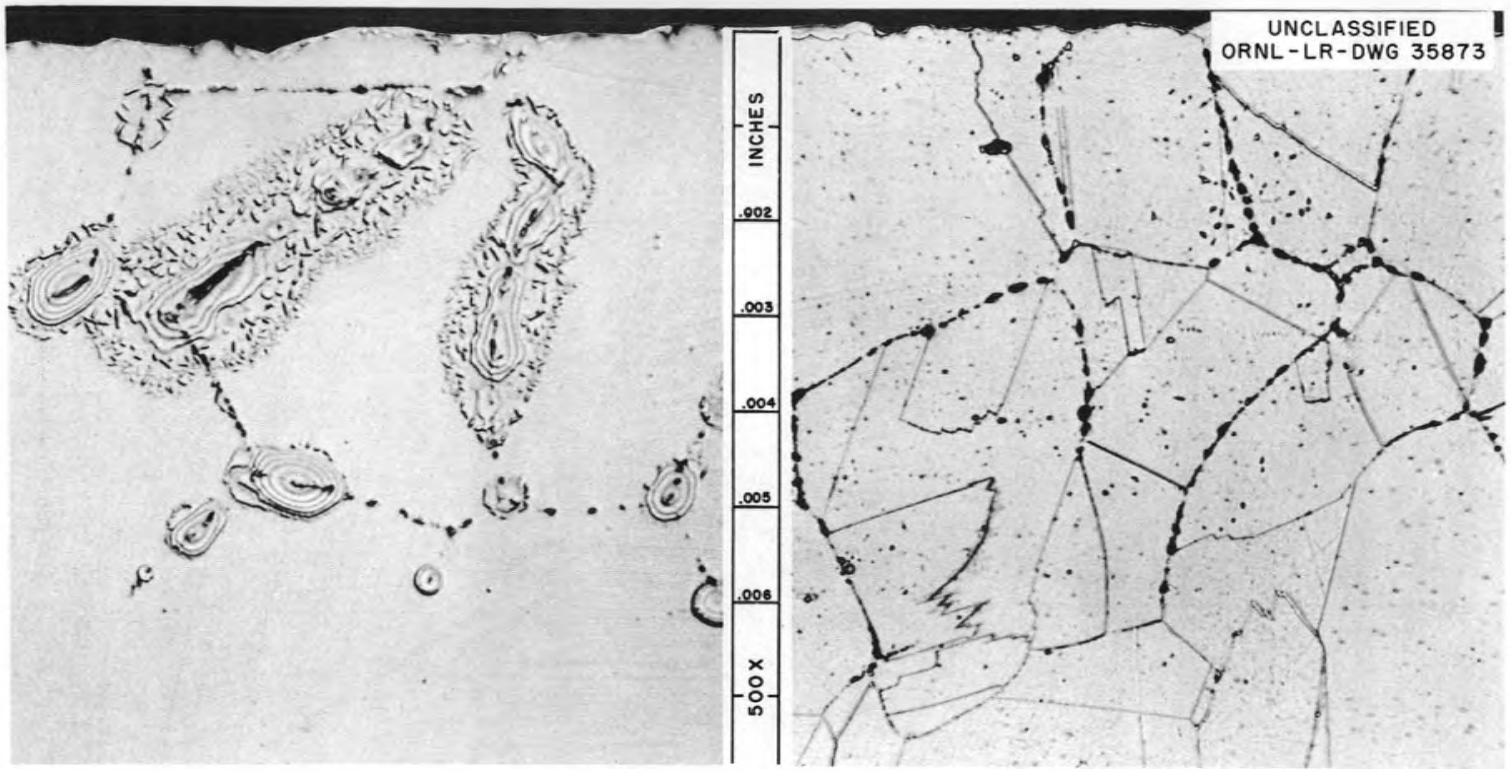

(*a*) AS POLISHED AND ALLOWED TO STAIN. 500X. (*b*) ETCHED. 500X.

Figure 40. Type 310 Stainless Steel Specimen Following Exposure to Lithium. Test Conditions: Static, 1500°F (816°C), 100 Hours. (*a*) Specimen Allowed to Stain in Air to Reveal Areas of Penetration by Lithium. (*b*) Note Grain-Boundary Attack and Thin Carbide Layer on Surface. Etched with Glyceria Regia. 500X.

namely the metallic crystal deposition and intergranular penetration by lithium.

To investigate the metallic crystal deposition, two type 446 stainless steel static capsule tests were conducted at 1900°F (1038°C). The capsules are shown schematically in Figure 41. The purpose of these tests was to determine whether the metallic crystal deposition noted in static tests occurred during the test or during cooling of the test capsule to room temperature.

After 100 hours, Capsule A, shown in Figure 41, was inverted and allowed to cool in air. Metallic crystals were found in the region which had been the vapor zone of the capsule during the test. No crystals were found on the specimen or the bath zone walls of the capsule.

Capsule B was allowed to cool slowly in the test furnace at the completion of the test. The specimen and the bath zone walls of the capsule were covered with hollow hexagonal "pipe-like" crystals. The specimen is shown at low magnification in Figure 42a. The surface of the specimen* and a cross sectional view of one of the deposited crystals is shown in Figure 42b. The crystals were analyzed and found to contain 80 iron – 18 chromium (weight per cent) which indicated a slight preferential enrichment in iron content since the before-test analysis of the capsule was 73 iron – 25 chromium (weight per cent).

---

*Specimen was nickel plated following test to preserve edge during metallographic polishing.

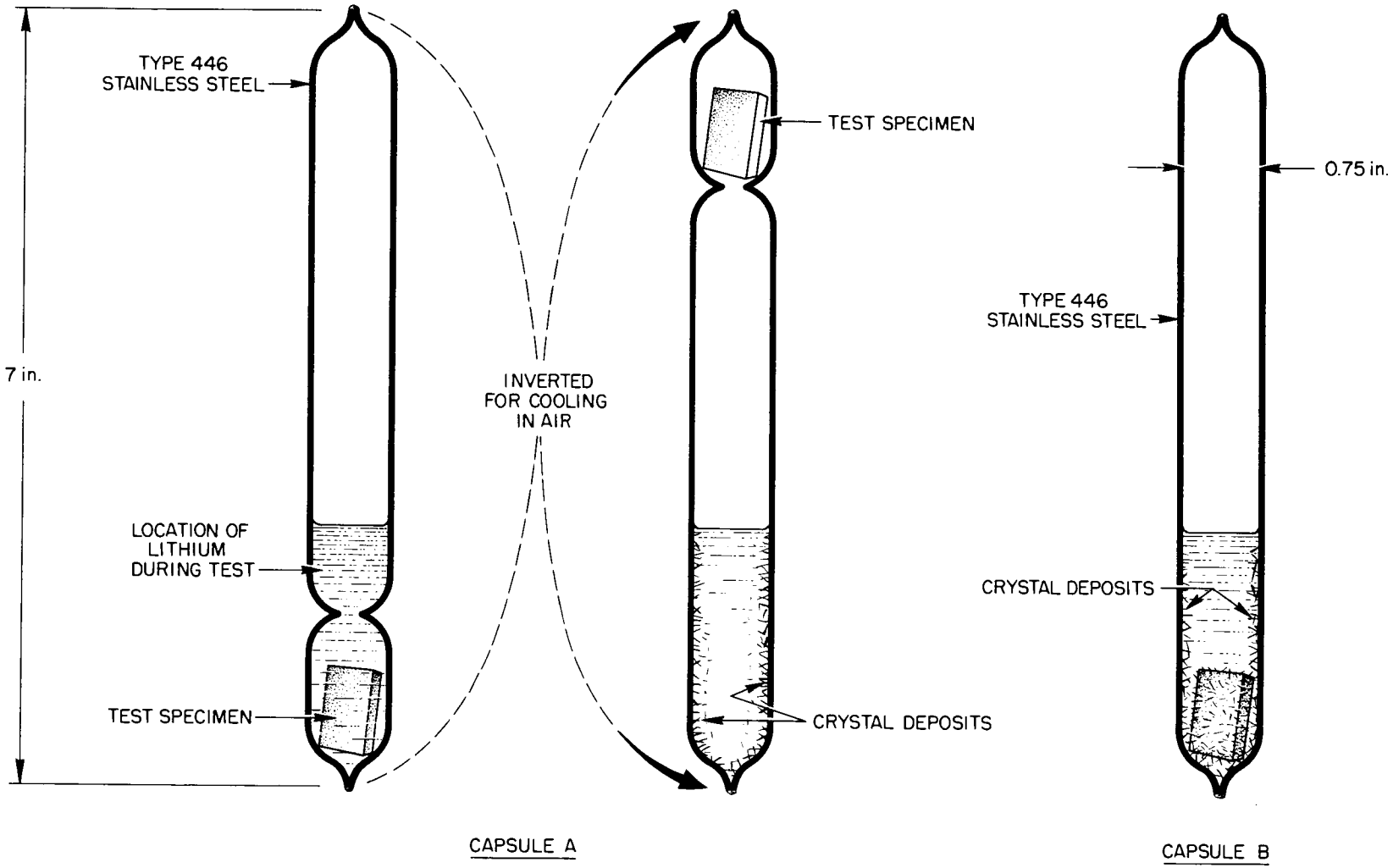

Figure 41. Type 446 Stainless Steel–Lithium "Solubility" Experiment. Test Conditions: Static, 1900°F (1038°C), 100 Hours. Capsule A Inverted Following Test to Drain Lithium away from Specimen, Cooled in Air. Capsule B Allowed to Furnace Cool Slowly.

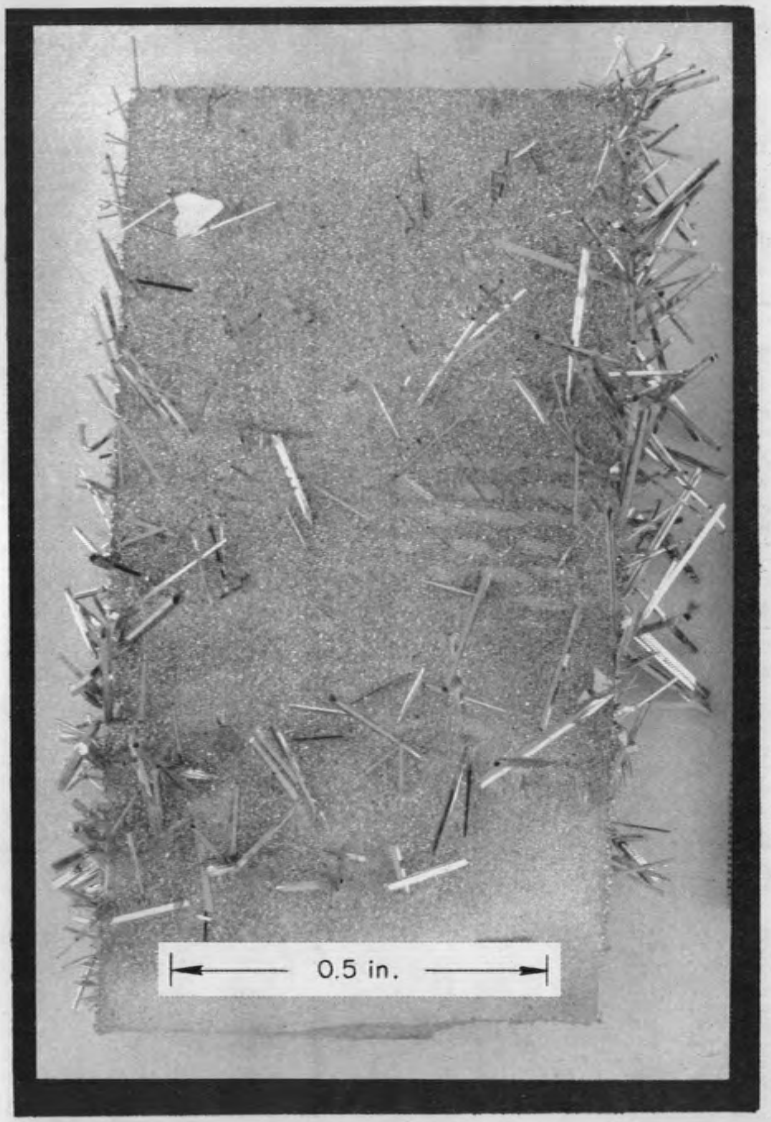

(*a*) 4X.

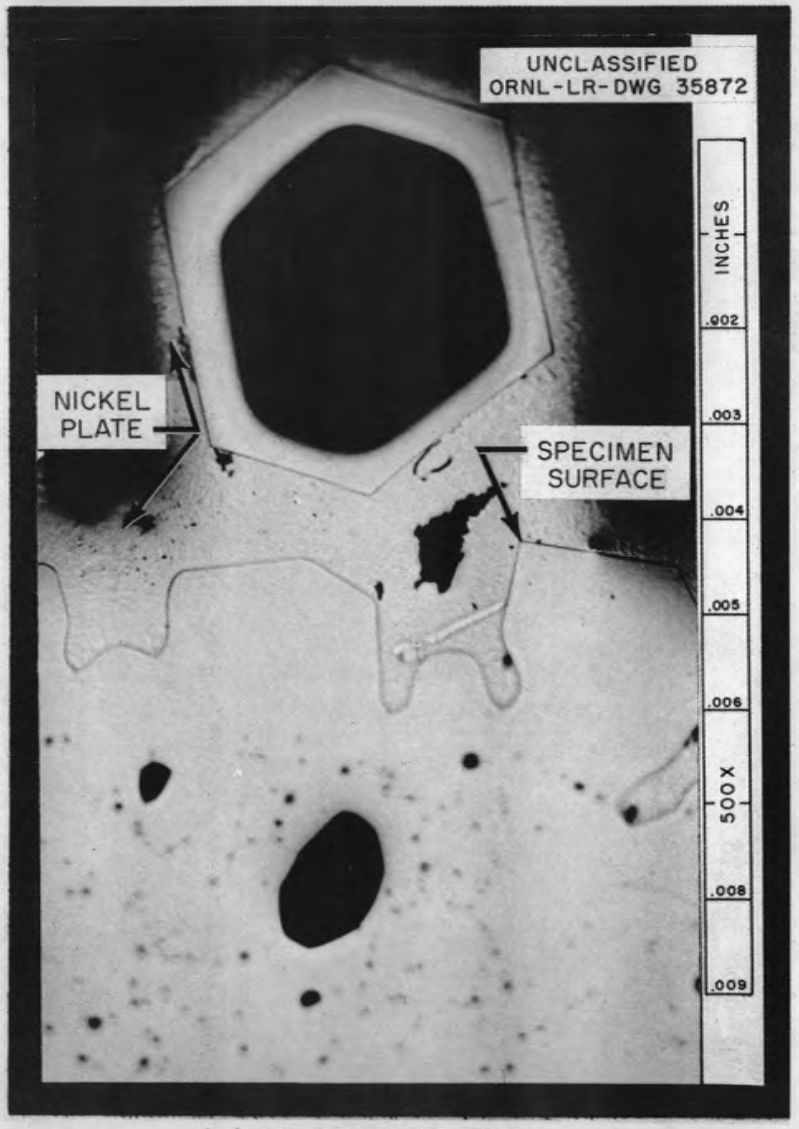

(*b*) AS POLISHED. 500X.

Figure 42. Type 446 Stainless Steel Specimen Following Exposure to Lithium. Test Conditions: Static, 1900°F (1038°C), 100 Hours. (*a*) Shows Hexagonal "Pipe-Like" Crystals Attached to Specimen. (*b*) Shows the As-Polished Specimen with its Very Irregular Surface and Attached Crystal. "Pipe" Axis of Crystal Approximately Perpendicular to Polished Surface.

An approximate value for the solubility of iron plus chromium in lithium at 1900°F (1038°C) was calculated to be 2.7 weight per cent from the specimen weight loss of 36 mg/in.^{2} in Capsule A. This calculation was based on the assumptions that (a) all crystal deposition occurred on cooling, as indicated by the results on Capsule A, and (b) the dissolution of the specimen and capsule wall was fairly uniform as indicated by the crystal analysis.

In connection with the intergranular penetration by lithium, it is in order to note that other investigators[64,65] who have observed this phenomenon have attributed it simply to the reaction of lithium with grain-boundary carbides.

In the present study, however, grain-boundary penetrations were often associated with tests in which the nitrogen content of the lithium was abnormally high. Since nitrogen is one of the major contaminants in lithium metal, a systematic investigation was undertaken to determine the effect of lithium nitride additions on the corrosiveness of lithium toward type 316 stainless steel.

The results of these tests are given in Table XII. In nearly all tests the capsule walls suffered complete grain-boundary penetration by lithium even for relatively small lithium nitride additions. The appearance of the capsule walls following tests is illustrated in Figure 43. The capsule walls are shown in three metallographic conditions: (a) as polished, (b) as polished and allowed to stain in air two days, and (c) as etched. The stained areas were found to be basic when tested with litmus paper

TABLE XII

EFFECT OF ADDITIONS OF LITHIUM NITRIDE[a] TO LITHIUM[b] ON THE CORROSION RESISTANCE OF TYPE 316 STAINLESS STEEL

TEST CONDITIONS: 100 hour; Surface Area/Volume = 13 $in.^2/in.^3$

Test No.	Temperature °F	Temperature °C	Lithium Nitride Addition to Lithium Weight Per Cent	Weight Change $mg/in.^2$	Metallographic Observations
1	1500	816	0.5	+ 2.4	8 mils of intergranular attack.
2	1500	816	1.0	- 12.3	35-mil tube wall completely penetrated intergranularly.
3	1500	816	2.0	- 1.0	35-mil tube wall completely penetrated intergranularly.
4	1600	871	0.1	0	35-mil tube wall completely penetrated intergranularly.
5	1600	871	0.25	- 4.0	35-mil tube wall completely penetrated intergranularly.
6	1600	871	1.0	- 14.8	35-mil tube wall completely penetrated intergranularly.

[a]Lithium nitride analysis: 58.4 Li – 37.1 N_2 – 1.5 CO_3 (weight per cent).

[b]Nitrogen content of lithium prior to addition of lithium nitride: 0.05 weight per cent.

UNCLASSIFIED
ORNL-LR-DWG 35566

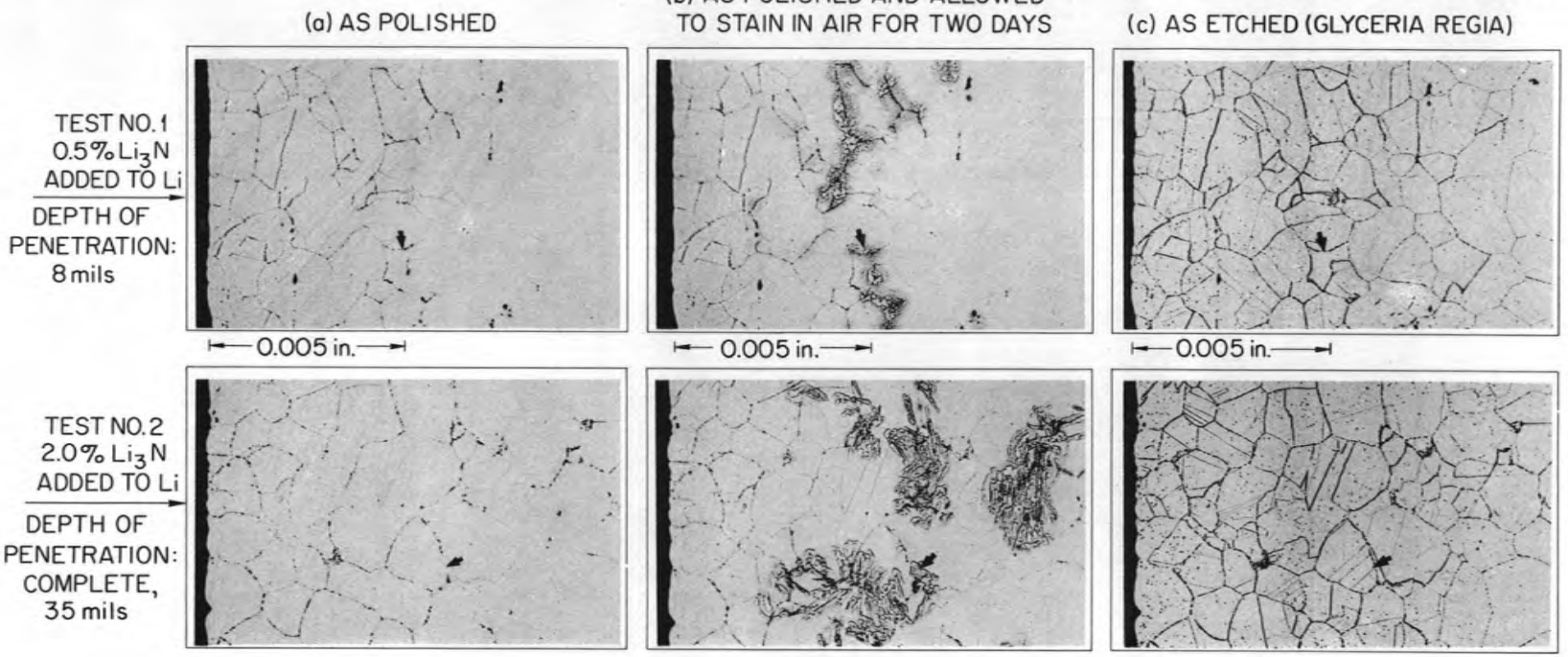

Figure 43. Effect of Additions of Lithium Nitride to Lithium on the Corrosion Resistance of Type 316 Stainless Steel. Test Conditions: 100 hr–1500°F (816°C) (Arrows Indicate Identical Areas in Photomicrographs.)

indicating that staining was due to the formation of lithium hydroxide by reaction of lithium, or a compound containing lithium, with moisture in the atmosphere. It is to be noted that the penetration of grain boundaries by lithium is difficult to detect by examination of specimens in the etched condition only. This may account for the fact that some investigators[66] have not reported grain-boundary penetrations.

The nature of this intergranular attack and its relation to the lithium nitride contamination in the lithium is not understood. One possible reaction might be the formation of the double nitride, $Li_3N{:}FeN$, which has been described by Frankenburger et al.,[67] as a salt with a definite melting point. In any event it is felt that the nitrogen concentration of the lithium has a definite effect because grain-boundary penetration of austenitic stainless steels by lithium (a) has been observed in only a few cases (and then to depths of less than ten mils) in standard tests with no nitride addition, and (b) has been observed consistently in those tests to which nitride additions have been made.

Mechanical property studies on exposed type 316 stainless steel have confirmed the detrimental effects of nitrogen contamination in lithium. These studies are described in Appendix II.

Three-Component Static Test Results

Metals. The following metals were tested in three-component static systems: beryllium, chromium, cobalt, nickel, rhenium, tungsten, yttrium, and zirconium. The results are listed in Table XIII.

Beryllium was observed to suffer considerable attack under the conditions of these experiments, especially at 1832°F (1000°C). The effect of the iron capsule on the corrosion resistance of beryllium is illustrated in Figure 44. The specimen tested in an iron container was attacked uniformly to a depth of nine mils as a result of mass transfer to the iron. A similar specimen tested in a beryllium container, however, exhibited no significant weight change. The alloying which occurred at the inner surface of the iron container is illustrated in Figure 45 at two different magnifications. The phase Be_2Fe was identified by x-ray analysis.

Chromium tested in an iron container was attacked uniformly to a depth of only one mil. Chromium was detected on the surface of the iron container by spectrographic analysis.

Corroded surfaces of cobalt and nickel specimens, tested in a columbium container, are shown in the photomicrographs of Figure 46. Nickel exhibited extensive dissolution and was attacked both intergranularly and along certain crystallographic planes, while cobalt underwent only minor solution attack.

TABLE XIII

RESULTS OF LITHIUM CORROSION TESTS ON METALS IN THREE-COMPONENT STATIC TEST SYSTEMS

Metal Specimen	Container	Temperature °F	Temperature °C	Time Hours	$\frac{A_s^*}{A_c}$ in.^{2}/in.^{2}	$\frac{A_s^*}{V}$ in.^{2}/in.^{3}	Weight Change mg/in.^{2}	Metallographic Observations
Beryllium	Armco Iron	1500	(816)	100	0.3	1.7	−25	4 mils of intergranular attack and void formation; 2 mils of alloying of beryllium with iron container wall.
Beryllium	Armco Iron	1832	(1000)	100	0.3	1.7	−422	9 mils of solution attack plus 5 mils of grain-boundary attack and void formation; 15 mils of alloying of beryllium with iron container wall.
Chromium	Armco Iron	1500	(816)	100	0.1	0.6	−162	1 mil of uniform solution; 3 mils of chromium diffusion into iron container wall.
Cobalt	Columbium	1500	(816)	100	0.1	0.4	−94	0.5 mil of uniform solution.
Nickel	Columbium	1500	(816)	100	0.1	0.4	−2427	20 mils of uniform solution attack plus an additional 15 mils of intergranular attack.
Rhenium	Columbium	1500	(816)	100	0.1	0.8	+0.7	No attack
Tungsten	Columbium	1500	(816)	100	0.1	0.4	0	No attack
Yttrium	Columbium	1500	(816)	100	0.1	1.2	−100	2 mils of solution attack in some areas; 2 mils of grain-boundary attack. Yttrium crystals found on columbium wall.
Zirconium	Armco Iron	932	(500)	100	0.2	1.0	+2.2	No attack.
Zirconium	Armco Iron	1112	(600)	100	0.2	1.0	+5.8	No attack.
Zirconium	Armco Iron	1292	(700)	100	0.2	1.0	+1.7	No attack; 0.2 mils of ZrN on surface.
Zirconium	Armco Iron	1472	(800)	100	0.2	1.0	−453	14 mils of uniform solution; 100 mils of iron capsule wall removed at bath level; approximately 2 grams of mass transfer crystals containing zirconium and iron.

*A_s and A_c are surface areas of specimen and container wall exposed to lithium, respectively; V = volume of lithium.

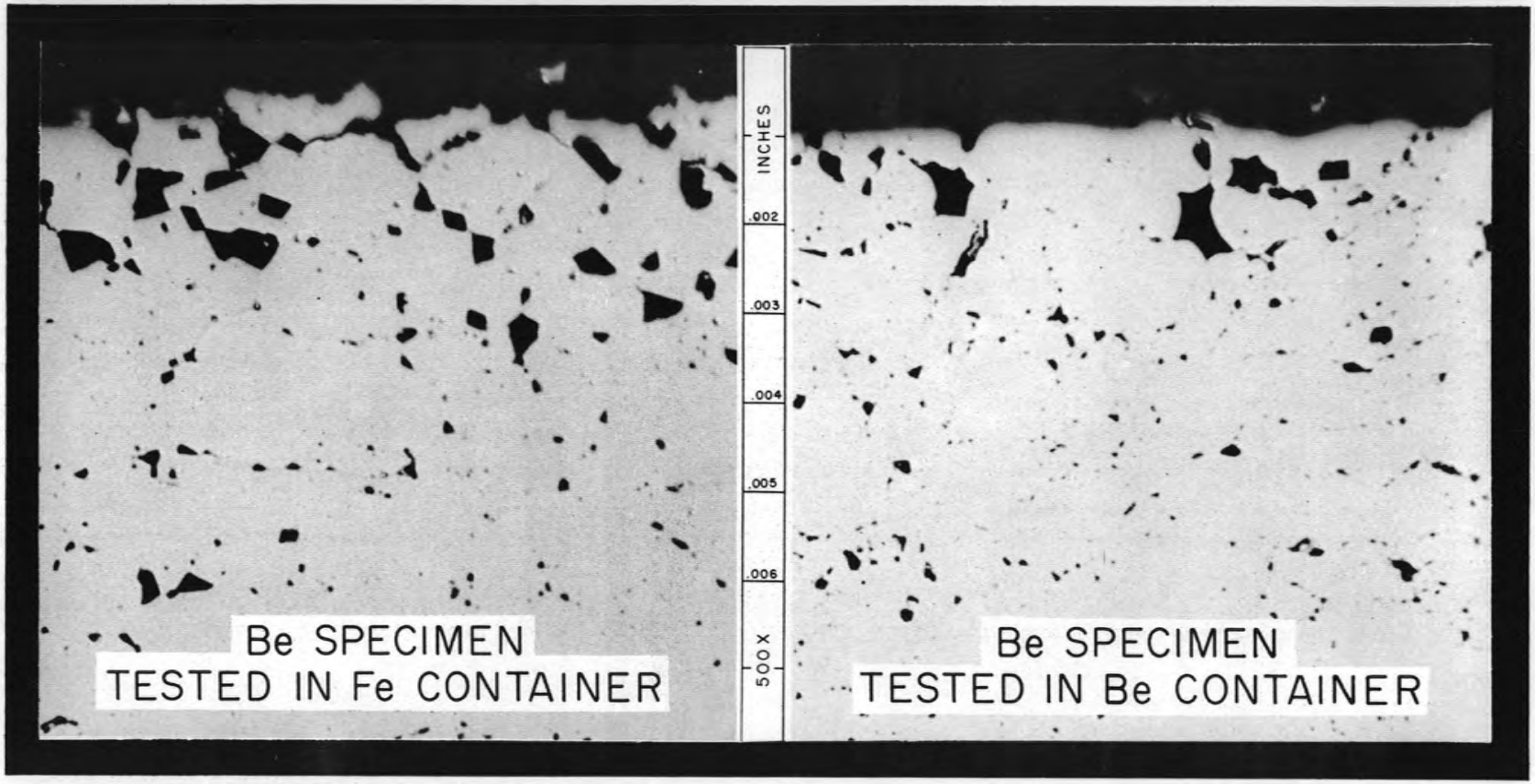

WEIGHT CHANGE = −422 mg/in.^{2} WEIGHT CHANGE = + 1.7 mg/in.^{2}

Figure 44. Effect of Container Material on the Corrosion Resistance of Beryllium Specimens Exposed to Lithium. Test Conditions: Static, 1832°F (1000°C), 100 Hours. As Polished. 500X.

[redacted]
Y-27314

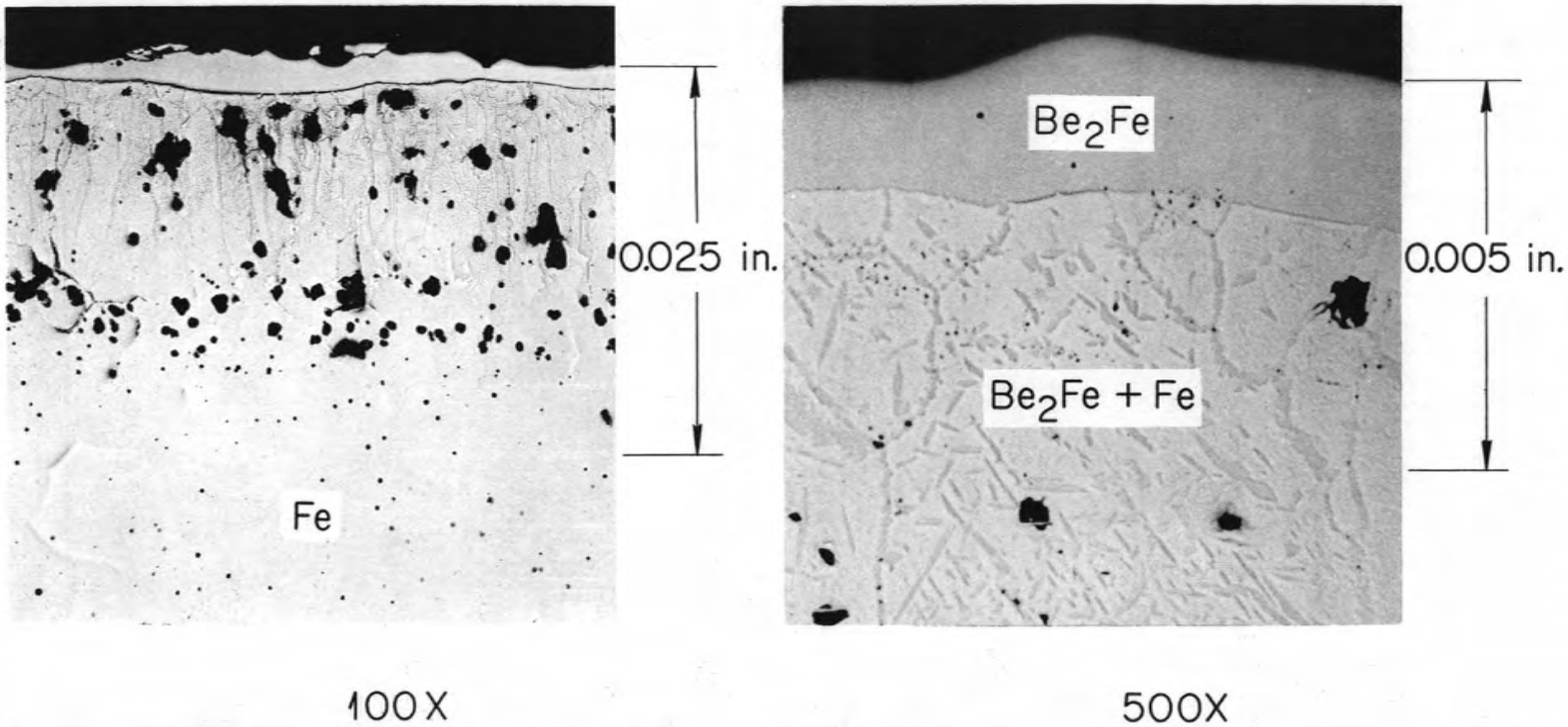

Figure 45. Wall of an Iron Container in Which a Beryllium Specimen was Exposed to Lithium. Test Conditions: Static, 1832°F (1000°C), 100 Hours. As-Polished. Reduced 18%.

UNCLASSIFIED
ORNL-LR-DWG 35871

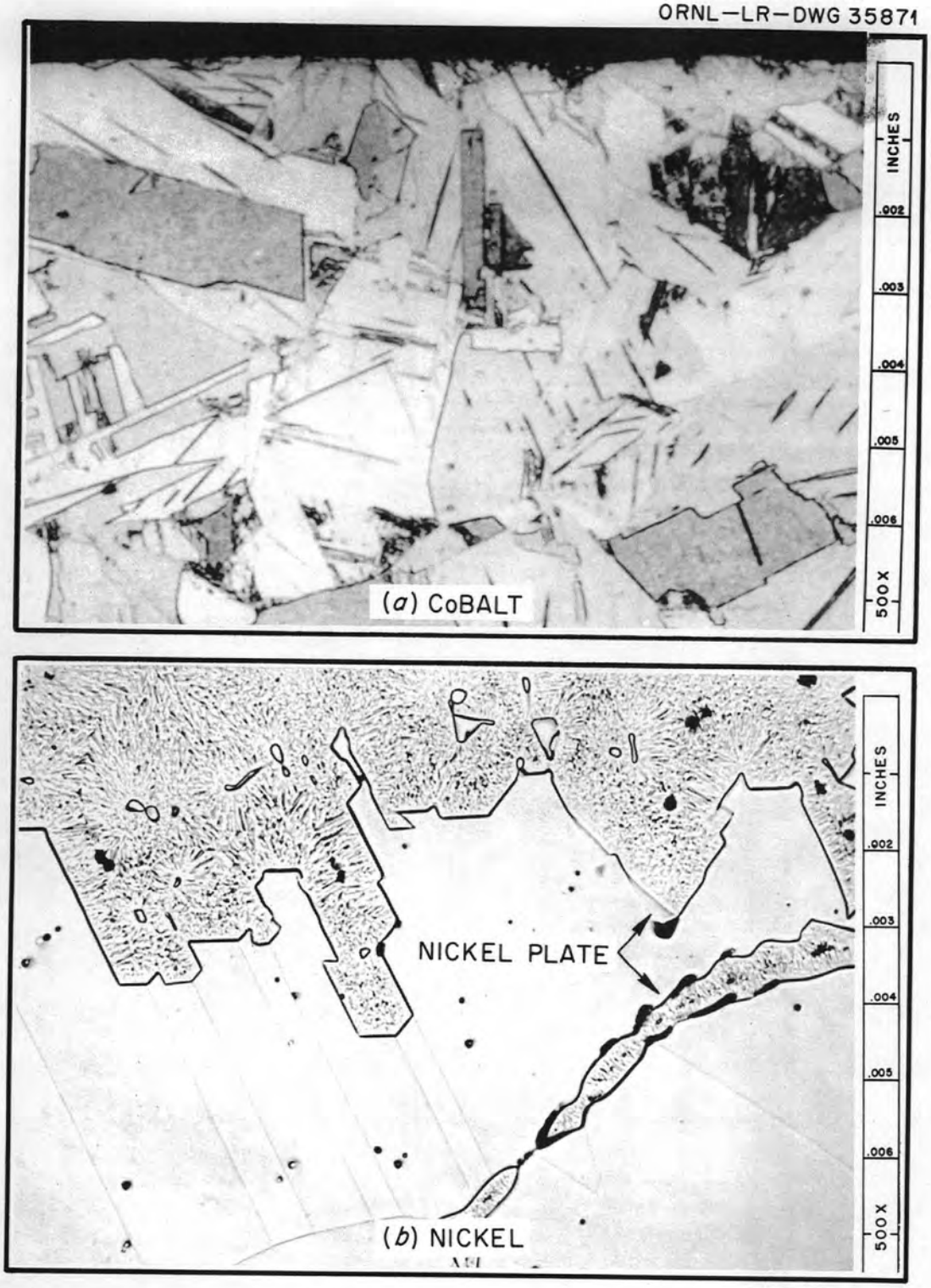

Figure 46. Cobalt and Nickel Following Exposure to Lithium. Test Conditions: Static, 1500°F (816°C), 100 Hours. Etchant: KCN, H_2O_2 (90–10 Volume Per Cent). 500X. Reduced 6%.

Rhenium and tungsten tested in a columbium capsule, showed excellent corrosion resistance. The metallographic appearance of rhenium following test is illustrated in Figure 47.

Yttrium, tested in a columbium container, however, exhibited both intergranular and solution attack as shown in Figure 48. Yttrium crystals were deposited on the container wall although no alloying of yttrium with the columbium could be detected.

Very little attack or weight change was observed on zirconium specimens tested in iron containers in the temperature range 932 to 1292°F (500 to 700°C). At 1472°F (800°C), however, both the specimen and the capsule underwent very severe solution attack and, as shown in Figure 49, massive quantities of iron-rich, iron-zirconium crystals in the form of hexagonal-shaped pipes were deposited on the capsule wall.

Alloys. Alloys based on nickel, cobalt, iron, zirconium, silver, gold, and palladium were tested in three-component static systems.

1. Nickel- and Cobalt-Base Alloys. The results of tests on hard-facing alloys based on nickel and cobalt are listed in Table XIV. Except for the two cases indicated in the table, test specimens were taken from "hard-faced" type 347 stainless steel plate, upon which the alloy under consideration had been deposited, and were tested in type 347 stainless steel containers. Unit weight changes for these specimens were computed using the exposed area of the deposited alloy only, type 347 stainless steel being relatively inert to lithium under the conditions of the tests. The results showed that while the cobalt-base

UNCLASSIFIED
ORNL—LR—DWG 35865

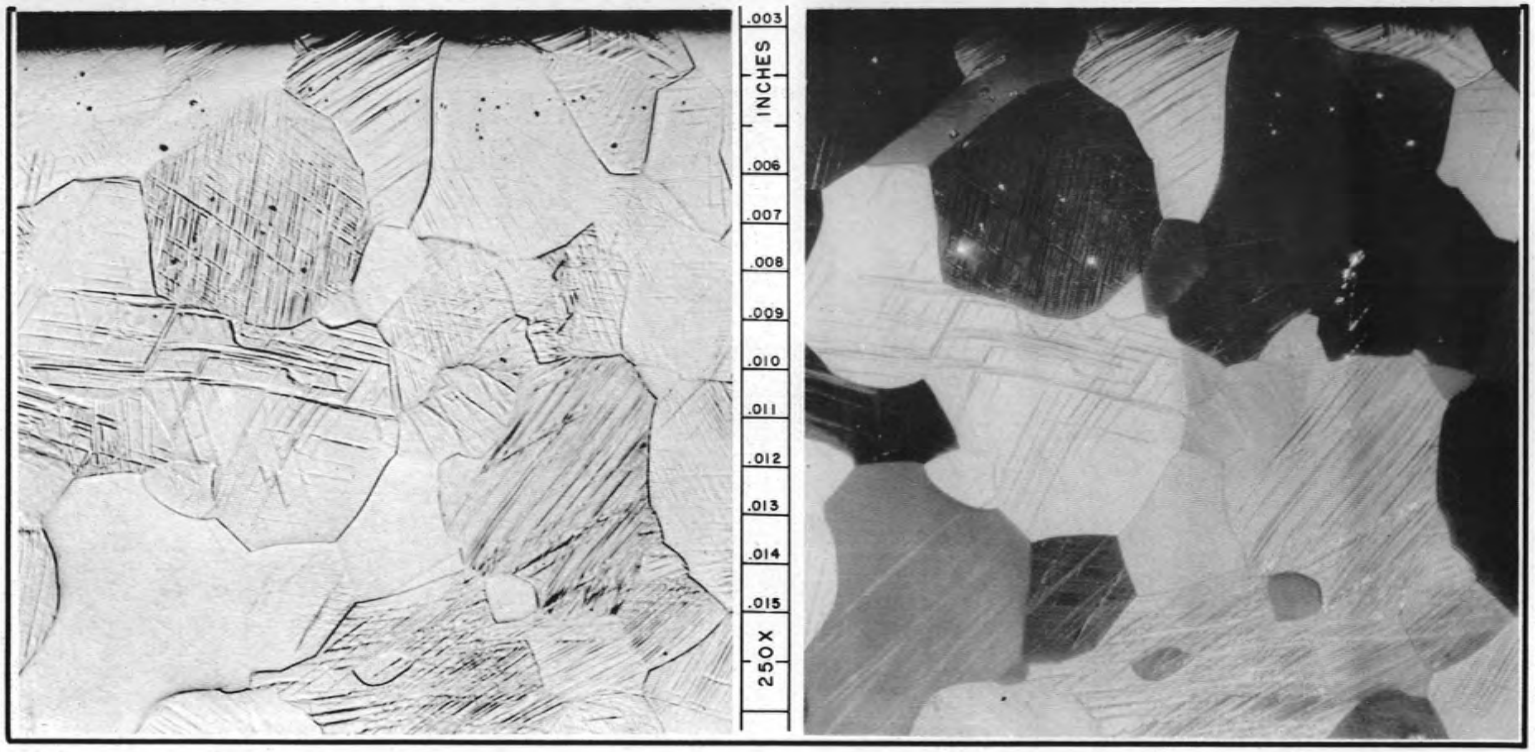

(*a*) BRIGHT FIELD (*b*) POLARIZED LIGHT

Figure 47. Rhenium Following Exposure to Lithium. Test Conditions: Static, 1500°F (816°C), 100 Hours. Cathodic Etch. 250X.

UNCLASSIFIED
Y-27328

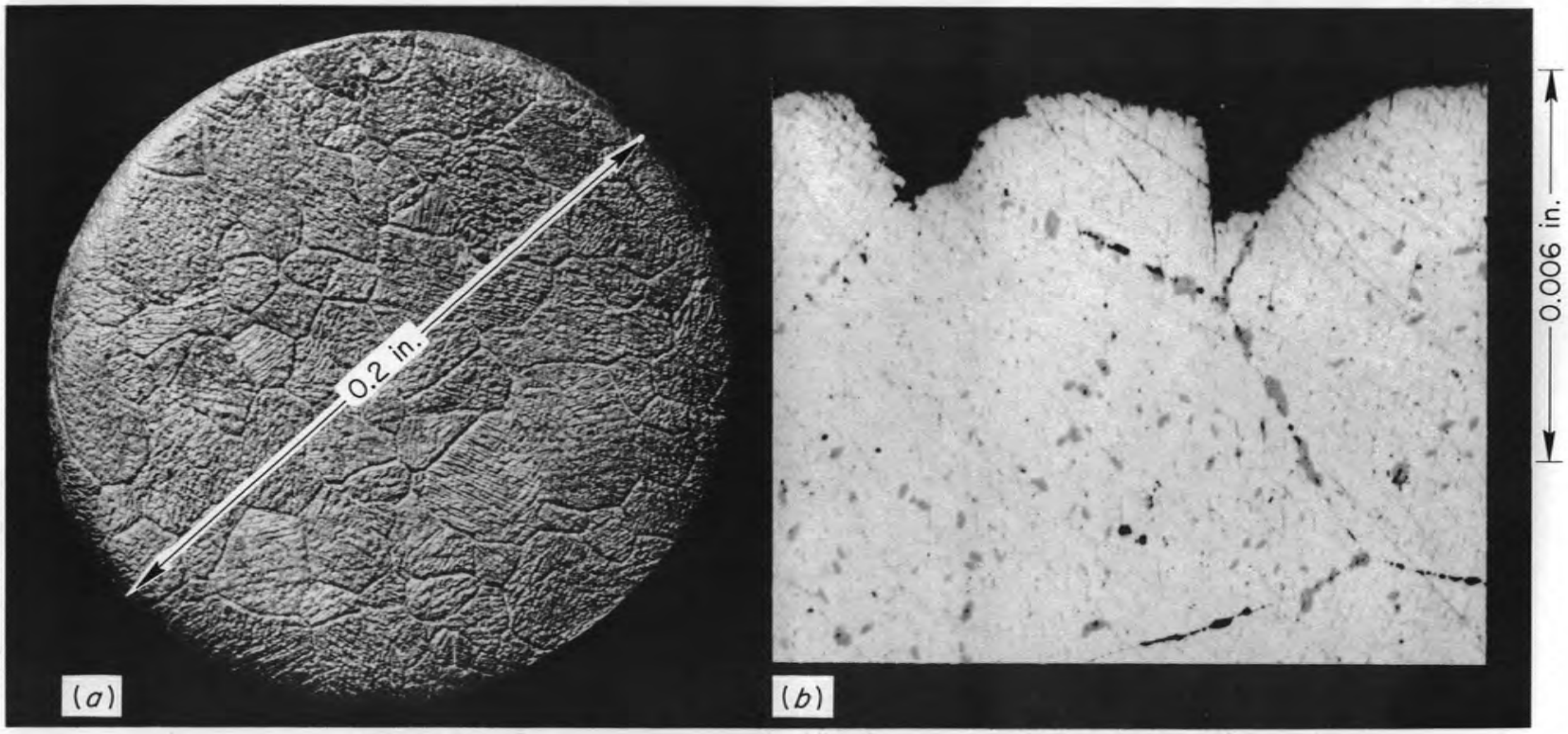

26X UNETCHED – 500X

Figure 48. (*a*) End of Yttrium Specimen Which had Been "Etched" During Exposure to Lithium in a Columbium Container. (*b*) Photomicrograph of Exposed Yttrium Surface. Test Conditions: Static, 1500°F (816°C), 100 Hours. Reduced 16%.

UNCLASSIFIED
Y-8021

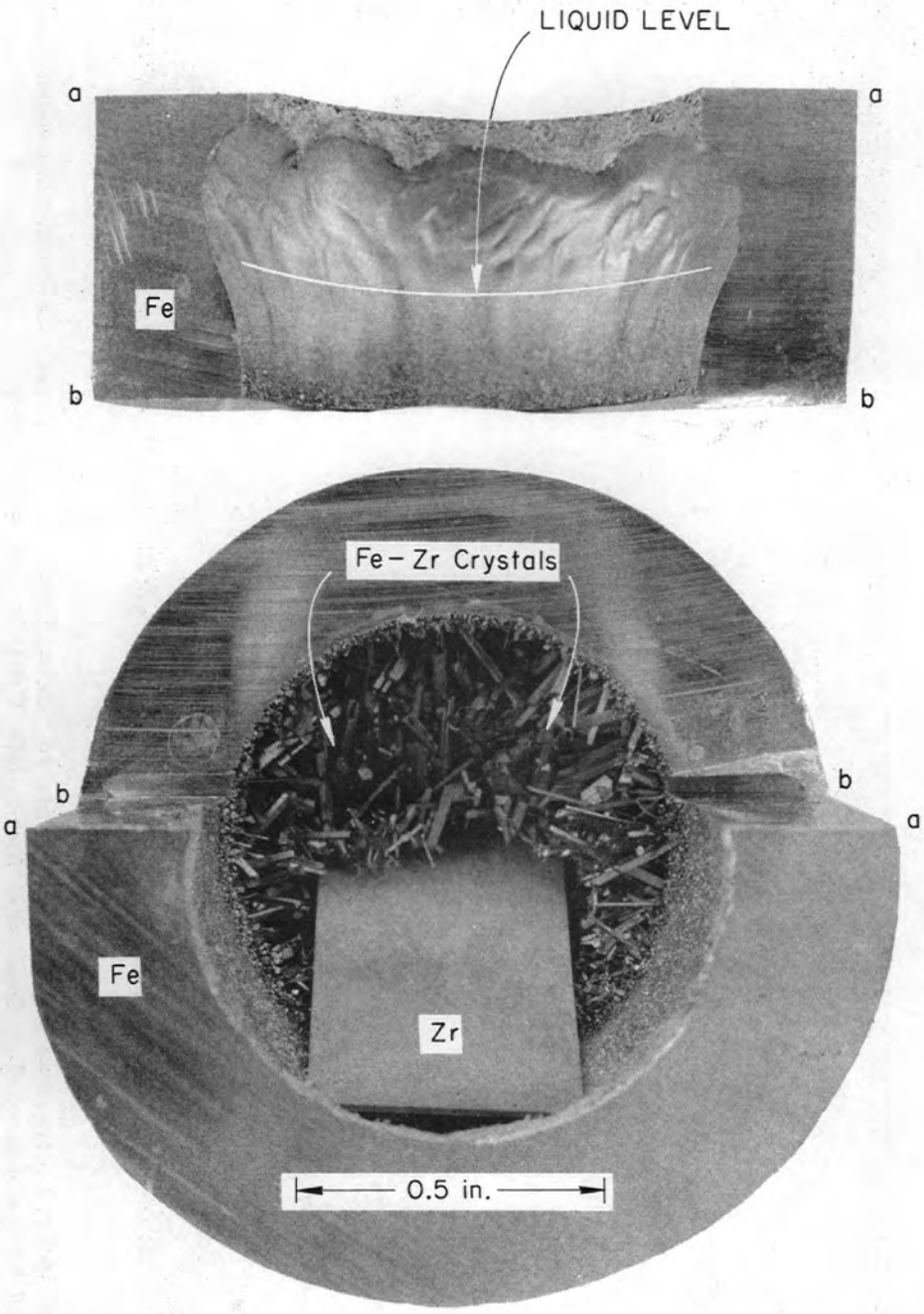

Figure 49. Armco Iron Capsule Containing Zirconium Specimen Following Exposure to Lithium. Test Conditions: Static, 1472°F (800°C), 100 Hours.

TABLE XIV

RESULTS OF LITHIUM CORROSION TESTS ON NICKEL-BASE AND COBALT-BASE ALLOYS IN THREE-COMPONENT STATIC TEST SYSTEMS

TEST CONDITIONS: 1500°F (816°C) – 100 HOURS

Alloy	Nominal Composition Weight Per Cent	Container	$\frac{A_s^*}{A_c}$ in.^{2}/in.^{2}	$\frac{A_s^*}{V}$ in.^{2}/in.^{3}	Weight Change[a] mg/in.^{2}	Metallographic Observations
Hastelloy D[b]	82Ni–9Si–3Cu–2Fe–0.12C	347 SS[c]	0.07	0.3	–129	4 to 6 mils subsurface voids.
Stellite No. 41[b]	76Ni–12Cr–5Fe–4Si–0.42C	347 SS	0.07	0.3	–577	10 to 15 mils subsurface voids.
Stellite No. 40[b]	73Ni–13Cr–5Fe–4Si–3B–0.42C	347 SS	0.07	0.3	–655	10 mils subsurface voids.
Hastelloy B[b]	61Ni–28Mo–5Fe–3Co–0.05C	347 SS	0.07	0.3	–85	5 mils subsurface voids.
Hastelloy C[b]	52Ni–17Mo–16Cr–5Fe–4W–0.15C	347 SS	0.07	0.3	–108	4 to 8 mils subsurface voids.
Stellite No. 6[b]	64Co–27Cr–4W–2Fe–1C	347 SS	0.07	0.3	–36	4 to 6 mils subsurface voids.
Stellite No. 21[b]	62Co–27Cr–5Mo–2Fe–0.3C	347 SS	0.07	0.3	–28	1 mil subsurface voids.
Stellite (Heat B)	58Co–35Cr–5W–1C	Armco Iron	0.25	1.4	–46	3 mils small subsurface voids.
Stellite (Heat C)	56Co–28Cr–12Mo–3Ni–0.3C	Armco Iron	0.25	1.4	–69	3 mils large subsurface voids.
Stellite No. 12[b]	56Co–29Cr–8W–2Fe–1.4C	347 SS	0.07	0.3	–26	0.5 mils attack on carbide network.
Stellite No. 1[b]	50Co–30Cr–12W–3Fe–2.5C	347 SS	0.07	0.3	–32	1 mil attack on carbide network.
Stellite No. 25[b]	50Co–20Cr–15W–10Ni–0.15C	347 SS	0.07	0.3	–31	2 mils solution-type attack plus 4 mils intergranular penetration.

*A_s and A_c are surface areas of specimen and container walls exposed to lithium, respectively; V = volume of lithium.

[a]Weight changes based on surface areas of test alloys only.

[b]These alloys tested as deposited on 0.25 inch type 347 stainless steel plate.

[c]SS stands for stainless steel.

alloys suffered much less weight loss and attack than did the nickel-base alloys, none of the hard-facing alloys studied are sufficiently corrosion resistant to be recommended for use in systems containing molten lithium at 1500°F (816°C). The detrimental effects of silicon and boron in nickel-base alloys are apparent.

Tests were also conducted on a series of nickel-base brazing alloys. Type 316 stainless steel strips were brazed together in the form of T-joints, as illustrated in Figure 50, using the following brazing alloys:

	Nominal Composition (weight per cent)
a.	90 Ni – 10 P
b.	80 Ni – 10 Cr – 10 P
c.	80 Ni – 6 Fe – 5 Cr – 5 Si – 3 B – 1 C
d.	73.5 Ni – 16.5 Cr – 10 Si
e.	71 Ni – 16.5 Cr – 10 Si – 2.5 Mn
f.	70 Ni – 14 Cr – 6 Fe – 5 B – 4 Si – 1 C
g.	69 Ni – 20 Cr – 10 Si

Specimens cut from these assemblies were tested in a capsule of the type shown in Figure 6a. All of the brazing alloys were attacked to depths of 35 mils or more and therefore would not be satisfactory for use in systems exposed to molten lithium.

The effect of the base material on the corrosion resistance of a brazing alloy is illustrated in Figure 51, which shows that a nickel-base brazing alloy, known commercially as Nicrobraz, exhibited better corrosion resistance when applied to nickel-rich Inconel than

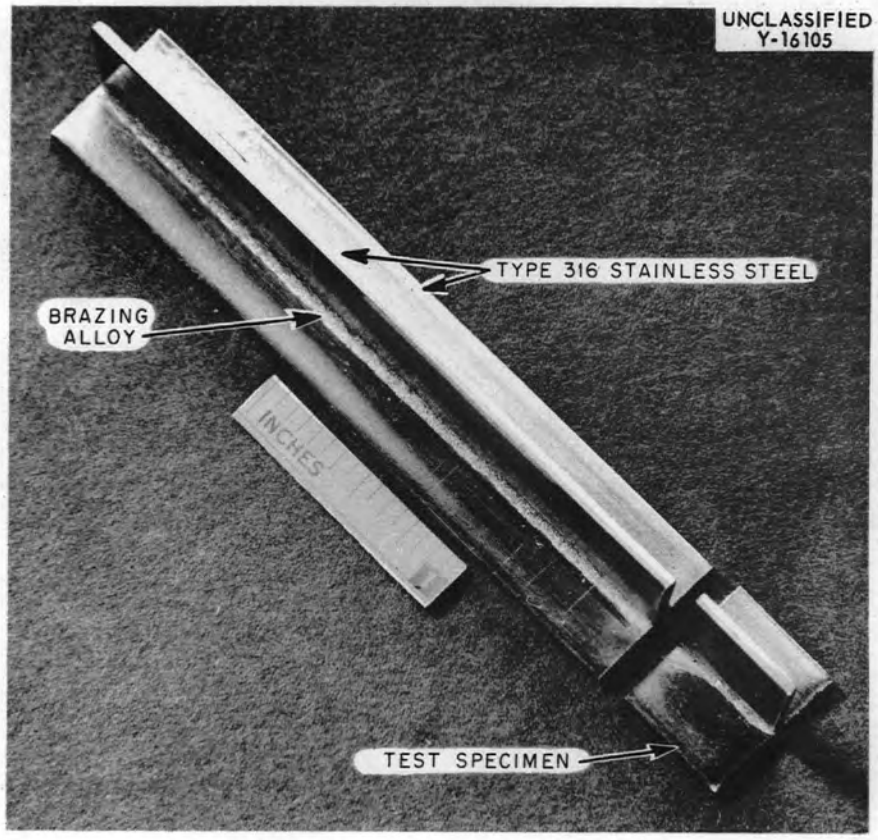

Figure 50. Type 316 Stainless Steel Brazed T-Joint Prepared by Placing a Controlled Quantity of Brazing Alloy at One End and Heating to the Flow Point in a Dry-Hydrogen Atmosphere.

UNCLASSIFIED
ORNL-LR-DWG 35866

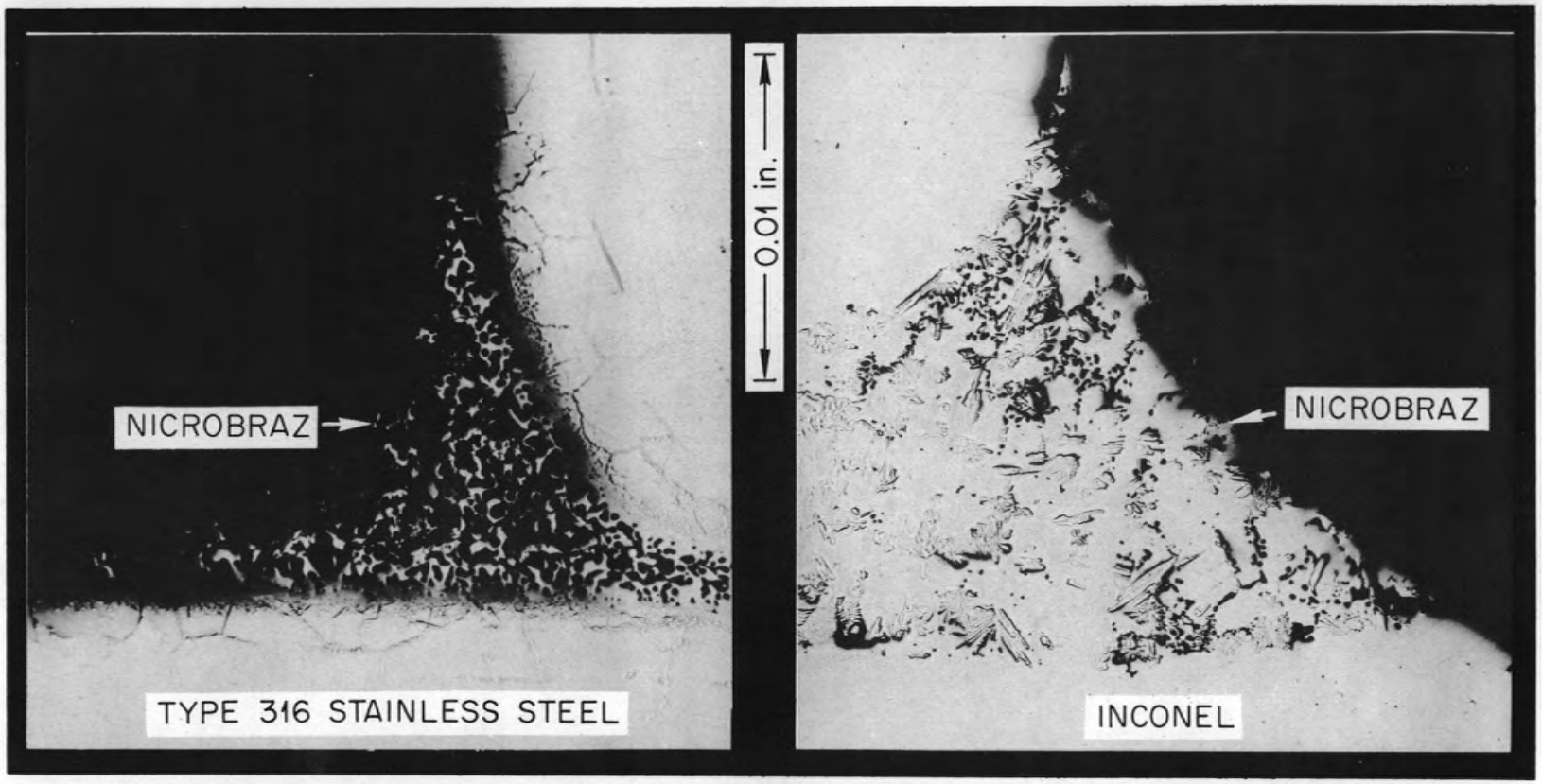

Figure 51. T-Joints Brazed with Nicrobraz (70Ni-14Cr-6Fe-5B-4Si-1C) Following Exposure to Lithium. Test Conditions: Static, 1500°F (816°C), 100 Hours. As Polished.

when applied to a stainless steel containing about 9 per cent nickel by weight. It appears that when the stainless steel was used as the base metal most of the nickel required to saturate the lithium was supplied by the brazing alloy, which accordingly underwent extensive attack. The solubility of nickel in lithium is approximately 0.3 weight per cent at 1292°F (700°C).[68]

2. Iron-Base Alloys. Three-component static tests were performed on the following iron-base alloys: 1035 steel, an experimental brazing alloy, Alfenol (84 Fe – 16 Al), and type 316 stainless steel. Armco iron containers were used for all specimens with the exception of the brazing alloy, which was tested in type 347 stainless steel. The results of these tests are given in Table XV.

The plain-carbon 1035 steel specimen exhibited very poor corrosion resistance, a result which is in agreement with that of an earlier study[69] on mild steel in Armco iron containers and with the two-component data presented in Table X of this report. The reduction by lithium of iron carbide was found to be primarily responsible for the poor corrosion resistance of the 1035 steel. Attack was observed to proceed along channels in grain boundaries, as shown in Figure 52, and no pearlite was visible in the microstructure of corroded specimens. The dark areas in the structure shown in Figure 52 were filled with a material which could not be preserved during metallographic preparation. The 1035 steel, which after slow cooling from 1500°F (816°C) normally contains about 45 per cent pearlite, was converted to a low-carbon iron. Gas evolved by specimens immersed in

TABLE XV

RESULTS OF LITHIUM CORROSION TESTS ON IRON-BASE ALLOYS IN THREE-COMPONENT STATIC TEST SYSTEMS

Alloy	Nominal Composition Weight Per Cent	Container	$\frac{A_s}{A_c}$* in.^{2}/in.^{2}	$\frac{A_s}{V}$* in.^{2}/in.^{3}	Weight Change mg/in.^{2}	Metallographic Observations
1500°F (816°C) – 100 Hours						
1035 Steel	99Fe–0.35C	Armco Iron	0.3	2.0	–4.5	Complete penetration of 0.25-inch thick specimen by lithium. Extensive decarburization throughout steel specimen.
CM-H-1762[a]	86Fe–5Si–5Cu–4B	Type 347 SS[b]	0.03	0.2	–10	3 mils of subsurface voids in braze.
Alfenol	84Fe–16Al	Armco Iron	0.1	0.5	–250	Complete intergranular penetration of 0.25-inch thick specimen; specimen separated into individual grains following test.
1832°F (1000°C) – 100 Hours						
Type 316 SS	67Fe–17Cr–12Ni–2Mo	Armco Iron	0.3	1.0	–15	5 mils of intergranular attack; slight amount of austenite transformed to ferrite.
1832°F (1000°C) – 400 Hours						
Type 316 SS	67Fe–17Cr–12Ni–2Mo	Armco Iron	0.3	1.0	–94	18 mils of heavy intergranular attack; some austenite transformed to ferrite.

*A_s and A_c are surface areas of specimen and container walls exposed to lithium, respectively; V = volume of lithium.

[a]Coast Metals Experimental Brazing Alloy applied to type 347 stainless steel T-joint.

[b]SS stands for stainless steel.

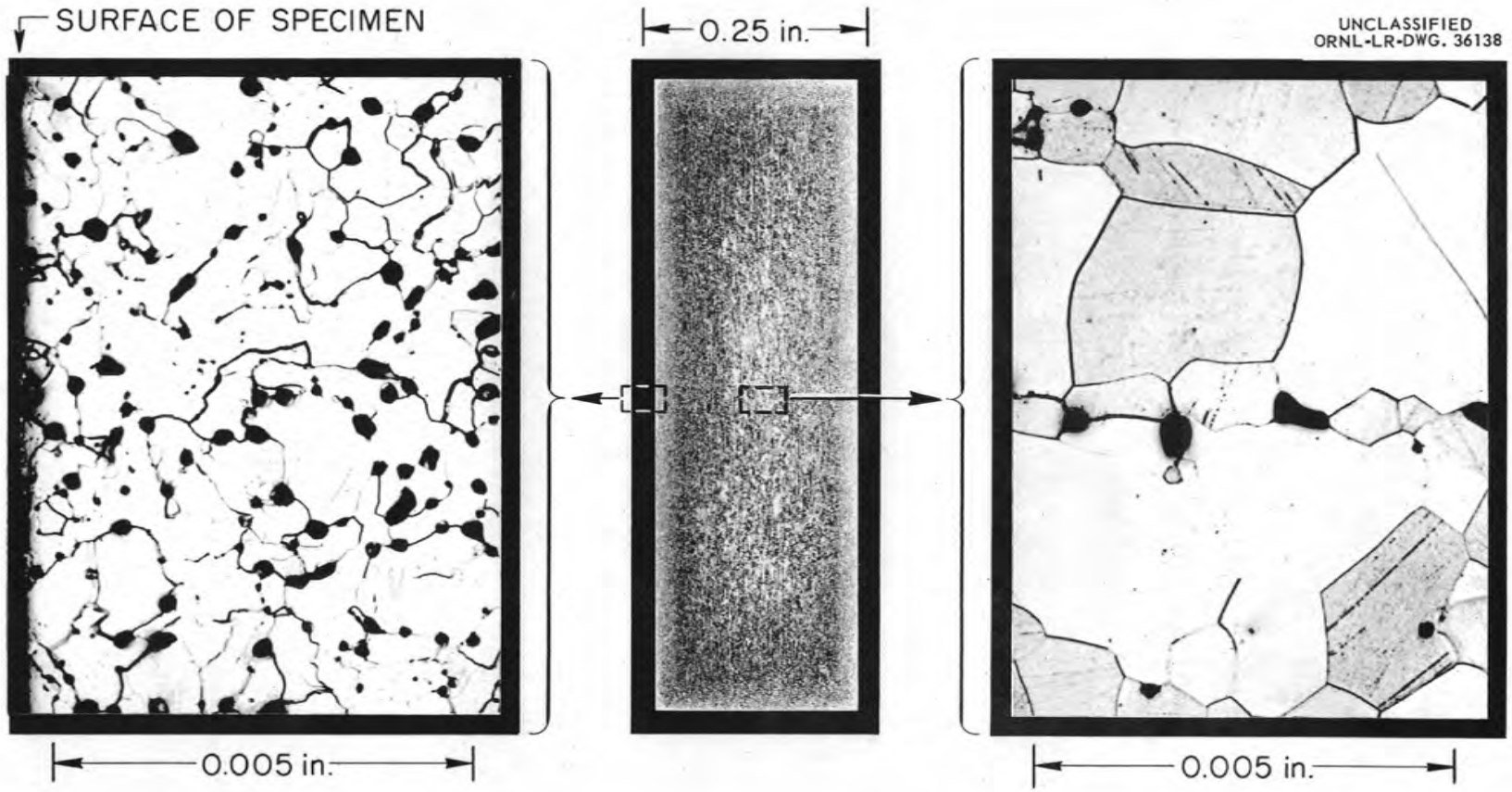

Figure 52. 1035 Steel Specimen Following Exposure to Lithium in an Armco Iron Capsule. Test Conditions: Static, 1500°F (816°C), 100 Hours. Note the Absence of Pearlite Both at the Surface (View on Left) and in the Center of the Specimen (View on Right). Etchant: Nital.

water after dry polishing was analyzed by gas chromotographic techniques and found to contain acetylene (C_2H_2) and hydrogen, the latter being a product of the lithium-water reaction. Acetylene is believed to have been produced by the following endothermic reaction:[70]

$$Li_2C_2 + 2H_2O = 2LiOH + C_2H_2$$

Penetration of the grain boundaries during the early stages of the test apparently restricted grain growth near the surface and led to a duplex grain structure. The results of chemical analyses of successive cuts machined from the 1035 steel specimens are listed in Table XVI. The carbon content of a ten-mil layer of the iron capsule increased from 0.010 weight per cent to 0.024 weight per cent during the test, indicating that the iron capsule wall acted as a sink for a large portion of the carbon removed from the steel specimen.

An iron-base brazing alloy, CM-H-1762, applied to type 347 stainless steel exhibited fair corrosion resistance to lithium, even though this alloy contained alloying additions of copper and silicon, both of which are appreciably soluble in lithium.

Alfenol (84 Fe – 16 Al) suffered complete intergranular attack and a very large weight loss. The heavy grain-boundary attack, shown in Figure 53, was probably due to the high solubility[71] of aluminum in lithium. The appearance of the Alfenol specimen following test is illustrated in Figure 53.

Austenitic stainless steel specimens were observed, in a previous study, to suffer extensive grain-boundary attack to depths of 16 mils when tested at 1832°F (1000°C) in Armco iron capsules.[72]

TABLE XVI

CARBON AND LITHIUM CONTENT OF TURNINGS MACHINED FROM A 1035 STEEL[a] SPECIMEN FOLLOWING EXPOSURE TO LITHIUM FOR 100 HOURS AT 1500°F (816°C) IN AN ARMCO IRON CONTAINER

Location of Turnings (mils)	Weight Per Cent	
	Carbon[b]	Lithium
0 (surface) – 10	0.057	--[c]
10 – 20	0.059	--[c]
20 – 30	0.072	--[c]
30 – 60	0.061	0.34
60 – 90	0.078	0.42
90 – 120 (center)	0.054	0.42

[a]Carbon content prior to exposure, 0.35 weight per cent.

[b]Some carbon lost from turnings due to evolution of acetylene (C_2H_2) while samples were being machined.

[c]Not enough sample for lithium determination.

UNCLASSIFIED
ORNL-LR-DWG 35876

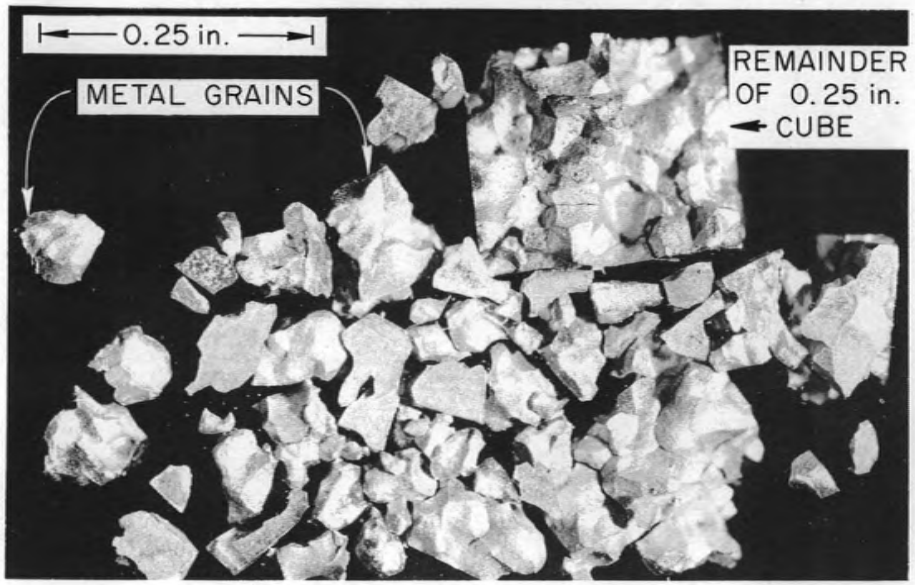

(a)

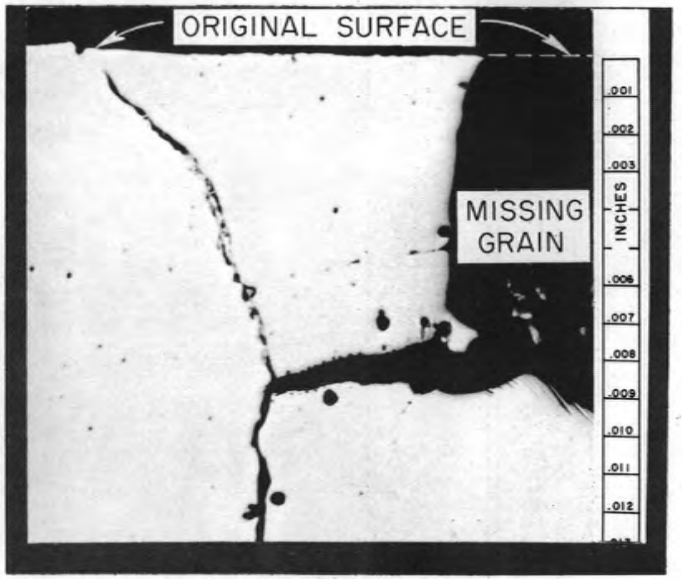

(b)

Figure 53. Alfenol (84Fe–16Al) Specimen Following 100 Hour Exposure to Lithium at 1500°F (816°C). (a) 0.25 Inch Cube Specimen Disintegrated by Grain-Boundary Attack. (b) Photomicrograph Showing Grain-Boundary Attack at Surface of Specimen. As Polished.

However, in the present investigation, when a type 316 stainless steel capsule was substituted for the Armco iron capsule, much less attack occurred on the stainless steel specimen (see Figure 54). In order to study this dissimilar-metal mass transfer phenomenon in a more quantitative fashion, the two tests listed at the bottom of Table XV were conducted.

The test capsule assembly and photomicrographs of the specimens from the two tests are shown in Figure 55. The extensive transformation of austenite to ferrite, especially in the 400-hour test, is quite apparent. The ferritic phase was identified by x-ray analysis of the surface and by use of the magnetic-etch technique.[73,74]

The chemical analysis data obtained on five successive ten-mil cuts from the surface of the 400-hour test specimen illustrated in Figure 55 are plotted in Figure 56. The selective leaching of chromium from the surface of the stainless steel is quite apparent. The nickel composition appears to have remained essentially constant. The preferential leaching of both chromium and nickel is evident in the plot of weight per cent ratios of iron/chromium and iron/nickel in various cuts shown in Figure 56, and is responsible for the martensitically-formed ferrite at the surface, shown in Figure 55.

Using the empirical formula of Monkman et al.,[75] the M_s temperature of the first cut was calculated to be approximately 245°F (118°C) as compared to a M_s value of approximately -370°F (-223°C) for the fifth cut. Changes in the carbon, nitrogen, manganese, and silicon content of the first cut were found to have only

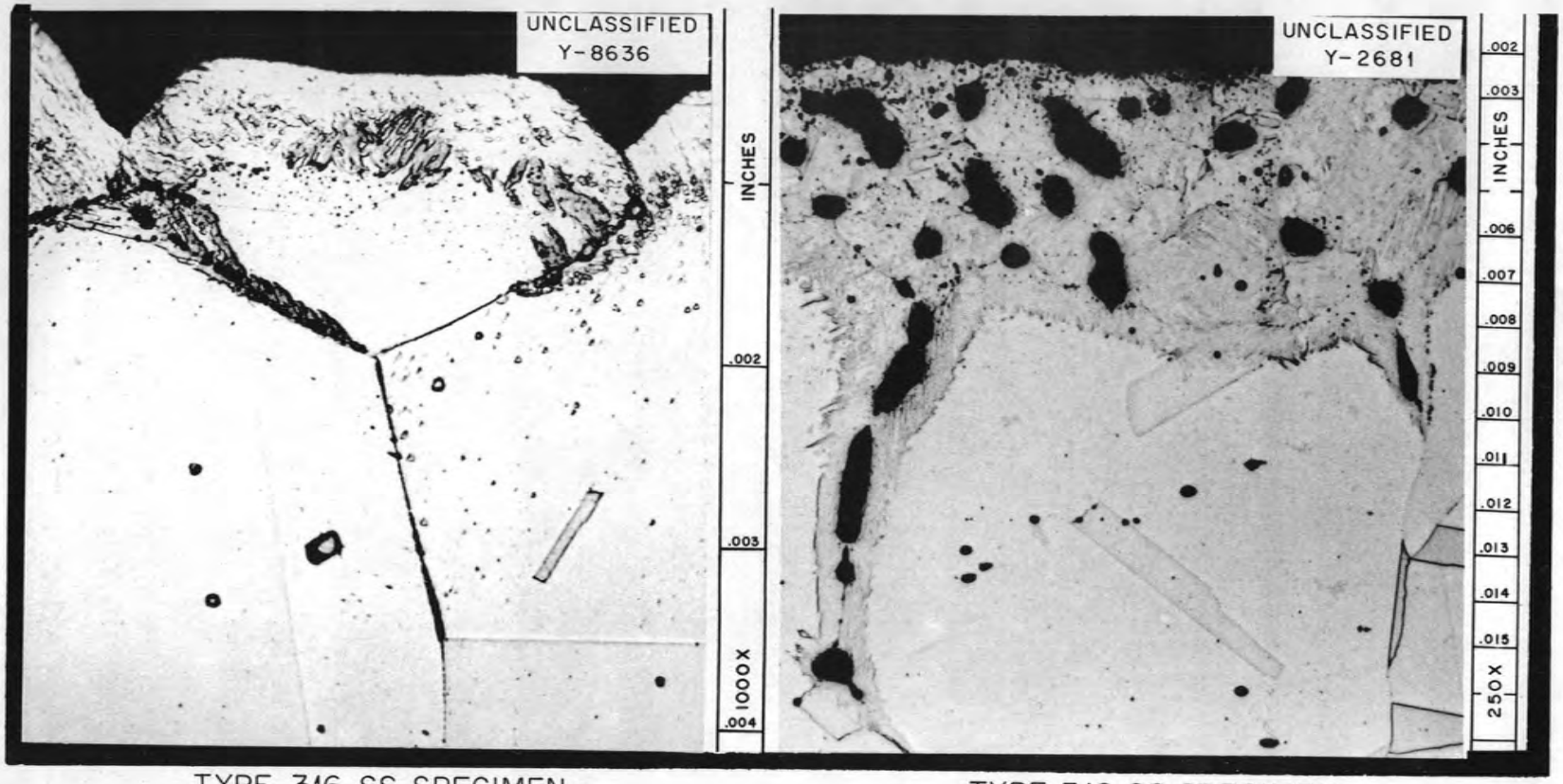

TYPE 316 SS SPECIMEN
FOLLOWING TEST IN 316 SS CAPSULE (1000 X)

TYPE 316 SS SPECIMEN
FOLLOWING TEST IN IRON CAPSULE (250 X)

Figure 54. Effect of Dissimilar Metal Container on the Extent of Attack Observed on Type 316 Stainless Steel Exposed to Lithium. Test Conditions: Static, 1832°F (1000°C), 400 Hours. Etchant: Glyceria Regia.

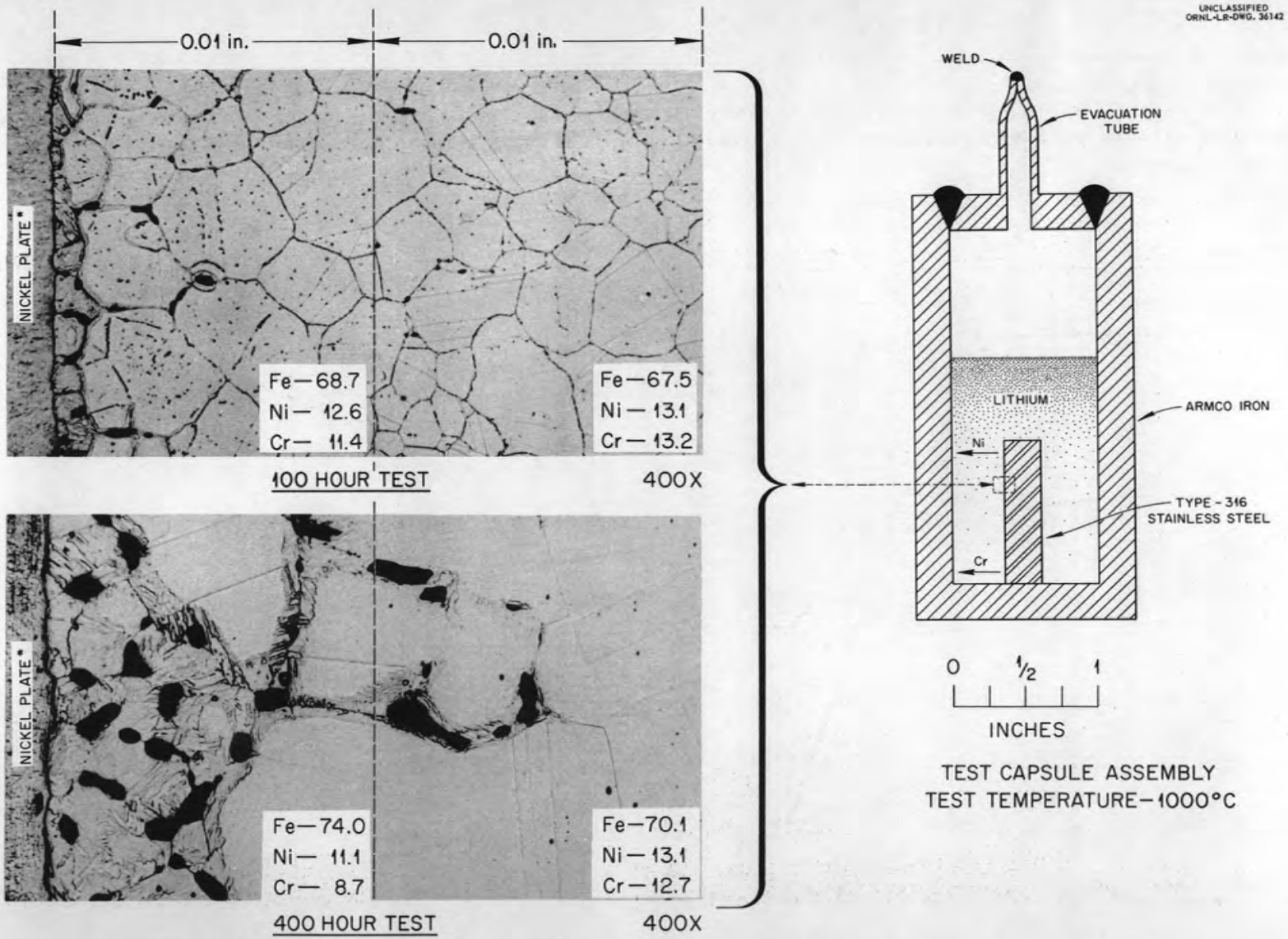

Figure 55. Preferential Leaching by Lithium of Nickel and Chromium from an Austenitic Stainless Steel. Specimens Nickel Plated for Edge Preservation. Etchant: Glyceria Regia. Reduced 41%.

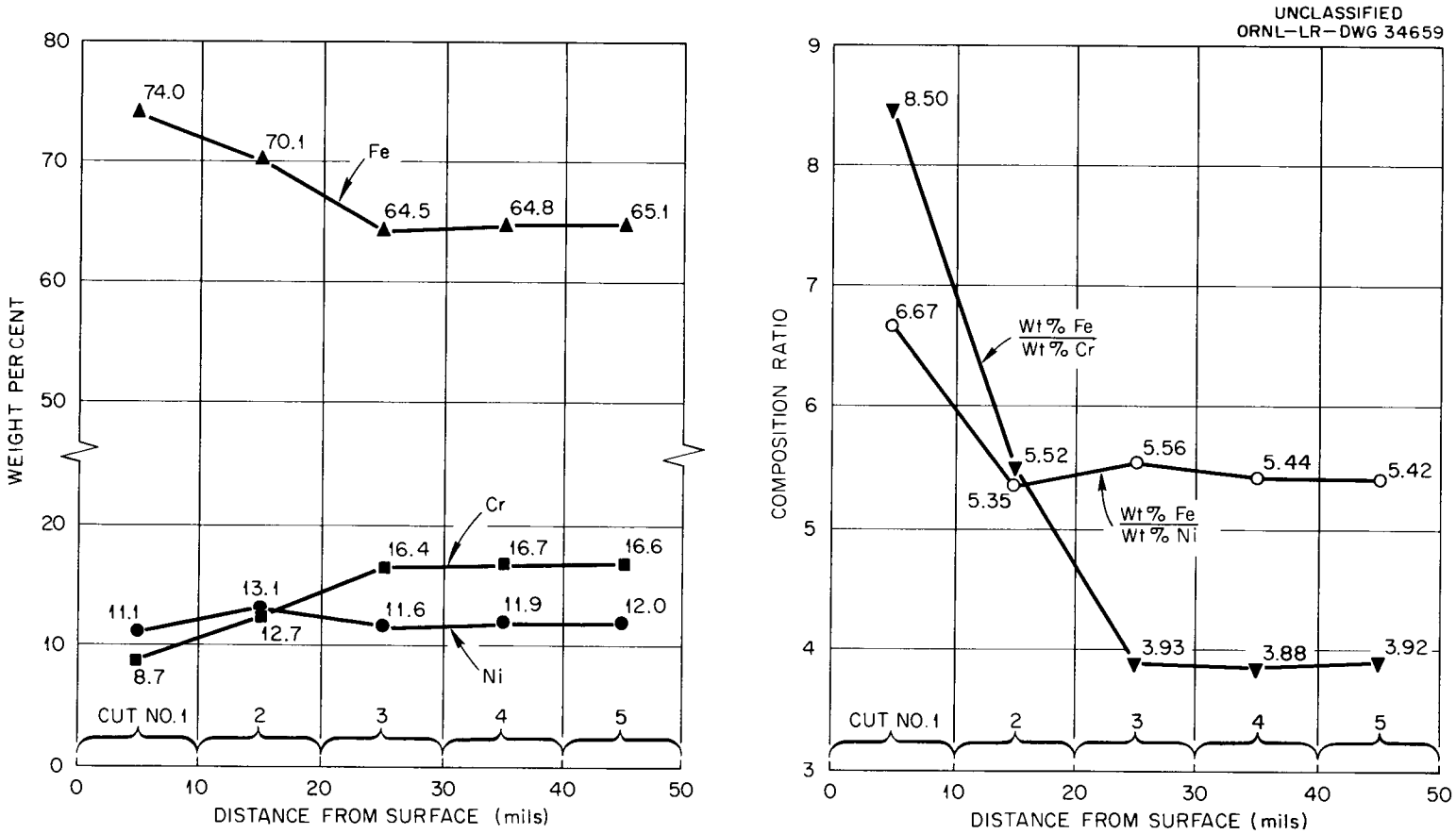

Figure 56. Chemical Compositions of Turnings Machined in 10-mil Increments from the Surface of a Type 316 Stainless Steel Specimen Following Exposure to Lithium. Test Conditions: Static, Armco Iron Capsule, 1832°F (1000°C), 400 Hours.

a minor effect on the M_s temperature when compared to the effect of the reduced chromium and nickel content.

Chemical analysis of the Armco iron capsule wall revealed an increase in both the chromium and nickel composition as a result of dissimilar-metal mass transfer from the stainless steel specimen.

3. Zirconium-Base Alloys. A series of zirconium-base alloys were corrosion tested in columbium containers. The results of these tests are listed in Table XVII.

An examination of the test results indicates that zirconium-base alloys containing additions of beryllium, columbium, and molybdenum were quite corrosion resistant to attack by lithium. Alloys containing columbium and molybdenum were studied at temperatures as high as 1832°F (1000°C). The unattacked surfaces of these alloys following test are shown in Figure 57. Chromium, iron, vanadium, and germanium appeared to lower the corrosion resistance of zirconium alloys.

4. Precious Metal-Base Alloys. The following precious metal-base brazing alloys were tested in three-component systems:

Nominal Composition (weight per cent)

a. 75 Ag – 20 Pd – 5 Mn

b. 64 Ag – 33 Pd – 3 Mn

c. 90 Au – 10 Cu

d. 82 Au – 18 Ni

e. 60 Pd – 40 Ni

f. 60 Pd – 37 Ni – 3 Si

TABLE XVII

RESULTS OF LITHIUM CORROSION TESTS ON ZIRCONIUM-BASE ALLOYS IN 100-HOUR THREE-COMPONENT[a] STATIC TESTS

Nominal Composition Weight Per Cent	$\frac{A_s}{A_c}$* in.^{2}/in.^{2}	$\frac{A_s}{V}$* in.^{2}/in.^{3}	Weight Change mg/in.^{2}	Metallographic Observations
1500°F (816°C)				
85Zr–15Cb	0.02	0.3	+2	No attack.
84Zr–16Fe	0.2	2.0	–61	0.5 mils uniform solution.
75Zr–15Cr–10Fe	0.2	2.0	–205	1.5 mils uniform solution.
1700°F (927°C)				
95Zr–5Be	0.2	2.0	–3	0.5 mils small subsurface voids.
82Zr–18Cr	0.2	2.0	–194	1.5 mils uniform solution.
75Zr–25Cb	0.2	2.0	–17	No attack.
70Zr–30V	0.2	2.0	–600	10 mils surface zone depleted in second phase.
69Zr–31Mo	0.2	2.0	–109	0.5 mils uniform solution.
65Zr–25V–10Fe	0.2	2.0	–387	3 mils solution.
65Zr–25V–10Ge	0.2	2.0	–387	3 mils solution.
1832°F (1000°C)				
85Zr–15Cb	0.1	1.0	+2	No attack.
80Zr–15Cb–5Mo	0.1	1.0	0	No attack.

*A_s and A_c are surface areas of specimen and container walls exposed to lithium, respectively; V = volume of lithium.
[a]Columbium used as the container material for all tests in this table.

UNCLASSIFIED
ORNL-LR-DWG 35868

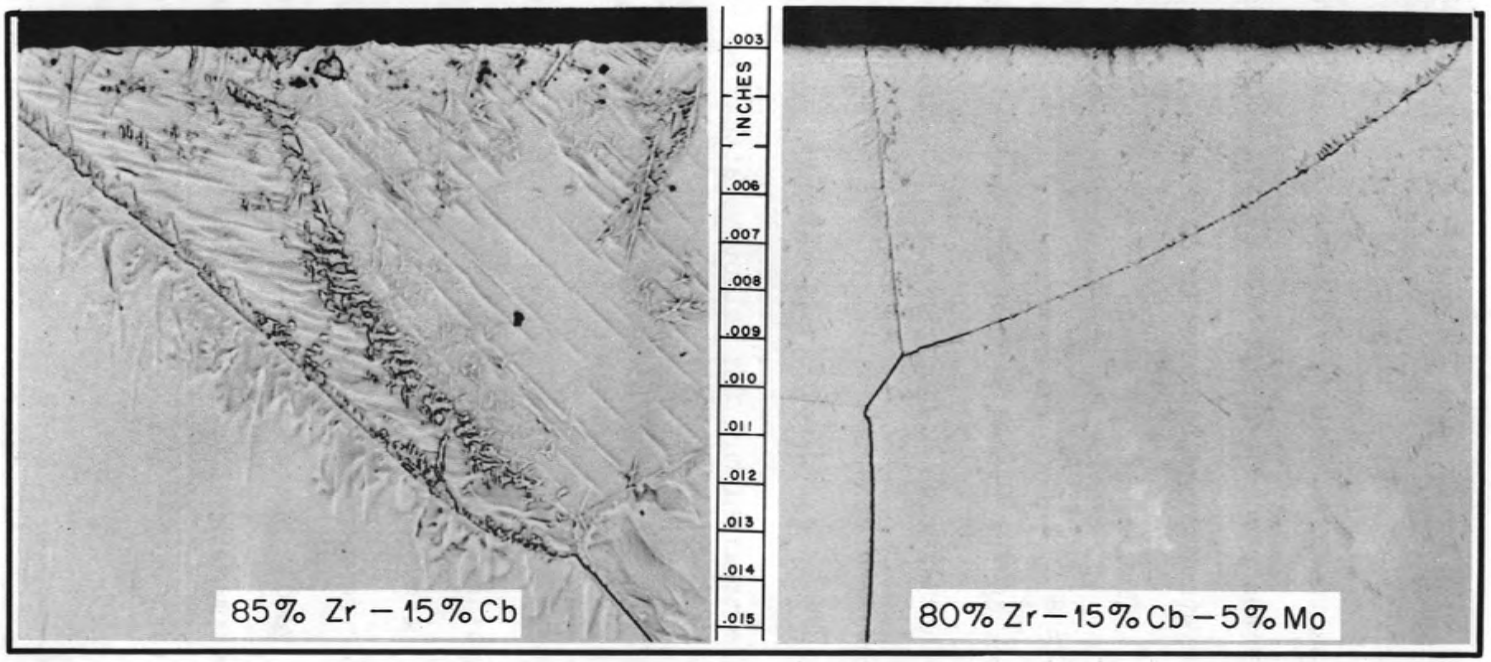

Figure 57. Surfaces of Two Zirconium-Base Alloys Following Exposure to Lithium. Test Conditions: Static, 1832°F (1000°C), 100 Hours. Cathodic Etch. 250X.

The braze alloys were tested in the form of T-joint specimens as previously illustrated (Figure 50) with type 316 stainless steel as the base material. In every case the alloys were attacked across the entire thickness (0.040 inch) of the brazed T-joint.

These results agree with the findings of past investigators[76] and indicate that the precious metal-base alloys should not be considered for use in systems containing molten lithium.

Cermets.* The results of tests on various nickel- and cobalt-bonded cermets are given in Table XVIII.

The attack on the nickel-bonded TiC cermets occurred primarily on the nickel-rich binder phase and the depth and severity of the attack increased with increasing nickel content. Figure 58 shows cross sections of two of the nickel-bonded cermet specimens following exposure to lithium. The selective attack of the nickel-rich binder phase is evident in Figure 59 which is an enlarged view of the zone in which the continuous corrosion terminated.

Several WTiC and WC cermets, bonded with cobalt, were tested in columbium containers. The results of these experiments are listed in Table XVIII. Based on both weight loss data and metallographic examination the corrosion resistance of the cermets studied in lithium was very good. Extensive cracking was observed on several of the cermet specimens but this was attributed to the thermal stresses during test rather than attack by lithium, except where noted otherwise.

---

*Ceramic-metal combinations, usually containing from a few to approximately fifty weight percent of pure metals or alloys.

TABLE XVIII

RESULTS OF LITHIUM CORROSION TESTS ON CERMETS[a] IN THREE-COMPONENT STATIC TESTS

Cermet Designation	Nominal Composition Weight Per Cent	$\frac{A_s}{A_c}$* in.^{2}/in.^{2}	$\frac{A_s}{V}$* in.^{2}/in.^{3}	Weight Change mg/in.^{2}	Metallographic Observations
K150A[b,c]	80TiC–10CbTaTiC$_3$–10Ni	0.08	0.4	–72	Nickel-binder phase attacked to a depth of 12 mils.
K151A[b,c]	70TiC–10CbTaTiC$_3$–20Ni	0.08	0.4	–690	Specimen cracked during test. Nickel-binder phase attacked to a depth of 65 mils.
K152B[b,c]	64TiC–6CbTaTiC$_3$–30Ni	0.08	0.4	–954	Specimen cracked during test. Nickel-binder phase attacked to a depth of 90 mils.
K162B[b,c]	64TiC–6CbTaTiC$_3$–25Ni–5Mo	0.08	0.4	–668	Specimen cracked during test. Nickel-binder phase attacked to a depth of 40 mils
K138A[d,e]	81TiC–19Co	0.18	2.0	–23	Cobalt-binder phase attacked slightly to a depth of 10 mils.
K21[d,e]	90WTiC–10Co	0.18	2.0	–31	Cobalt-binder phase attacked slightly to a depth of 6 mils.
AA[d,e]	97WC–3Co	0.18	2.0	–2	Specimen cracked during test. No attack.
A[d,e]	94WC–6Co	0.18	2.0	–9	Specimen cracked during test. No attack.
GG[d,e]	88WC–12Co	0.18	2.0	–22	Attacked erratically from 1 to 7 mils with the attack concentrated in the metal phase.

*A_s and A_c are surface areas of specimen and container walls exposed to lithium, respectively; V = volume of lithium.

[a]Specimen size: 0.25 × 0.25 × 0.50 inch.

[b]Designations assigned by manufacturer: Kennametal, Inc., Latrobe, Pennsylvania.

[c]Armco Iron used as the container material.

[d]Designations assigned by manufacturer: Adamas Carbide Corporation, Kenilworth, New Jersey.

[e]Columbium used as the container material.

UNCLASSIFIED
ORNL-LR-DWG 35869

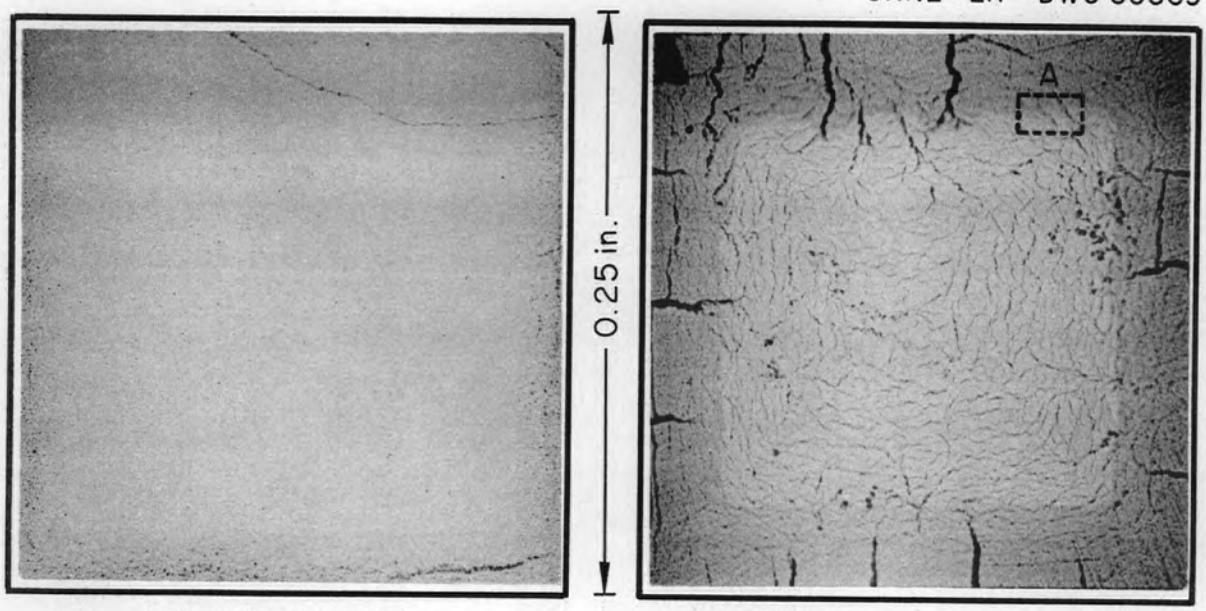

(*a*) 90 TiC – 10 Ni (*b*) 64 TiC – 6 CbTaTiC – 25 Ni – 5Mo

Figure 58. Cross Sections of Cermet Specimens Following Exposure to Lithium. Test Conditions: Static, 1500°F (816°C), 100 Hours. Crack Across Upper Right Corner of (*a*) Occurred During Sectioning Following Test. As Polished.

UNCLASSIFIED
ORNL-LR-DWG. 36140

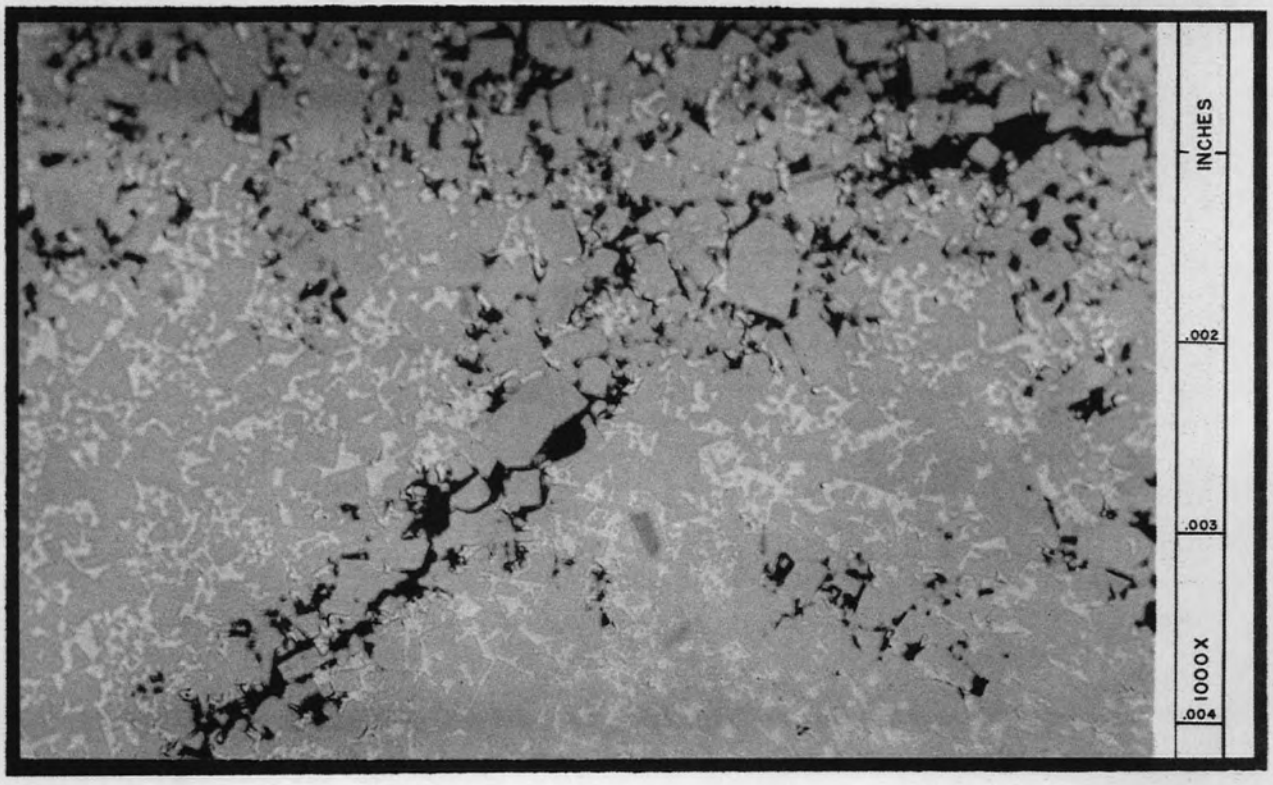

Figure 59. Region A shown in Figure 58 Illustrating the Leaching Action of Lithium on the Nickel-Rich Binder Phase (White) Surrounding the Angular Carbide Particles (Gray). As Polished. 1000X.

Ceramics. A limited number of corrosion tests[77] in liquid lithium demonstrated that the common ceramics, glasses and glass-bonded ceramics, were heavily attacked. An effort was made, therefore, to use very pure, crystalline ceramics for the present study utilizing Armco iron as the container material.

Metallographic examination of the specimens was considered the most important basis for evaluating the corrosion resistance. Due to the porous nature of many ceramics, weight change data were usually difficult to interpret.

The results of test on various ceramic materials are listed in Figure 60.* In the tests on single crystal specimens of MgO, Al_2O_3, and Mg Al_2O_4, the ratio of the surface areas of specimen-to-container was 0.03 in.^{2}/in.^{2}, while the ratio of specimen surface area-to-volume of lithium was 0.7 in.^{2}/in.^{3}. In the tests on other ceramics in lithium, the ratio values were 0.09 in.^{2}/in.^{2} and 0.09 in.^{2}/in.^{3}. Results obtained on similar tests in sodium and lead are included in Figure 60, since it is felt that only by such a comparison can the relative corrosiveness of lithium be appreciated.

Of the ceramics tested in lithium, carbides of titanium, zirconium, and chromium were the only materials to withstand attack. The edges of titanium carbide specimens before and after exposure to lithium are shown in Figure 61, indicating no change as a result of

---

*The tests in lithium were performed in collaboration with W. H. Cook of the General Corrosion Group. The tests in sodium and lead were performed by W. H. Cook.

UNCLASSIFIED
ORNL-LR-DWG 18435

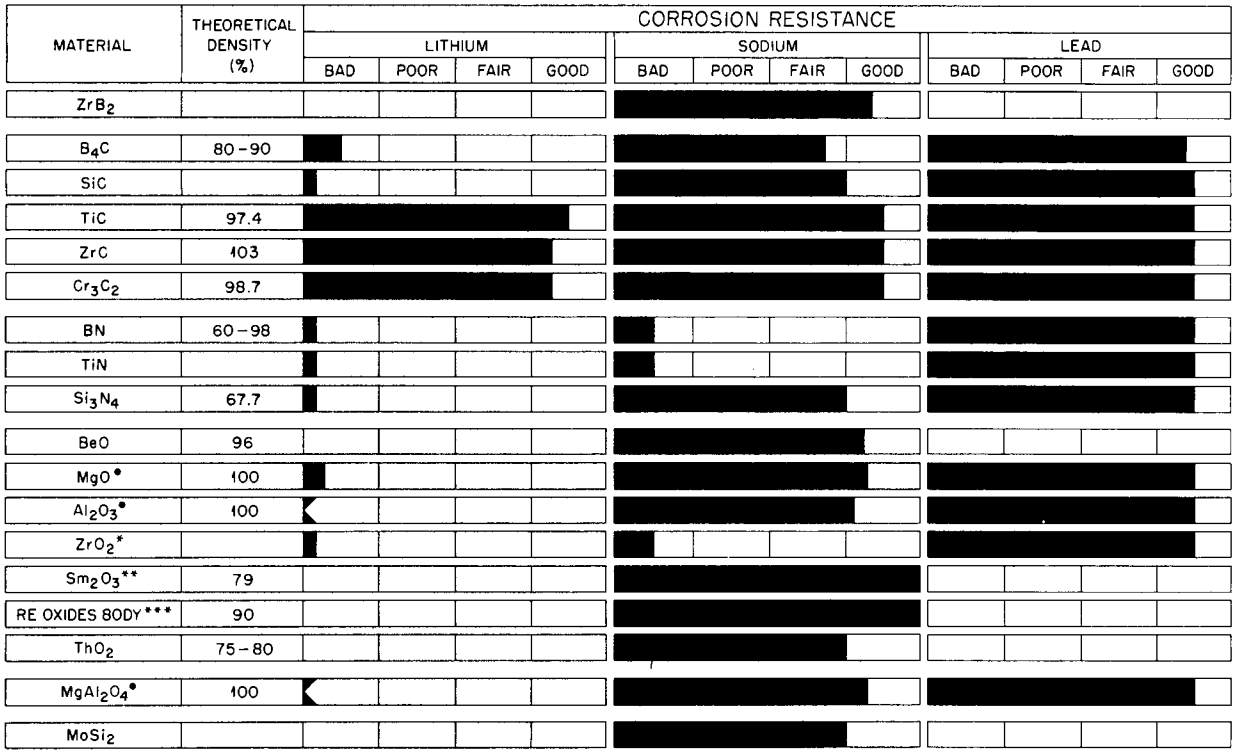

SIGNIFICANCE OF SHORTEST BARS:

- ▮ PIECES OF THE TESTED SPECIMEN REMAINED.
- ◤ THERE WAS NO VISIBLE TRACE OF THE TESTED SPECIMEN.

• A SPECIMEN FROM A SINGLE CRYSTAL.
* CaO-STABILIZED.
** A 1000-hr TEST.
*** A 500-hr TEST. (BODY COMPOSITION: 45.0 TO 49.5 % Sm_2O_3 – 22.5 TO 27 % Gd_2O_3 – BALANCE PRIMARILY OTHER RARE-EARTH OXIDES.)

TYPE OF DATA	ARBITRARY CORROSION RATINGS AND DATA RANGE BASES			
	BAD	POOR	FAIR	GOOD
DEPTH OF ATTACK, mils*	3	2	1	0
WEIGHT CHANGE (%) **	6	4	2	0
DIMENSIONAL CHANGE (%)	3	2	1	0

* MEASURED IN METALLOGRAPHIC EXAMINATIONS.
** DETERMINED BY DIRECT MEASUREMENT AND/OR BY CALCULATIONS BASED ON THE MATERIAL(S) FOUND IN THE TEST MEDIUM BY CHEMICAL ANALYSES.

Figure 60. Corrosion Resistance of Various Ceramics in Lithium, Sodium and Lead. Test Conditions: Static, 1500°F (816°C), 100 Hours.

UNCLASSIFIED
ORNL-LR-DWG 35870

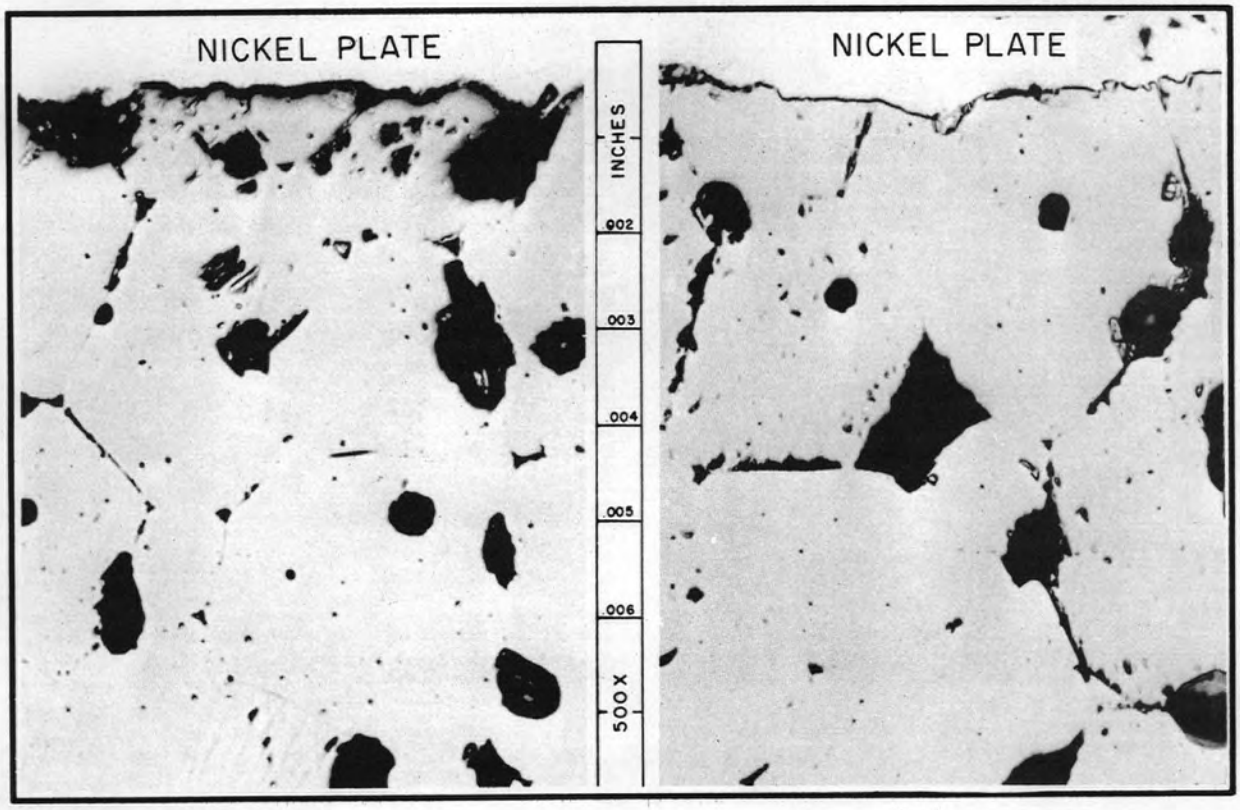

(*a*) (*b*)

Figure 61. Titanium Carbide (TiC), (97.4% of Theoretical Density), (*a*) Before and (*b*) Following Exposure to Lithium in an Iron Container. Test Conditions: Static, 1500°F (816°C), 100 Hours. As Polished. 500X.

the exposure to lithium. The dark areas are voids and illustrate the porous nature of the material.

Severe attack on the nitrides, BN, TiN, and Si_3N_4, produced pieces from each test with phases that could not be identified by x-ray diffraction.

Single crystals of MgO (periclase), Al_2O_3 (sapphire), and $MgAl_2O_4$ (spinel) were heavily attacked by lithium under the conditions of these tests. Zirconia was also severely attacked.

Ceramics in general were found to have very limited corrosion resistance. However, several of the carbides, which are the major constituents of many of the cermets discussed above, apparently have excellent corrosion resistance to lithium.

Seesaw Furnace Test Results

Seesaw furnace tests were conducted primarily to study the tendency of various metals and alloys to undergo temperature-gradient mass transfer in non-isothermal, low-velocity (one to three feet per minute) flow systems. These tests were performed for the most part on refractory metals and stainless steels which had exhibited good corrosion resistance in static test systems. In addition, two relatively low-temperature tests were performed on the nickel-base alloy, Inconel.

Metals

The metals studied were molybdenum, columbium, vanadium, and zirconium. Since most of these metals possess limited oxidation resistance at the temperatures investigated, it was necessary to encapsulate the test components in a protective Inconel container (see Figure 9c). The results, which are given in Table XIX, showed that in respect to all acceptability criteria — solution attack, intergranular attack, and mass transfer — these metals were highly resistant to corrosion by lithium under the conditions of the tests. The shallow subsurface void formation observed in vanadium is considered to be of minor significance.

It is to be noted that molybdenum was tested at higher temperatures and for longer times than the other metals in this series. The absence of attack on molybdenum in both hot and cold regions of the 150-hour test is shown in Figure 62, which is representative of all

TABLE XIX

RESULTS OF LITHIUM CORROSION TESTS ON VARIOUS REFRACTORY METALS IN SEESAW FURNACE TEST SYSTEMS

Furnace Tilting Rate: ½ cycle per minute

Metal	Hot Zone		Cold Zone		Length of Test, Hours	Specimen Weight Change (mg/in.^{2})		Metallographic Observations
	°F	°C	°F	°C		Hot Zone	Cold Zone	
Molybdenum[a]	1700	(927)	1000	(538)	500	−0.1	+0.4	Hot Zone: No attack. Cold Zone: No attack or crystal deposition.
Molybdenum	1800	(982)	1000	(538)	100	−0.3	−0.7	Hot Zone: No attack. Cold Zone: No attack or crystal deposition.
Molybdenum	1800	(982)	1050	(566)	500	−0.1	+2.2	Hot Zone: No attack. Cold Zone: No attack or crystal deposition.
Molybdenum	1900	(1038)	1000	(538)	100	−0.4	−0.8	Hot Zone: No attack. Cold Zone: No attack or crystal deposition.
Molybdenum	1900	(1038)	1100	(593)	150	−0.3	+0.4	Hot Zone: No attack. Cold Zone: No attack or crystal deposition.
Columbium[b]	1600	(871)	1100	(593)	300	+0.1	0	Hot Zone: No attack. Cold Zone: No attack or crystal deposition.
Vanadium[c]	1500	(816)	900	(482)	100	−1.3	0	Hot Zone: 1 mil subsurface attack. Cold Zone: No attack or crystal deposition.
Zirconium[d]	1500	(816)	1100	(593)	100	+0.2	0	Hot Zone: No attack. Cold Zone: No attack or crystal deposition.

[a]Molybdenum – 0.46 Ti, 0.0012 O_2, 0.0006 N_2, 0.030 C (weight per cent).
[b]Columbium – 0.23 Zr, 0.0071 O_2, 0.0088 N_2, 0.0066 C (weight per cent).
[c]Vanadium – 0.15 O_2, 0.14 C, 0.041 N_2, 0.0001 H_2 (weight per cent).
[d]Reactor Grade Zirconium – 0.120 O_2, 0.0047 N_2, 0.0036 H_2 (weight per cent).

[redacted]

ORNL-LR-DWG 35731

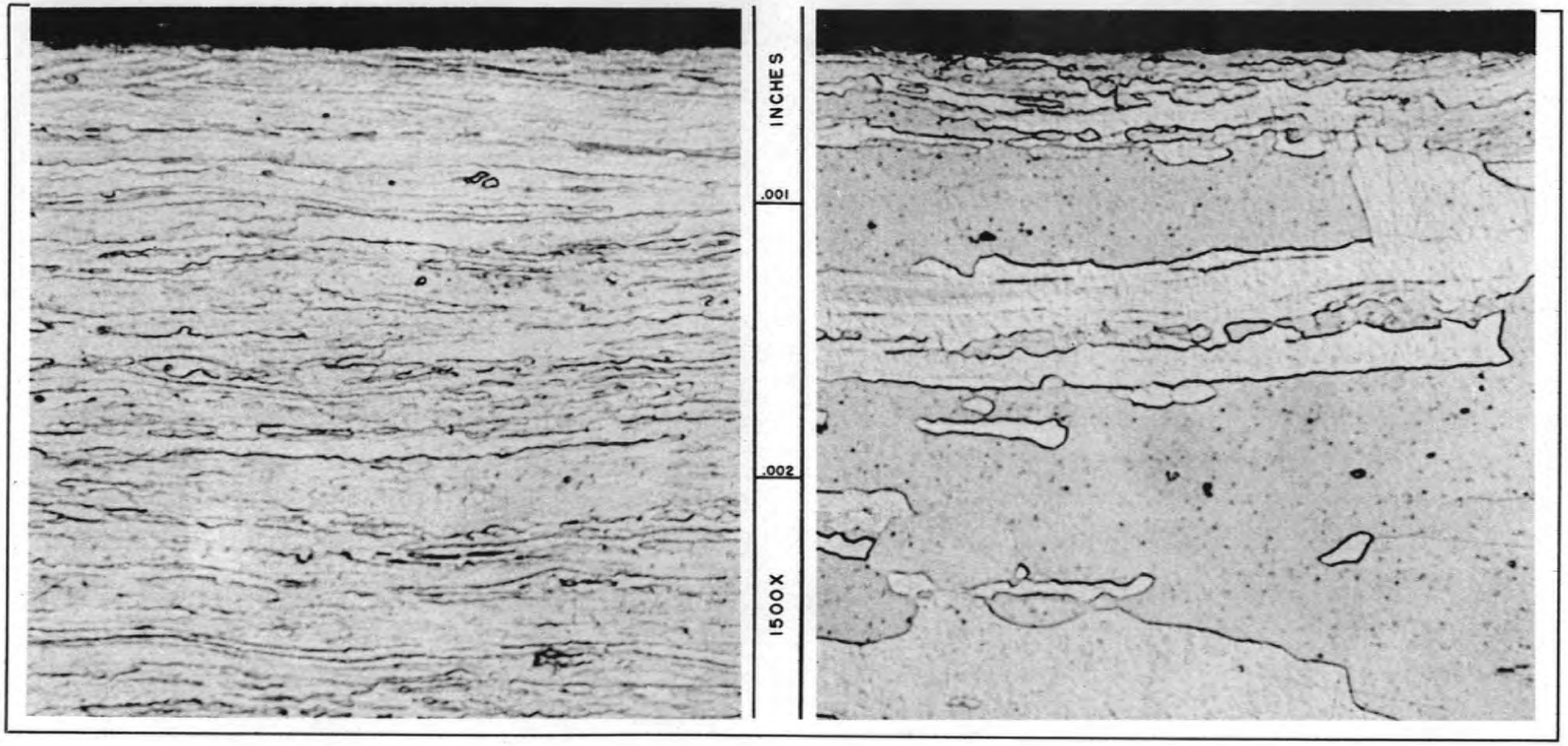

(*a*) COLD ZONE–1100°F (593°C)

(*b*) HOT ZONE–1900°F (1038°C)

Figure 62. Cold- and Hot-Zone Specimens from Molybdenum Seesaw Capsule Following Exposure to Lithium. Test Conditions: ½ Cycle Per Minute, 150 Hours (4500 Cycles). Etchant: HF, HNO_3, H_2SO_4, H_2O (25-10-10-55 Volume Per Cent).

molybdenum runs. In the photomicrograph of the hot-zone region shown in Figure 62 it is evident that recrystallization and grain growth occurred during the test.

Alloys

Iron-Base Alloys. Seesaw tests on iron-base alloys were limited to three austenitic stainless steels and one ferritic stainless steel.

1. Austenitic Stainless Steels. The austenitic stainless steels studied were types 304, 316, and 347, with the major effort on type 316. The results, which are listed in Table XX, showed that, in general, complex interactions occurred in all regions of the test components. It is evident that the austenitic stainless steels are definitely inferior to the refractory metals, discussed previously, under the conditions which obtain in seesaw-type tests. Pertinent experimental observations made in connection with the tests under consideration may be summarized as follows:

(a) For the type 316 alloy, the amounts of both hot-zone dissolution of test metal and crystal deposition in the cold zones were observed to increase with increasing hot-zone temperature, as shown in Figure 63.

(b) Metallic mass transfer crystals were visible in the cold zones of all but one of the capsules operated at hot-zone temperatures in excess of 1300°F (704°C). The crystals shown in Figure 63 on the cold-zone wall of the 1600°F (871°C) test on type 316 were found to be high in nickel and low in chromium relative to the before-test container analysis.

TABLE XX

RESULTS OF LITHIUM CORROSION TESTS ON AUSTENITIC STAINLESS STEELS IN SEESAW FURNACE TEST SYSTEMS

Furnace Tilting Rate: 1 cycle per minute

Material[a]	Hot Zone		Cold Zone		Length of Test, Hours	Appearance of Cold Zone	Metallographic Observations
	°F	°C	°F	°C			
304[b] SS[c]	1500	(816)	1350	(732)	100	Crystals	Hot Zone: ½-mil GBA[d]. Cold Zone: No attack, 1 mil metallic crystals.
316[e] SS	1300	(704)	960	(516)	100	No crystals	Hot Zone: ½-mil GBA; ½-mil carbide crystals. Cold Zone: No attack or crystals.
316 SS	1400	(760)	900	(482)	500	Crystals	Hot Zone: 1 mil GBA. Cold Zone: ½-mil metallic crystals.
316 SS	1500	(816)	1130	(610)	100	Crystals	Hot Zone: 1 mil GBA. 1 mil carbide crystals. Cold Zone: 1 mil metallic crystals.
316 SS	1500	(816)	1075	(590)	100	Crystals	Hot Zone: 1 mil GBA. Cold Zone: No attack, ½-mil metallic crystals.
316 SS	1500	(816)	900	(482)	100	No crystals	Hot Zone: 3 mils of subsurface voids. Cold Zone: No attack or crystals.
316 SS	1500	(816)	1000	(538)	500	Crystals	Hot Zone: 2 mils of subsurface voids. Cold Zone: No attack; 10-mil metallic crystals.
316 SS	1500	(816)	900	(482)	500	Crystals	Hot Zone: 7 mils of subsurface voids. Cold Zone: No attack; 4 mil metallic crystals.
316 SS	1600	(871)	1100	(593)	500	Crystals (71.4Fe, 3.4Cr, 23.5Ni)	Hot Zone: 4 mils of subsurface voids. Cold Zone: 3 mil carbide crystals. 13 mil metallic crystals.
347[f] SS	1500	(816)	1000	(538)	100	Crystals	Hot Zone: 4 mils of subsurface voids. Cold Zone: 2 mil metallic crystals.
347 SS	1500	(816)	1100	(593)	100	Crystals	Hot Zone: 4 mils of subsurface voids. Cold Zone: ½-mil metallic crystals.

[a]Dimensions of containers: Length, 15 inches; outside diameter, 0.75 inches; wall thickness, 0.035 inches.

[b]Nominal composition in weight per cent: 69Fe, 19Cr, 10Ni, 0.08C max.

[c]SS stands for stainless steel.

[d]GBA stands for grain-boundary attack.

[e]Nominal composition in weight per cent: 67Fe, 17Cr, 12Ni, 2Mo, 0.10C max.

[f]Nominal composition in weight per cent: 69Fe, 18Cr, 10Ni, 1Cb, 0.08C max.

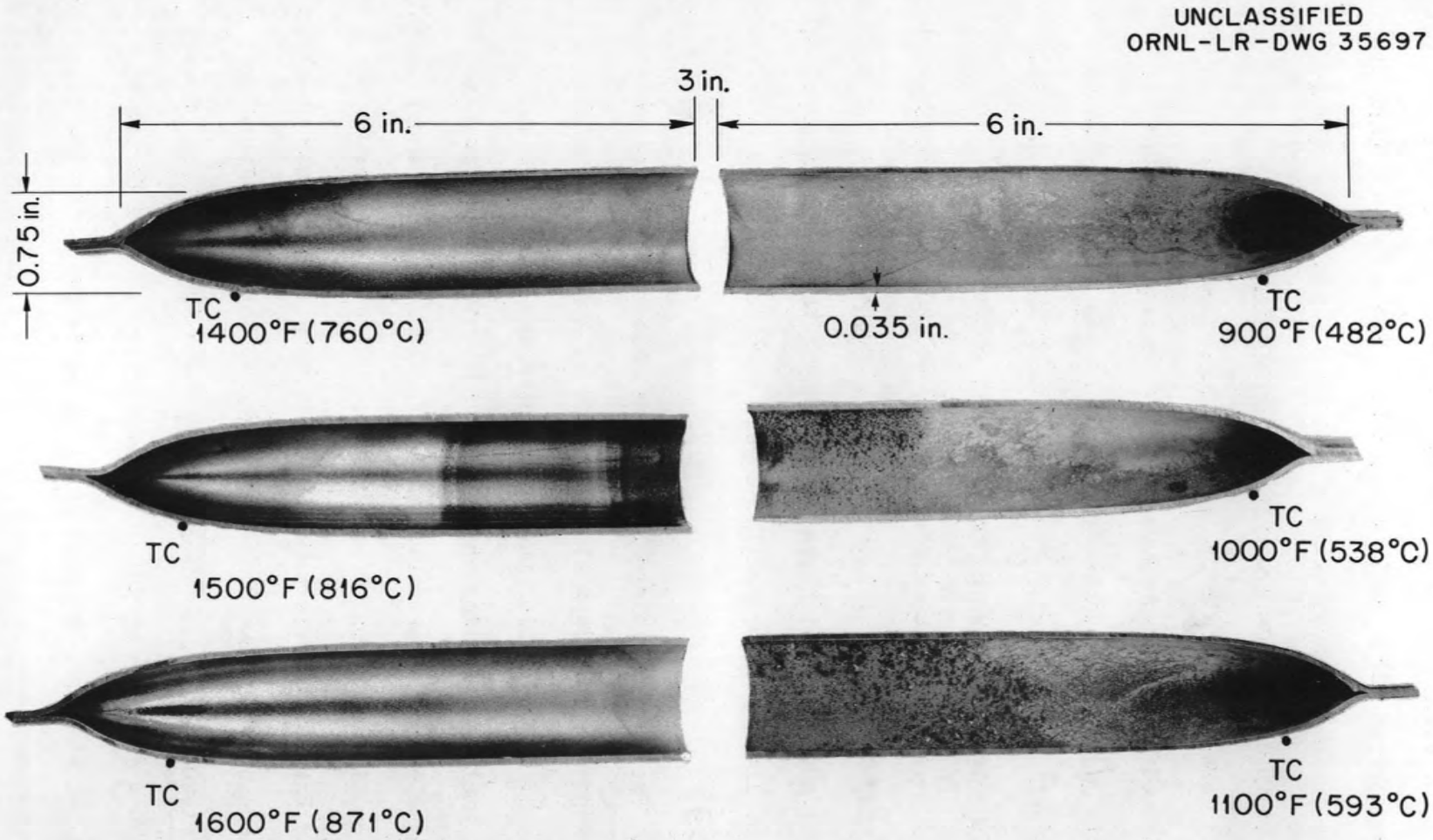

Figure 63. Type 316 Stainless Steel Seesaw Test Capsules Following Exposure to Lithium. Test Conditions: 1 Cycle Per Minute, 500 Hours (30,000 Cycles); 5 Inches of Lithium in Capsule.

(c) The attack in hot zones was found to be quite shallow and generally occurred along grain boundaries. The metallographic appearance of the hot-zone walls of the capsules shown in Figure 63 is illustrated in the photomicrographs of Figure 64.

(d) Carbide crystals of the type described in the section of this report covering two-component static tests on iron-base alloys (see Figure 38) were found on hot-zone walls in two tests and on the cold-zone wall in one test. The formation of the carbide crystals could not be correlated with specific test conditions.

(e) X-ray analysis of the hot-zone walls of all capsules which were operated in excess of 1300°F (704°C) indicated the presence of a ferrite surface layer which was attributed to the leaching of alloying elements by lithium. The ferrite layers were not detected metallographically.

2. Ferritic Stainless Steel. The results of six seesaw-type tests on type 446 stainless steel are listed in Table XXI. The complexity of the corrosion phenomena which can occur in a multicomponent, multiphase alloy when placed in contact with flowing lithium at elevated temperatures was well illustrated by these tests. The most prominent corrosion reactions are discussed below:

(a) Extensive temperature-gradient mass transfer was observed in tests operated for 100 hours or longer at hot-zone temperatures in excess of 1400°F (760°C). The rapid increase in the amount of mass transfer as a function of hot-zone temperature is illustrated in Figure 65, which shows the cold zones of three test capsules following

UNCLASSIFIED
ORNL-LR-DWG 35695

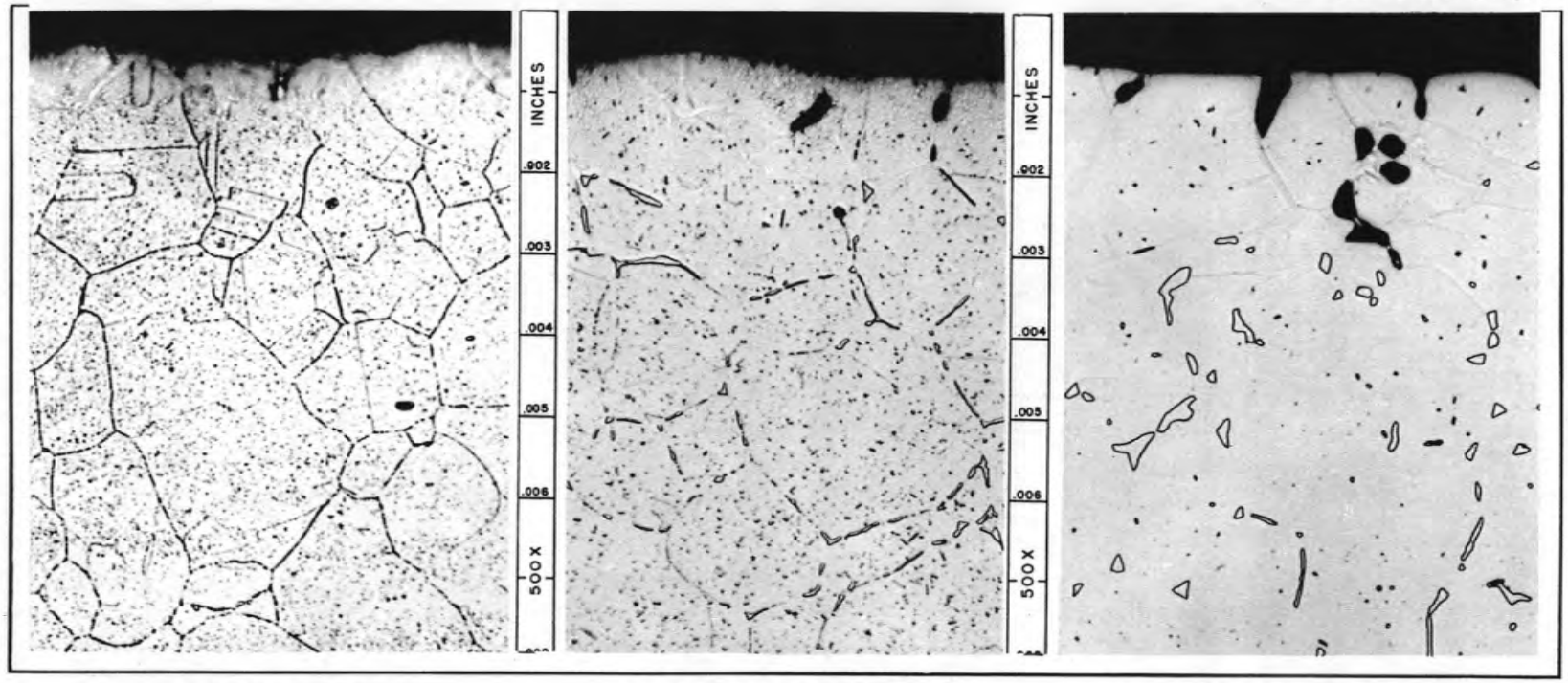

(*a*) 1400°F (760°C) (*b*) 1500°F (816°C) (*c*) 1600°F (871°C)

Figure 64. Hot-Zone Sections from Type 316 Stainless Steel Seesaw Capsules Following Exposure to Lithium. Test Conditions: 1 Cycle Per Minute, 500 Hours (30,000 Cycles); Hot-Zone Temperatures Indicated. Etchant: Glyceria Regia. Reduced 10.5%.

TABLE XXI

RESULTS OF LITHIUM CORROSION TESTS ON TYPE 446 STAINLESS STEEL AND INCONEL IN SEESAW FURNACE TEST SYSTEMS

Furnace Tilting Rate: 1 cycle per minute

Material[a]	Hot Zone		Cold Zone		Length of Test, Hours	Appearance of Cold Zone	Metallographic Observations
	°F	°C	°F	°C			
446 SS[b]	1200	(649)	1050	(566)	100	No crystals	Hot Zone: 57 mils GBP[c]. Cold Zone: 21 mils GBP.
446 SS	1400	(760)	1130	(610)	100	No crystals	Hot Zone: 20 mils GBP. Cold Zone: 52 mils GBP, ½-mil carbide crystals.
446 SS	1500	(816)	1130	(610)	100	Crystals	Hot Zone: 10 mils GBP. Cold Zone: 45 mils GBP, 2 mil metallic crystals.
446 SS	1500	(816)	1200	(650)	100	Crystals (0.25 grams) (87.7Fe, 11.7Cr, 0.6Ni)	Hot Zone: 12 mils GBP. Cold Zone: 40 mils of GBP, 2 mil duplex crystals.
446 SS	1600	(871)	1250	(677)	24	Crystals	Hot Zone: 10 mils GBP. Cold Zone: 35 mils GBP. No crystals.
446 SS	1800	(982)	1300	(704)	100	Crystals (2.0 grams) (86.7Fe, 11.5Cr, 0.9Ni)	Hot Zone: 25 mils GBP, 3 mil solution attack. Cold Zone: 35 mils GBP, 6 mil duplex crystals.
Inconel[d]	1200	(649)	1100	(593)	100	Crystals (0.38 grams)	Hot Zone: 5 mils GBA[e]. Hard, unidentified phase in attacked areas. Cold Zone: 0.5 mil metallic crystals.
Inconel	1200	(649)	1100	(593)	500	Crystals (0.7 gram) (95.5Ni, 3.1Cr, 1Fe)	Hot Zone: 10 mils GBA. Hard, unidentified phase in attacked areas. Cold Zone: 2 mil crystals.

[a]Dimensions of containers: Length, 15 inches; outside diameter, 1.0 inch; wall thickness, 0.075 inches.

[b]Nominal composition in weight per cent: 73Fe, 25Cr, 0.5Ni, 0.35C (max.); SS stands for stainless steel.

[c]GBP stands for grain-boundary penetration.

[d]Nominal composition in weight per cent: 80Ni, 14Cr, 6Fe.

[e]GBA stands for grain-boundary attack.

UNCLASSIFIED
ORNL-LR-DWG 35732

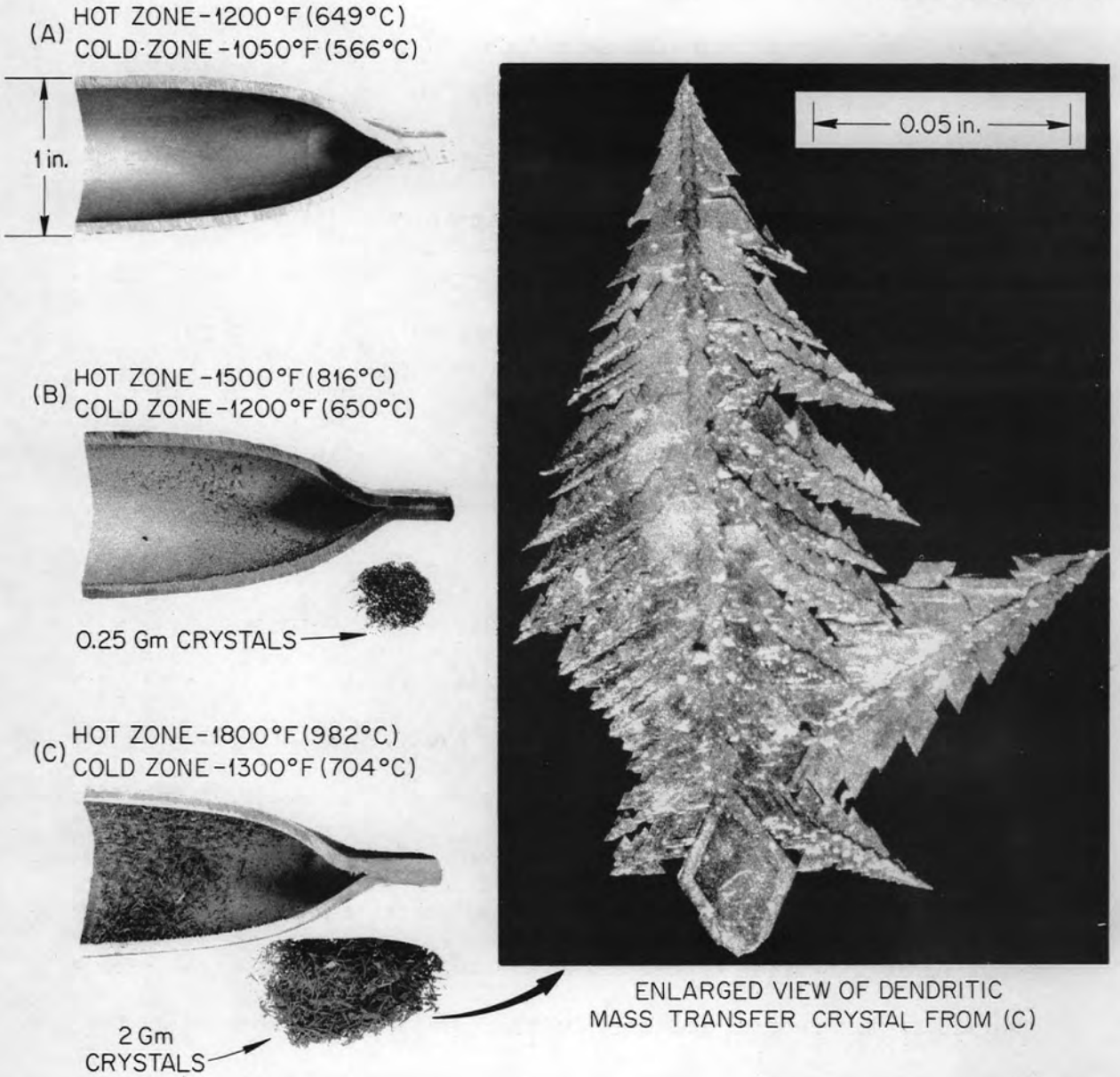

Figure 65. Cold-Zone Sections from Type 446 Stainless Steel Seesaw Capsules Following Exposure to Lithium. Test Conditions: 1 Cycle Per Minute, 100 Hours (6000 Cycles).

100-hour seesaw tests. The dendritic nature of the crystal deposits is quite apparent. As indicated in Table XXI, these deposits were high in iron and low in chromium relative to the before-test container analysis. No crystal deposits were found in the test conducted at a hot-zone temperature of 1200°F (649°C).

(b) Grain-boundary carbide precipitates in type 446 stainless steel were found to be particularly susceptible to attack by lithium. The deepest intergranular attack was observed in those regions which operated in the temperature range 1100 – 1200°F (593 – 649°C). Penetrated regions such as that shown in the photomicrograph in Figure 66 were found by chemical analysis to contain as much as one weight per cent of lithium.

(c) Abnormally large grains were observed to develop in the central regions of hot-zone wall thicknesses, and chromium carbide crystals were deposited on cold-zone walls. These effects, which are illustrated in Figures 67 and 68, respectively, were investigated and found to be related to the reaction between lithium and grain-boundary carbides in the hot zones. The dissolution of carbides near the surface of the hot wall produced a carbon concentration gradient resulting in diffusion of carbon to the surface and the dissolution of carbides in the central portions of the wall. In the absence of the grain-boundary carbides, very rapid grain growth occurred. Similar grain-size variations were observed by McKee[78] in a type 316 stainless steel-lithium system operated at 1800°F (982°C). Chemical, metallographic, microhardness, and x-ray diffraction studies showed

UNCLASSIFIED
ORNL-LR-DWG 35864

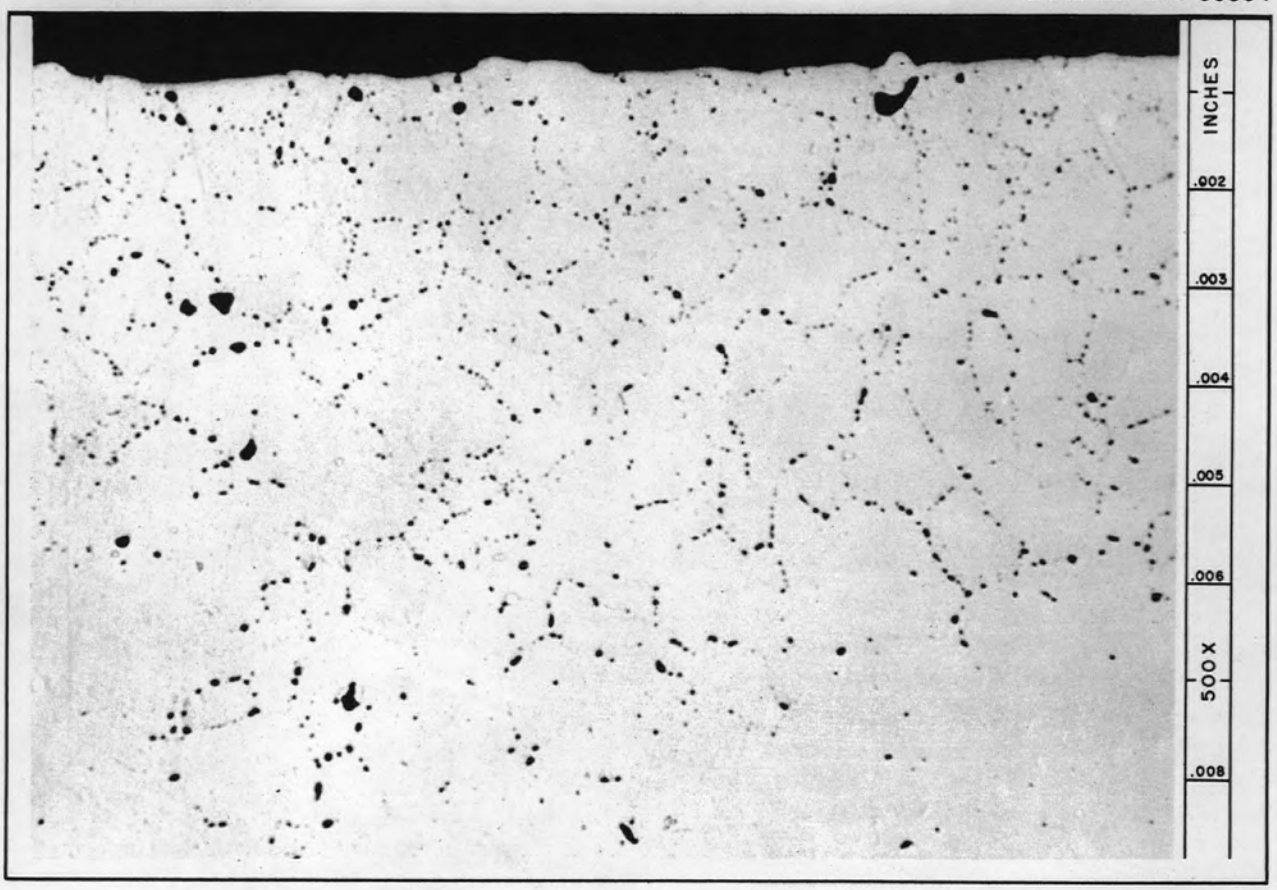

Figure 66. Hot-Zone Wall of Type 446 Stainless Steel Seesaw Test Capsule. Test Conditions: 1 Cycle Per Minute, 24 Hours (1440 Cycles); Hot Zone – 1600°F (871°C), Cold Zone – 1250°F (677°C). As Polished. 500X.

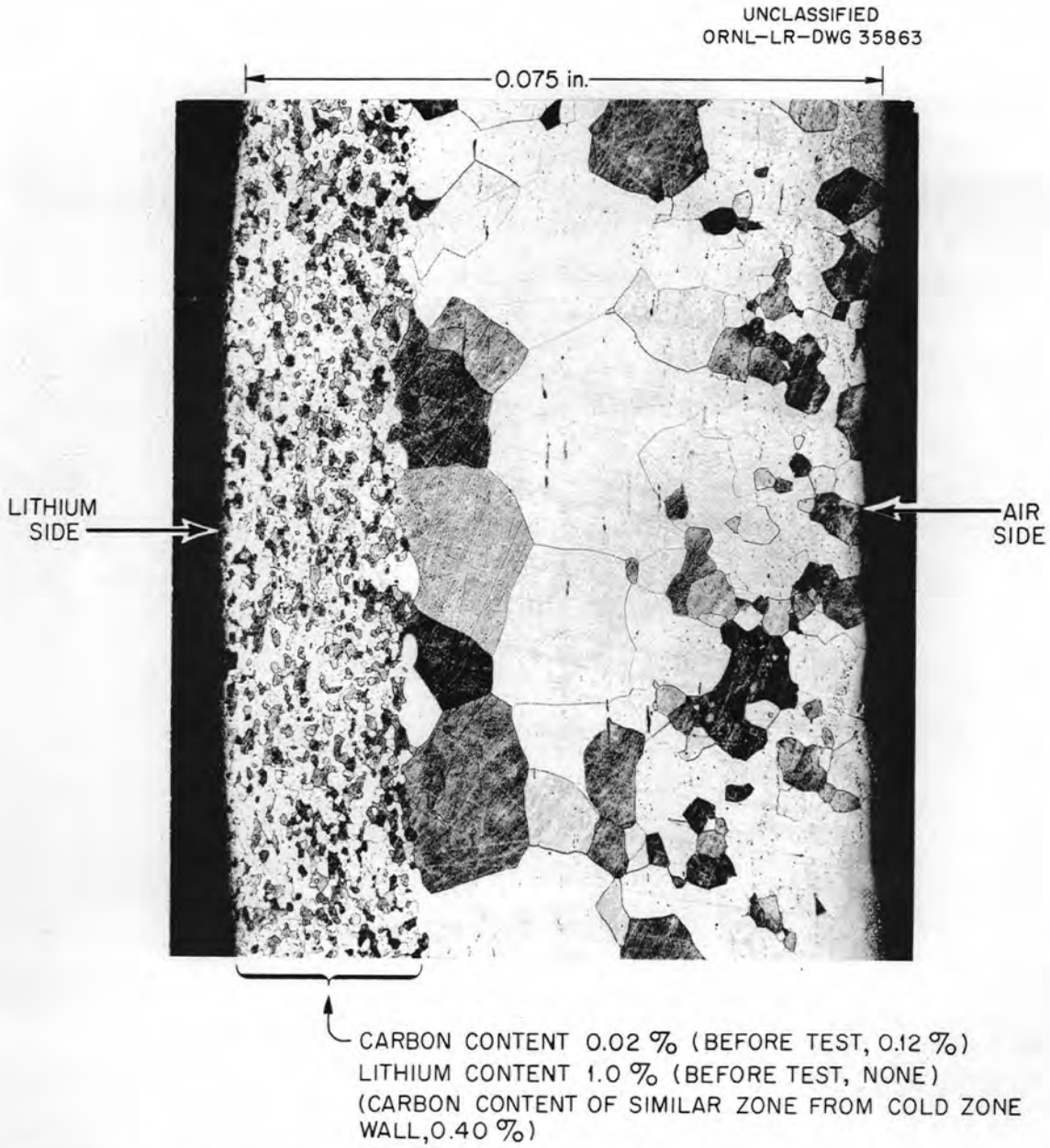

Figure 67. Hot-Zone Wall of Type 446 Stainless Steel Seesaw Test Capsule. Test Conditions: 1 Cycle Per Minute (6000 Cycles), Hot Zone – 1800°F (982°C), Cold Zone – 1300°F (704°C), 100 Hours. Etched with Glyceria Regia. 50X.

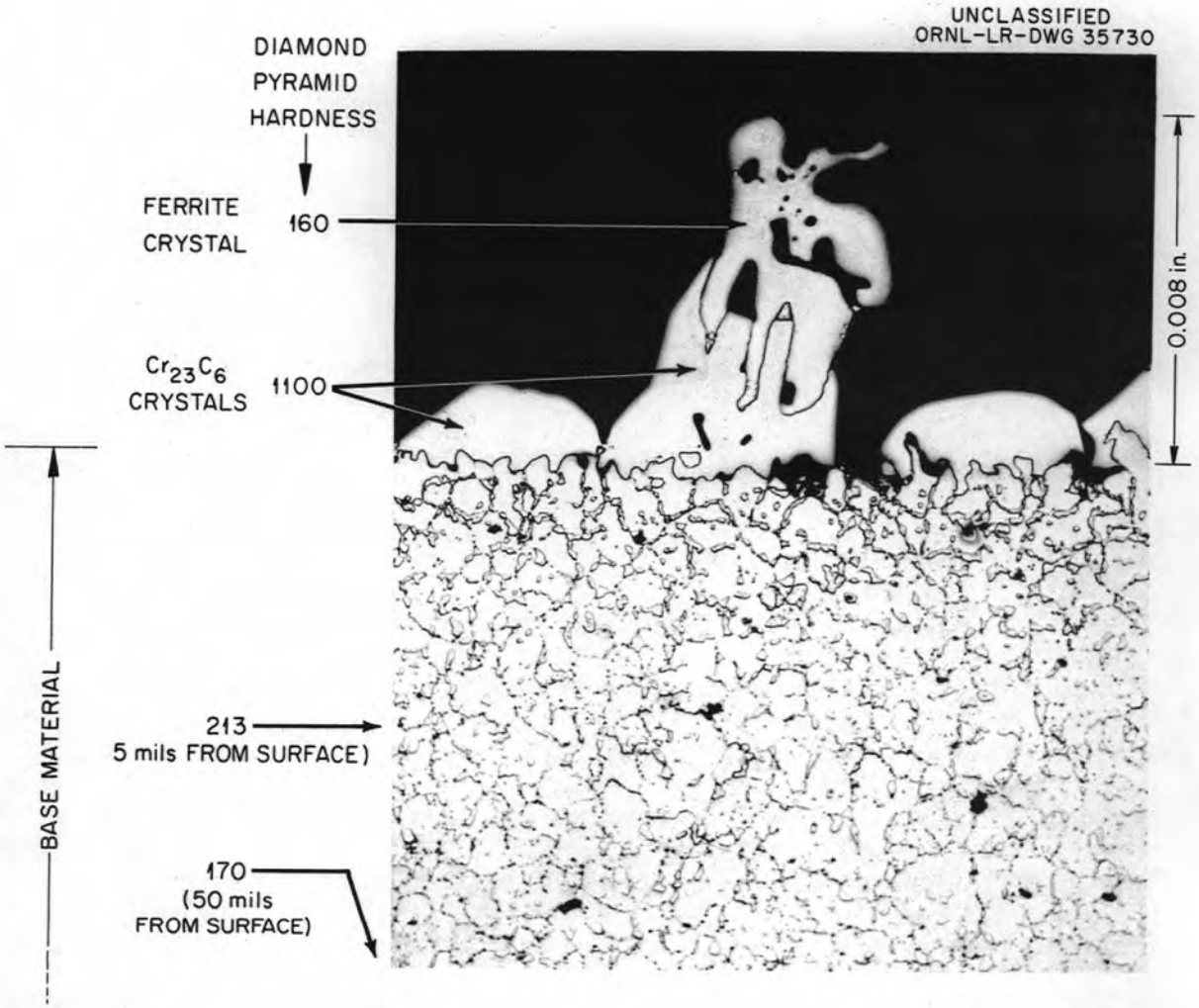

Figure 68. Cold-Zone Wall of Type 446 Stainless Steel Seesaw Test Capsule. Test Conditions: 1 Cycle Per Minute, 100 Hours (6000 Cycles); Hot Zone – 1800°F (982°C), Cold Zone – 1300°F (704°C). Etchant: Glyceria Regia. 250X.

that considerable carbon enrichment had occurred at the cold-zone wall (Figure 68) during the test. A 25-mil layer machined from the inside surface was found to contain 0.40 weight per cent carbon as compared to 0.12 per cent before test and a carbide gradient was metallographically evident. X-ray analysis of the surface indicated the presence of $Cr_{23}C_6$ and ferrite.

Nickel-Base Alloys. The appreciable solubility of nickel in molten lithium[79] suggested that nickel-base alloys would experience extensive temperature-gradient mass transfer. Consequently, the corrosion behavior of only one such alloy, Inconel, was investigated in the seesaw test apparatus. The results of two tests conducted at hot-zone temperatures of 1200°F (649°C) with a relatively small temperature gradient of 100 Fahrenheit degrees are given in Table XXI. Extensive mass transfer was observed in test periods as short as 100 hours. The mass transfer crystals were found to be preferentially enriched in nickel and low in chromium and iron relative to the before-test capsule analysis. A hard phase (Diamond Pyramid Hardness-850, 25 gram load), similar in metallographic appearance to the chromium-rich sigma phase frequently observed in stainless steels, was observed in the microstructure of attacked hot-zone regions.

Thermal Convection Loop Test Results

Thermal convection loop tests were performed with columbium, several austenitic and ferritic stainless steels, and to a very limited extent with the nickel-base alloy, Inconel. The three basic apparatus designs utilized are described in detail in Chapter VI (p 34). Loop Type "A" represented an early loop design and was used in testing Inconel and some of the stainless steels. Loop Type "B" was an improved version of Type "A" and was used in the later tests of the stainless steels. The tests with columbium were performed in Type "C" loops which were designed to be operated inside either evacuated or inert-gas-filled enclosures. In some experiments small specimens of the test metal were suspended in the loop in order to determine weight changes resulting from corrosion.

Columbium

Six columbium thermal convection loop tests were conducted using two methods of preventing oxidation of the columbium. The loop test conditions and results are summarized in Table XXII.

Loops Nos. 51, 52, 54, and 55 were fabricated from welded columbium tubing prepared from sintered columbium stock. A columbium filler wire was used in making the saddle-welds* at the top of the hot legs. The first of these loops (No. 51) was also clad with type 310 stainless steel to protect the columbium from oxidation.

---

*All welding on columbium described in this section was performed in an inert-gas atmosphere chamber.

TABLE XXII

RESULTS OF LITHIUM CORROSION TESTS ON COLUMBIUM IN THERMAL CONVECTION LOOP TEST SYSTEMS

Lithium Flow Velocity = 2–3 feet per minute

Loop Number	Hot Leg °F	Hot Leg °C	ΔT[a] °F	ΔT[a] °C	Length of Test, Hours	Specimen Weight[b] Change (mg/in.^{2}/100 hours)	Metallographic Observations
51[c]	1500	(816)	250	(139)	500	No specimen	Hot Leg: Complete penetration (20 mils) of saddle-weld zone. ½-mil GBA[d] of base material. Cold Leg: No attack.
52[e]	1600	(871)	300	(167)	155	−0.1	Hot Leg: Complete penetration (20 mils) of saddle-weld zone. 10 mils GBA of heat affected zone. No attack of base material. Cold Leg: No attack.
54[e]	1600	(871)	300	(167)	23	+2.2	Hot Leg: Complete penetration (20 mils) of saddle-weld zone and longitudinal tube weld. 10 mils GBA of base material. Cold Leg: No attack.
55[e]	1600	(871)	200	(111)	55	−5.2	Hot Leg: Complete penetration (20 mils) of saddle-weld zone and base material. Cold Leg: 3 mils GBA in longitudinal tube weld.
58[f]	1600	(871)	200	(111)	36	−14.0	Hot Leg: 10 mils GBA of arc-cast insert. Complete penetration (30 mils) of longitudinal tube weld and 8 mils GBA of base material. Cold Leg: 6 mils of attack in longitudinal tube weld. No attack of base material.
59[f]	1500	(816)	200	(111)	115	+0.1	Hot Leg: 9 mils GBA of arc-cast insert. Complete penetration (30 mils) of longitudinal tube weld. 16 mils GBA of base material. Cold Leg: 4 mils GBA of longitudinal tube weld. No attack of base material

[a]ΔT stands for the maximum temperature difference between hot and cold legs.

[b]Specimen suspended in hot leg of loop.

[c]Welded columbium tubing 0.5 inch outside diameter by 0.020 inch wall thickness; analysis: O_2–0.007, N_2–0.018, C–0.010, Zr–0.08, (weight per cent); clad with type 310 stainless steel; 0.020 inch wall thickness.

[d]GBA stands for grain-boundary attack.

[e]Welded columbium tubing, 0.5 inch outside diameter by 0.020 inch wall thickness; analysis: O_2–0.038, N_2–0.014, C–0.015, Zr–0.49, (weight per cent).

[f]Two-inch length of arc-cast columbium tubing, 0.5 inch outside diameter by 0.030 inch wall thickness; analysis: O_2–0.045, N_2–0.009, C–0.015, Zr–0.06, (weight per cent). Remainder of loop of welded tubing 0.5 inch outside diameter by 0.030 inch wall thickness; analysis: O_2–0.027, N_2–0.016, C–0.016, Zr–0.06, (weight per cent).

The cladding was omitted in the fabrication of subsequent loops, and they were operated in the stainless steel vacuum box shown in Figure 12 (p 37).

Loop No. 51 was terminated after 500 hours. Extreme grain-boundary cracking in the columbium saddle weld at the top of the hot leg was revealed when the stainless steel shroud was removed (Figure 17, p 57). Lithium penetration of the saddle-weld areas also caused the termination of test Loops Nos. 52, 54, and 55. In the case of Loop No. 52, attack was limited to the weld itself and to the heat-affected zone adjacent to the weld. No penetration of the base material was observed. In Loops Nos. 54 and 55, however, attack of the longitudinal tube weld and the base material was also detected.

In order to eliminate the problem of penetration of the grain boundaries in the columbium saddle welds, and 85 Zr – 15 Cb (weight per cent) alloy, which had shown good resistance in a static test at 1832°F (1000°C), was utilized in the braze-welding of the saddle joints of Loops Nos. 58 and 59. In addition, two-inch lengths of arc-cast, seamless columbium tubing were inserted in the hot legs of these loops as shown in Figure 69; the butt joints for these inserts were also braze-welded with the Zr-Cb alloy.

The inserts were added in order to compare the corrosion resistance of columbium tubing made from arc-cast stock and sintered stock in the same loop test. These loops failed as a result of lithium penetration through the longitudinal tube welds in the hot legs. The outside surface of a penetrated weld zone and a transverse

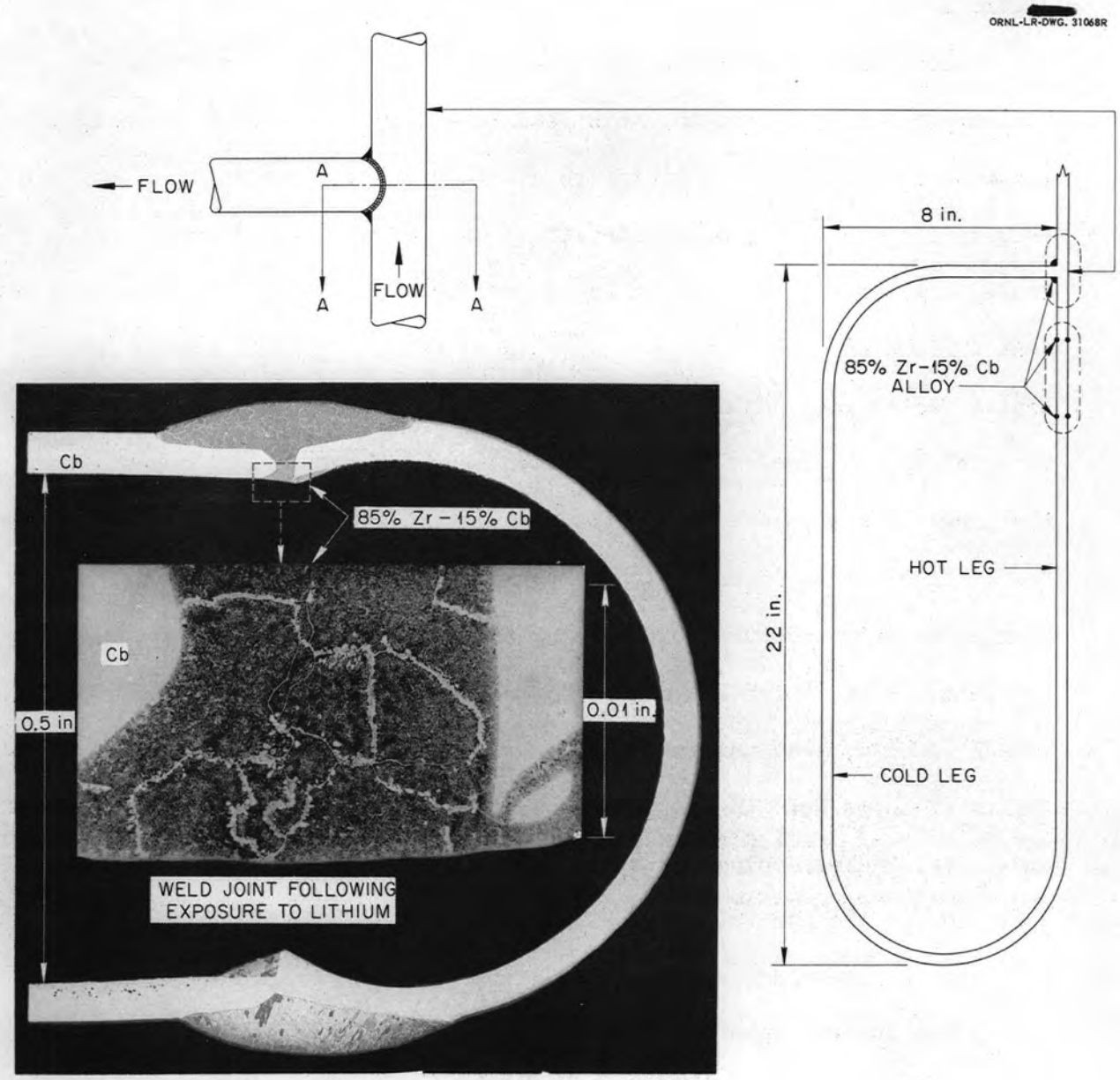

SECTION A-A THROUGH SADDLE WELD AREA SHOWN ABOVE

Figure 69. Columbium Saddle Joint Braze Welded with 85Zr–15Cb (Weight Per Cent) Alloy Following Exposure to Lithium. Thermal Convection Loop No. 59. Test Conditions: Hot-Leg Temperature – 1500°F (816°C); Cold-Leg Temperature – 1300°F (704°C); 115 Hours. As-Polished.

section of the tube wall showing the grain-boundary path of the penetration of the weld zone are illustrated in Figure 70. The metallographic appearance of the arc-cast insert and the sintered tubing are illustrated in Figure 20 (p 63). Both the arc-cast inserts and the adjacent sintered tubing were attacked to depths of eight mils or more in Loops Nos. 58 and 59. These loops also failed as a result of lithium penetration through the longitudinal tube welds in the hot legs of the loops.

Weight-loss specimens of the type illustrated in Figure 13.2 (p 41) were suspended in the hot legs of five of the loops listed in Table XXII. Small weight gains or weight losses were found, and due to the relatively short test times no conclusions could be reached concerning the temperature-gradient mass transfer tendencies of columbium in dynamic lithium systems.

The investigation on columbium described in the section of this chapter (see p 55) indicated that oxygen contamination of the columbium was responsible for the severe grain-boundary attack described above. The variation in the amount of oxygen contamination in the various parts of the sintered columbium could account for the "scatter" in the depths of attack reported in Table XXII.

Alloys

Thermal convection loop tests on alloys were confined to the austenitic and ferritic stainless steels with the exception of one test on Inconel. Four austenitic and two ferritic stainless steels

[redacted]

Y-26678

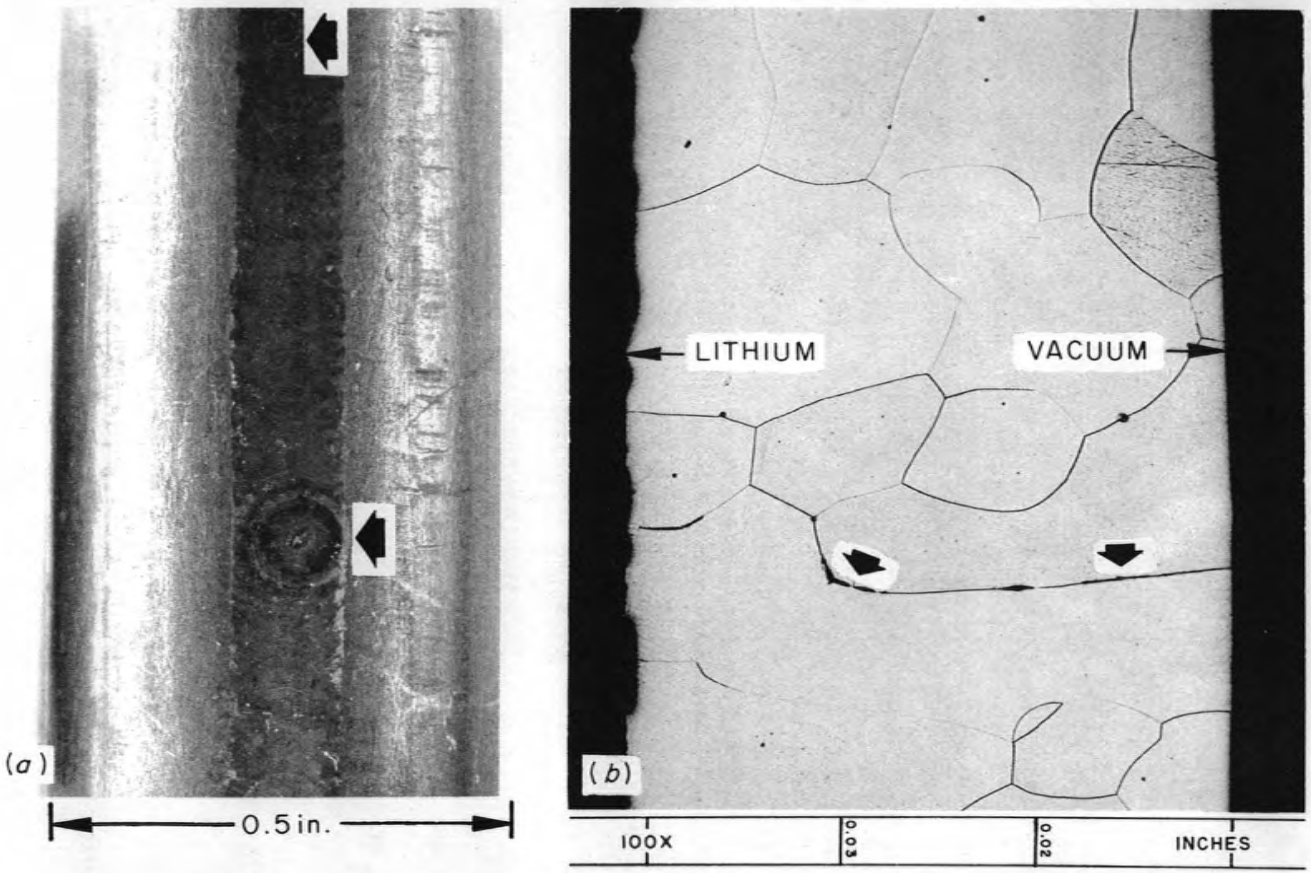

Figure 70. (*a*) Low Magnification View of the Longitudinal Weld Zone in the Hot Leg of Columbium Thermal-Convection Loop No. 58 Which Leaked During Test. (*b*) High Magnification View of Tube Wall Showing Path of Lithium Penetration. Etchant: HF-H_2SO_4-HNO_3-H_2O, 25-10-10-55, Volume Per Cent.

were studied with thirteen of the twenty-four stainless steel loop tests being performed on type 316 stainless steel. Loop tests on alloys were conducted at hot-leg temperatures ranging from 1000 to 1600°F (538 to 871°C) for time periods of 88 to 3,000 hours.

The most important factors considered in evaluating thermal convection loop test results for these alloys were: (1) weight-losses from specimens suspended in the hot legs of the loops, (2) the corrosion revealed by metallographic examination of the hot- and cold-leg walls, (3) the weight of mass-transferred crystals found in the loop following test, and (4) the time required for the loop to plug, if plugging occurred. Chemical analyses were obtained for the mass-transferred crystals found in the cold legs of loops, and these data were correlated with analyses of metal machined from the hot- and cold-leg surfaces of the loops following test. In this manner the preferential leaching of alloying elements could be followed.

Nickel-Base Alloy (Inconel). It was shown previously that Inconel experienced extensive mass transfer in seesaw furnace tests. Nevertheless, because of the importance of Inconel as a commercial high-temperature structural material, it was considered desirable to ascertain the extent and nature of corrosion suffered by this alloy in a thermal convection loop. Accordingly, a single Inconel loop was operated under the relatively mild test conditions afforded by a hot-zone temperature of 1300°F (704°C) with a thermal gradient of 100°F (56°C) between the hot and cold legs. A loop of the

Type "A" design was utilized and the test was of 1000 hours duration.

Photomicrographs of transverse sections through the hot and cold legs of this loop are shown in Figure 71. The hot leg was heavily attacked to a depth of about sixteen mils, while both crystal deposition and intergranular attack occurred in the cold zone.

Although the temperature gradient in the loop was rather small, massive quantities of crystals were detected in the cold leg (1.5 g) and the fill pot (13.5 g) of the loop. These crystals were analyzed and found to contain 92.4 Ni – 7.0 Cr – 0.6 Fe (weight per cent). In view of the nominal composition of Inconel (80 Ni – 14 Cr – 6 Fe, weight per cent), it is apparent that the mass-transfer process for Inconel involved the preferential leaching of nickel from the walls of the hot zone.

Iron-Base Alloys (Austenitic and Ferrite Stainless Steels). Thermal convection loop tests of iron-base alloys were restricted to studies of the austenitic and ferritic stainless steels.

1. Preliminary Tests with Type "A" Loops. A total of seventeen loop tests were conducted with types 316, 321, 347, 430, and 446 stainless steels. All loops were of the Type "A" design (see Figure 11, p 36). The hot-leg temperatures in these tests ranged from 1000 – 1500°F (538 – 816°C) with temperature gradients of 140 – 400°F (79 – 223°C) between the hot and cold zones. The experiments varied from 204 to 3,000 hours in length. Results of these tests are summarized in Tables XXIII, XXIV, and XXV.

UNCLASSIFIED
ORNL-LR-DWG. 36136

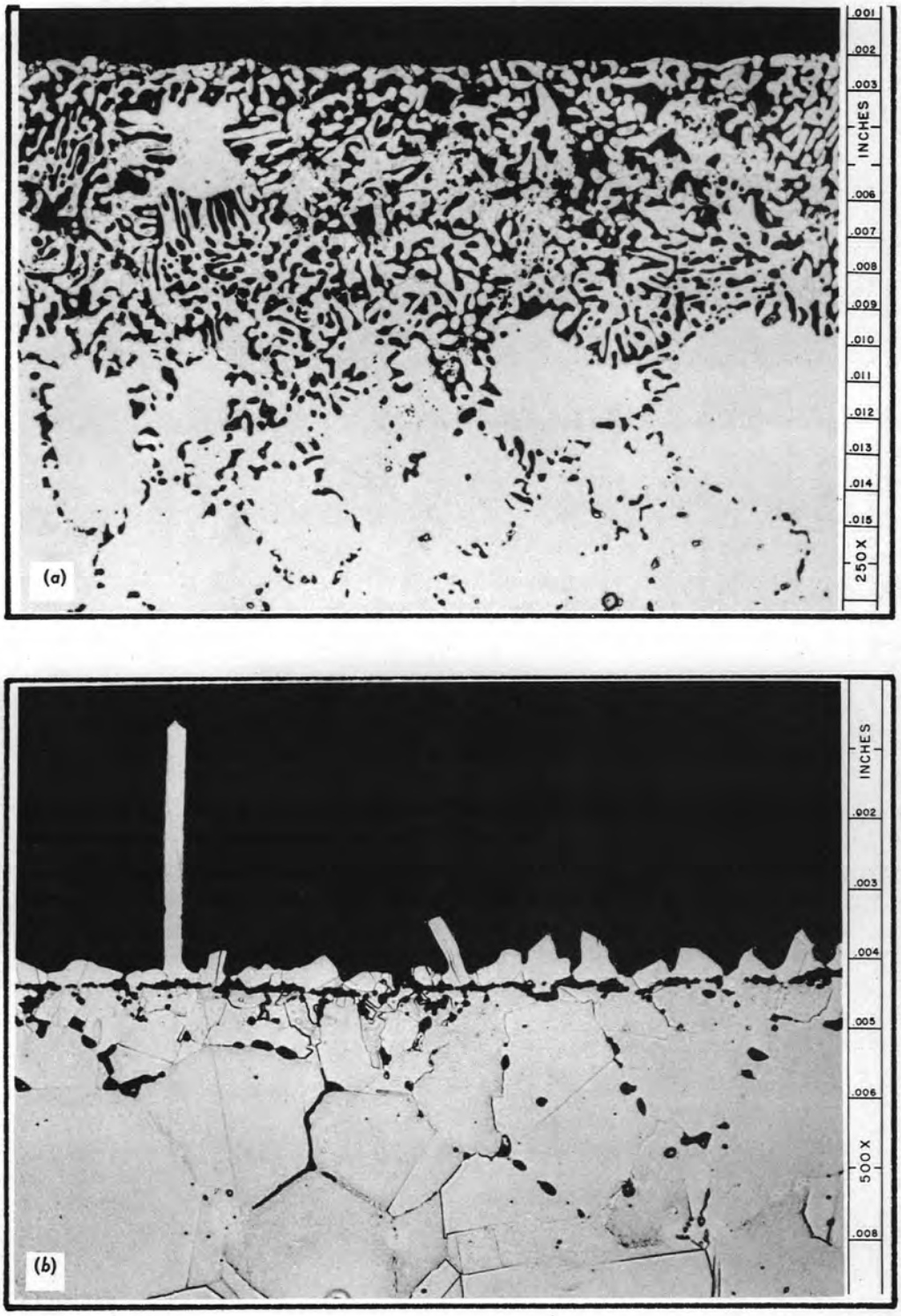

Figure 71. (*a*) Hot-Leg and (*b*) Cold-Leg Sections from Inconel Loop Following Exposure to Lithium. Test Conditions: Hot-Leg Temperature – 1300°F (704°C); Cold-Leg Temperature – 1200°F (649°C); 1000 Hours. (*a*) As-Polished, (*b*) Etchant: Glyceria Regia. Reduced 15%.

TABLE XXIII

RESULTS OF LITHIUM CORROSION TESTS ON TYPE 316 STAINLESS STEEL[a] IN THERMAL CONVECTION LOOP TEST SYSTEMS[b]

Lithium flow velocity = 3–4 feet per minute

Loop Number	Hot Leg °F	Hot Leg °C	ΔT[c] °F	ΔT[c] °C	Length of Test, Hours	Total Mass Transfer[d] mg	Metallographic Observations
1	1500	(816)	200	(111)	500	500	Hot Leg: 15 mils GBA[e] Cold Leg: 14 mils GBA. 2-mil duplex[f] crystals.
2	1500	(816)	280	(157)	1000	100	Hot Leg: 2 mils GBA. Cold Leg: 1 mil GBA. 1-mil duplex crystals.
3	1470	(798)	140	(79)	1000	10	Hot Leg: 5 mils GBA. Cold Leg: 1 mil GBA. No crystals.
4	1400	(760)	270	(150)	2150[g]	4700	Hot Leg: 23 mils GBA. Cold Leg: 5 mils GBA. 5-mil duplex crystals.
5	1310	(708)	250	(137)	290[g]	900	Hot Leg: 3 mils subsurface voids. 1-mil carbide crystals. Cold Leg: No attack, 2-mil duplex crystals.
6	1300	(704)	200	(111)	1000	250	Hot Leg: 15 mils GBA. 1-mil carbide crystals. Cold Leg: 10 mils GBA. 1-mil duplex crystals.

[a] Pipe size: 0.84 inch outside diameter by 0.109 inch wall thickness, pipe analysis: Fe–68.7, Cr–15.4, Ni–11.5, Mo–2.1, Mn–1.8, C–0.06 (weight per cent).

[b] All loops of type "A" design without diffusion cold trap.

[c] ΔT is the maximum temperature difference between hot and cold legs.

[d] Weight of crystals collected from loop following test.

[e] GBA stands for grain-boundary attack.

[f] Duplex crystal is carbide-metal crystal.

[g] Loop plugged with mass transfer crystals.

TABLE XXIV

RESULTS OF LITHIUM CORROSION TESTS ON TYPES 321[a] AND 347[b] STAINLESS STEEL IN THERMAL CONVECTION LOOP TEST SYSTEMS[c]

Lithium Flow Velocity = 3–4 feet per minute

Loop Number	Material[h]	Hot Leg °F	Hot Leg °C	ΔT[d] °F	ΔT[d] °C	Length of Test, Hours	Total Mass Transfer[e] mg	Metallographic Observations
7	321	1500	(816)	280	(157)	204[f]	1000	Hot Leg: 1 mil GBA[g]. Cold Leg: No attack. 1 mil metallic crystals.
8	321	1300	(704)	240	(133)	1230[f]	700	Hot Leg: 3 mils GBA. Cold Leg: No attack. 1 mil duplex crystals.
9	347	1500	(816)	400	(223)	280[f]	1500	Hot Leg: 3 mils GBA. Cold Leg: 5 mils GBA. 2 mil duplex crystals.
10	347	1300	(704)	240	(133)	1000	1300	Hot Leg: 6 mils GBA. 1 mil carbide crystals. Cold Leg: 4 mils GBA. 1 mil metallic crystals.
11	347	1000	(538)	380	(212)	1000	0	Hot Leg: 1 mil of subsurface voids. Cold Leg: No attack. 0.2 mil metallic crystals.
12	347	1000	(538)	380	(212)	3000	0	Hot Leg: 3 mils irregular surface attack. Cold Leg: No attack. 0.3 mil metallic crystals.

[a]Pipe size: 0.84 inch outside diameter by 0.109 inch wall thickness. Pipe analysis: Fe–68.5, Cr–15.9, Ni–11.5, Mn–1.4, Ti–0.4, Si–0.5, C–0.05 (weight per cent).

[b]Pipe size: 0.84 inch outside diameter by 0.109 inch wall thickness. Pipe analysis: Fe–70.4, Cr–12.1, Ni–12.0, Mn–1.3, Cb–0.8, Si–0.4, C–0.05 (weight per cent).

[c]All loops of type "A" design without diffusion cold trap.

[d]ΔT is the maximum temperature difference between hot and cold legs.

[e]Weight of crystals collected from loop following test.

[f]Loop plugged with mass transfer crystals.

[g]GBA stands for grain-boundary attack.

[h]Stainless steel.

TABLE XXV

RESULTS OF LITHIUM CORROSION TESTS ON TYPES 430[a] AND 446[b] STAINLESS STEEL IN THERMAL CONVECTION LOOP TEST SYSTEMS[c]

Lithium Flow Velocity: 3–4 feet per minute

Loop Number	Material[f]	Hot Leg °F	Hot Leg °C	ΔT[d] °F	ΔT[d] °C	Length of Test, Hours	Total Mass Transfer[e] mg	Metallographic Observations
13	430	1500	(816)	280	(157)	1500	1000	Hot Leg: 4 mils GBA[g]. 50 mils decarburized. Cold Leg: 5 mils GBA. 6 mils duplex crystals.
14[h]	430	1300	(704)	350	(194)	1530[i]	1400	Hot Leg: 4 mils GBA. 6 mils decarburized. Cold Leg: 7 mils GBA. 2 mil duplex crystals.
15	446	1500	(816)	330	(185)	864[i]	9000	Hot Leg: 8 mils GBA. 30 mils decarburized. Cold Leg: Complete GBA of 84 mil pipe wall. 4 mil layer of duplex crystals.
16	446	1500	(816)	300	(168)	700[i]	6800	Hot Leg: 15 mils GBA. 20 mils decarburized. Cold Leg: Complete GBA of 84 mil pipe wall. 2 mil duplex crystals.
17	446	1300	(704)	240	(133)	1500	200	Hot Leg: 25 mils GBA. 1 mil carbide crystals. Cold Leg: 65 mils GBA. 1 mil duplex crystals.

[a]Pipe size: 0.84 inch outside diameter by 0.109 inch wall thickness. Pipe analysis: Fe–82.3, Cr–15.7, Ni–0.3, Mn–0.5, Si–0.4, C–0.08 (weight per cent).

[b]Pipe size: 0.84 inch outside diameter by 0.109 inch wall thickness. Pipe analysis: Fe–73.2, Cr–22.7, Ni–0.6, Mn–0.6, Si–0.02, C–0.30 (weight per cent).

[c]All loops of type "A" design without diffusion cold trap.

[d]ΔT is the maximum temperature difference between hot and cold legs.

[e]Weight of crystals collected from loop following test.

[f]Stainless steel.

[g]GBA stands for grain-boundary attack.

[h]High nitrogen content of lithium (1300 ppm as compared with normal concentration of 300–400 ppm) following test indicated that loop had leaked during test.

[i]Loop plugged with mass transfer crystals.

Appreciable mass transfer deposits (see Figure 72) were observed in all tests when the hot-leg temperature was equal to, or greater than, 1300°F (704°C), although not all of these loops plugged completely during the course of the tests. Only in the case of the type 347 stainless steel loops (Nos. 11 and 12) operated at hot-leg temperatures of 1000°F (538°C) was mass transfer insignificant. Mass transfer crystals were found on the cold-leg surface of Loop No. 12 which was operated for 3,000 hours, but could be detected only at very high magnification (see Figure 73).

Serious inconsistencies existed, however, in the results of the higher temperature tests, particularly with regard to the time required for plugging as a function of hot-leg temperature. The weight of mass-transferred material necessary to plug a loop also varied widely. The distribution of deposited material in the cold leg and the shape of the mass-transferred crystals exerted a marked influence on the plugging time and on the quantity of crystals required for plugging. It was concluded, therefore, that plugging time was not a useful parameter in gauging the corrosion characteristics of materials in thermal convection loop tests.

Although the experimental difficulties just cited prevented a quantitative evaluation of this set of test results, the corrosion processes observed have a general applicability to the more refined tests described in the following section and are, therefore, summarized as follows:

UNCLASSIFIED
ORNL-LR-DWG 35981

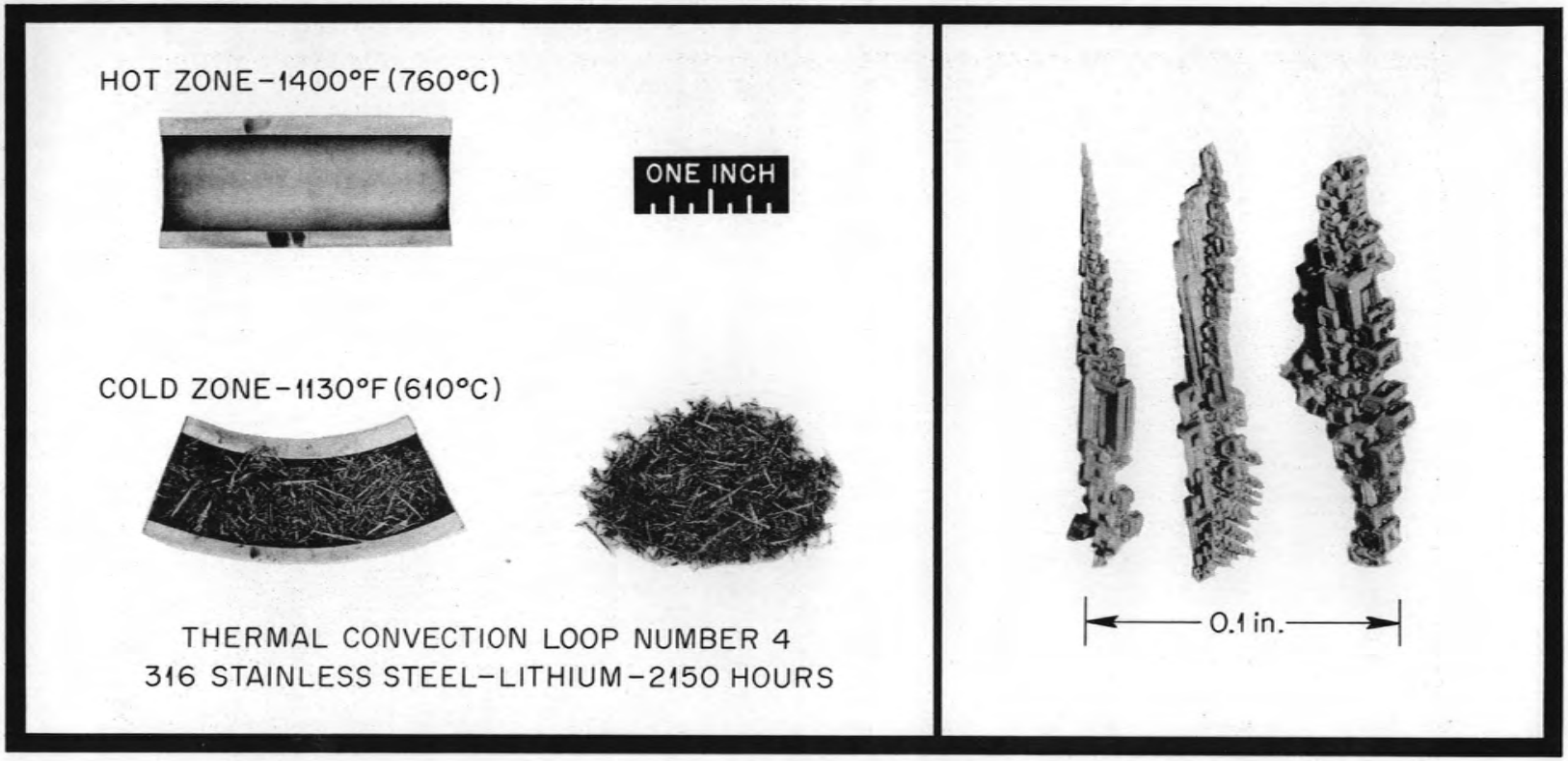

(*a*) (*b*)

Figure 72. (*a*) Hot- and Cold-Leg Sections from Thermal-Convection-Loop Test. (*b*) Enlarged View of Mass-Transfer Crystals.

UNCLASSIFIED
ORNL-LR-DWG 35953

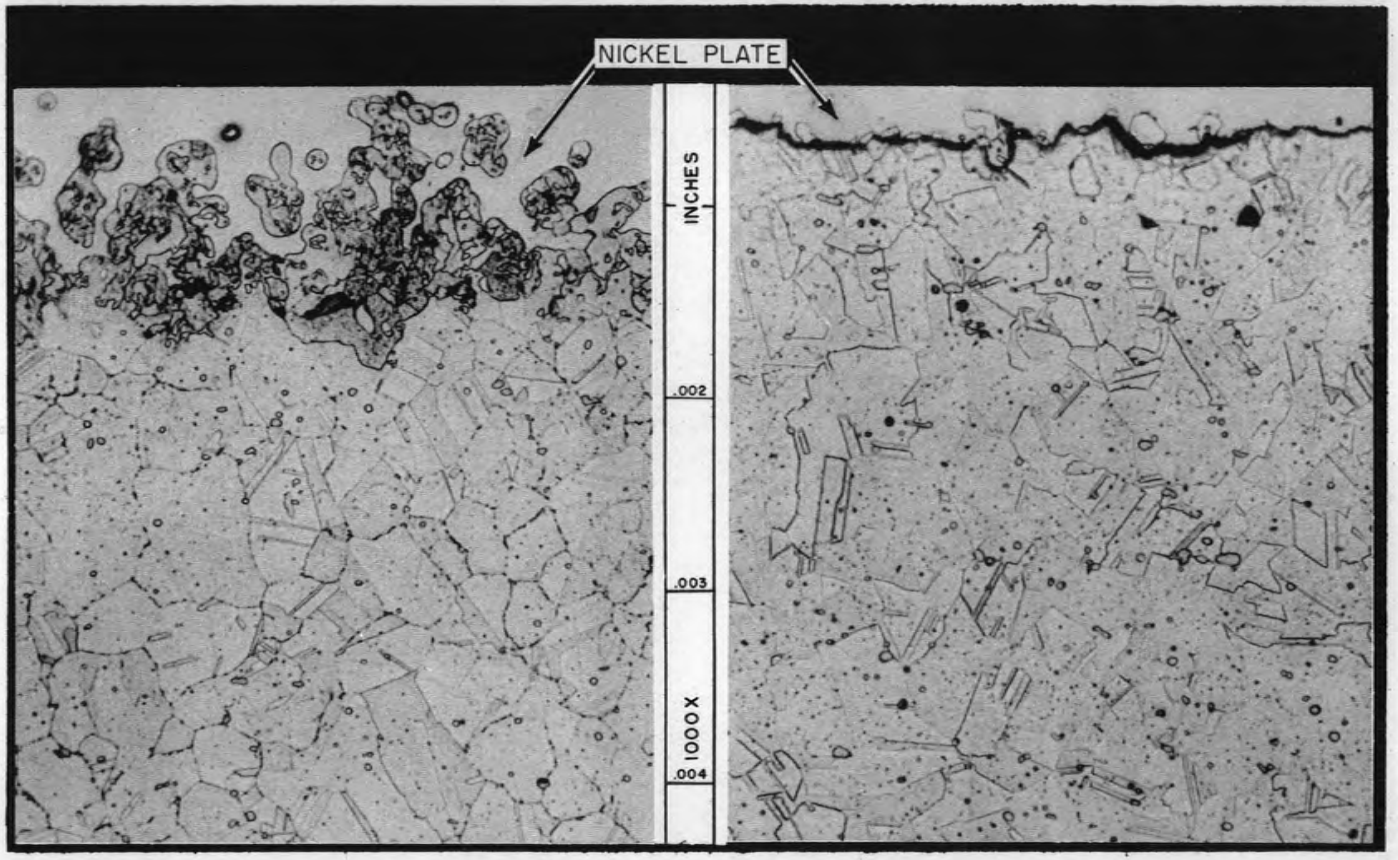

HOT LEG—1000°F (538°C)

COLD LEG—620°F (326°C)

Figure 73. Hot- and Cold-Leg Sections from a Type 347 Stainless Steel Thermal Convection Loop (No. 12) Following Exposure to Lithium for 3000 Hours. Etchant: Glyceria Regia. 1000X.

(a) Mass Transfer Effects. As indicated before, extensive mass transfer occurred at temperatures from 1300 – 1500°F (704 – 816°C). Most of this mass-transferred material was deposited in the form of loose aggregates of metallic crystals, the compositions of which are discussed in more detail in Section 3 below. In addition, a tightly adherent layer of "duplex" crystals was frequently observed on the walls of both the hot and cold legs of the loops. These crystals consisted of a carbide phase, $Cr_{23}C_6$, and a metallic phase of unknown composition but similar in metallographic appearance to the metallic crystals responsible for plugging. A typical example of such a deposit is shown in Figure 74. In a few cases carbide crystals alone were observed attached to the walls of the hot legs of the loops.

(b) Grain-Boundary Attack. The depth of grain-boundary penetration was found to vary widely from loop to loop. However, the deepest penetrations were detected in those loops which circulated lithium that contained more than 500 ppm nitrogen at the completion of the test. A typical example of such attack is shown in Figure 74. Penetration appeared to be slightly less severe for the titanium- and columbium-stabilized stainless steels, types 321 and 347, respectively, than for the unstabilized grade, type 316. Ferritic type 446 stainless steel, which contained considerably more carbon than the other grades tested (0.30 versus 0.05 – 0.08 weight per cent), exhibited significantly more grain-boundary attack than the low-carbon alloys. This effect was especially pronounced in the cold legs of the type 446 stainless steel loops where the cold-zone temperature was

UNCLASSIFIED
ORNL-LR-DWG. 36134

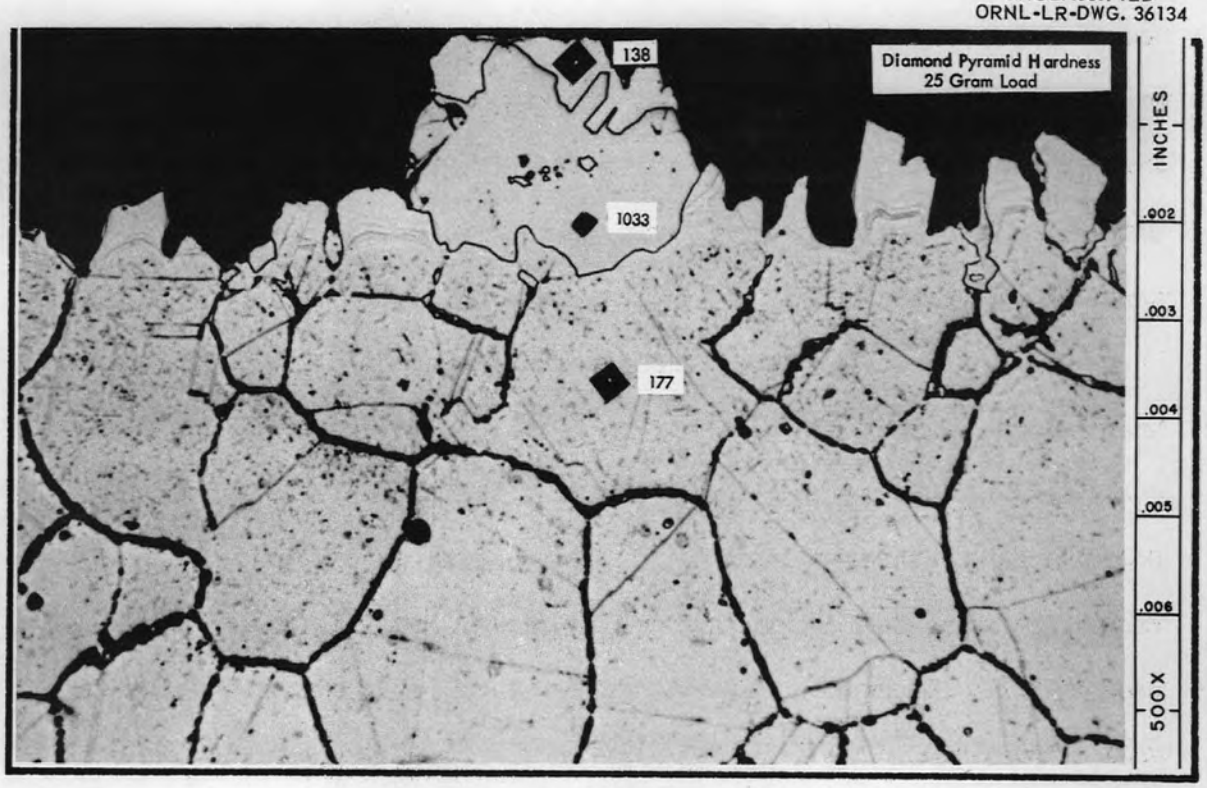

Figure 74. Cold Leg Surface of Type 316 Stainless Steel Loop (No. 1) Following Exposure to Lithium. Test Conditions: Hot Leg – 1500°F (816°C), Cold Leg – 1300°F (704°C), 500 Hours. Note Metallic Crystal (D.P.H.-138), Carbide Crystal (D.P.H.-1033) and Grain Boundary Attack. Etched with Glyceria Regia. 500X.

nearly optimum for the grain-boundary precipitation of carbides. This particularly severe attack of lithium on grain-broundary carbides has already been discussed on page 154.

Special comment is required for the surface attack which occurred in the hot-leg sections of the two type 347 stainless steel loops (Nos. 11 and 12), which were operated at a hot-zone temperature of 1000°F (538°C). As may be seen in Figure 73, the depth of surface attack was limited to one and one-half mils, but the surface was roughened in an extremely irregular manner which can scarcely be described as grain-boundary penetration.

(c) Austenite-to-Ferrite Phase Transformations. Metallographic examination of the hot-leg sections of all of the austenitic stainless steel loops revealed, without exception, the presence of areas of ferrite one to three mils thick. This austenite-to-ferrite phase transformation, as illustrated in Figure 73, resulted from the preferential leaching of the austenite stabilizing elements from the wall surfaces.

2. Tests with Modified Types "A" and "B" Loops. In an effort to obtain more quantitative mass transfer data in the thermal convection loop test, modifications were made in the original loop design. Weight-loss specimens in the form of sleeve inserts and tab inserts, as illustrated on page 41, were incorporated into the hot leg in the zone having the maximum temperature during loop operation. Tests were conducted on type 316 stainless steel only. The selection of this alloy was based on two factors: (1) the background of corrosion

information previously obtained in static and seesaw tests and (2) its high-temperature strength properties. Tests were conducted to determine the influence of (a) hot-leg temperature, (b) diffusion cold trap,* (c) additions of lithium nitride or lithium oxide to lithium, and (d) flow velocity. The effect of hot-leg temperature was investigated using three Type "A" loops (15-inch, hot and cold legs) while the other variables were studied in five Type "B" loops (30-inch, hot and cold legs).

(a) Effect of Hot-Leg Temperature. Three type 316 stainless steel loops of the modified Type "A" design containing both sleeve and tab inserts and with a diffusion cold trap attached were operated at hot-leg temperatures of 1400, 1500, and 1600°F, respectively, (760, 816, and 871°C) and with temperature gradients ranging from 490 to 630°F (273 to 350°C). The results of these tests were summarized in Table XXVI.

Extensive mass transfer occurred in all three of these tests, two of the loops plugging completely during the test period. As in the preliminary studies with type 316 stainless steel, large quantities of metallic crystals were recovered from the cold legs of

---

*Diffusion cold trap is simply an air-cooled extension of the loop pipe from the bottom of the cold leg (see Figure 11, p 36). The use of such a trap was shown in previous work to be effective in reducing the mass transfer tendencies in sodium systems by reducing the oxygen content of the sodium.

TABLE XXVI

RESULTS OF LITHIUM CORROSION TESTS ON TYPE 316 STAINLESS STEEL[a] IN THERMAL CONVECTION LOOP TEST SYSTEMS[b]

Lithium Flow Velocity = $3\frac{1}{2}$–$4\frac{1}{2}$ feet per minute

Purpose of Test: To study the affects of hot-leg temperature on corrosion in stainless steel systems

Loop Number	Hot Leg		ΔT[c]		Length of Test, Hours	Hot-Leg Specimen (Tab)			Total Mass Transfer[d] mg	Metallographic Observations
						Weight Loss	Thickness Loss (mils)			
	°F	°C	°F	°C		mg/in.^{2}/100 hr	Maximum	Minimum		
18	1400	(760)	630	(350)	1090	5.8	$\frac{3}{4}$	$\frac{1}{2}$	100	Hot Leg: 4 mils of subsurface voids. 10 mil crystals. Cold Leg: $\frac{1}{2}$ mil crystals. No attack.
19	1500	(816)	490	(273)	500[e]	17.8	1	$\frac{1}{2}$	823	Hot Leg: 5 mils of subsurface voids. Cold Leg: 3 mil duplex crystals. No attack.
20	1600	(871)	605	(336)	437[e]	42.8	2	1	521	Hot Leg: 6 mils of subsurface voids. Cold Leg: 3 mil duplex crystals. No attack.

[a]Pipe size: 0.84 inch outside diameter by 0.109 inch wall thickness. Pipe analysis: Fe–65.0, Cr–17.5, Ni–12.3, Mo–2.2, Mn–1.8, C–0.10 (weight per cent).

[b]All loops of type "A" design with diffusion cold trap.

[c]ΔT is the maximum temperature difference between hat and cold legs.

[d]Weight of crystals collected from loop following test.

[e]Loop plugged with mass transfer crystals.

the loops at the completion of the tests, and many of the usual manifestations of surface corrosion (see below) were observed in the loops.

In an effort to obtain a more quantitative means for describing mass transfer, it was assumed that the weight losses of the tab inserts were a measure of the extent of mass transfer. These weight-loss data were converted into "mass transfer rates" by computing the weight loss per 100 hours of test time, assuming weight loss to vary linearly with time. As may be seen from Table XXVI, the rate of mass transfer, expressed in these terms, increased consistently with increasing hot-leg temperature.

A plot of the rate of specimen weight loss versus hot-leg temperature is shown in Figure 75. In interpreting this graph, it should be observed that the temperature gradients were not the same in the three loops. The temperature difference, ΔT, between the hot and cold legs of Loop No. 19 (hot-leg temperature, 1500°F) was only 490°F (273°C) as compared to 605 and 630°F (336 and 350°C) for the other two loops. Had the ΔT for Loop No. 19 also been in the neighborhood 600°F (333°C), the mass transfer rate for this loop would have been increased somewhat as a result of the increased flow rate of lithium in the loop. Thus, for equal temperature gradients, it appears reasonable to postulate an approximately linear relationship between the rate of mass transfer and hot-leg temperature in the limited temperature range 1400 – 1600°F (760 – 871°C).

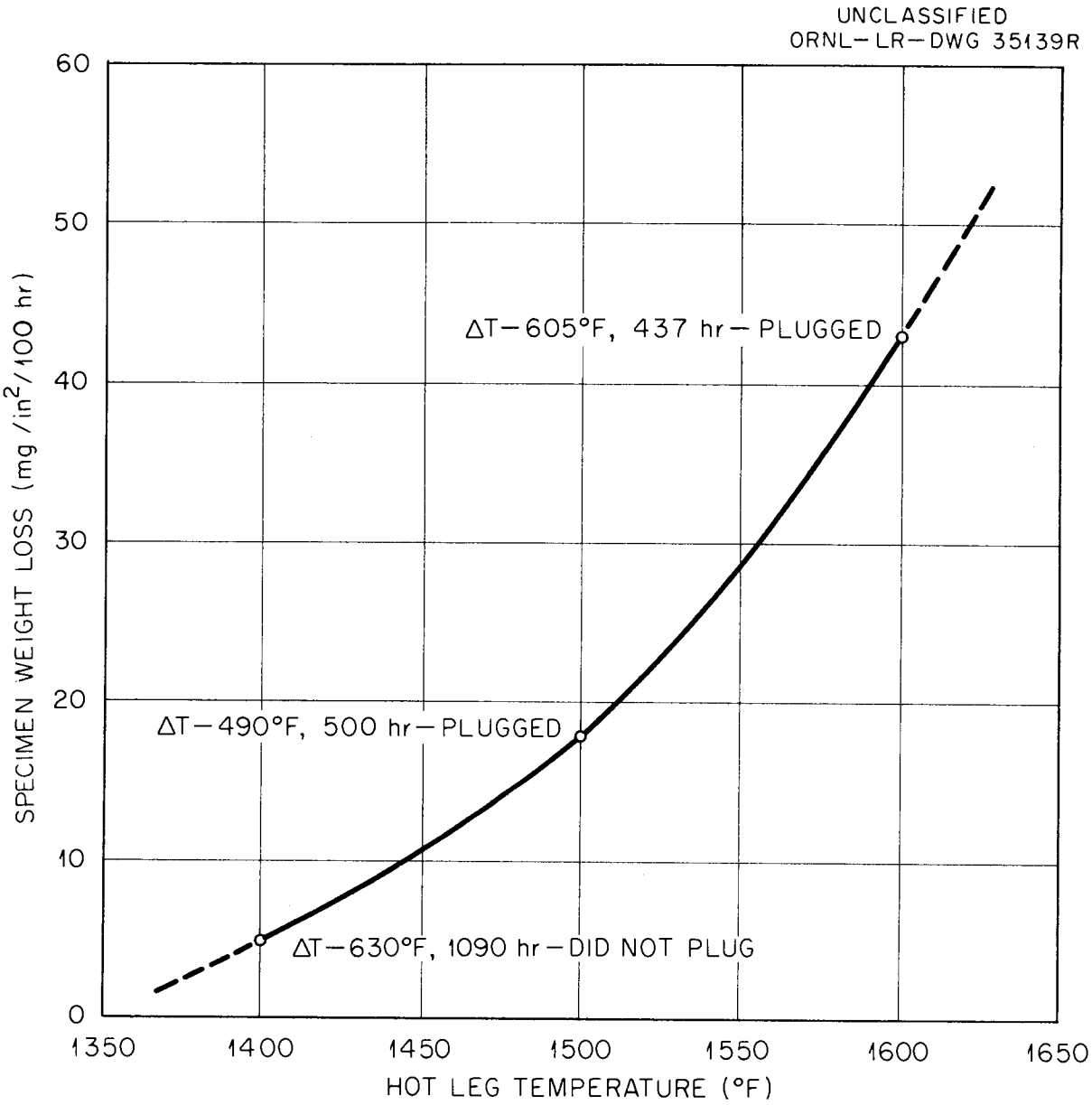

Figure 75. Effect of Hot Leg Temperature in Type 316 Stainless Steel-Lithium Thermal Convection Loop System on the Rate of Removal of Metal from a Specimen Suspended in the Hot Leg.

Weight losses suffered by the sleeve inserts in these and all subsequent tests with type 316 stainless steel loops were only 30 to 50 per cent as large as the weight losses for corresponding tab inserts. On the tab specimens there was a visible and measurable increase in the rate of attack near edges and around the supporting wire where higher liquid velocities developed due to local turbulences in the flow pattern. This effect was responsible for the irregular thickness changes of tab specimens cited in Table XXVII and is illustrated in Figure 77.

The various surface corrosion phenomena observed in these loops were similar in several respects to those encountered in the preliminary thermal convection loop tests. Coarse aggregates of metallic crystals in the cold leg, duplex crystal deposition in both the hot and cold legs, and the austenite-to-ferrite phase transformation in the hot leg were all observed. On the other hand, substantial subsurface void formation rather than grain-boundary attack occurred at all three of the test temperatures. Transverse sections through typical regions of the hot legs of Loops Nos. 18 and 20 are shown in Figure 76.

(b) The Influence of the Diffusion Cold Trap. The reduction of mass transfer in thermal convection loops through the use of a diffusion cold trap is illustrated by the results obtained with Loops Nos. 21 and 22 (see Table XXIX). The two loops were operated under identical conditions and had identical designs except that the cold trap was omitted in Loop No. 22. The rate of mass transfer for

TABLE XXVII

RESULTS OF LITHIUM CORROSION TESTS ON TYPE 316[a] STAINLESS STEEL IN THERMAL CONVECTION LOOP TEST SYSTEMS[b]

Lithium Flow Velocity = 6–8 feet per minute

Purpose of Tests: To study important variables which might affect corrosion in stainless steel systems

Loop Number	Test Variable	Hot Leg		ΔT[c]		Length of Test, Hours	Hot-Leg Specimen (Tab)			Total Mass Transfer[d] mg	Metallographic Observations
							Weight Loss mg/in.^{2}/100 hr	Thickness Loss (mils)			
		°F	°C	°F	°C			Maximum	Minimum		
21 316 SS[e]	Base-line loop with cold trap	1500	(816)	430	(239)	293[f]	94.2	7	3	1940	Hot Leg: 3 mils of subsurface voids. Cold Leg: 1 mil duplex crystals. 1 mil GBA.[g]
22 316 SS	Base-line loop no cold trap	1500	(816)	430	(239)	96[f]	509.5	12	6	5050	Hot Leg: 4 mils of subsurface voids. Cold Leg: 1 mil crystals. 1 mil GBA.
23 316 SS	1000 ppm nitrogen added.[h] No cold trap.	1500	(816)	350	(195)	88[f]	272.3	6	3	2560	Hot Leg: 4 mils GBA. Cold Leg: 2 mil crystals. 1 mil GBA.
24 316 SS	1000 ppm oxygen added.[i] No cold trap.	1500	(816)	250	(139)	210[f]	79.0	6	2	1870	Hot Leg: 1 mil of subsurface voids. Cold Leg: 1 mil duplex crystals. ½ mil GBA.

[a]Pipe size: 0.84 inch outside diameter by 0.109 inch wall thickness; pipe analysis: Fe–65.0, Cr–17.5, Ni–12.3, Mo–2.2, Mn–1.8, C–0.10 (weight per cent).

[b]All loops of type "B" design.

[c]ΔT is the maximum temperature difference between hot and cold legs.

[d]Weight of crystals collected from loop following test.

[e]SS stands for stainless steel.

[f]Loop plugged with mass transfer crystals.

[g]GBA stands for grain-boundary attack.

[h]Nitrogen added as lithium nitride. (Analysis of lithium nitride: Li plus N_2–96.8 weight per cent).

[i]Oxygen added as lithium oxide. (Analysis of lithium oxide: Li plus O_2–98.9 weight per cent).

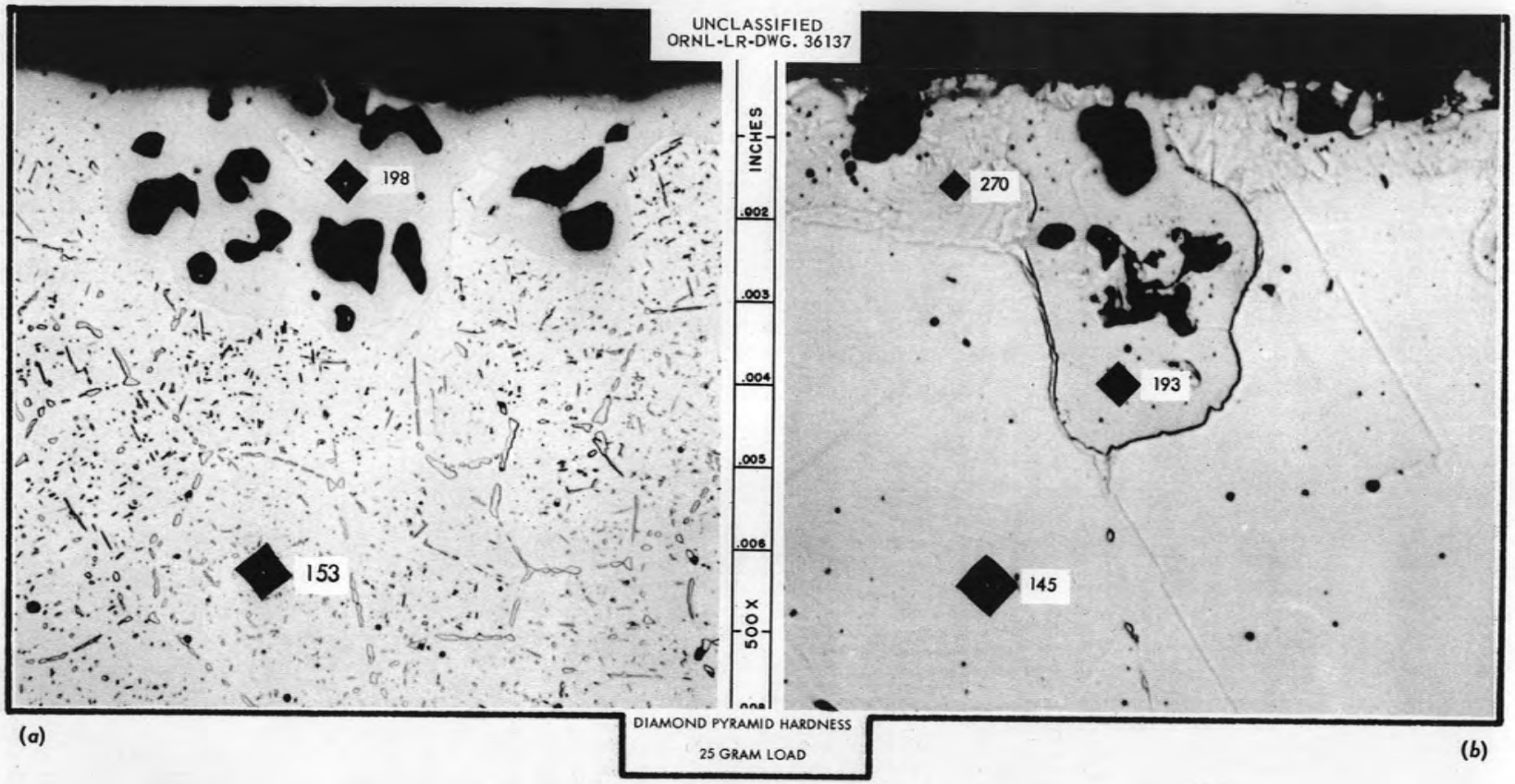

Figure 76. The Effect of Temperature on the Corrosion of the Hot Legs of Type 316 Stainless Steel Thermal Convection Loops by Lithium. (*a*) Loop No. 18, Hot-Leg Temperature – 1400°F (760°C), 1090 Hours. (*b*) Loop No. 20, Hot-Leg Temperature – 1600°F (871°C), 437 Hours. Etchant: Glyceria Regia. 500X. Reduced 6%.

UNCLASSIFIED
ORNL-LR-DWG. 36141

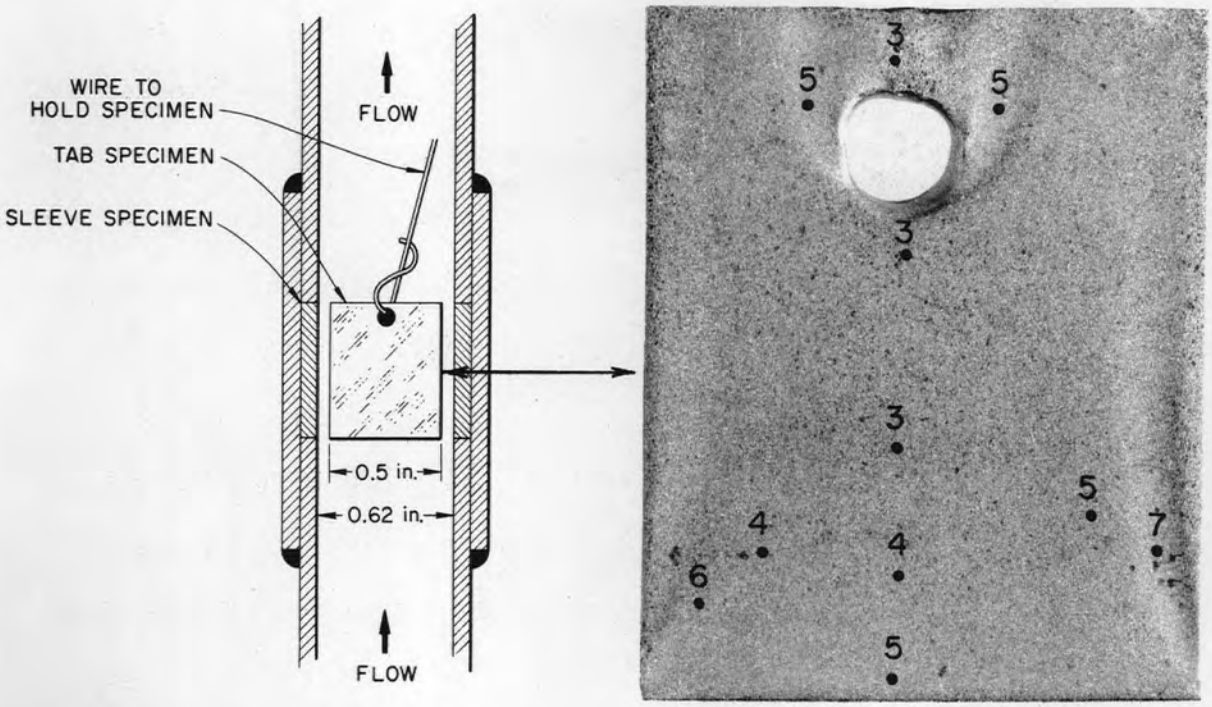

Figure 77. Weight-Loss Specimen from the Hot Leg of Type 316 Stainless Steel Loop No. 21 Following Exposure to Lithium. Note that Specimen Surface is "Grooved" in Areas of Highest Turbulence. Numbers on Specimen Indicate Loss in Thickness in Mils as a Result of Exposure to Lithium. Test Conditions: Hot Leg – 1500°F (816°C), Cold Leg – 1070°F (577°C), 293 Hours.

the loop without the cold trap was five times greater. Tests conducted by McKee[80] on loops of Type "B" design with diffusion cold traps, which were constructed from the same heat of type 316 stainless steel used in the present study, showed specimen weight-loss rates approximately equal to those obtained with the base-line cold trap loop (No. 21). McKee's tests were performed at hot- and cold-leg temperatures of 1600 and 1100°F (871 and 593°C), respectively.

Originally, it was felt that the cold trap served to remove impurities from the lithium, thus reducing attack; however, the results obtained upon the deliberate contamination of the lithium with Li_3N and Li_2O (see below) do not support this contention. At the present time the function of the diffusion cold trap is not understood.

(c) The Effect of Oxygen and Nitrogen Additions to Lithium. Lithium nitride and lithium oxide were added to Loops Nos. 23 and 24, respectively, (see Table XXVII) in order to determine the effect of these impurities on the rate of mass transfer. As a result of these additions, concentrations of 1000 ppm of nitrogen and oxygen, respectively, were built up in the two loops. Both loops were of the modified Type "B" design except that the diffusion cold traps were omitted to avoid precipitation of the added impurities. The hot-leg temperature in both cases was 1500°F (816°C).

As indicated in Table XXVII, the mass transfer rates for Loops Nos. 23 and 24 were markedly less than that for the base-line loop, No. 22. The influence of the additives is brought into question, however, by the fact that the thermal gradients in the former loops were

substantially less than that for the base-line loop. In an attempt to clarify this issue, the mass transfer rates for the three loops were divided by the respective ΔT for each loop and the resulting values were plotted against ΔT. It was found that the three data points lay very close to a straight line, suggesting that the mass transfer rates for all three loops would have been the same had the loops been operated with identical thermal gradients. In view of the obvious inadequacies of the data, however, it is only tentatively suggested that the nitrogen and oxygen additions to lithium had no effect on the mass transfer rate at 1500°F (816°C).

The details of the corrosion phenomena in Loops Nos. 23 and 24 differed somewhat from those for other loops operated at 1500°F (816°C). The hot leg of the loop to which nitrogen was added exhibited marked grain-boundary penetration (Figure 78a) in contrast with the sub-surface void formation (Figure 78b) observed in the base-line loop, No. 22. Metallographic examination of the hot leg of Loop No. 24 to which oxygen was added revealed the occurrence of neither grain-boundary attack nor a phase transformation. Surface attack was very uniform and only a few widely scattered sub-surface voids at a depth of less than one mil were observed. As in the case of the mass transfer rates, however, these observations must be considered as tentative on account of the relatively small thermal gradients in the loops.

(d) Effect of Flow Velocity. The primary difference between the Types "A" and "B" loop designs lay in the increased lengths of the vertical sections of the hot and cold legs of the Type "B" loops. This

UNCLASSIFIED
ORNL-LR-DWG. 36135

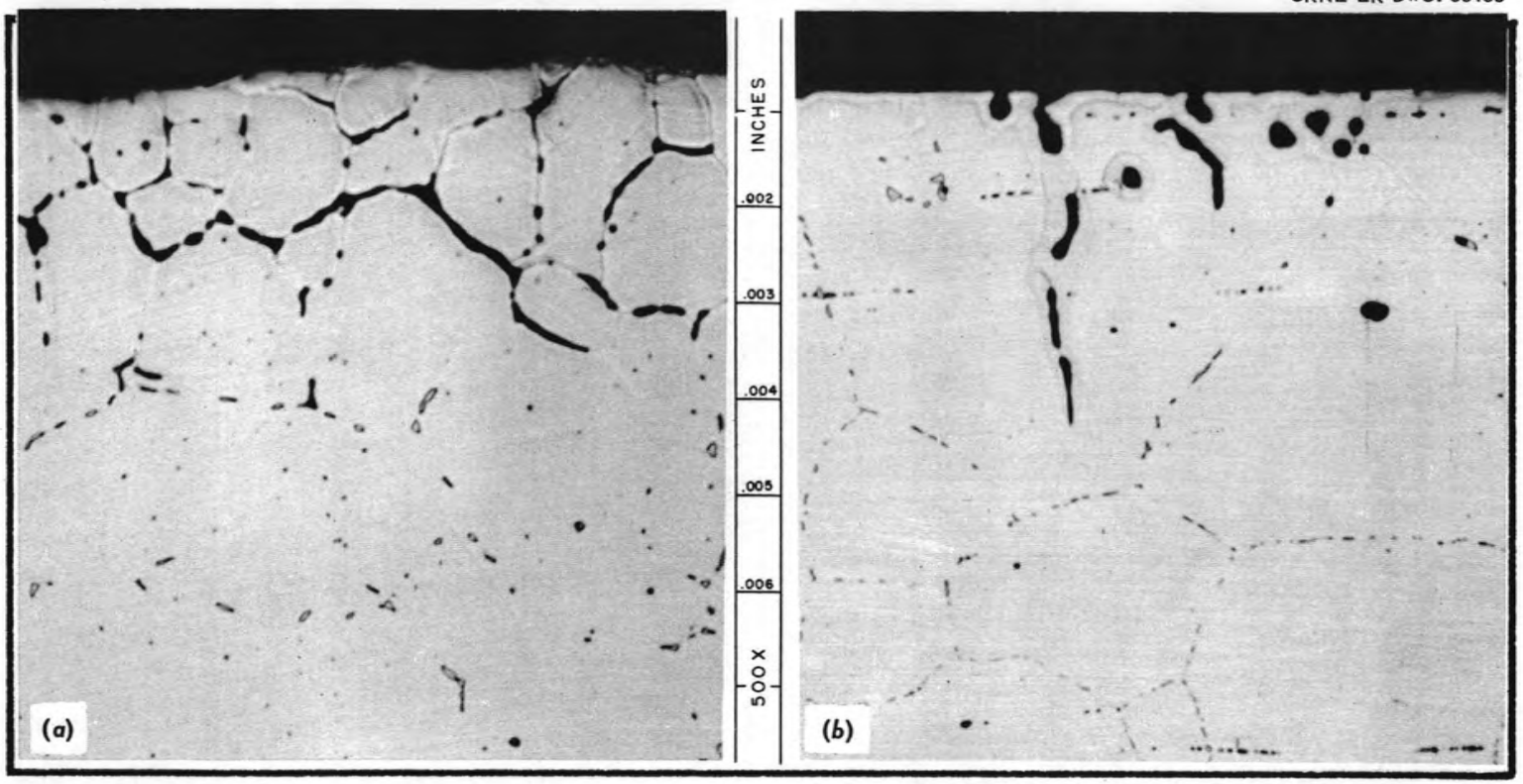

Figure 78. Effect of Nitrogen Addition to Lithium on the Corrosion in the Hot Leg of a Type 316 Stainless Steel Loop. (*a*) Loop No. 23: 1000 ppm Nitrogen Added , (*b*) Loop No. 22: Standard Loop with no Nitrogen Added. Etchant: Glyceria Regia. 500X.

feature permitted the attainment of a flow velocity in the Type "B" loops nearly double that of the Type "A" loops. The influence of velocity alone was illustrated by a comparison of Loop No. 19 (Type "A") with Loop No. 21 (Type "B"). These loops were operated under almost identical temperature conditions, but the mass transfer rate for the higher velocity loop was more than five times greater. The effect discussed on page 185 in connection with the influence of the magnitude of the thermal gradient in a loop on mass transfer also suggested that an increase in flow velocity led to increased mass transfer. Finally, the drastic effects of localized variations in flow patterns and flow velocities was noted on page 178 in connection with the "grooving" of the tab insert specimens (see Figure 77). Thus, it is apparent that flow velocity was of paramount importance in determining mass transfer rates under the loop test conditions described.

3. Chemical Analyses of Mass Transfer Deposits and Hot- and Cold-Leg Surfaces. The bulk of the crystal deposition observed in the stainless steel thermal convection loops occurred in the vicinity of the lower T-joints which were the coldest sections of the loops. Because of the difficulty experienced in retaining the crystals in position during the stripping operation, the loops were radiographed at the completion of the tests. A radiograph of a typical crystal deposit "plug" is illustrated in Figure 79. Deposition was not confined entirely to the bottom of the cold leg; minor quantities of crystals were frequently found on the weight-loss specimen in the hot leg and at the lithium-gas interface at the top of the loop.

UNCLASSIFIED
ORNL-LR-DWG 35952

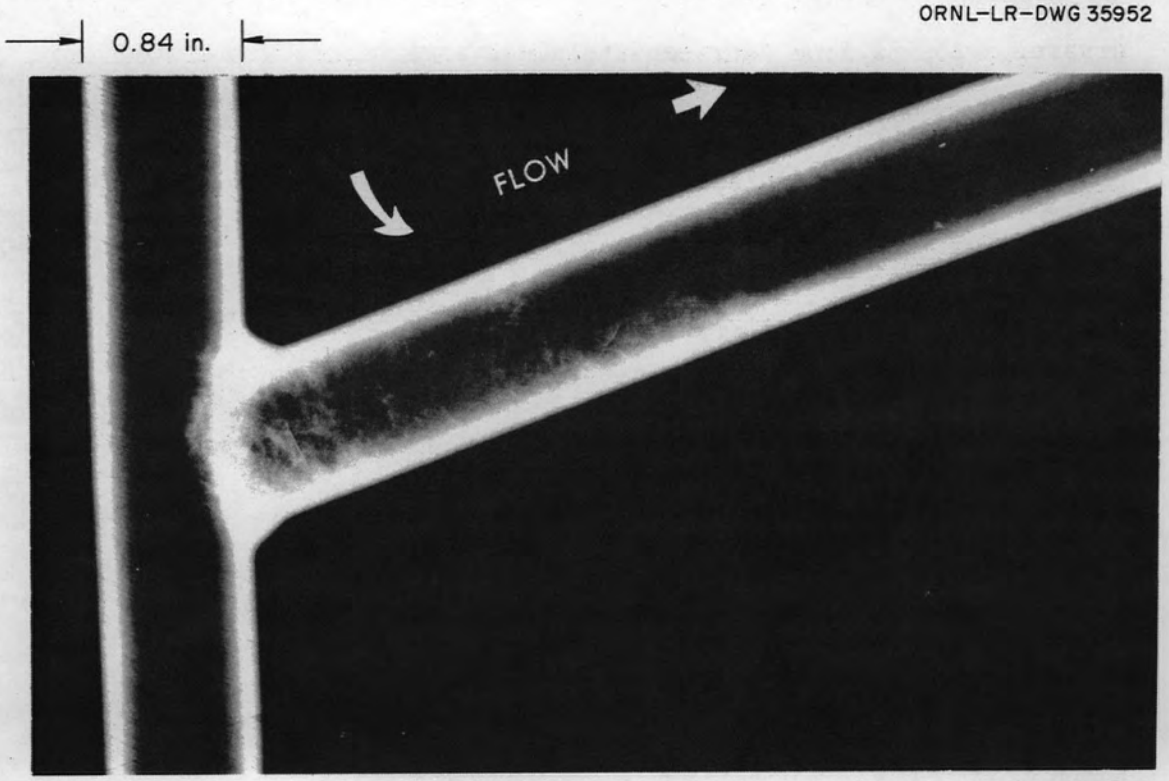

Figure 79. Radiograph of the Bottom of the Cold Leg of a Type 316 Stainless Steel Thermal Convection Loop (No. 22) Which Plugged After 96 Hours of Operation. White "Feathery" Areas Indicate Location of Mass Transfer Crystals. Note the Low Density of the Crystal "Plug" Relative to the Weld Zone at the Saddle Joint.

Duplicate chemical analyses were performed on the crystals in all tests when the weight of crystals recovered made such determinations possible. The results of the chemical analyses performed on the crystal deposits from fourteen stainless steel loops are listed in Table XXVIII. These analyses were intended to show whether any of the components of the stainless steel had mass transferred preferentially from the hot-leg pipe wall. An over-all summary of the findings listed in detail in Table XXVIII is given in Table XXIX. Although the deposits were generally found to be somewhat enriched in particular elements relative to the pipe composition before test, it should be emphasized that all major elements found in the original pipe were present in fairly large concentrations in the crystals.

Despite several inconsistencies in the analytical data, the general trend of the compositional changes accompanying mass transfer was established. The crystals were usually significantly enriched in nickel and manganese, and smaller enrichments in iron were frequently observed. The chromium content of the metallic crystals was low in all cases, a result attributable to the fact that most of the chromium and carbon removed from the hot leg deposited as $Cr_{23}C_6$ crystals firmly bonded to the cold-leg surface. These crystals were not removed during the stripping operation following test.

In order to determine the extent of compositional changes in the loop walls, ten-mil cuts were machined from the hot- and cold-leg surfaces of four type 316 stainless steel loops. In the case of one of these loops, five-mil cuts were also obtained. Analyses of these

TABLE XXVIII

COMPARISON OF MASS TRANSFER CRYSTAL ANALYSIS[a] WITH THE BEFORE-TEST ANALYSIS OF THE THERMAL CONVECTION LOOP PIPE

Loop Number	Loop Material	Weight Per Cent						
		Fe	Ni	Cr	Mn	Mo	Si	C
	316 SS[b] pipe before test	68.7	11.5	15.4	1.8	2.1	0.4	0.06
4	crystals	90.6[c]	1.2	7.1	1.0	0.1	0.1	0.04
5	crystals	72.1[c]	22.1[c]	2.3	3.6[c]	0.1	0.1	
	316 SS pipe before test	65.0	12.2	17.5	1.8	2.2	0.6	0.10
19	crystals	55.5	26.3[c]	13.1	4.7[c]	0.4		
20	crystals	60.8	23.5[c]	11.1	3.4[c]	0.6		
21	crystals	68.2[c]	11.6	16.5	1.2	1.3	0.2	
22	crystals	73.7[c]	17.3[c]	5.4	2.9[c]	0.1	0.5	0.10
23	crystals	66.9[c]	19.5[c]	6.1	3.3[c]	0.1	4.0[c]	
24	crystals	73.1[c]	13.1[c]	12.3	0.9	0.5		
	321 SS pipe before test	68.5	11.5	15.9	1.4		0.5	0.06
7	crystals	58.5	23.8[c]	13.2	4.0[c]		0.4	
	347 SS pipe before test	70.4	12.0	12.1	1.3		0.4	0.05
9	crystals	58.5	26.7[c]	10.2	4.2[c]		0.3	
10	crystals	65.6	24.1[c]	5.8	4.0[c]		0.1	
	430 SS pipe before test	82.3	0.3	15.8	0.6		0.4	0.08
14	crystals	97.9[c]	0.7[c]	1.1	0.3		0.1	0.01
	446 SS pipe before test	73.2	0.6	22.7	0.6		0.1	0.30
15	crystals	85.6[c]	8.1[c]	5.2	1.2[c]		0.1	0.04
16	crystals	83.4[c]	6.6[c]	8.5	1.4[c]		0.1	0.03

[a]The analyses of the elements listed totaled 90 to 97 weight per cent of the crystals in all cases. Duplicate analyses performed on the crystals from each loop. Compositions adjusted to 100 per cent.

[b]SS stands for stainless steel.

[c]Indicates that crystals found in the loop were rich in this particular element as compared to the concentration of the element in the pipe before test.

TABLE XXIX

SUMMARY OF ANALYTICAL RESULTS ON MASS TRANSFER CRYSTALS FOUND IN FOURTEEN STAINLESS STEEL THERMAL CONVECTION LOOP TESTS

12 of 14 loops had crystals rich* in nickel
10 of 14 loops had crystals rich* in manganese
9 of 14 loops had crystals rich* in iron
1 of 11 loops had crystals rich* in silicon
0 of 14 loops had crystals rich* in chromium
0 of 8 loops had crystals rich* in molybdenum
0 of 5 loops had crystals rich* in carbon

*Rich in particular element as compared to the concentration of that element in the stainless steel pipe before test.

layers of material were obtained, and the results are shown in Table XXX. The compositional differences between hot- and cold-leg samples obtained from the ten-mil cuts were minor and somewhat erratic. The large quantity of base material contained in the ten-mil cuts probably masked the effect of the surface reactions since the analyses of the five-mil cuts indicated a significant enrichment of the cold-leg surface in chromium and nickel relative to the hot leg.

The analyses of the deposited metallic crystals and of the machined layers suggest that the preferential leaching which occurred in the hot leg was relatively minor compared to the solution attack on the hot-leg surface. During deposition, however, a "partitioning" of the precipitated material appeared to have occurred with the chromium and carbon forming $Cr_{23}C_6$ crystals, while the metallic deposits were relatively enriched in nickel, manganese, and, in most cases, iron.

4. Summary of Austenitic and Ferritic Stainless Steel Thermal Convection Loop Results. The stainless steel loop test investigations can be summarized by considering three aspects of the corrosion results:

(a) Temperature Limitations for the Containment of Lithium. A few general statements may be made concerning the useful temperature limits of austenitic or ferritic stainless steels for the containment of lithium. The corrosion and mass transfer rates of both the austenitic and ferritic stainless steels at hot-leg temperatures above 1300°F (704°C) were found to be excessive for heat-transfer systems designed for 1000-hour operation. In addition, the corrosion rates

TABLE XXX

CHEMICAL ANALYSIS ON 5- AND 10-MIL CUTS MACHINED FROM THE HOT- AND COLD-LEG SURFACES OF TYPE 316 STAINLESS STEEL THERMAL CONVECTION LOOPS

Loop Number	Section Analyzed	Weight Per Cent						
		Fe	Ni	Cr	Mn	Mo	Si	C
	Type 316 SS[a] pipe before test	65.0	12.2	17.5	1.8	2.2	0.6	0.10
19[b]	10 mil cut from hot-leg surface	67.4	11.5	16.7	1.7	2.2	0.4	0.02
	10 mil cut from cold-leg surface	66.5	11.9	17.2	1.6	2.2	0.5	0.06
20[c]	10 mil cut from hot-leg surface	68.2	11.8	17.5	1.6	2.2	0.4	0.01
	10 mil cut from cold-leg surface	65.5	12.5	17.5	1.8	2.2	0.5	0.06
	5 mil cut from hot-leg surface	68.3	10.4	15.6				
	5 mil cut from cold-leg surface	65.1	12.6	17.4				
21[d]	10 mil cut from hot-leg surface	66.2	11.9	16.0	2.0	2.2	0.4	0.08
	10 mil cut from cold-leg surface	67.0	12.1	16.9	2.0	2.2	0.5	0.24
22[e]	10 mil cut from hot-leg surface	66.7	12.0	16.6	1.8	2.0	0.6	0.08
	10 mil cut from cold-leg surface	66.8	12.0	16.4	1.9	2.0	0.6	0.08

[a]SS stands for stainless steel.
[b]Test conditions: Hot Leg: 1500°F (816°C), Cold Leg: 1010°F (543°C), 500 hours.
[c]Test conditions: Hot Leg: 1600°F (871°C), Cold Leg: 995°F (535°C), 437 hours.
[d]Test conditions: Hot Leg: 1500°F (816°C), Cold Leg: 1070°F (577°C), 293 hours.
[e]Test conditions: Hot Leg: 1500°F (816°C), Cold Leg: 1070°F (577°C), 96 hours.

were found to increase rapidly with increasing hot-leg temperatures so that even shorter times of operation would not be feasible at higher temperatures. In tests operated at a hot-leg temperature of 1000°F (538°C), small amounts of both hot-leg corrosion and crystal deposition in cold legs were detected. Thus, systems operating at maximum temperatures as low as 1000°F (538°C) might become plugged under long-time operating conditions.

(b) General Nature of the Corrosion Process. The corrosion in stainless steel-lithium thermal-convection loop systems occurred by a mass transfer process. Although some preferential leaching of nickel and chromium from the hot-leg wall was observed, iron was also found to mass transfer rapidly. A large portion of the chromium and carbon that was removed from the hot leg was deposited in the form of adherent crystals of chromium carbide ($Cr_{23}C_6$) on the cold-leg wall. The remainder of the material removed from the hot leg precipitated as metallic crystals in the cold leg. The composition of the metallic crystals was variable and depended on the test conditions.

(c) Factors Affecting Rate of Mass Transfer. The experimental results clearly indicate that an increase in flow velocity of the lithium increased the rate of mass transfer. The role of velocity must be considered from two standpoints: (1) its obvious connection in the transport of solute atoms from the hot leg to the cold leg, and (2) its effect on other possible major rate-controlling steps, such as liquid or solid diffusion.

In regard to the transport step, a calculation of the solute-element transport per circuit of lithium around the loop on the basis of flow velocity, loop dimensions, and the weight of crystals recovered, revealed that approximately one ppm of solute elements per circuit was deposited in the cold leg. This result is to be compared with the 1300 ppm per circuit which would have been deposited if transport rate were a major limiting factor. [The 1300 ppm value is based on recent published data[81] which indicate that the total equilibrium solubility of iron, nickel, and chromium, from type 316 stainless steel in lithium is approximately 2600 ppm at 1450°F (788°C) and 1300 ppm at 1250°F (677°C).] Thus, the observed mass transfer rates were much too low for transport of solute atoms to have been a major limiting factor.

The effect of velocity on liquid diffusion may be considered in terms of alterations in the characteristics of the laminar liquid sublayer across which solute elements are considered to diffuse at metal surfaces in the loop. The thickness of the laminar layer decreases with increasing velocity. The following experimental observations can be understood in terms of changes in this laminar layer resulting from changes in flow characteristics: (1) grooving of the tab-insert specimens (Figure 77) was produced in areas where specimen geometry resulted in localized increases in flow velocities, and (2) the weight losses for the sleeve-insert specimens were only 30 to 50 per cent as great as those for the tabs even though the average temperature of the sleeves was higher than that of the tabs.

The leaching of alloying elements from hot legs posed the question as to whether solid state diffusion was a major factor in the over-all mass transfer process. On first consideration it would appear that if solid state diffusion were a major factor no effect of velocity on mass transfer rates should have been observed in the velocity range studied. This, however, would not necessarily be the case. If, for example, liquid diffusion and solid diffusion each contributed comparable major resistances in the mass transfer circuit, a significant velocity effect on the over-all rate might still be expected. The fact that the mass transfer rate was increased by a factor of five on only doubling the flow rate, however, suggests that the effect of solid state diffusion was probably a minor one.

Based on these observations it was concluded that the rate of mass transfer in stainless steel-lithium systems was probably controlled to a major degree by liquid diffusion in the hot leg.

Unfortunately, little information could be derived from the experimental data regarding the influence of other factors on the mass transfer process. The extent to which cold-leg processes determined the rate of mass transfer, for example, is unknown. The limited studies of the effect of nitride and oxide additions to the lithium led to inconclusive results, thus prohibiting any definite conclusions concerning the effect of impurities in the lithium.

CHAPTER VIII

CONCLUSIONS AND RECOMMENDATIONS

Conclusions

The corrosion resistance of a large number of materials in molten lithium under various test conditions was studied in this investigation. The results of the study together with pertinent information from other sources are combined in the bar graph shown in Figure 80. It is the purpose of this graph to provide a condensed guide for the evaluation of available corrosion data for a large variety of materials under a wide range of test conditions.

These data in several instances represent the "best-estimate" extrapolation of existing experimental results. They are valid for systems where the surface-to-volume ratio is approximately 13:1 and, in dynamic tests, for flow rates and container dimensions as indicated on the chart. It should also be emphasized that the data for the metals, especially for the refractory metals, pertain to tests with high-purity materials. The presence of certain impurities or contaminants in any of the materials listed or in the lithium itself may significantly alter the test results, and the reader is referred to specific sections of this report for more detailed discussions of such instances.

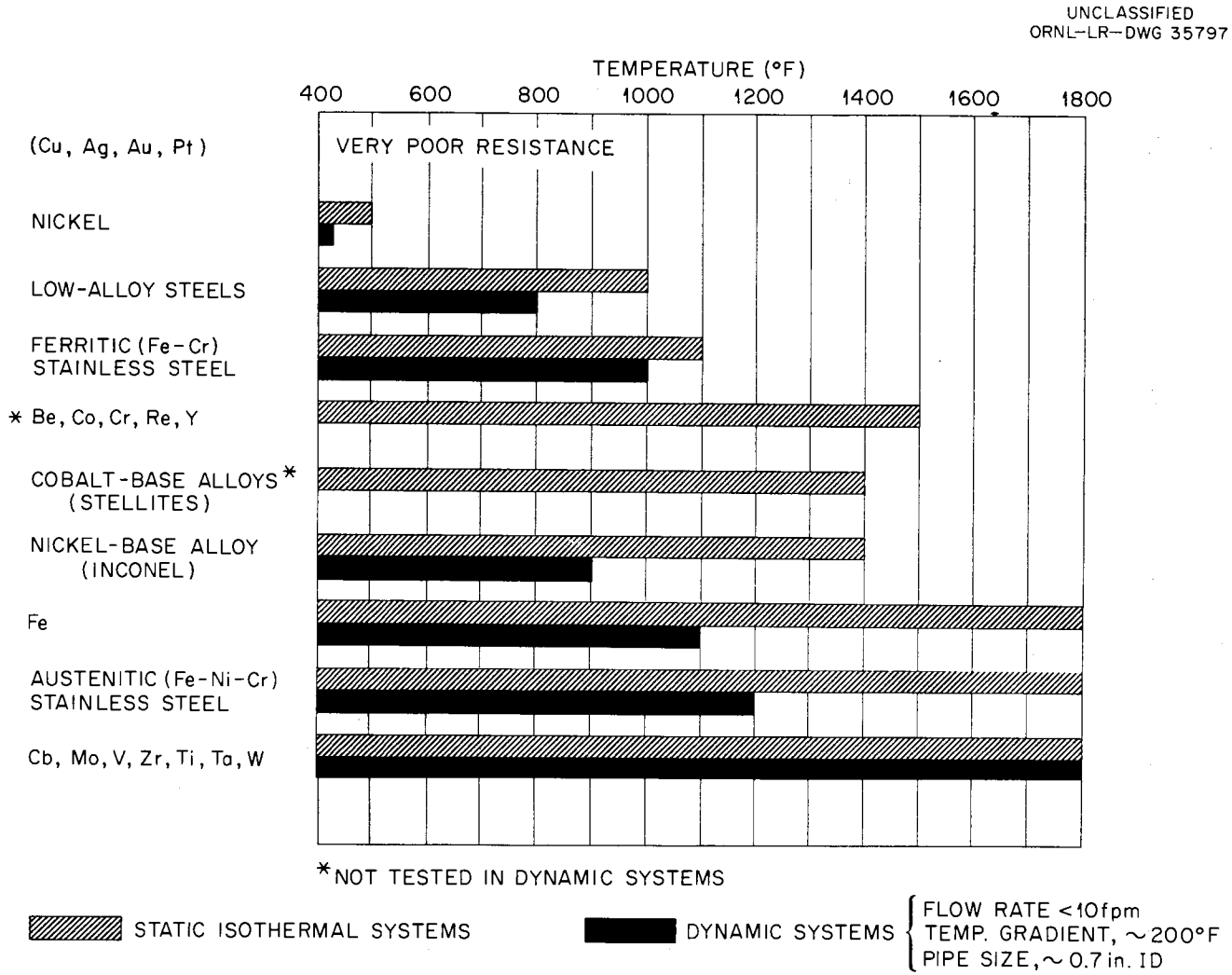

BARS INDICATE APPROXIMATE TEMPERATURES BELOW WHICH A TWO COMPONENT SYSTEM COULD BE OPERATED FOR 1000 HOURS WITH LESS THAN 0.005 in. OF ATTACK OR CONTAINER SURFACE REMOVAL.

Figure 80. Corrosion Resistance of Various Metals and Alloys in Molten Lithium.

Based on an analysis of the data shown in the graph and other more specific results from the present study, the following general conclusions may be drawn:

1. Copper, Nickel, Nickel-Base Alloys, Precious Metals, and Precious-Metal-Base Alloys. Metals with relatively large solubilities in molten lithium exhibited poor corrosion resistance even at low temperatures. Examples of such behavior are afforded by the corrosion results for copper, nickel, the nickel-base brazing alloys, nickel-base hard-facing alloys, the precious metals, and brazing alloys based on the precious metals. Inconel was an exception to this general rule in that it exhibited good corrosion behavior in static tests. On the other hand, it suffered extensive mass transfer in dynamic tests at 1200°F (649°C).

2. Iron. Iron exhibited excellent corrosion resistance in static systems as long as the carbon content of the iron was so low as to prevent the existence of a carbon-rich austenite phase at the test temperature. Although iron was not tested in a dynamic system, the results obtained with iron-base alloys suggested that iron itself might have acceptable corrosion properties in flowing systems at temperatures below 1200°F (649°C).

3. Low-Alloy Steels. Low-alloy steels possessed limited resistance to corrosion by lithium. Grain-boundary penetration occurred in these steels, and this effect increased with increasing carbon content.

4. Ferritic Stainless Steels. The limited corrosion resistance of the ferritic stainless steels was related to the preferential attack of grain-boundary carbides. Less grain-boundary penetration occurred in the low carbon grades of ferritic stainless steels.

5. Austenitic Stainless Steels. The austenitic stainless steels were found to be the most corrosion resistant of the commercially available, high-temperature alloys for the containment of lithium. However, these alloys suffered extensive mass transfer at temperatures of 1300°F (704°C) and above in dynamic test systems. In some tests with these alloys grain-boundary attack occurred, and this effect was greatly increased when the lithium in the test system was contaminated with lithium nitride. The attack appeared to be less severe in some of the stabilized grades. In those systems where preferential leaching of alloying elements occurred, surface regions were observed to have transformed from austenite to ferrite.

6. Beryllium, Cobalt, Chromium, Rhenium, and Yttrium. These metals showed good corrosion resistance at temperatures as high as 1500°F (816°C) in static, isothermal systems but were not tested in dynamic systems.

7. Cobalt-Base Alloys. Cobalt-base alloys of the hard-facing type were tested in static systems and were found to possess varying degrees of corrosion resistance depending on the concentration of alloying elements. The higher carbon alloys generally exhibited less resistance to attack.

8. Refractory Metals. The refractory metals, columbium, molybdenum, vanadium, and zirconium were found to possess excellent

corrosion resistance to lithium in both static and dynamic test systems. Molybdenum performed well in dynamic tests at temperatures as high as 1900°F (1038°C). The corrosion of columbium was strongly dependent upon oxygen concentration in the test metal; detectable grain-boundary attack was observed in specimens containing in excess of 100 ppm oxygen. Thus columbium to be used as a container material for lithium should be very low in oxygen content, and all welding operations should be performed under high purity, inert-gas atmospheres. Static corrosion results obtained in this investigation and recent dynamic test data obtained in three-component test systems[69,70] indicated that titanium, tantalum, and tungsten also possessed good resistance to lithium in both static and dynamic systems.

9. Cermets. Nickel-bonded cermets experienced severe corrosion in static systems, a fact presumably related to the high solubility of nickel in lithium. Cobalt-bonded cermets possessed acceptable corrosion resistance, but corrosive attack increased with increasing cobalt concentrations.

10. Ceramics. A large number of oxides, nitrides, borides, and carbides were tested in static systems, but only chromium-, titanium-, and zirconium-carbide bodies exhibited acceptable corrosion resistance.

The following conclusions can be drawn relative to phenomena which occurred in the molten lithium metal in these studies:

1. Carbon Transfer. Extensive transfer of carbon by lithium was detected in: (a) three-component, static, isothermal systems in

which carbon was transferred from alloys of high-carbon content to alloys of lower carbon content; and (b) in dynamic systems in which carbon was transferred from hot to cold zones.

2. Oxygen and Nitrogen Solubilities. The relatively high solubility of oxygen in lithium at temperatures just above the melting point of lithium raised a question as to the usefulness of a cold trap for the removal of oxygen from dynamic lithium systems. The reverse conclusion was reached in the case of nitrogen removal.

3. Sampling Techniques. The research performed relative to analyses for oxygen and nitrogen in lithium indicated the necessity for special sampling and handling techniques to avoid atmospheric contamination of the specimens. Techniques suitable for these purposes were developed in this study.

4. Lithium Purification Techniques. Titanium and zirconium reduced the nitrogen concentration in lithium very effectively, and yttrium showed promise of significantly reducing the oxygen concentration.

5. Velocity Effects. Thermal convection loop tests on type 316 stainless steel showed that flow velocity had a major influence on the rate of mass transfer. An analysis of these data indicated that this effect was primarily attributable to the velocity dependence of liquid diffusion in the hot leg.

Recommendations

Recommendations for future studies of the corrosion of materials by lithium include:

1. Further studies of the effect of oxygen contamination on the corrosion resistance of the refractory metals.

2. High-temperature dynamic tests on refractory metals at high flow velocities and with large temperature differences for extended time periods.

3. Determination of the relationship between hot- and cold-leg temperature differences and the rate of mass transfer in dynamic tests with austenitic stainless steels.

4. Further studies on the effect of flow velocity under equal temperature conditions in dynamic tests with austenitic stainless steels.

5. Determination of the limiting temperature conditions for austenitic stainless steel systems employing high flow rates and large temperature differences.

6. Detailed determinations of the rates of solution and deposition as functions of temperature and flow velocity in various regions of dynamic test systems. Such information might be obtained, for example, from a series of weight-loss sleeve-insert specimens incorporated in the hot and cold legs of thermal or forced convection loop systems.

LIST OF REFERENCES

LIST OF REFERENCES

1. Kitzes, A. S., A Discussion of Liquid Metals as Pile Coolants, ORNL-360, pp. 5, 34 (August 10, 1949)

2. Sullivan, W. H., Trilinear Chart of Nuclides, Oak Ridge National Laboratory, U. S. Government Office, Washington, D. C. (January, 1957)

3. Jackson, C. B. (Ed.), Liquid-Metals Handbook, Sodium-NaK Supplement, Atomic Energy Commission, Department of Navy, Washington, D. C., p. 162 (1955)

4. Goldstein, H., The Attenuation of Gamma Rays and Neutrons in Reactor Shields, NDA-34, U. S. Government Printing Office, Washington 25, D. C., pp. 33, 34, 67 (May 1, 1957)

5. Nuclear Propulsion Program Engineering Progress Report No. 24, PWAC-582, p. 25 (June 30, 1957) SECRET C-85

6. Nesterenko, G. N., Sobolev, A. I. and Syshkob, Yu. N., Application of Atomics Engines in Aviation, Military Press of the Ministry of Defense of the U.S.S.R., Moscow (1957). Translation (NP-TR-81), p. 67, prepared by Technical Documents Liaison Office, MCLTD, Wright-Patterson Air Force Base, Ohio

7. Silberstein, A., Hearings before Subcommittees of the Joint Committee on Atomic Energy, Congress of the United States, Eighty-Fifth Congress, Second Session on Outer Space Propulsion by Nuclear Energy, January 22, 23, and February 6, 1958. U. S. Government Printing Office, Washington, D. C., p. 72 (1958)

8. Spitzer, L., Jr., et al., Problems of the Stellarator as a Useful Power Source, U. S. Atomic Energy Commission Report PM-S-14, NYO-6047 (August, 1954) OFFICIAL USE ONLY

9. Separation of Lithium-7, Y-1243 (To be issued)

10. Hoffman, E. E. and Manly, W. D., Lithium as a Nuclear Reactor Coolant, ORNL-2538, p. 30 (August 8, 1958) SECRET C-81

11. Hoffman, E. E. and Manly, W. D., "Corrosion Resistance of Metals and Alloys to Sodium and Lithium," Handling and Uses of the Alkali Metals, Advances in Chemistry, Am. Chem. Soc., Series 19, pp. 82 – 92 (1957)

12. Manly, W. D., "Fundamentals of Liquid-Metal Corrosion," Corrosion, 12, 336 – 342 (July, 1956)

13. Gurinsky, D. H., "The Behavior of Materials in Aggressive Liquid Metals," Nuclear Metallurgy, A Symposium on Behavior of Materials in Reactor Environment, Institute of Metal Division, A.I.M.M.E., p. 6 (February 20, 1956)

14. Burton, W. N., Coffman, S. W. and Randolph, C. L., A Compendium of Information Concerning Lithium, Aerojet Engineering Corporation Report RTM-57, pp. 17 – 25, 56 (September 16, 1949) CONFIDENTIAL

15. DeVries, G., Pfefferkorn, O. T. and Wetmore, W. O., The Corrosion of Metals by Molten Lithium, NP-3120 (March 21, 1950) CONFIDENTIAL

16. Edler, H. G., The Corrosion of Metals in Molten Lithium, RTM-69 (October 11, 1950) CONFIDENTIAL

17. Wilkinson, W. D. and Yaggee, F. L., Attack on Metals by Lithium, ANL-4990 (October 13, 1950)

18. Wilkinson, W. D. and Yaggee, F. L., Attack on Uranium by Lithium at 600°C, ANL-4991 (October 13, 1950)

19. Jessman, D. S., et al., Preliminary Investigation of Metallic Elements in Molten Lithium, NEPA-1465 (June, 1950) CONFIDENTIAL

20. Anderson, R. and Stephen, H., Progress Report on Materials Tested in Lithium, NEPA-1652 (August, 1950) CONFIDENTIAL

21. Dana, A. W., Jr., Baker, O. H. and Ferguson, M., Investigation of Constant Temperature, Forced Circulation Liquid Lithium Systems, Technical Report Quarter 3, B and W Report No. 5528, DC-52-5-19 (April, 1952)

22. Dana, A. W., Jr., Baker, O. H. and Ferguson, M., Investigation of Metal Transport by Liquid Lithium, Technical Report Quarter 5, B and W Report No. 5230, DC-52-27-45 (May, 1952)

23. Cunningham, J. E., Interim Report on the Resistance of Metallic Materials to Corrosion Attack by High Temperature Lithium, ORNL CF-51-7-135 (July 23, 1951)

24. Brasunas, A. de S., Interim Report on Static Liquid-Metal Corrosion, ORNL-1647, pp. 32 – 44 (May 11, 1954)

25. Lyon, R. N. (Ed.), Liquid-Metals Handbook (revised ed.), Office of Naval Research, NAVEXOS-P-733, pp. 158 – 161 (June, 1952)

26. Parkinson, W., Jr., Stability of Iron Toward Lithium at Elevated Temperatures under Cyclotron Irradiation, NAA-SR-73 (August, 1952)

27. McKee, J. M., Effect of Nitrogen on Corrosion by Lithium, NDA-40 (June 14, 1957) SECRET

28. Minushkin, B., Determinations of the Solution Rate of Metals in Lithium, NDA-44 (June 30, 1958) SECRET

29. Nuclear Propulsion Program Engineering Progress Report No. 16, PWAC-552, p. 78 (April 1 – June 30, 1955)

30. Nuclear Propulsion Program Engineering Progress Report No. 17, PWAC-553, p. 83 (July 1 – September 30, 1955)

31. Nuclear Propulsion Program Engineering Progress Report No. 18, PWAC-554, p. 91 (October 1 – December 31, 1955)

32. Nuclear Propulsion Program Engineering Progress Report No. 19, PWAC-561, p. 104 (January 1 – March 31, 1956)

33. Nuclear Propulsion Program Engineering Progress Report No. 20, PWAC-562, p. 99 (April 1 – June 30, 1956)

34. Nuclear Propulsion Program Engineering Progress Report No. 21, PWAC-563, p. 102 (July 1 – September 30, 1956)

35. Nuclear Propulsion Program Engineering Progress Report No. 23, PWAC-571, pp. 138, 140 (January 1 – March 31, 1957)

36. Nuclear Propulsion Program Engineering Progress Report No. 24, PWAC-572, pp. 128 – 131 (April 1 – June 30, 1957)

37. Nuclear Propulsion Program Engineering Progress Report No. 25, PWAC-573, pp. 111, 113 – 119 (July 1 – September 30, 1957)

38. Nuclear Propulsion Program Engineering Progress Report, PWAC-574, pp. 109 – 122, 136 – 140, 143 – 150 (October 1 – December 31, 1957)

39. Nuclear Propulsion Program Engineering Progress Report, PWAC-581, pp. 121, 122, 138 – 142, 148 – 154 (January 1 – March 31, 1958)

40. Nuclear Propulsion Program Engineering Progress Report, PWAC-582, pp. 119 – 126, 143, 145 – 148, 153 (April 1 – June 30, 1958)

41. Nuclear Propulsion Program Engineering Progress Report, PWAC-583, pp. 97 – 104, 108 – 111, 121, 123 (July 1 – September 30, 1958)

42. Hoffman, E. E. and Jansen, D. H., Lithium Symposium – Analytical Procedures and High-Temperature Corrosion – Reading List, ORNL CF-57-10-6 (Rev. January 20, 1958)

43. Cunningham, J. E., Interim Report on the Resistance of Metallic Materials to Corrosion Attack by High Temperature Lithium, ORNL CF-51-7-135, p. 15 (July 23, 1951)

44. Vreeland, D., Hoffman, E. E. and Manly, W. D., "Corrosion Tests for Liquid Metals, Fused Salts at High Temperatures," Nucleonics, 11(11), 36 – 39 (1953)

45. Brasunas, A. de S., Interim Report on Static Liquid-Metal Corrosion, ORNL-1647, p. 2 (May 11, 1954)

46. Brasunas, A. de S., A Simplified Apparatus for Making Thermal Gradient Dynamic Corrosion Tests (Seesaw Tests), ORNL CF-52-3-123 (March 13, 1952)

47. Gurinsky, D. H., "The Behavior of Materials in Aggressive Liquid Metals," A Symposium on Behavior of Materials in Reactor Environment, IMD Special Report Series No. 2, AIME, pp. 5, 6 (February 20, 1956)

48. Hackett, H. N., "Mercury for the Generation of Light, Heat, and Power," Trans. ASME, 647 – 655 (October, 1942)

49. McKee, J. M., Effect of Nitrogen on Corrosion by Lithium, NDA-40, p. 13 (June 14, 1957) SECRET

50. Gray, R. J., Crouse, R. and Roche, T. K., Metallurgy Division Quar. Progr. Rep., ORNL-1302, pp. 105 – 107 (September 2, 1952)

51. Avery, H., Homerberg, V. and Cook, E., "Metallographic Identification of Ferromagnetic Phases," Metals and Alloys, 10, 353 (1939)

52. Cunningham, J. E., Interim Report on the Resistance of Metallic Materials to Corrosion Attack by High Temperature Lithium, ORNL CF-51-7-135 (July 23, 1951)

53. DeVries, G., Pfefferkorn, O. and Wetmore, W., "The Corrosion of Metals by Molten Lithium," U. S. Naval Ordinance Test Station, Inyokern, California, NP-3120, p. 8 (March, 1950) CONFIDENTIAL

54. Webber, H., Goldstein, D. and Fellinger, R., "Determination of the Thermal Conductivity of Molten Lithium," Trans. ASME, 77(2), 100 (February, 1955)

55. Begley, R., Development of Niobium-Base Alloys, Wright Air Development Center Technical Report 57-344, p. 93 (May, 1958)

56. Tottle, C., "The Physical and Mechanical Properties of Niobium," J. Inst. Metals, 85, 377 (April, 1957)

57. Heestand, R. L. and Hoffman, E. E., Welding of Columbium, Part I. Joining Techniques for Systems to Contain Lithium, ORNL-2423 (To be published)

58. Seybolt, A. U., "Solid Solubility of Oxygen in Niobium," J. Metals, 6, 774 – 776 (June, 1954)

59. Ang, C. Y. and Wert, C., "Some Properties of Columbium Containing Nitrogen," J. Metals, 5, 1032 – 1036 (August, 1953)

60. Glassner, A., The Thermochemical Properties of the Oxides, Fluorides, and Chlorides to 2500°K, U. S. Government Printing Office, Washington 25, D. C.

61. Brewer, L., et al., Chemistry and Metallurgy of Miscellaneous Materials: Thermodynamics, p. 42, ed. by L. L. Quill, McGraw-Hill, New York (1950)

62. Darnell, J. R. and Yntema, L. F., Technology of Columbium (Niobium), pp. 2, 4, ed. by B. W. Gonser and E. M. Sherwood, John Wiley and Sons, Inc., New York (1958)

63. Hodgman, C. D., et al., Handbook of Chemistry and Physics, p. 540, Chemical Rubber Pub. Co., Cleveland, Ohio (1953)

64. Wilkinson, W. and Yaggee, F., Attack on Metals by Lithium, ANL-4990, p. 32 (October 13, 1950)

65. Anderson, R. and Stephan, H., Progress Report on Materials Tested in Lithium, NEPA-1652, p. 17 (August, 1950)

66. McKee, J., Effect of Nitrogen on Corrosion by Lithium, NDA-40, p. 10 (June 14, 1957)

67. Frankenburger, W., Andrussow, L. and Durr, F., "A New Complex Compound of Lithium, Iron and Nitrogen," Zeitschrift fur Elektrocheme, 34(9), 632 – 637 (1928)

68. Bagley, K. Q. and Montgomery, K. R., The Solubility of Nickel in Lithium, United Kingdom Atomic Energy Authority, Industrial Group Report No. IGR-TN/C 250 (September 30, 1955)

69. Cunningham, J. E., Interim Report on the Resistance of Metallic Materials to Corrosion Attack by High Temperature Lithium, ORNL CF-51-7-135, pp. 1, 54 (July 23, 1951)

70. Gunty, M., "Sur la Chaleur de Formation du Carbure de Lithium," Comptes Rendus, 126, 1866 (June 27, 1898)

71. Hansen, M., Constitution of Binary Alloys, McGraw-Hill Book Co., p. 104 (1958)

72. Cunningham, J. E., Interim Report on the Resistance of Metallic Materials to Corrosion Attack by High Temperature Lithium, ORNL CF-51-7-135, p. 12 (July 23, 1951)

73. Gray, R. J., Crouse, R. and Roche, T. K., Metallurgy Division Quar. Progr. Rep., ORNL-1302, pp. 105 – 107 (September 2, 1952)

74. Avery, H., Homerberg, V. and Cook, E., "Metallographic Identification of Ferromagnetic Phases," Metals and Alloys, 10, 353 (1939)

75. Monkman, F., Cuff, F., Jr. and Grant, N., "Computation of M_s for Stainless Steels," Metal Progr., 71(4), 95 (April, 1957)

76. Lyon, R., Liquid-Metals Handbook, NAVEXOS P-733 (Rev.) Atomic Energy Commission and Department of the Navy, p. 161 (1952)

77. Lyon, R., Liquid-Metals Handbook, NAVEXOS P-733 (Rev.) Atomic Energy Commission and Department of the Navy, pp. 152, 156, 157 (1952)

78. McKee, J., The Effect of Nitrogen on Corrosion by Lithium, NDA-40, p. 33 (June 14, 1957) SECRET

79. Bagley, K. Q. and Montgomery, K. R., The Solubility of Nickel in Lithium, UKAEA Industrial Group Report No. IGR-TN/C 250 (September 30, 1955)

80. McKee, J., The Effect of Nitrogen on Corrosion by Lithium, NDA-40, p. 23 (June 14, 1957)

81. Nuclear Propulsion Program Engineering Progress Report, PWAC-574, p. 150 (October 1 – December 31, 1957)

82. Nuclear Propulsion Program Engineering Progress Report, PWAC-581, pp. 144, 148 (January 1 – March 31, 1958)

83. Nuclear Propulsion Program Engineering Progress Report, PWAC-582, p. 153 (April 1 – June 30, 1958)

BIBLIOGRAPHY

BIBLIOGRAPHY

Andrade, E. N. da C. and Dobbs, E. R., "The Viscosities of Liquid Lithium, Rubidium and Cesium," Proc. Roy. Soc. London, 211-A, 12 – 13 (1952)

Baker, P. S., Duncan, F. R. and Greene, H. B., "Preparation of High-Purity Lithium Metal by Vacuum Distillation," Science, 118, 778 – 780 (1953)

Bost, W. E., Thermal and Corrosion Properties of Solid and Liquid Lithium, TID-3605 (August, 1957) CONFIDENTIAL

Brasunas, A. de S., "Liquid Metal Corrosion," Corrosion, 9, 78 – 84 (1953)

Brewer, L. and Margrave, J., "The Vapor Pressures of Lithium and Sodium Oxides," J. Phys. Chem., 59, 421 – 425 (1955)

Crocker, A. R. et al., Design, Operation, and Test of a Sodium-to-Lithium-to-Air Heat Transfer System, APEX-327 (August, 1957)

DeVries, G., Pfeffkorn, O. T. and Wetmore, W. U., The Corrosion of Metals by Molten Lithium, NP-3120 (March, 1950) CONFIDENTIAL

Eigo, D. P., Franklin, J. W. and Cleaver, G. H., "Lithium," Eng. and Mining J., 156, (9) 75 (September, 1955)

Epstein, L. F., "Corrosion by Liquid Metals," Proceedings of the International Conference on the Peaceful Uses of Atomic Energy, 9, 311 – 317, United Nations (1956)

Epstein, L. F. and Howland, W. H., "The Distillation of Lithium Metal," Science, 114, 443 – 444 (1951)

Evans, W. et al., "Thermodynamic Properties of the Alkali Metals," J. Research Nat. Bur. Standards, 55, (2) 83 – 96 (August, 1955)

Fenton, W. M. et al., "Uses of Lithium Metal," Handling and Uses of the Alkali Metals, Advances in Chemistry, Series 19, Am. Chem. Soc. pp. 16 – 26 (1957)

Hader, R. N., Nielsen, R. L. and Herre, M. G., "Lithium and Its Compounds," Ind. Eng. Chem., 43, 26 – 36 (1951)

Hampel, C. A., "Lithium," Chap. 12, Rare Metals Handbook, Reinhold Pub. Co. (1956)

Herold, A., Muller, P. and Albrecht, P., Compt. Rend., 235, 658 – 659 (September 29, 1952) (In French)

Hoffman, E. E., "Liquid Metal Corrosion," Corrosion Fundamentals, University of Tennessee Press (1956)

Hoffman, E. E. and Manly, W. D., "Comparison of Sodium Lithium, and Lead as Heat Transfer Media from a Corrosion Standpoint," Problems in Nuclear Engineering, 1, 128, Pergamon Press, New York (1957)

Hoffman, E. E. and Trotter, L. R., "Corrosion and Mass Transfer by Lithium at Elevated Temperatures," Metallurgy Information Meeting, Ames, Iowa, May 1956, TID-7526 (Pt. 1) (1957)

Horsley, G. W., A Filtration and Vacuum Distillation Unit for the Purification of Alkali Metals, AERE M/R-1706 (1955)

Howland, W. H. and Epstein, L. F., "Binary System Sodium-Lithium," Handling and Uses of the Alkali Metals, Advances in Chemistry, Series 19, Am. Chem. Soc., pp. 34 – 42 (1957)

Kolodney, M. and Minushkin, B., A Method for Determining the Solution Rate of Container Metals in Lithium, NDA-41, (75 – 17) (June, 1957)

Landolt, P. E., "New Horizons for Lithium," Mining Eng., 9, (4), 460 (April, 1957)

Lockhart, R. W., "Liquid-Metal Cooled Systems," The Reactor Handbook, 2, Engineering, AECD-3643, 245 – 366 (May, 1955)

Luckenbach, W. F., "Lithium Metal," Metal Progr., 22, (2) 142 – 144 (August, 1957). (Digest of an article from Foote Prints, 28, (2) 23 – 28 (1956) Foote Mineral Co.

Meyer, H. C., Jr., "Some Practical Aspects of Handling Lithium Metal," Handling and Uses of the Alkali Metals, Advances in Chemistry, Series 19, Am. Chem. Soc., pp. 9 – 16 (1957)

Mote, M. W. and Foust, P. D., "Lithium and Its Alloys," The Reactor Handbook, 3, Materials, AECD-3647 (March, 1955)

Osborg, H., Lithium, Theoretical Studies and Practical Applications, Electrochem. Soc. (1935)

Rogers, R. R. and Viens, G. E., "Effect of Pressure on the Refining of Lithium by Distillation," J. Electrochem. Soc., 98, (12) 483 – 487 (1951)

Rogers, R. R. and Viens, G. E., "Refining Lithium by Vaporization at Low Pressure," Can. Mining and Met. Bull., pp. 15 – 20 (January, 1951)

Rogers, R. R. and Viens, G. E., "The Production of Lithium Metal," Can. Mining and Met. Bull., pp. 623 – 628 (November, 1948)

Sanderson, L., "Lithium," Can. Mining J., 77, (7), 70 (July, 1956)

Sneed, M. C. and Brasted, R. C., "The Alkali Metals," Comp. Inorg. Chem., 6, (Pt. 1) Nostrand Co. (1957)

Taylor, J. W., "Role of Liquid Metals in Nuclear Power Development," Research, 8, (3) 102 – 105 (March, 1955)

Tyzack, C. and Longton, P. B., The Oxidation of Lithium, RDB(D) TN-131, (June 15, 1955)

van Arkel, A. D., Spitsbergen, U. and Heyding, R. D., "Volatility of Lithium Oxide," Can. J. Chem., 33, 446 – 447 (1955)

Verdieck, R., "Lithium: The Element with a Dual Personality," Chem. Proc. (July, 1957)

Woodruff, O. J., McShane, W. J. and Purchell, W. J., "Coolants," Nucleonics, 11, (6) 27 – 34 (June, 1953)

APPENDICES

APPENDIX I

IMPURITIES IN LITHIUM

The most common impurities found in commercial lithium are the non-metals: hydrogen, oxygen, nitrogen, and chlorine; the metalloids: carbon and silicon; and the metals: sodium, potassium, calcium, aluminum, copper, iron, and nickel. Of these elements, oxygen and nitrogen have generally been regarded as being most influential in increasing the corrosiveness of lithium.[1] The techniques which were developed and the experiments conducted in order to study the effects of these impurities are discussed briefly in the sections which follow.

A. Sampling Techniques

Inconsistencies in analytical results on duplicate samples of lithium taken from the various test systems were observed throughout the early portions of the corrosion study. In addition, the concentrations of nitrogen and, particularly, oxygen of given lithium samples often were found to be inconsistent with the past history of the particular specimen. Although analytical difficulties were thought to be responsible for some of the inconsistencies observed, it was recognized that inadequate sampling procedures also represented a major contribution to the experimental errors.

The sampling procedure developed to overcome these problems is illustrated in Figure 81. In order to obtain meaningful analytical

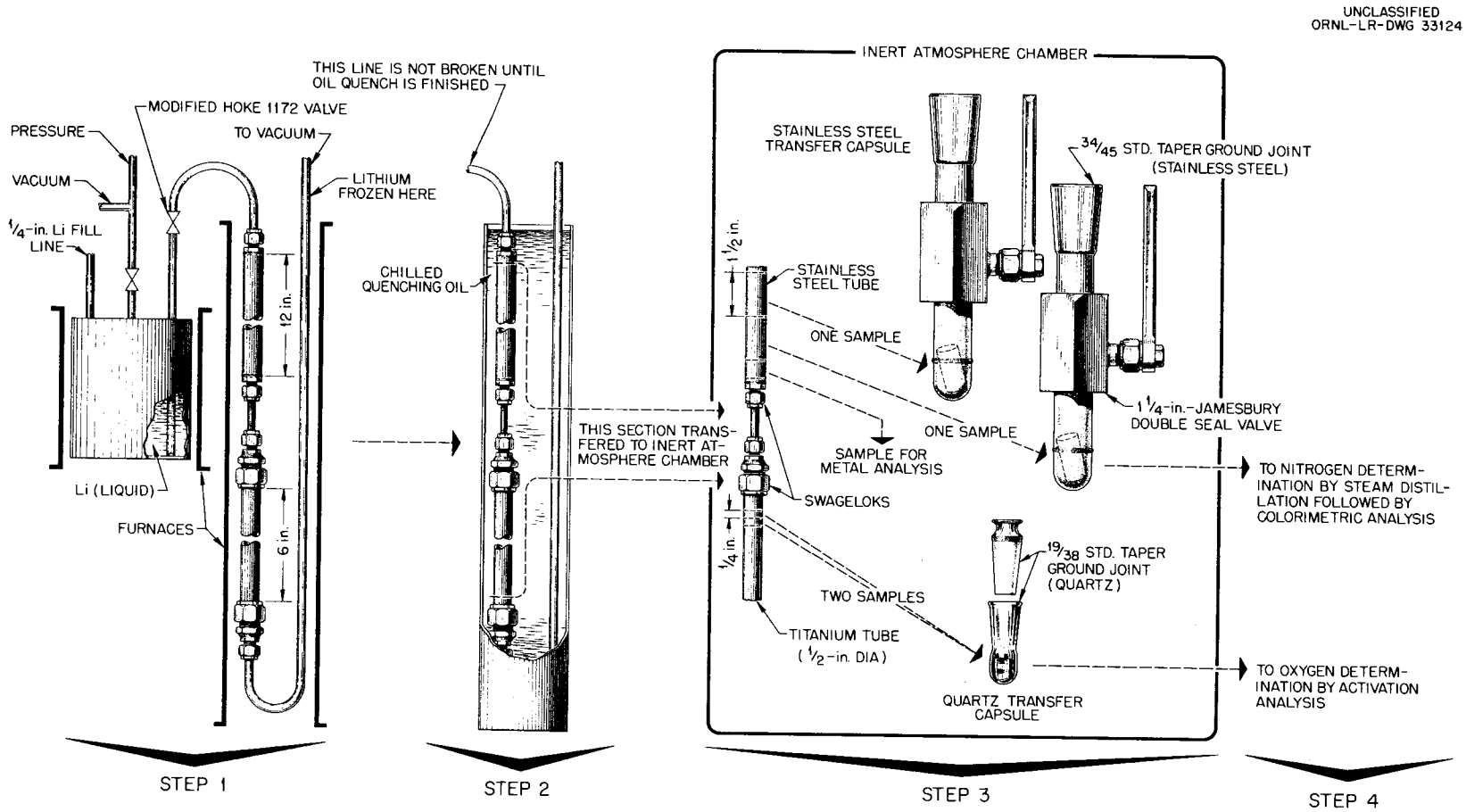

Figure 81. Lithium Sampling Procedure.

results, it was necessary to take samples at temperatures of interest in inert containers, quench them rapidly from the test temperature to avoid segregation of the impruity elements, and protect them from atmospheric contamination at all times. The procedure consisted of the following steps:

1. Pressurization of the container to be sampled with argon, forcing lithium into a heated sampling tube.

2. Removal of the furnace from around the sampling tube and rapid quenching of the sample by means of a chilled-oil bath.

3. Cutting of the sampling tube and transference to the inert atmosphere chamber for sectioning and loading of samples into the transfer capsules which were submitted for chemical analysis.

B. Analytical Methods for Determining Nitrogen and Oxygen in Lithium

A co-operative program was conducted with the Analytical Chemistry Division of the Oak Ridge National Laboratory and with the Nuclear Development Corporation of America to establish the most reliable methods for determining nitrogen and oxygen in lithium in the concentration range from 10 to 2000 ppm. The sampling technique described in Figure 81 was used in this program.

Nitrogen was determined by the methods described by White[2,3] and Sax *et al.*,[4] and the results obtained on the same samples of lithium by both analytical groups were found to agree to within ± 50 ppm at the 300 ppm level and ± 100 ppm at the 2200 ppm level.

On the other hand, the agreement among oxygen analyses, as determined by five different methods, was very poor. The methods used involved activation analysis,[5] mercury amalgamation,[6,7] butyl bromide,[6,7] butyl iodide,[8,9,10] and methanol.[11,12] Several hundred lithium samples were subsequently analyzed for oxygen using the activation analysis technique and this method was found to be the most reliable in terms of reproducibility and sensitivity particularly at oxygen concentrations less than 200 ppm.

C. Purification Experiments

In order to study the effects of nitrogen and oxygen contamination on the corrosiveness of lithium, it was necessary to devise methods of purifying the metal. The purest lithium (LC Grade) obtained from the manufacturer was found to contain 390 ppm oxygen* and 605 ppm nitrogen.[13] The methods used in attempts to purify lithium included low-temperature filtration, vacuum distillation, and gettering with active metals, such as titanium, zirconium, and yttrium.

Filtration through 10-micron stainless steel filters at 482°F (250°C) did not reduce the nitrogen or oxygen content of lithium.

---

*All oxygen concentrations listed in Appendix I were determined by activation analysis.

Vacuum distillation of lithium at 1202°F (650°C) in the apparatus illustrated in Figure 82 was also found to be ineffective in lowering the nitrogen and oxygen concentrations. The results of these experiments are listed in Table XXXI. The failure of this method is probably attributable to the rather high pressure (10^{-4} mm Hg) under which the distillations were performed. However, it should be noted that Arbiter and Lazerus,[14] using distillation equipment and test conditions somewhat similar to those employed in this study, were successful in reducing the nitrogen content of lithium to less than 50 ppm. In the cited work, the presence of titanium sponge in the boiler could have been responsible for the reduced nitrogen content of the distillate. The results listed in Table XXXI were obtained in a distillation system which did not have titanium sponge in the lithium boiler.

The addition to lithium of metals whose oxides and nitrides are more stable than those of lithium was found to be the most practical and effective purification method investigated. Standard free energies of reaction of various metals with lithium nitride and lithium oxide calculated from standard free energies of formation were used as guides in the selection of metals for the gettering studies. On the basis of the possible reduction reactions for lithium nitride[15] listed in Table XXXII, titanium, zirconium, and yttrium were selected for study as potential purifying agents for nitrogen. Both titanium and zirconium were found to be very effective in gettering nitrogen from lithium at 1500°F (816°C) but were not effective in reducing the

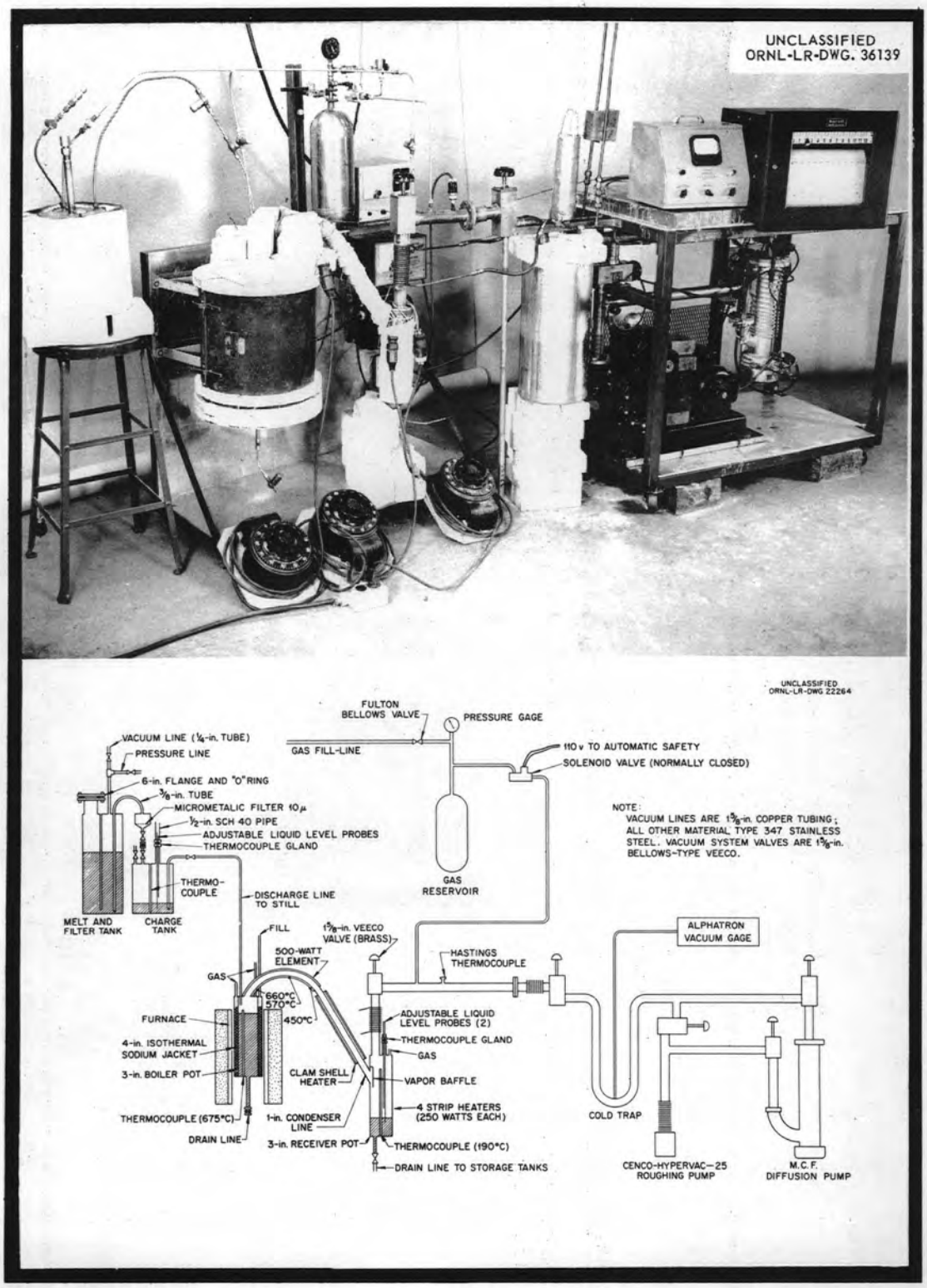

Figure 82. Lithium Distillation System.

TABLE XXXI

EFFECT OF VACUUM DISTILLATION[a] AT 1202°F (650°C) ON THE NITROGEN AND OXYGEN CONTENT OF LITHIUM

Pressure at cold trap with system cold: 2×10^{-5} mm Hg
Pressure at cold trap with system at temperature: 1×10^{-4} mm Hg
Distillation rate: 30 grams per hour

Distillation No.	Nitrogen (ppm) Separate Analyses[b]	Nitrogen (ppm) Average	Oxygen[b] (ppm) Separate Analyses	Oxygen[b] (ppm) Average	Remarks
Charge to still (1100 grams)	1170, 1250	1210	226	(226)	As received and filtered at 300°C through a 5-micron filter.
1	1400, 1300	1350	370, 285	330	
2	1260, 1150, 885, 1010	1080	700, 389, 376, 533	500	
3	3000, 1900	2450	375	(375)	Condenser leaked near end of run.
4	4200, 5300	4750	1120, 1210	1170	Some contamination of system occurred during repair of leak following Distillation No. 3.
5	1600, 1600, 2000	1730	203, 198	200	
6	1800, 2100 2700, 3100	2430	701, 758, 688, 630	690	

[a]80 per cent of each charge was distilled and the remaining 20 per cent was discharged through the drain line.
[b]All samples obtained at end of 80 per cent distillation.

TABLE XXXII

STANDARD FREE ENERGY CHANGES FOR REACTIONS BETWEEN Li_3N AND VARIOUS METALS

$$Li_3N + \frac{x}{y} M = \frac{1}{y} M_xN_y + 3\ Li$$

M_xN_y	ΔF°_{298} Kcal/g-atom of N
ZrN	- 38.0
UN	- 37.7
TiN	- 36.2
Th_3N_4	- 33.6
YN	- 26.7
Be_3N_2	- 23.4
CbN	- 15.7
TaN	- 14.9
Mg_3N_2	- 10.8
Ca_3N_2	- 9.3
Ba_3N_2	+ 0.6

oxygen content, a result to be expected from the oxide-free energy data[16] shown in Figure 83. Typical test results are shown in Table XXXIII which gives data obtained for titanium. In these tests, flat titanium specimens having measurable surface areas were used so that the gettering rate as a function of the surface area could be determined. The metallographic appearance of the titanium before and after the gettering experiment is illustrated in Figure 84.

Titanium sponge was used in subsequent purification experiments. These tests were conducted at 1500°F (816°C) for 24 hours on 40-pound batches of commercial lithium utilizing five pounds of titanium sponge and resulted in reduction of the nitrogen content of lithium to less than 10 ppm. This procedure was used routinely to produce low-nitrogen lithium for the latter portion of the thermal convection loop test investigations. Since it was clear that no significant improvement could be achieved using the more expensive zirconium sponge, no further testing on zirconium was undertaken.

The results of preliminary studies using yttrium indicated that this metal is more effective than either titanium or zirconium in reducing the oxygen content of molten lithium. Lithium purified by exposure to yttrium turnings at 1500°F (816°C) for 100 hours resulted in lithium containing less than 100 ppm each of oxygen and nitrogen. Chemical analyses obtained on yttrium metal specimens exposed to impure lithium for various time periods in another series of tests are listed in Table XXXIV and are indicative of the relative effectiveness of yttrium as a gettering agent for these impurities. Additional tests will be required to confirm the results of these preliminary studies.

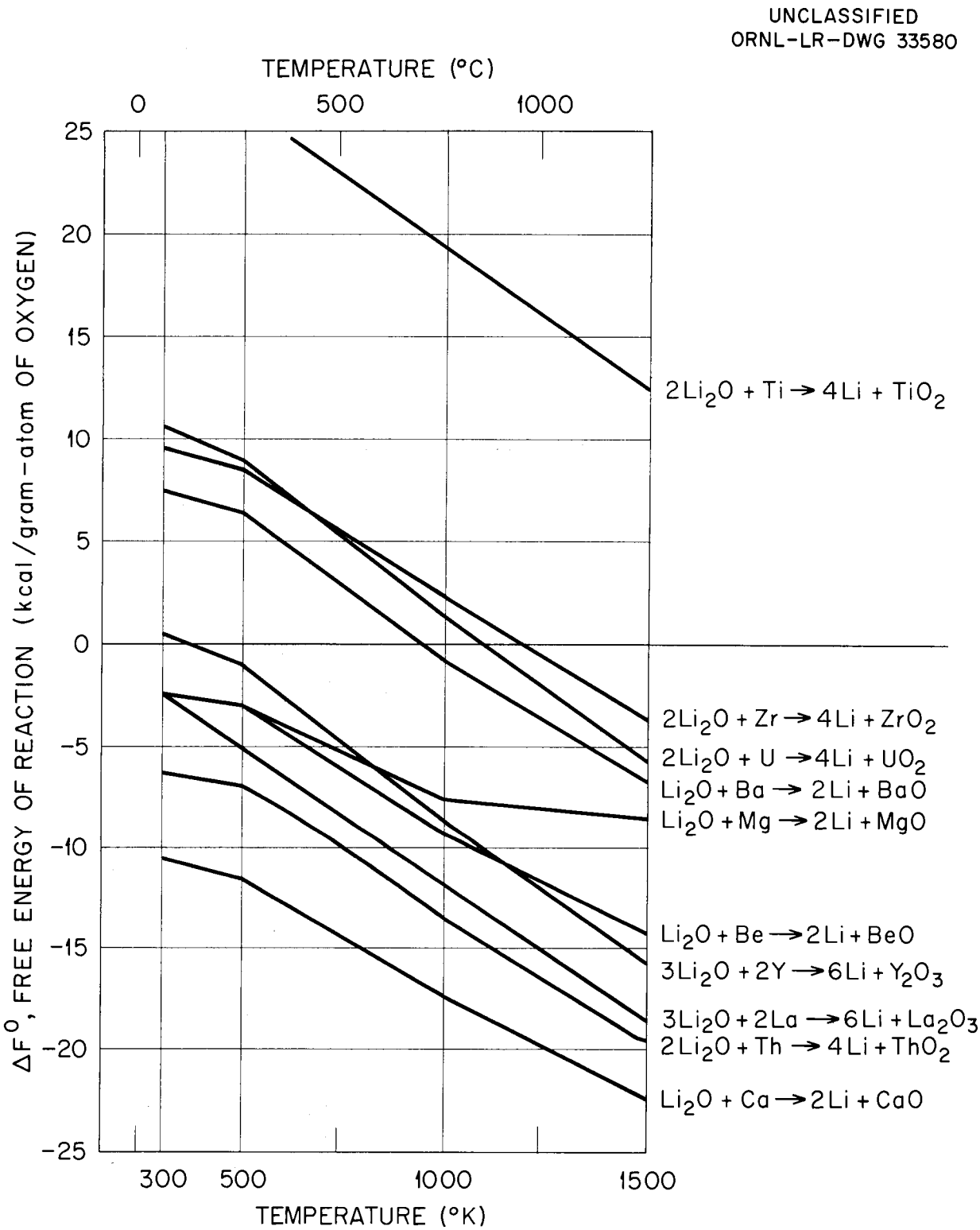

Figure 83. Standard Free Energy Changes for Lithium Oxide Reduction Reactions.

TABLE XXXIII

RESULTS OF LITHIUM PURIFICATION EXPERIMENT UTILIZING TITANIUM SHEET AS THE GETTERING METAL

Test Conditions:
- Temperature: 1500°F (816°C)
- Container: Type 347 Stainless Steel
- Weight of Lithium: 730 grams
- Volume of Lithium: 94.8 in.^{3}
- Dimensions of Titanium Sheets: 8.0 x 1.75 x 0.012 inches
- Number of Titanium Sheets: 10
- Total Weight of Titanium Sheets:[a] 130 grams
- Ratio of Total Surface Area of Titanium to Lithium Volume: 2.98 in.^{2}/in.^{3}

Material Analyzed	Impurity Content (ppm)		Remarks
	N_2	O_2	
Lithium			
Before test	2450	370	
After 24 hours	740	910	Rate of N_2 loss (0 – 24 hours), 71 ppm/hr.
After 48 hours	380	730	Rate of N_2 loss (24 – 48 hours), 15 ppm/hr.
Titanium Sheet			
Before test	74	1500	
After 24 hours	1600	1000	X-ray examination of surface showed TiN; metallographic examination showed 0.0004-inch layer of TiN.
After 48 hours	3200	1400	X-ray examination of surface showed TiN; metallographic examination showed 0.0006-inch layer of TiN.

[a]Weight change of titanium specimens during 48-hour test: 1.0 gram (3.55 mg/in.^{2}).

UNCLASSIFIED
ORNL-LR-DWG 35962

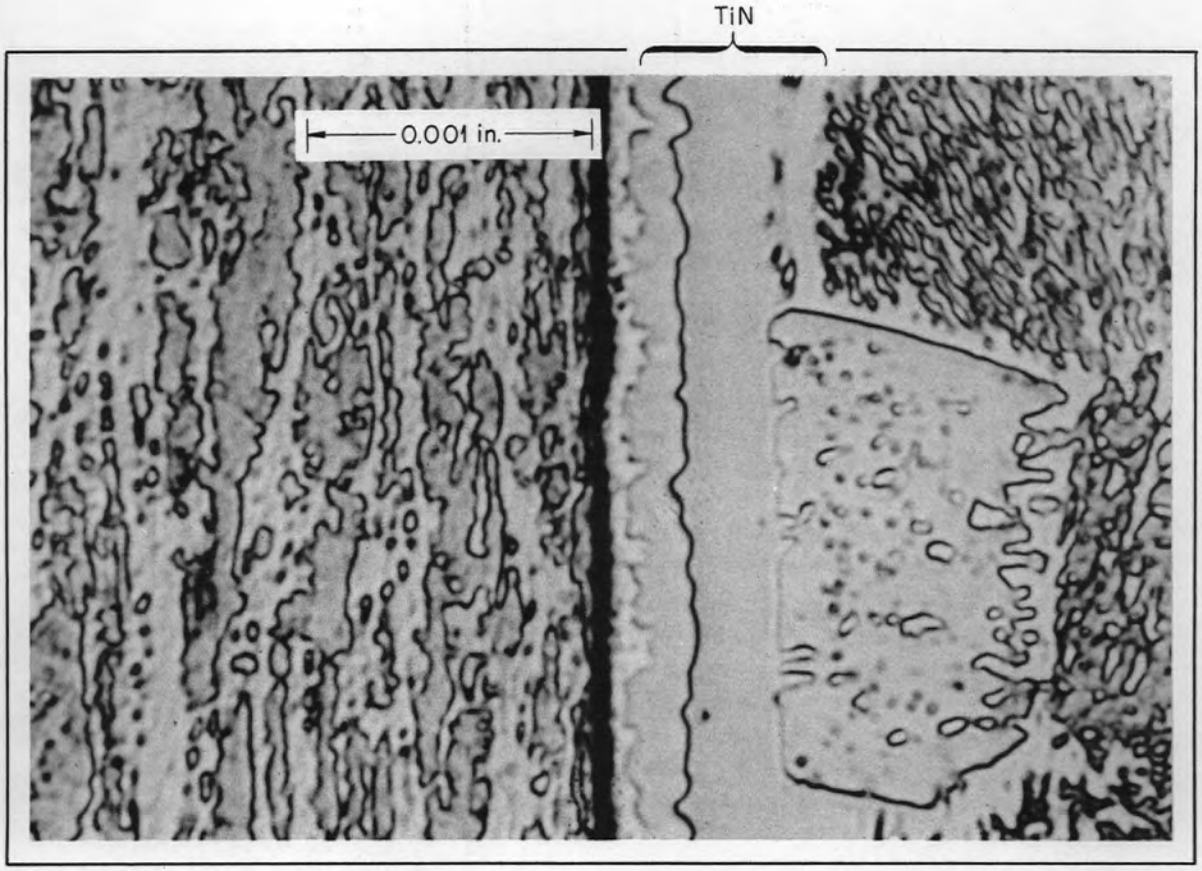

Figure 84. Surface of Titanium Gettering Specimen Before and Following Exposure to Lithium. Gettering Test Conditions: 1500°F (816°C), 100 Hours; Ratio of Titanium Surface Area to Lithium Volume – 2.98 in.^{2}/in.^{3}; Specimen Thickness – 0.012 Inches. Nitrogen Content of Lithium: Before Test – 2450 ppm, After Test – 380 ppm. Etchant: HF, HNO_3, Glyceria (25-25-50 Volume Per Cent).

TABLE XXXIV

COMPOSITIONS[a] OF YTTRIUM GETTER SPECIMENS[b] BEFORE AND AFTER EXPOSURE TO LITHIUM CONTAINING NITROGEN AND OXYGEN

Test Temperature: 1500°F (816°C)
Total Time of Test: 72 hours

Yttrium Specimen Number	Time Period of Exposure, Hours	Oxygen Content of Yttrium (ppm)			Nitrogen Content of Yttrium (ppm)		
		Before Test	After Test	Change	Before Test	After Test	Change
1	0 – 72	1300	3800	+ 2500	450	1100	+ 650
2	24 – 72	1400	3900	+ 2500	570	850	+ 280
3	48 – 72	940	1800	+ 860	110	170	+ 60

[a]As determined by vacuum-fusion analysis.

[b]Dimensions of cylindrical specimens: Diameter, 0.3 inch; Length, 1.0 inch.

D. Solubility of Lithium Nitride and Lithium Oxide in Lithium

No information was found in the literature relative to the equilibrium solubilities of lithium nitride or lithium oxide in molten lithium. Such information was needed in order to determine the potential usefulness of cold-trapping* as a method of continually purifying lithium circulating systems.

Solubility experiments were conducted in the sampling apparatus shown in Figure 85, using high-purity lithium nitride** and lithium oxide*** which were prepared especially for this study. For each solubility determination, sufficient oxide or nitride was added to bring the impurity level of the bath to 5 weight per cent. Samples of the lithium were taken by forcing the lithium through a 20-micron stainless steel filter after allowing the system to equilibrate at the sampling temperature for 24 hours. The solubility samples were quenched and prepared for analysis by the techniques illustrated in Figure 81.

The results of this work showed that the solubility of nitrogen is 1290 ± 150 ppm at 482°F (250°C) and 1830 ± 150 ppm at 572°F (300°C).

---

*Cold-trapping is a method of liquid metal purification which is based upon the temperature dependence of solubility of impurities in the liquid metal.

**Lithium nitride analysis: 98.7 weight per cent Li_3N.

***Lithium oxide analysis: 99.8 weight per cent Li_2O.

UNCLASSIFIED
ORNL-LR-DWG 24830

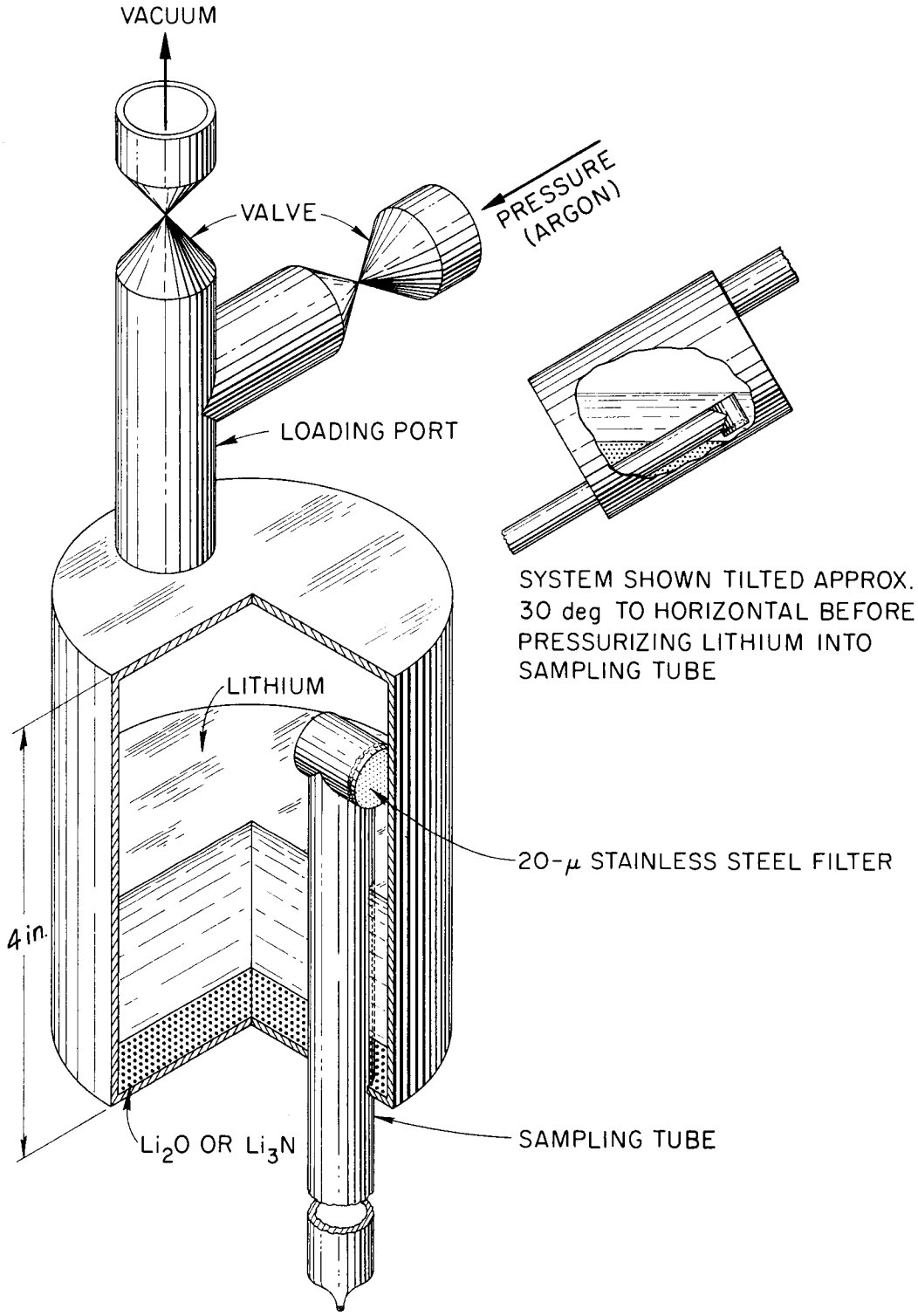

Figure 85. Sampler Used in Li_3N and Li_2O Solubility Studies.

These results, which are based on the analyses of three samples at each temperature, explain the ineffectiveness of low-temperature filtration and cold-trapping in reducing the nitrogen content of lithium.

The solubility of lithium oxide was determined at four temperatures with a minimum of seven samples taken at each temperature. The results, which are listed and plotted in Figure 86, show that the solubility of lithium oxide at temperatures slightly above the melting point of lithium is less than 100 ppm. This result is not consistent with the reported ineffectiveness of cold-trapping[17] as a method of reducing the oxygen content of lithium, but this inconsistency may be related to the inadequacy of previous analytical techniques.

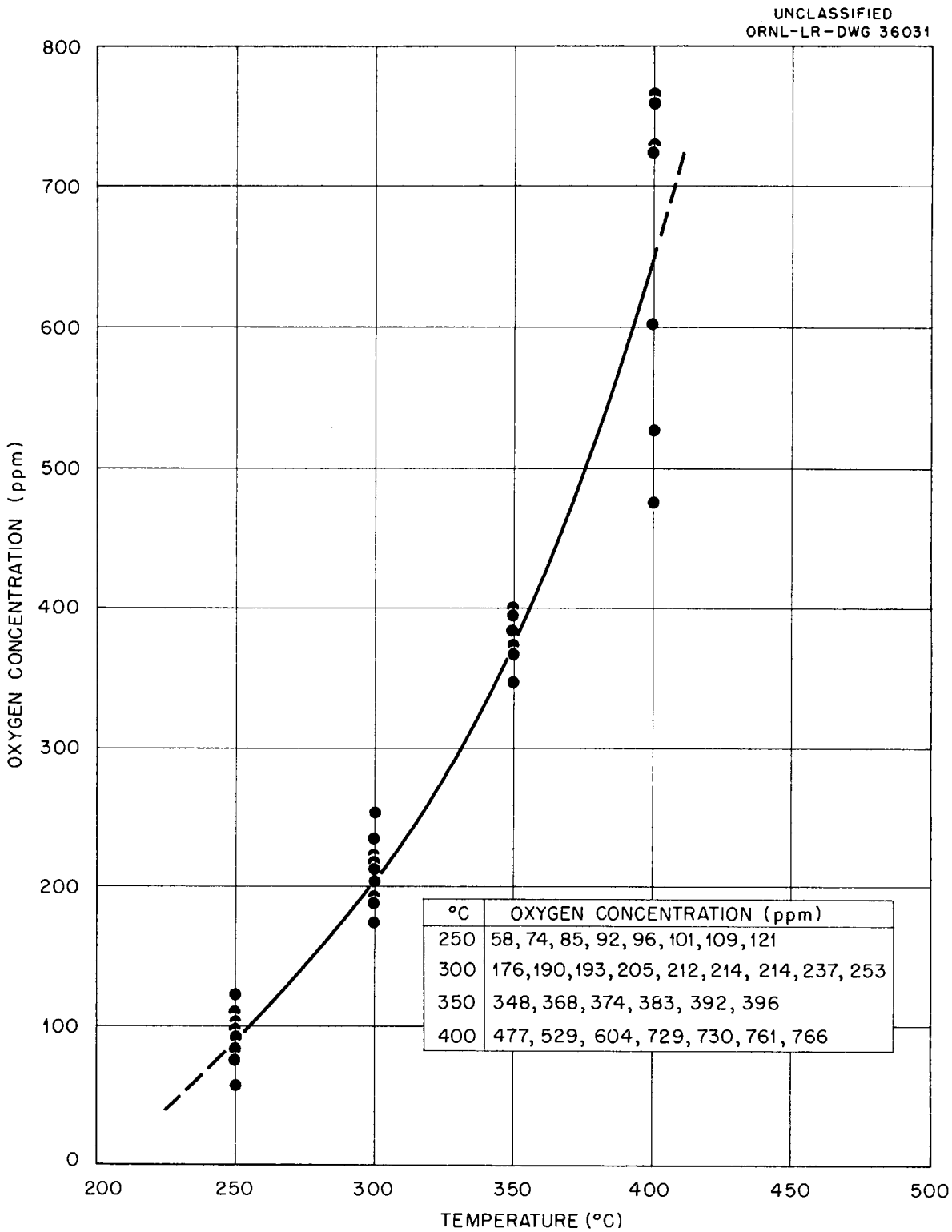

Figure 86. Solubility of Lithium Oxide in Lithium.

APPENDIX II

MECHANICAL PROPERTY STUDIES ON TYPE 316 STAINLESS STEEL AFTER EXPOSURE TO LITHIUM OF VARYING PURITY

In the present corrosion study, it was shown that type 316 stainless steel was particularly susceptible to grain-boundary penetration when exposed to lithium of high-nitrogen content (see Figure 43, p 108). The effect of this grain-boundary attack on the room-temperature tensile properties of the steel was determined using flat tensile specimens 0.05 inch in thickness which had been exposed for 100 hours at 1500°F (816°C), to static lithium containing two weight per cent lithium nitride. For purposes of comparison, tensile specimens were also exposed to lithium containing two weight per cent lithium oxide and to "pure" lithium under the same test conditions.

Photomicrographs of transverse sections through the specimens prior to tensile testing but after exposure to lithium are shown in Figure 87. As may be seen, grain-boundary attack was most pronounced in the specimen exposed to the high-nitrogen lithium* and was essentially absent in the specimen exposed to "pure" lithium.

---

*The specimen exposed to lithium which contained the large nitrogen addition was slightly ferromagnetic and covered with a poorly adherent, one-mil thick metallic film. The chemical composition of this film was 87Fe – 12Ni – 0.8Cr (weight per cent) as compared to 71Fe – 10Ni – 18Cr (weight per cent) for the specimens before tests. The corrosion process responsible for this film formation was not investigated.

UNCLASSIFIED
ORNL-LR-DWG 35696

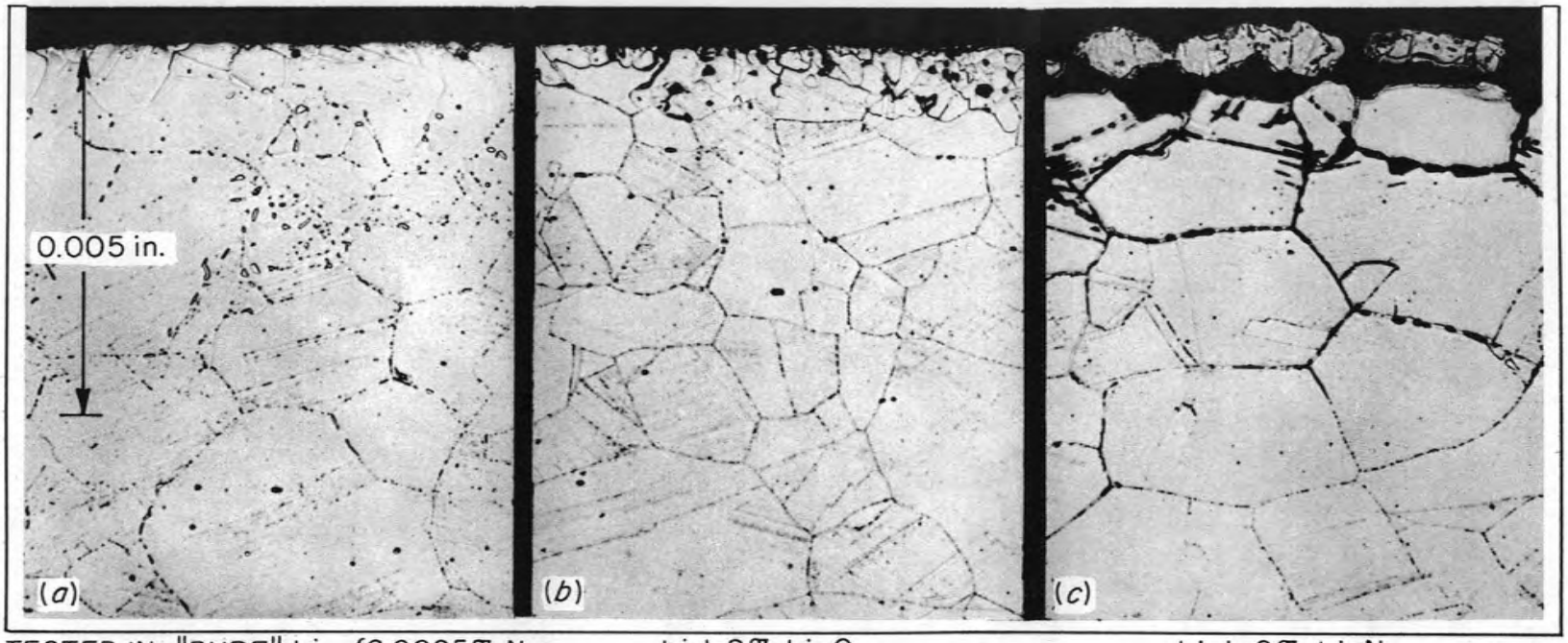

TESTED IN: "PURE" Li {0.0025% N_2, 0.0135% O_2} Li + 2% Li_2O Li + 2% Li_3N

Figure 87. The Effect of Adding Li_2O and Li_3N to Lithium on the Corrosion Resistance of Type 316 Stainless Steel. Test Conditions: Static, 1500°F (816°C), 100 Hours. Etchant: Glyceria Regia.

The results of the tensile tests and photographs of the ruptured specimens are shown in Figure 88. A control specimen that was heated in argon for 100 hours at 1500°F (816°C) in order to duplicate the heat treatment given the other specimens was also included for comparison purposes. It is evident that the nitride impurity has a greater effect on the strength, the ductility, and the grain-boundary cracking than does the oxide impurity.

UNCLASSIFIED
ORNL-LR-DWG 35698

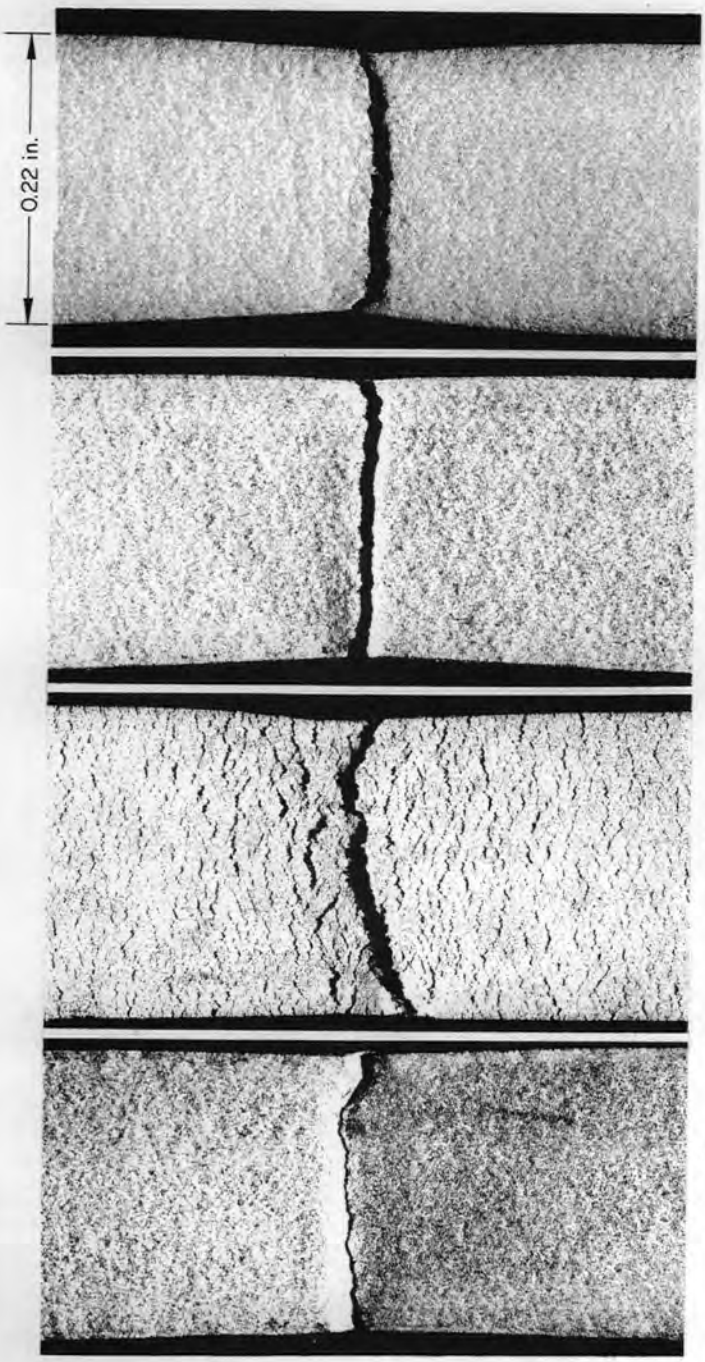

TENSILE SPECIMENS TREATED FOR 100 hr AT 1500°F (816°C) IN THE FOLLOWING ENVIRONMENTS:

ARGON
% EXTENSION = 31.5 % (2-in. GAGE LENGTH)
TENSILE STRENGTH = 98,555 psi

LITHIUM (0.0025 % N_2, 0.0135 % O_2)
% EXTENSION = 32.2 % (2-in. GAGE LENGTH)
TENSILE STRENGTH = 96,005 psi

LITHIUM + 2 % LITHIUM NITRIDE
% EXTENSION = 19.2 % (2-in. GAGE LENGTH)
TENSILE STRENGTH = 88,908 psi

LITHIUM + 2 % LITHIUM OXIDE
% EXTENSION = 30.5 % (2-in. GAGE LENGTH)
TENSILE STRENGTH = 91,992 psi

Figure 88 Type 316 Stainless Steel Specimens Tested in Tension at Room Temperature Following Treatments Indicated. Note Intergranular Cracking in the Specimen Exposed to Lithium Containing 2% Lithium Nitride. 10X. Reduced 29%.

APPENDICES REFERENCES

1. Horsley, G., The Purification of Commercial Lithium, AERE-M/R-1251, p. 1 (September 26, 1953)

2. Aircraft Nuclear Propulsion Project Quar. Progr. Rep., ORNL-2157 (Pts. 1 – 5), p. 128 (September 30, 1956)

3. ANP Project Quar. Progr. Rep., ORNL-2221 (Pts. 1 – 5), pp. 162, 163 (December 31, 1956)

4. Sax, N., Chu, N., Miles, R. H. and Miles, R. W., Determination of Nitrogen in Lithium, NDA-38 (June 14, 1957)

5. Leddicotte, G., Anal. Chem. Ann. Progr. Rep., ORNL-2453, p. 30 (December 31, 1957)

6. ANP Project Quar. Progr. Rep., ORNL-2157 (Pts. 1 – 5), pp. 127, 128 (September 30, 1956)

7. ANP Project Quar. Progr. Rep., ORNL-2221 (Pts. 1 – 5), pp. 163, 164 (December 31, 1956)

8. ANP Project Quar. Progr. Rep., ORNL-2340 (Pts. 1 – 5), p. 167 (June 30, 1957)

9. ANP Project Quar. Progr. Rep., ORNL-2387 (Pts. 1 – 5), pp. 149 – 150 (September 30, 1957)

10. ANP Project Quar. Progr. Rep., ORNL-2517, p. 57 (March 31, 1958)

11. Sax, N. and Steinmetz, H., Determination of Oxygen in Lithium Metal, ORNL-2570 (October 15, 1958)

12. ANP Project Quar. Progr. Rep., ORNL-2274 (Pts. 1 – 5), pp. 138, 139 (March 31, 1957)

13. ANP Project Semiann. Progr. Rep., ORNL-2599, p. 12 (September 30, 1958)

14. Arbiter, W. and Lazerus, S., Purification of Lithium by Vacuum Distillation, NDA-39 (June 14, 1957)

15. Quill, L. L., The Chemistry and Metallurgy of Miscellaneous Materials, McGraw-Hill Book Co., Inc., p. 42 (1950)

16. Glassner, A., The Thermochemical Properties of the Oxides, Fluorides, and Chlorides to 2500°K, U. S. Government Printing Office, Washington, D. C. (1957)

17. Arbiter, W. and Lazerus, S., Purification of Lithium by Vacuum Distillation, NDA-39, p. 7 (June 14, 1957)

ORNL-2674
C-84 — Reactors-Special Features of Aircraft Reactors
M-3679 (22nd Ed., Rev. 1)

INTERNAL DISTRIBUTION

1. G. M. Adamson, Jr.
2. C. J. Barton
3. M. Bender
4. D. S. Billington
5. F. F. Blankenship
6. E. P. Blizard
7. E. S. Bomar, Jr.
8. W. F. Boudreau
9. G. E. Boyd
10. E. J. Breeding
11. F. R. Bruce
12. A. D. Callihan
13. J. V. Cathcart
14. C. E. Center (K-25)
15. R. A. Charpie
16. G. W. Clark
17. R. L. Clark
18. R. E. Clausing
19. C. E. Clifford
20. J. H. Coobs
21. W. H. Cook
22. W. B. Cottrell
23. R. S. Crouse
24. F. L. Culler
25. J. E. Cunningham
26. J. H. DeVan
27. J. R. DiStefano
28. L. M. Doney
29. D. A. Douglas
30. L. B. Emlet (K-25)
31. D. E. Ferguson
32. A. P. Fraas
33. J. H. Frye, Jr.
34. W. T. Furgerson
35. R. G. Gilliland
36. R. J. Gray
37. W. R. Grimes
38. A. G. Grindell
39. R. L. Heestand
40. M. R. Hill
41. T. Hikido
42-43. E. E. Hoffman
44. H. Inouye
45. D. H. Jansen
46. W. H. Jordan
47. G. W. Keilholtz
48. F. L. Keller
49. F. Kertesz
50. J. J. Keyes
51. G. Leddicotte
52. C. F. Leitten, Jr.
53. R. B. Lindauer
54. R. S. Livingston
55. R. N. Lyon
56. H. G. MacPherson
57. R. E. MacPherson
58. F. C. Maienschein
59. W. D. Manly
60. E. R. Mann
61. L. A. Mann
62. H. E. McCoy, Jr.
63. W. B. McDonald
64. F. R. McQuilkin
65. R. P. Milford
66. A. J. Miller
67. J. G. Morgan
68. J. P. Murray (Y-12)
69. M. L. Nelson
70. G. J. Nessle
71. L. G. Overholser
72. P. Patriarca
73. A. M. Perry
74. M. L. Picklesimer
75. A. E. Richt
76. M. T. Robinson
77. T. K. Roche
78. H. W. Savage
79. D. Scott
80. J. L. Scott
81. E. D. Shipley
82. A. Simon
83. O. Sisman
84. J. Sites
85. M. J. Skinner
86. G. M. Slaughter
87. C. O. Smith
88. G. P. Smith, Jr.
89. A. H. Snell
90. C. D. Susano
91. J. A. Swartout
92. A. Taboada
93. R. E. Thoma

94. W. C. Thurber
95. D. F. Toner
96. D. B. Trauger
97. L. R. Trotter
98. G. M. Watson
99. R. C. Waugh
100. A. M. Weinberg
101. J. C. White
102. G. D. Whitman
103. J. C. Wilson
104. C. E. Winters
105. J. L. Gregg (consultant)
106. W. O. Harms (consultant)
107. J. H. Koenig (consultant)
108. H. Leidheiser, Jr. (consultant)
109. C. S. Smith (consultant)
110. W. T. Smith (consultant)
111. E. E. Stansbury (consultant)
112. E. P. Wigner (consultant)
113. H. A. Wilhelm (consultant)
114. Central Research Library
115. ORNL Y-12 Technical Library
Document Reference Section
116. Metallurgy Library
117-204. Laboratory Records Department
205. Laboratory Records, ORNL RC

EXTERNAL DISTRIBUTION

206. AiResearch Manufacturing Company
207-210. Air Force Ballistic Missile Division
211. AFPR, Boeing, Seattle
212. AFPR, Boeing, Wichita
213. AFPR, Douglas, Long Beach
214-216. AFPR, Douglas, Santa Monica
217-218. AFPR, Lockheed, Marietta
219. AFPR, North American, Canoga Park
220. AFPR, North American, Downey
221-222. Air Force Special Weapons Center
223-224. Air Research and Development Command (RDZN)
225. Air Technical Intelligence Center
226-228. ANP Project Office, Convair, Fort Worth
229. Albuquerque Operations Office
230. Argonne National Laboratory
231. Armed Forces Special Weapons Project, Sandia
232. Armed Forces Special Weapons Project, Washington
233-234. Army Ballistic Missile Agency
235. Army Rocket and Guided Missile Agency
236. Assistant Secretary of the Air Force, R and D
237-242. Atomic Energy Commission, Washington
243. Atomics International
244. Battelle Memorial Institute
245-247. Bettis Plant (WAPD)
248. Brookhaven National Laboratory

249. Bureau of Aeronautics
250. Bureau of Aeronautics General Representative
251. BAR, Aerojet-General, Azusa
252. BAR, Chance Vought, Dallas
253. BAR, Convair, San Diego
254. BAR, Grumman Aircraft, Bethpage
255. BAR, Martin, Baltimore
256. Bureau of Yards and Docks
257-258. Chicago Operations Office
259. Chicago Patent Group
260. Director of Naval Intelligence
261. duPont Company, Aiken
262. Engineer Research and Development Laboratories
263-270. General Electric Company (ANPD)
271-272. General Electric Company, Richland
273. General Nuclear Engineering Corporation
274. Hartford Aircraft Reactors Area Office
275. Idaho Test Division (LAROO)
276-277. Knolls Atomic Power Laboratory
278. Lockland Aircraft Reactors Operations Office
279. Los Alamos Scientific Laboratory
280. Marquardt Aircraft Company
281. Martin Company
282. National Aeronautics and Space Administration, Cleveland
283. National Aeronautics and Space Administration, Washington
284. National Bureau of Standards
285. Naval Air Development Center
286. Naval Air Material Center
287. Naval Air Turbine Test Station
288. Naval Research Laboratory
289. New York Operations Office
290. Nuclear Development Corporation of America
291. Nuclear Metals, Inc.
292. Oak Ridge Operations Office
293. Office of Naval Research
294. Office of the Chief of Naval Operations
295. Patent Branch, Washington
296-297. Phillips Petroleum Company (NRTS)
298-301. Pratt and Whitney Aircraft Division
302. San Francisco Operations Office
303. Sandia Corporation
304-305. School of Aviation Medicine
306. Sylvania-Corning Nuclear Corporation
307. Technical Research Group
308. Thompson Products, Inc.
309. USAF Headquarters
310. USAF Project RAND
311. U. S. Naval Radiological Defense Laboratory
312-313. University of California Radiation Laboratory, Livermore
314-325. Wright Air Development Center
326-350. Technical Information Service Extension